Multi-loop investigations of strong interactions at high temperatures

Inauguraldissertation
der Philosophisch-naturwissenschaftlichen Fakultät
der Universität Bern

vorgelegt von
Philipp Maximilian Schicho
von Graz / Österreich

Leiter der Arbeit:
Prof. Dr. Mikko Laine
Albert Einstein Center for Fundamental Physics
Institute for Theoretical Physics, Universität Bern

Multi-loop investigations of strong interactions at high temperatures

Inauguraldissertation
der Philosophisch-naturwissenschaftlichen Fakultät
der Universität Bern

vorgelegt von
Philipp Maximilian Schicho
von Graz / Österreich

Leiter der Arbeit:
Prof. Dr. Mikko Laine
Albert Einstein Center for Fundamental Physics
Institute for Theoretical Physics, Universität Bern

Von der Philosophisch-naturwissenschaftlichen Fakultät angenommen.

Bern, 23/04/2020 Der Dekan:

Prof. Dr. Zoltan Balogh

Abstract

Matter alters its properties remarkably when confronted with extreme conditions such as temperatures as high as in the early universe. The emergence of the Quark-Gluon Plasma and restoration of electroweak symmetry through phase transitions are but the most prominent phenomena to invigorate studies of gauge theories at finite temperatures. If the temperature is sufficiently high, static observables are effectively described in a reduced dimension by a framework known as Dimensional Reduction.

The computer algebraic multi-loop treatment of perturbation theory for finite-temperature theories is at the core of this thesis. It adopts sophisticated tools from zero temperature to decimate typically vast numbers of Feynman integrals with the objective to automate the dimensional reduction. To accomplish this, integration-by-parts identities pertinent to both massless and massive loops at finite temperature are illuminated. Additionally, an inclusion of higher-dimensional operators in these theories is first motivated and then generalised.

The developed tools are applied to review the advancements of [1] in chapter 4 and [2] in chapter 5. There, we analyse the dimensionally reduced theories of high-temperature QCD, namely electrostatic and magnetostatic QCD.

We inspect three-loop contributions stemming from non-static modes to the magnetostatic coupling in dimensionally reduced hot Yang-Mills theory [1]. By including dimension-six operators the result is found to be infrared finite and influenced by all scales in the QCD hierarchy. Incorporating also electrostatic effects indicates a non-perturbative ultrasoft gauge coupling at $\mathcal{O}(\alpha_{\mathrm{s}}^{3/2})$.

Based on its relevance in cosmology, we determine another low-energy coefficient in electrostatic QCD, the Debye mass. By including effects from massive fermions up to two loops [2], energy ranges of (1 GeV–10 TeV) are scanned to show the smooth crossing of quark mass thresholds.

Acknowledgements

I wish to express my gratitude to Mikko Laine for his thorough discussions, guidance and of course patience throughout the various stages of collaboration during the evolution of this work. I thank Gert Aarts for agreeing to co-referee this thesis and being the external expert on the defence committee. I specially thank York Schröder for hosting me during my visit in Chile, our fruitful collaboration, and the many `FORM` language lessons. Additionally, I want to emphasise former and current members of the Thermal Field Theory and Particle Cosmology group at the University of Bern namely Greg, Tuomas, Simone, and Germano for their dedicated conversations, programming advice, and inspirations during the preparation of my dissertation.

However, none of this could have worked out without my friends Andrew, Conny, Irina, Markus, Tanja, Vivi, and Rose that constantly succeeded to put everything back into perspective. Finally, I wish to thank my parents for their unconditional support that opened the door for many opportunities during my studies – I could not appreciate it more.

Contents

Notation

Throughout this thesis natural units are used if not stated otherwise: $c = k_{\mathrm{B}} = \hbar = 1$. To regulate divergences in the occurring theories, a mass-independent regularisation scheme, the modified Minimal Subtraction scheme ($\overline{\mathrm{MS}}$), is employed. It rescales the arbitrary renormalisation scale parameter μ

$$\bar{\mu}^2 = 4\pi e^{-\gamma_{\mathrm{E}}}\,\mu^2\,, \tag{0.1}$$

in dimensional regularisation where γ_{E} is the Euler-Mascheroni constant. Therein, momentum integrations are regulated by defining the spatial measure in $d = 3 - 2\epsilon$ dimensions, whereas the spacetime dimensionality is denoted by $D = d + 1 = 4 - 2\epsilon$. While Greek indices assume values in $\mu, \nu \in \{0, \ldots, d\}$, Latin indices take up $i, j \in \{1, \ldots, d\}$. The integration in Euclidean position space is performed along imaginary time τ and spatial coordinates x_i with four-vectors $X = (\tau, x_i)$:

$$\int_X \equiv \int_0^\beta \mathrm{d}\tau \int_{\mathbf{x}} = \frac{1}{T}\int_{\mathbf{x}}\,, \quad \int_{\mathbf{x}} \equiv \int \mathrm{d}^d\mathbf{x}\,, \quad \beta \equiv \frac{1}{T}\,. \tag{0.2}$$

Sum-integrals with Euclidean momenta $K = (k_n, k_i)$ are comprised of

$$\sum\!\!\!\!\!\!\int_K \equiv T\sum_{\omega_n}\int_{\mathbf{k}}\,, \quad \int_{\mathbf{k}} \equiv \int \frac{\mathrm{d}^d\mathbf{k}}{(2\pi)^d}\,, \tag{0.3}$$

implicitly defined in the Matsubara four-momenta $\omega_n = (2n+\sigma)\pi T$ with $\sigma = 0(1)$ and $n \in \mathbb{Z}$ for bosons(fermions), respectively. In contrast energies are denoted as

$$\omega_i^k = \sqrt{k^2 + m_i^2}\,. \tag{0.4}$$

Chapter 1

Motivation

Nature spreads over a broad range of scales of which some are well separated and a unified theoretical description of physics across the whole spectrum appears on the outset to be an untenable task. In fact, some theories that work well at large distances will fail to give precise predictions for short distances. It is then rather natural to exploit the hierarchy of a multi-scale system to construct effective theories that focus on the degrees of freedom relevant to the problem at hand. This is the concept of Effective Field Theories (EFT).

One such successful EFT is the Standard Model (SM). Underpinned by precision experiments at the LHC, it proves a viable contender to study the physics on the subatomic level on the basis of its theoretical building blocks

$$\mathcal{G}_{\mathrm{SM}} = \mathrm{SU}(3)_{\mathrm{QCD}} \times \mathrm{SU}(2)_{\mathrm{weak}} \times \mathrm{U}(1)_{\mathrm{Y}} \ . \tag{1.1}$$

These consist of quantum electrodynamics and Electroweak (EW) theory which undergoes spontaneous symmetry breaking at the scale of the vacuum expectation value of the Higgs field at $v = 246$ GeV [3]. The other sector is Quantum Chromodynamics (QCD), the theory of quarks and gluons, which describes interactions mediated by the strong force.

The framework of Thermal Field Theory (TFT) studies these and other field theories at finite temperature. Together finite chemical potential and temperature span the equilibrium phase diagram of the theory. Scanning its phase structure over a vast range of scales should reproduce the thermal history of the universe and how it cooled down starting from a very hot and dense state. One yet puzzling question is how accurately the Standard Model describes this evolution. Testing its phase transition and description of nature under extreme conditions allows to uncover theoretical shortcomings such as its failure to explain the net baryonic asymmetry [4] or produce detectable gravitational wave signatures [5, 6, 7]. Whereas these are phenomena related to electroweak theory, we focus on the QCD sector $\mathcal{G}_{\mathrm{QCD}}$ of the SM gauge group at small chemical potential.

In this regime the finite-temperature picture of QCD comprises two phases. At low temperatures confinement [8] constitutes a hadronic phase in which particles are colour-neutral built from quarks and gluons. In this region the strong coupling is truly strong and adequately described with non-perturbative methods. By raising temperature and density, different confinement arrangements begin increasingly to overlap and their confinement becomes ambiguous – the quark-gluon plasma (QGP) emerges. Thus, at high temperatures asymptotic freedom [9, 10] asserts a small (or not so strong) coupling that allows to employ perturbation theory [11]. The transition between the two phases is a smooth crossover for physical quark masses. Consequently its critical temperature T_{c} is ambiguous and depends on the observables that are considered. The current definition finds it at $T_{\mathrm{c}} \simeq 155$ MeV [12, 13, 14, 15].

However, Linde's infamous infrared (IR) problem [16] corrupts perturbative calculations below a certain temperature scale in a TFT. This relates to the fact that at finite temperature

certain modes with large correlation lengths, so-called *soft* modes, become non-perturbative. In turn, their presence compromises perturbation theory in the IR regime of the theory. For a non-Abelian gauge theory like QCD, this happens close to the confinement-deconfinement phase transition crossover temperature T_c. Indeed, it directly roots in the colour-magnetic fields, the spatial components of the gauge field, that directly affect the IR dynamics. Since their perturbative treatment fails, a possible cure of this impasse is a resummation of loops generated from the soft modes by summing IR divergent terms to all orders. A systematisation in this approach is less straightforward when advancing to higher-loop orders which is already conceivable at two-loop level.

High-temperature Dimensional Reduction (DR) provides an automatic all-order resummation which systematically by-passes the IR problem. Since the perturbative integration over ultraviolet (UV) modes is infrared safe it ensures that the weak-coupling expansion in the UV is under control. The remaining effective theory is one of light *static*, time-independent, modes in a reduced dimension. Owing to a clean dissection of scales within a TFT, temperature normally sets the shortest scale besides degrees of freedom with much larger correlation lengths. To them spacetime effectively appears to be 3-dimensional which entails all the low energy physics of the full theory for non-dynamical observables. This allows to conflate the best features of both worlds, the perturbative and non-perturbative ones by using them at energy ranges where they apply best. By construction, the matching of the EFT is purely perturbative for which the effective coupling is required to be small. Once the EFT is constructed, further UV scales can be integrated out iteratively until the new effective theory becomes non-perturbative. The IR dynamics of the modes related to this sector can then be studied with lattice methods.

This thesis focuses on strongly coupled interactions at high temperatures addressing an automated pipeline for performing dimensional reduction. We motivate the necessity of an augmented basis of higher-dimensional operators inside electrostatic QCD (EQCD) and magnetostatic QCD (MQCD), the dimensionally reduced effective theories of QCD. Thereby, we compute two matching coefficients of EQCD, namely the 3-loop effective gauge coupling g_{E} and the 2-loop Debye mass m_{E} including quark mass effects in the latter. An algorithmic automation for potentially interesting scalar extensions of the SM is envisaged.

The machinery of Feynman rules expresses a QFT as a diagrammatic theory and systemises the computation of amplitudes. Any succession of this diagrammatic computation ties together three stages: combinatorics, algebra, and analyticity. The combinatorial part encompasses the generation of Feynman diagrams based on the field content of the considered theory. As computations typically encounter a few thousands of diagrams, an automated approach becomes indispensable already at this step.

At zero temperature a plethora of sophisticated automated methods exists for perturbative loop computations in contrast to finite-T algorithms. The demand for unprecedented precision in calculations for hadron collider physics entices more activity in the development of new techniques. These pushed the limit to 5-loop computations tackling the QCD β-function [17, 18, 19] and fermion anomalous dimension [20, 21].

Finite-temperature enhances the complexity of the occurring integrals by their sum-integral analytical structure of the propagators. While the rest of the Feynman rules remains unaltered, most algebraic methods can be recycled. A common strategy to decimate the number of integrals is to find algebraic relations among them based on the symmetries of the integrand and measure. Especially the reduction by integration-by-parts (IBP) bears great potential in this simplification and was established for finite-T in [22]. The reduction concludes once a finite set of irreducible master diagrams [23] is assembled. Their total number depends on how many scales appear in the integrals.

The analytic evaluation of those leftover master sum-integrals poses a core difficulty because only a specific class of diagrams allows to be treated generically. Merely few systematic

methods are available because different observables usually bear different mass dimensions. Now every computation of a new physical problem requires to evaluate a whole set of new sum-integrals of the corresponding mass dimension. At orders beyond 2-loops these known techniques only work on a few of the appearing integrals while some are still completely unknown – even for fully massless bosonic cases.

The first chapter introduces prerequisites how to perturbatively study theories at finite temperature. Hence, sec. 2.1 addresses equilibrium perturbative Thermal Field Theory. One prominent subtlety, the IR divergence problem, is addressed alongside the implementation of renormalisation for the UV in sec. 2.2 and resummation for IR divergences in sec. 2.3. To tackle the latter, in sec. 2.4 scale separation at high temperatures is used to introduce Dimensional Reduction as a means to construct a suitable EFT that provides an alternative for resummation to evade the IR problem.

Beyond the introduction, the thesis scopes the following topics. Chapter 3 outlines a state-of-the-art automation of DR for a general thermal field theory and consecutively QCD. We follow a specific diagrammatic example through all the steps of the automation and discuss the algebraic and analytic treatment therein. Based on these algorithmic implementations, chapter 4 studies the cancellation of IR divergences in the dimensionally reduced EFT of hot Yang-Mills wherein the inclusion of higher-dimensional operators is motivated and becomes inevitable. In chapter 5, we investigate cosmologically relevant temperature ranges of a Debye mass within QCD and focus on mass effects stemming from fermions. Additionally, appendix A provides the reader with thermal and vacuum integrals while appendix B lists the employed integration-by-parts reductions and identities.

Chapter 2

Introduction

The two main formalisms developed for the treatment of quantum field theories at finite temperature are the real-time (Schwinger-Keldysh) formalism [24, 25] appropriate for out-of-equilibrium systems and the imaginary-time (Matsubara) formalism [26] adequate for theories in thermal equilibrium. Computations of thermodynamic equilibrium properties provide an initial point for non-equilibrium evaluations. Setting the stage in the following chapter, we concentrate on the latter formalism pertinent to the research publications described in this thesis.

A pedagogical account on both formalisms is collected in [27, 28, 29].

2.1 Perturbative Thermal Field Theory

Throughout most epochs during its evolution the universe is thermalised. This assumption of equilibrium is justified because time scales of external observations are large enough such that time scales on which dynamical, statistical processes occur are suppressed in comparison. As a result, distribution functions of bosons and fermions are exponentially close to their equilibrium values.

Relativistic quantum field theory is a theory describing multi-particle creation and annihilation. The most fitting description of the statistical behaviour of such a theory leaves the particle number unrestricted but imposes conditions on the conservation of energy and commuting number operator. This is captured by the grand canonical ensemble. In order to fix the conserved mean values of energy and particle number, Lagrange multipliers are installed, namely temperature $\beta = 1/T$ through a heat bath and chemical potential μ_i with a particle reservoir.

At equilibrium the density matrix $\rho(\beta) = e^{-\beta\mathcal{H}}$ encompasses all the information of the system with the Hamiltonian $\mathcal{H} = H - \mathcal{N}\mu$ and the charge density $\mathcal{N} = \int_{\mathbf{x}} \psi^\dagger\psi$. For the remainder of this thesis we are interested in the situation where $\mu = 0$ equivalent to inspecting the canonical ensemble. The central object to access thermodynamic quantities is the partition function

$$\mathcal{Z}(\beta) = \mathrm{Tr}\,\rho(\beta)\ , \tag{2.1}$$

and derivatives thereof. For an observable $\mathcal{O}$ the expectation value is defined

$$\langle\mathcal{O}\rangle_\beta = \frac{1}{\mathcal{Z}(\beta)}\mathrm{Tr}\,\rho(\beta)\mathcal{O}\ . \tag{2.2}$$

The cyclicity of the trace gives rise to the KMS (Kubo-Martin-Schwinger) [30, 31] relation for the 2-point function

$$\langle\mathcal{O}_1(t)\mathcal{O}_2(t')\rangle_\beta = \langle\mathcal{O}_2(t')\mathcal{O}_1(t+i\beta)\rangle_\beta\ . \tag{2.3}$$

The key to the Imaginary Time Formalism (ITF) is to interpret the Boltzmann weight $e^{-\beta\mathcal{H}}$ as a time evolution operator $\mathcal{U}(t) = e^{-i\mathcal{H}t}$. Since β is real the system evolves along the negative imaginary time axis [32] by a time period of $\Delta t = -i\beta$.

Time evolution has a well defined representation within the path integral formalism. By extending it to said imaginary time evolution it reproduces eq. (2.1) with the generating functional

$$\mathcal{Z} = C \int_{\text{b.c.}} \mathcal{D}\Phi \, \exp\left[i \int_{t_\text{i}}^{t_\text{i} - i\beta} \mathrm{d}t \int_{\mathbf{x}} \mathcal{L}_\text{M}(\Phi, \partial_\mu \Phi) \right] , \tag{2.4}$$

where Φ collects a set of different fields and C is a (infinite) normalizing factor. The integration spans over the interval $[t_\text{i}, t_\text{f}]$ between initial time t_i and final time $t_\text{f} = t_\text{i} - i\beta$ equal to the initial time with imaginary shift.

The analytic continuation of time to complex values $t \in \mathbb{C}$ adds additional freedom in the choice of the integration path $\mathcal{C}$ in the complex plane. The imaginary part of this path must be monotonically decreasing in order for the propagators to be analytic in time. The simplest curve compatible with this and further restrictions [27] parameterises time vertical in the complex plane $t(\tau) = t_\text{i} - i\tau$

$$\mathcal{Z} = C \int_{\text{b.c.}} \mathcal{D}\Phi \, \exp\left[- \int_0^\beta \mathrm{d}\tau \int_{\mathbf{x}} \mathcal{L}_\text{E}(\Phi, \partial_\mu \Phi) \right] , \tag{2.5}$$

with real-valued $\tau \in [0, \beta]$ and independent of the initial time $t_\text{i} = 0$ which drops out after a linear variable transformation provided $\mathcal{H}$ is t-independent. This imaginary-time path integral is the ITF. In this implementation a finite-temperature D-dimensional quantum field theory is equivalent to a $D = d + 1$ theory with d spatial dimensions and one compact time dimension. Through the previous analytic continuation $t(\tau) = -i\tau$ the Minkowskian Lagrangian converts into the Euclidean Lagrangian $\mathcal{L}_\text{E} = -\mathcal{L}_\text{M}(t \to t(\tau))$ and on the finite-τ interval bosonic (fermionic) fields $\phi(\psi)$ assume (anti-)periodic boundary conditions (b.c.)

$$\phi(0, x) = \phi(\beta, x) \, , \tag{2.6}$$
$$\psi(0, x) = -\psi(\beta, x) \, . \tag{2.7}$$

These arise as a consequence of the trace in eq. (2.2) and the Grassmann nature of the fermionic fields. In the description of a field theory in the ITF, a temporal discrete Fourier sum decomposes the particle fields into Matsubara [26] modes

$$\phi(\tau, x) = T \sum_{n=-\infty}^{\infty} \phi_n(x) e^{i\omega_n \tau} \, , \quad \omega_n = \begin{cases} \omega_n^\text{B} = 2n\pi T & \text{(bosons)} \\ \omega_n^\text{F} = (2n+1)\pi T & \text{(fermions)} \end{cases} , \quad n \in \mathbb{Z} \, . \tag{2.8}$$

The so-called Matsubara frequencies ω_n^B, ω_n^F arise through the (anti-)periodicity conditions of the fields in a finite time interval which dictates discrete energy levels k_0. Alternatively they can also be established by the (anti-)periodicity of the corresponding Fourier transformed propagators together with the KMS condition eq. (2.3) and the definition of the time ordered product.

The topology of spacetime corresponds to that of $\mathbb{R}^3 \times S^1_\beta$ similar to that of a Kaluza-Klein theory. The sums of Green's functions that are encountered as a consequence of eq. (2.8) can also be understood as a sum over images tagged with the corresponding winding number n in ω_n and for every full circle in the compactified time direction the price of $e^{-\beta\omega_n}$ is paid.

Indeed, the Matsubara imaginary time formalism is ideal for studying equilibrium systems. Setting the integration limits in eq. (2.5) trades the time variable for the temperature $t \to \beta$ of the heat bath. This swap discards most the dynamics of the temporal direction but gains a theoretical description of the static behaviour of system at finite-T.

The advantage of the ITF is that the zero-temperature Feynman diagram machinery of perturbative computations extends straightforwardly. To reason this, we summarise the mappings from the vacuum theory

$$\begin{aligned} \int_K &\mapsto \not{\sum}_K \,, \\ G_{\mathrm{M}}(K_1,\dots,K_n) &\mapsto G_{\mathrm{E}}(k_1,\dots,k_n)\,, \\ (2\pi)^{d+1}\delta^{(d+1)}(K) &\mapsto \delta(K)\,, \end{aligned} \tag{2.9}$$

by introducing the notation $\delta(K) \equiv \beta\delta_{k_n,0}(2\pi)^d\delta^{(d)}(\mathbf{k})$ and $\int_K \equiv \int \frac{\mathrm{d}^{d+1}k}{(2\pi)^{d+1}}$. The first line indicates that Euclidean Green's functions G_{E} depend dynamically only on the d-dimensional momenta (k). The Matsubara frequencies act like mass parameters, mediate the temperature, and make themselves felt only inside the propagators. Where the free frequency-momentum space propagator amounts to

$$\Delta(\omega_n,k) = \frac{1}{\omega_n^2+k^2+m^2} = \frac{1}{\omega_n^2+\omega_k^2}\,, \tag{2.10}$$

with energies $\omega^k \equiv \omega_k$ in eq. (0.4). Concretely, Matsubara frequencies appear on internal and external lines of the Feynman diagrams. Taking functional derivatives of the path integral $\frac{\delta\mathcal{Z}[J]}{\delta J}$ in eq. (2.5) with respect to some external source J poses no structural difference such that vacuum vertices remain unmodified. At the vertex, momentum and mode conservation is deployed through the changed δ-function. Lastly, vacuum loop integration is replaced by sum-integrals.

For very high temperatures the non-static non-zero modes $\phi_{n\neq 0}$ become infinitely heavy. Intuitively infinitely heavy particles decouple at zero temperature [33]. However, at finite temperature this decoupling is incomplete and instead non-static modes generate a tower of effective vertices that affect the static modes which become non-perturbative. In general these corrections cannot be ignored.

First, we discuss the short and large distance properties of finite-temperature theories.

2.2 Regularisation of ultraviolet divergences

The processing of the short distance (large-k) or ultraviolet (UV) behaviour of a finite-temperature theory is already covered at zero temperature. In fact, the theory remains unaltered in the UV because modes with wavelengths shorter than the finite temporal extent $|\mathbf{x}|, |x_0| \ll \beta$ fail to perceive the (anti-)periodicity of time. To show this explicitly, the fermionic and bosonic imaginary-time propagators in mixed $(\tau,\mathbf{k})$ "Saclay" representation are employed by a discrete Fourier transformation [34]:

$$G(\tau) = T\sum_{\omega_n} e^{i\omega_n\tau}\Delta(\omega_n,k)\,, \tag{2.11}$$

$$G(\tau) = T\sum_{\omega_n^{\mathrm{B}}} \frac{e^{i\omega_n^{\mathrm{B}}\tau}}{[(\omega_n^{\mathrm{B}})^2+\omega^2]} = \frac{1}{2\omega}n_{\mathrm{B}}(\omega)\left[e^{(\beta-\tau)\omega}+e^{\tau\omega}\right]\,, \tag{2.12}$$

$$\tilde{G}(\tau) = T\sum_{\omega_n^{\mathrm{F}}} \frac{e^{i\omega_n^{\mathrm{F}}\tau}}{[(\omega_n^{\mathrm{F}})^2+\omega^2]} = \frac{1}{2\omega}\left[n_{\mathrm{F}}(\omega+\mu)e^{(\beta-\tau)\omega+\beta\mu} - n_{\mathrm{F}}(\omega-\mu)e^{\tau\omega}\right]\,. \tag{2.13}$$

The above identities are established by directly evaluating the sums as a contour integral in the complex plane using Cauchy's residue theorem with the single-particle distribution functions

$$n_{\mathrm{B/F}}(\omega) = \frac{1}{e^{\beta\omega}\mp 1}\,, \tag{2.14}$$

for Bose-Einstein (n_{B}) and Fermi-Dirac (n_{F}) distributions.

The frequency sums can be converted into a sum over vacuum propagators ($T = 0$) with a temporal shift $\sim n\beta$ [27] such that in Euclidean position space

$$G(\tau, \mathbf{x}; T) = \sum_{n=-\infty}^{\infty} G(\tau + n\beta, \mathbf{x}; T = 0) \, . \tag{2.15}$$

The UV sensitivity of the theory is related to singular points in Euclidean spacetime $X^2 = 0$ since the Euclidean vacuum propagator develops a pole $G(X; T = 0) \sim 1/|X|^{d-1} = |X|^{-2}$ in $d = 3$. Representing the thermal propagators by eq. (2.15) shifts $X^2 = (\tau + n\beta)^2 + \mathbf{x}^2$ which only becomes singular for the temperature-independent vacuum contribution ($n = 0$). Consequently, a direct evaluation of Matsubara sums splits sum-integrals Z into a vacuum part ($T = 0$) and analytic temperature-dependent pieces

$$Z = Z^{\mathrm{vac}} + Z^{T} \, . \tag{2.16}$$

In general the temperature-dependent terms mix with zero-T ones and renormalisation is not at all obvious. However, one can show that the above considerations still hold [35]. Therefore, the zero-temperature renormalisation machinery applies to render the theory finite in the UV.

The root source of these short-distance divergences are the theoretically *bare* unphysical parameters inside the Lagrangian [36]. As they are non-observable they appear in intermediate stages of calculations but can be systematically removed by undergoing the stages of (i) regularisation and (ii) renormalisation.

Regularisation controls arising divergences at large momenta in a mathematically transparent manner. Multiple viable choices to employ such a regulator exist such as a momentum cut-off or Pauli-Villars fictitious mass term [37]. Commonly for the resulting quantities to be physical they must be independent of their regulator. A practical candidate is dimensional regularisation proposed by t'Hooft and Veltman [38, 39]; for a review of the topic see [35, 40]. It introduces a regulator by analytically continuing the spacetime dimension to $d \in \mathbb{C}$. One choice is to shift $d \to d - 2\epsilon$ with a small deviation $\epsilon > 0$ from the actual dimension and UV divergences appear as $1/\epsilon$-poles.

The above shift affects the dimensions of the couplings of the theory. To retain the correct total integral dimension, an arbitrary but finite renormalisation scale μ is introduced. As an example, a bare coupling is dimensionful in general d which is of $[g_{\mathrm{B}}] = \mu^{\Delta}$ with canonical dimension $\Delta = \frac{4-d}{2}$ and renders combinations $\mu^{d-4} g_{\mathrm{B}}^2 = \mu^{-2\epsilon} g_{\mathrm{B}}^2$ dimensionless. This multiplicative dimensional factor is then compensated by the measure of the d-dimensional integral

$$\int_{\mathbf{k}} \equiv \mu^{-2\epsilon} \left[\left(\frac{\bar{\mu}^2 e^{\gamma_{\mathrm{E}}}}{4\pi} \right)^{\epsilon} \int \frac{\mathrm{d}^{d-2\epsilon}\mathbf{k}}{(2\pi)^{d-2\epsilon}} \right] \, , \tag{2.17}$$

wherein the parameter μ was inserted by $1 = \mu^{-2\epsilon}\mu^{2\epsilon}$. Thus, the square bracket in $\mu^{-2\epsilon}[\dots]$ has integer mass dimension. One other central feature of dimensional regularisation is the vanishing of scaleless integrals

$$\mu^{2\epsilon} \int_{\mathbf{k}} \frac{1}{[k^2]^{s_1}} = 0 \, , \tag{2.18}$$

which arises as a consequence of the limit $m \to 0$ in eq. (A.16). For multi-loop computations this proves a decisive simplification as it reduces the number of integrals immensely in most cases.

The second stage to render the theory UV-finite is renormalisation which is essentially a reparameterisation of bare parameters in terms of physical ones using a specific scheme. This absorbs divergences by the prescription of multiplicative renormalisation using the renormalisation constants Z_x that do not depend on dimensional parameters (masses, momenta) [41].

This rescaling recovers the original bare (unrenormalised) theory Lagrangian that features the set $x \in \{x_i\}$ of possible fields $\{\Phi_i\} \subseteq \{x_i\}$ and couplings $\{g_i\} \subseteq \{x_i\}$

$$x_{\mathrm{B}} = \mu^{\Delta_x} Z_x x_{\mathrm{R}} \; . \tag{2.19}$$

Here $\Delta_x(\epsilon)$ is the canonical dimensionality of the bare coupling x_{B}. The subscripts denote bare (B) and renormalised (R) quantities.

By scheme we refer to the specific choice of finite parts inside the renormalisation constants Z_x. The running of a generic coupling $g(\mu)$ in one scheme will then in general be different from the one in another scheme $g(\mu) \neq g'(\mu)$. Subsequently, the scale μ inside the square brackets of eq. (2.17) is rescaled by $\bar{\mu}^2 = 4\pi e^{-\gamma_{\mathrm{E}}} \mu^2$. This is the $\overline{\mathrm{MS}}$ scheme [42] wherein the renormalisation constants Z_x assume the form

$$Z_x = 1 + \delta Z_x = 1 + \sum_{\{x_i\}} \sum_{\ell=1}^{N_k} a_x^\ell \sum_{k=1}^{\ell} \frac{Z_x^{(\ell,k)}}{\epsilon^k} \; , \quad a_i = \frac{g_i^2}{(4\pi)^2} \; , \tag{2.20}$$

where the normalisation for the couplings is chosen as a_i. At N_k-loop order inverse ϵ-powers reach up to degree N_k which are weighted with powers of the couplings respective to the loop level. The general expression to absorb all these divergences is given by the renormalisation counterterms $\delta Z_x(\{x_i\})$ that depend on all couplings. All the $1/\epsilon$-divergent terms ($k > 0$) are determined through the UV behaviour of the theory. Finite terms ($k = 0$) in the expansion of Z_x are in principle allowed but depend on the renormalisation scheme; the $\overline{\mathrm{MS}}$-scheme omits $Z_x^{(l,0)} = 0$ and leaves them untouched.

Although physical quantities should be independent of the chosen renormalisation procedure they are still affected. The reason is that practical expansions merely reach up to fixed and finite order in perturbation theory. The appearance of the scale parameter $\bar{\mu}$ is a remnant of this fact and the Renormalisation Group Equation (RGE) monitors scaling properties of the renormalised quantities with the change of the renormalisation scale.

As a general concept, the anomalous dimension monitors the μ-dependence of the theory in physical parameters such as couplings or masses but also unphysical ones like wave functions. As a flow function of Z_x it is defined by

$$\gamma_x = -\frac{\mathrm{d} \ln Z_x}{\mathrm{d} \ln \mu^2} \; . \tag{2.21}$$

A special case of the definition in eq. (2.21) is the β-function which is but the anomalous dimension of the coupling g_i with different normalisation. It is solely concerned with the running of the couplings $\{g_i\} \subseteq \{x_i\}$ in the theory

$$\frac{\mathrm{d} a_i}{\mathrm{d} \ln \mu^2} = \beta_i(\{a_i\}) \; , \tag{2.22}$$

where $a_i = g_i^2/(4\pi)^2$ is the normalisation established in eq. (2.20) for a generic renormalised coupling $g_i = g_i(\mu^2)$. Qualitatively the β-function distinguishes three different scaling behaviours of a theory depending on its overall sign

- $\beta(g) > 0$, the coupling vanishes at small momenta as $\mu \to 0$, the theory is *infrared free* and confines in the UV.
- $\beta(g) < 0$, the coupling vanishes at large momenta as $\mu \to \infty$ the theory is *asymptotically free* and confines in the IR.
- $\beta(g) = 0$, the theory is scale invariant.

In the ensuing sections the focus lies on the second point and theories that show asymptotic freedom such as QCD.

We observed how to handle UV divergences in finite-temperature theories by recycling the well known counterterms from the vacuum. Next, we discuss ramifications for the infrared when putting a theory at finite temporal extent.

2.3 Resummation of infrared divergences

On the end of the spectrum where distances are large (small-k), the thermal character of the theory introduces new complications compared to zero-T. One issue is the infamous Linde Infrared (IR) problem [16] of thermal gauge theories which is fundamentally related to the bosonic nature of the constituent fields.

Fermionic degrees of freedom are not plagued with IR divergences as observed from their fermionic zero mode ($\psi_{n=0}$) integral with $\omega_0^{\mathrm{F}} = \pm\pi T$

$$\int_k \frac{1}{k^2 + M_0^2} \propto \sqrt{M_0^2}\,, \tag{2.23}$$

where $M_0^2 = m_i^2 + (\pi T)^2$. The limit $m_i \to 0$ faces no risk of IR divergences.

Contrarily, bosons experience an aggravated scenario. Their infrared sensitivity of arising diagrams is inspected starting from the massless bosonic two-loop sum-integral

$$= Z_{210} = Z_2 Z_1 = \sum\!\!\!\!\!\!\int_{K_1} \frac{1}{[K_1^2]^2} \sum\!\!\!\!\!\!\int_{K_2} \frac{1}{[K_2^2]}\,. \tag{2.24}$$

How the massless limit $m = 0$ affects this diagram is seen when evaluating its factorising one-loop components Z_1 and Z_2 which behave differently in the IR. By splitting the sum-integral measure

$$\begin{aligned} \sum\!\!\!\!\!\!\int_K &\equiv T \sum_{k_0=-\infty}^{\infty} \int_{\mathbf{k}} = \sum_{k_0 \neq 0} \int_{\mathbf{k}} + \sum\!\!\!\!\!\!\int_K \delta_{k_0} \\ &= \sum\!\!\!\!\!\!\int_K{}' + T \int_{\mathbf{k}}\,, \end{aligned} \tag{2.25}$$

we recover two parts, one for the non-zero modes and one for the zero mode. Conventionally $\sum\!\!\!\!\!\!\int'_K$ denotes a sum-integral over K, with the prime indicating that the Matsubara zero mode is omitted in eq. (0.3). Therefore, the most general 1-loop bosonic tadpole sum-integral Z_1 is computed which is split via eq. (2.25). While for the zero-mode a direct computation of the integral in dimensional regularisation is feasible, the non-zero ($n \neq 0$) contributions can be expanded in a series of small masses. For $\omega_n \neq 0$ this is allowed as integrands in the expansion are of

$$\int_k \frac{(m^2)^n}{[\omega_n^2 + k^2]^{n+1}}\,. \tag{2.26}$$

The bosonic and fermionic results are listed in eqs. (A.39) and (A.40).

Naively the zero mode of $Z_1^{(n=0)}$ is UV divergent while $Z_2^{(n=0)}$ is IR divergent. Due to the lack of a scale in the denominator both should vanish in dimensional regularisation. The strategy is to regulate both kinds of divergences, the IR by adding a mass regulator m to their zero mode ($n = 0$) propagator and the UV by using eq. (A.15) with dimensional regularisation $d = 3 - 2\epsilon$. Their radial contributions

$$Z_1^{(n=0)} = \int_{\mathbf{k}} \frac{1}{[k^2 + m^2]^1} \sim \int \mathrm{d}k\, k^{d-1} \frac{1}{[k^2 + m^2]^1} \sim m \overset{m\to 0}{\to} 0\,, \tag{2.27}$$

$$Z_2^{(n=0)} = \int_{\mathbf{k}} \frac{1}{[k^2 + m^2]^2} \sim \int \mathrm{d}k\, k^{d-1} \frac{1}{[k^2 + m^2]^2} \sim \frac{1}{m} \overset{m\to 0}{\to} \infty\,. \tag{2.28}$$

are UV finite but only the first one is also IR finite. In fact, an infinite number of integrals is plagued with IR divergences with increasing severity with the number of propagator powers.

This kind of divergence at $m_i = 0$ arises because bosons develop a dynamical mass at finite temperature

$$m_i(T) = g^n T + m_i \,, \tag{2.29}$$

where m_i is a zero-temperature mass. A perturbative treatment of bosonic propagators that disregards this mass inevitably leads to IR divergences.

Resummation [43, 44] provides a means to cure the theory of these IR divergences by shifting the pole mass. The integral in eq. (2.24) belongs to a general set of diagrams that needs to be summed to all orders. These arising $(N+1)$-loop "Daisy" ring diagrams factorise N-hard one-loops and one soft N-propagator loop

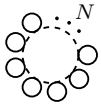

$$\begin{aligned} &\propto \; g^{2N}\left[\int_{k_1} \frac{T}{\left[k_1^2+m^2\right]^N}\right]\left[\sum\!\!\!\!\!\!\int_{K_2}{}' \frac{1}{K_2^2}\right]^N = g^{2N}\left[I_{N;m}\right]\left[Z_1\right]^N \\ &\propto \; g^{2N}\left[m^{3-2N}T\right]\left[\frac{T^2}{12}\right]^N \propto m^3 T\left[\frac{gT}{m(T)}\right]^{2N} \,, \end{aligned} \tag{2.30}$$

employing $m(T)$ inside the zero-T vacuum integrals $I_{N;m}$ from eq. (A.15). The soft thermal mass is kept only on the propagators while safely omitted in the hard loops. An analogous factorisation is absent at higher loop levels. Therefore, one is confronted with a case-by-case study rather than a systemisable problem. Alternatively, resummation can be achieved along a reorganisation of the Lagrangian by adding an effective mass term to the free theory Lagrangian while equally subtracting the same term in the interacting Lagrangian [45, 46].

While the weak-coupling expansion could be justified in the underlying theory it might be compromised for degrees of freedom sensitive to IR scales. We saw in eq. (2.30) that the perturbative expansion breaks down for $m(T) \leq gT$ starting from 3-loop order ($N = 2$). However, resummation remedies the IR divergent behaviour of the Daisy diagrams. A similar treatment is not feasible for diagrams that contribute at the order

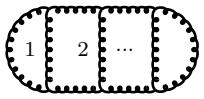

$$\propto \; g^6 T^4 \left[\frac{g^2 T}{m(T)}\right]^{N-3} \,, \tag{2.31}$$

with Matsubara zero modes on every line. While diagrams up to $N < 3$ are IR regular, modes with thermal masses of $m(T) \leq g^2 T$ contribute to $\mathcal{O}(g^6)$ at all loops $N > 3$. Consequently at finite order infinitely many diagrams need to be considered regardless the size of g. This invalidates perturbation theory and exposes the non-perturbative nature for said modes.

To be more concrete, we inspect the effective expansion parameter for light particles ($m_i \to 0$) at asymptotically high-T and weak-coupling $g \ll 1$

$$\epsilon_{\mathrm{B/F}} = g^2\, n_{\mathrm{B/F}}(\omega_p) = \frac{g^2}{e^{\frac{\omega_p}{T}} \mp 1} \overset{\omega_p \ll T}{\sim} \frac{g^2 T}{\omega_p}\left(\frac{1 \pm 1}{2} \mp \frac{\omega_p}{2T}\right) \,, \tag{2.32}$$

where $|p|$ is a typical momentum of the heat bath featuring in the energies $\omega_p = \sqrt{p^2 + m^2}$. The Bose-Einstein or Fermi-Dirac factors are a direct result of the explicit summation of the Matsubara frequencies inside propagators of the Feynman rules. Reflecting the constant interactions within the plasma this affirms that the weak-coupling expansion of the full theory is invalidated once values $\omega_p \geq m(T) \sim g^2 T$ are assumed for bosons; fermions remain perturbative. Then the respective expansion parameter $\epsilon_{\mathrm{B}} \sim g^2 T/\omega_p$ is of order unity regardless if temperatures are high. Thus, bosonic degrees of freedom with light thermal masses $\mathcal{O}(g^2 T)$ become non-perturbative which is the aforementioned Linde IR problem. As it relates directly to the Matsubara zero-mode, a physical interpretation is that of a massless particle in a reduced dimension. As seen in the d-dimensional vacuum tadpole integral $I_{N;m} \sim m^{d-2N}$ in eq. (A.15), a reduced dimension causes an increased IR sensitivity.

The following section aims to discriminate those degrees of freedom that are supposed to be treated non-perturbatively. Effective theories equip us with a framework to treat all IR-safe modes perturbatively because integrating out heavy degrees of freedom is a UV process and therefore IR-safe.

2.4 Effective theories at high temperatures

The idea behind Effective Theories (EFT) states that length scales much shorter than the actual physical problem are negligible for its description. An immediate example is the separation of scales visible by reading this thesis. Hierarchically grouped into chapters, paragraphs, and single words, the effect of omitting or misspelling certain words is next to irrelevant to comprehend the text as a whole. Intuitively we are even all experts of EFTs when throwing of a snowball. Neither do we have to probe the sub-atomic structure of the constituent snowflakes nor consider quantum gravity to be successful. It suffices entirely to operate on the level of Newtonian mechanics paired with a certain amount of aim.

In quantum field theories this principle is known as *decoupling*. Let us assume the fundamental theory consists of light fields (ϕ_l, m) and heavy fields (ϕ_h, M) with hierarchically ordered respective masses $m \ll M$. By integrating out the heavy degrees of freedom in the partition function eq. (2.5), an effective action for the light fields

$$S[\phi_l, \phi_h] \to S_{\text{eff}}[\phi_l] \,, \tag{2.33}$$

is constructed. An actual path integration over heavy fields gives rise to highly non-local operators [35] which, when perceived at length scales at which the effective theory is valid, will look local again. Since their treatment starting from the full theory causes many subtleties, a more economical and infrared-safe approach is the *matching* of Green's functions, interchangeably referred to as "integrating over" (although technically different).

The matching encodes the physics of the ultraviolet scales within the parameters of the EFT which is demanded to respect the symmetries of the fundamental theory. A viable form to write down a local effective action of the light fields $S_{\text{eff}}[\phi_l]$ is by means of higher-dimensional operators $\mathcal{O}_n$. With $n > 4$ it is of the form

$$S_{\text{eff}}[\phi_l] = \int_{\mathbf{x}} \left\{ \mathcal{L}_{\text{eff}}[\phi_l] + \sum_{n \geq 5} \mathcal{O}_n \left(\frac{p}{M} \right)^n \right\} , \tag{2.34}$$

where $\mathcal{L}_{\text{eff}}[\phi_l]$ is a renormalisable low energy Lagrangian with parameters dependent on the high scale theory and $\mathcal{O}_n$ are suppressed by the heavy mass M.

In the limit of asymptotically high masses ($M \to \infty$) the error made by neglecting these additional terms is diminished both in the action and the Green's functions. Therefore, inside an EFT at zero temperature infinitely heavy fields decouple from the theory which is known as the Appelquist-Carazzone decoupling theorem [33]. The next section argues why a similar intuition fails at finite temperature.

2.4.1 High-temperature Dimensional Reduction

We recall that the fields which reside in $(d+1)$-dimensions at finite temperature constitute a d-dimensional Euclidean theory at zero temperature with an infinite number of fields. Each of these modes corresponds to a propagator of the form $\Delta(\omega_n, p) = [\mathbf{p}^2 + M_n^2]^{-1}$ with masses $M_n^2 = \omega_n^2 + m_i^2$ and m_i are potential zero-temperature mass scales in the fundamental theory. Those IR modes with wavelengths much larger than the finite temporal extent $|\mathbf{x}|, |x_0| \gg \beta$ or vice versa $M_n \ll T$ cannot resolve the time coordinate. For them space appears to be effectively d-dimensional.

Possible scales $|p| \sim g^n T$ in the expansion eq. (2.32) induce a rigorous momentum scale hierarchy which is parameterised by powers of the coupling g. Typically the field modes of a TFT and the effective expansion parameter ϵ_{B} are discriminated along the following theoretical organising principle.

- The *hard* scale $|p| \sim g^0 T \sim \pi T$ or fully perturbative scale $\epsilon_{\mathrm{B}} \sim \mathcal{O}(g^2)$. Characteristic for individual particles in a thermal bath, these modes carry momenta or masses of the hard scale, are weakly coupled and influenced by the heat bath only at next-to-leading order. The corresponding modes are the non-static ($n \neq 0$) Matsubara modes of both fermions and bosons. Lacking a Matsubara zero mode, fermion fields are included altogether at this scale. Being only temperature-dependent, $g^0 T$ is also the highest scale in possible constructed EFTs and sets the upper limit of which scales these theories can resolve.

- The *soft* scale $|p| \sim gT$ or barely perturbative scale $\epsilon_{\mathrm{B}} \sim \mathcal{O}(g)$. Associated with collective excitations and interactions of the particles with the thermal bath, the related modes develop the aforementioned dynamical mass scales $m_i(T)$. At this order, these are related to the static degrees of freedom ($n = 0$) such that static temporal (colour-electric) modes of non-Abelian fields develop a Debye mass $m_{\mathrm{D}} \sim m_i(T)$.

- The *ultrasoft* scale $|p| \sim g^2 T/\pi$ or non-perturbative scale $\epsilon_{\mathrm{B}} \sim \mathcal{O}(1)$. Static spatial (colour-magnetic) modes of non-Abelian fields are strongly coupled amongst each other and also develop a thermal mass $m'_{\mathrm{D}} \sim m_i(T)$. The latter is, however, purely non-perturbative.

Because of this confining, non-perturbative, structure of the ultrasoft sector, additional smaller momentum scales are forbidden and cannot be generated dynamically. Note that, massive bosonic fields may assume all three scales depending on their zero-temperature mass m_i since all thermally generated masses will be either of the same or of lower order. Nothing forbids those scalar masses to be of the same order as the non-zero Matsubara modes $m_i \sim \pi T$, in which case those fields should also be integrated out together with the hard modes [47, 48].

If the coupling g in the fundamental theory is sufficiently small, the scales are split hierarchically $g^2 T/\pi \ll gT \ll \pi T$. Exploiting the above classification of the fields, an EFT is constructed for the light static degrees of freedom at the soft and ultrasoft scale. These modes perceive spacetime only in a reduced d-dimensional setting – this is the principle of Dimensional Reduction (DR).

The strategy behind every effective theory is to express the parameters of the effective theory in terms of the ones at the high scale. Thus, dimensional reduction integrates out hard (and soft) scales and maps the couplings and temperature from the $(d+1)$-dimensional to a d-dimensional theory (cf. fig. 2.1). By construction, the Green's functions of the remaining degrees of freedom reproduce the ones from the full theory up to a relative error [49]. Note that fermionic modes are hard modes and therefore the effective theory is purely bosonic.

The dimensionally reduced EFT is described by the effective action with sufficiently suppressed operators $\mathcal{O}_n$ with $n > 4$ of the form

$$S_{3d} = \frac{1}{T} \int_{\mathbf{x}} \left\{ \mathcal{L}_{3d} + \sum_{n \geq 5} \frac{\mathcal{O}_n}{(\pi T)^n} \right\} . \tag{2.35}$$

In contradistinction to eq. (2.34), non-vanishing higher-dimensional operators compromise an exact decoupling at finite-temperature [50]. The main reason is that now the parameters of the effective theory themselves depend on T. Interactions generate softer scales and dynamical masses $m_i(T) \sim g^n T$ with $n > 0$ – these are the screened masses [51]. The accuracy of a dimensionally reduced EFT, the second term in eq. (2.35), is bounded by errors

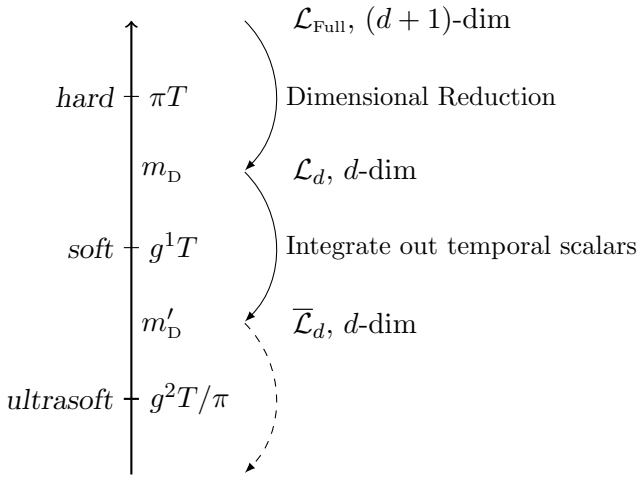

Figure 2.1: Scale hierarchy of a $(d+1)$-dimensional thermal field theory at high temperature, and construction of effective theories at different steps of the dimensional reduction. The first step integrates out all hard non-zero modes. The second step integrates out temporal scalars with soft thermal masses m_{D}. At the ultrasoft scale, light static scalars and gauge fields remain.

of $\mathcal{O}\left(m_i^2(T)/M^2(T)\right)$ with the UV scale $M(T) \sim g^m T$ and $m < n$. For the highest scale we have $M(T) \sim \pi T$. At low momenta and despite infinite-temperature or masses, DR proves merely to be valid up to g^{n-m}. In other words, the correction terms in the EFT operator expansion compete with terms from the perturbative expansion $g \ll 1$. In this setup an expansion in the weak-coupling is only valid if both corrections originating from the EFT as well as higher-order loops are included. This is an expression of how the decoupling theorem fails for thermal EFT.

At the same time it tells us how to deal with it, namely by establishing power counting arguments to determine which terms in the EFT expansion and which loop orders in the perturbative expansion ought to be considered. Lacking this amount of consistency in the renormalisation leads to non-vanishing IR divergences – as will be highlighted in chapter 4.

2.4.2 Parameter matching

The final ingredient in the construction of the dimensionally reduced EFT is the matching, the mapping of the UV parameters of the parent theory onto the effective ones. The procedure equates n-point correlation functions in the full- and effective theories inside their domain of mutual validity. As we demand, the EFT reproduces the infrared of the full theory and is valid below a certain scale $m(T)$ which is dubbed the matching scale. This is where the two theories get compared and all externally input scales such as external momenta are fixed at similar order $q_i \lesssim m(T)$.

For a theory with UV scales M, IR scales m, couplings g amongst light fields, and couplings G involving at least one heavy field, we obtain for a generic n-point Green's function

$$\text{Full theory}: \quad \Gamma_n(q_1, \ldots, q_n; g, m, G, M) \;, \tag{2.36}$$

$$\text{EFT}: \quad \overline{\Gamma}_n(q_1, \ldots, q_n; \overline{g}, \overline{m}) \;, \tag{2.37}$$

where $\overline{g}, \overline{m}$ are respective EFT parameters as functions of G and M. Since $\overline{\Gamma}_n$ is an expansion in inverse powers of the UV scale $1/M$ only the IR scales remain therein. The difference of the two renormalized correlators is the matching contribution

$$\Gamma_{\text{M}} = \Gamma_n - \overline{\Gamma}_n \;, \tag{2.38}$$

where Γ_{M} is analytic in m while the individual terms on the right can contain non-analyticities which cancel in the difference. Thus, treating IR scales as small perturbations, an expansion

in (m, q_i) of Γ_n and $\overline{\Gamma}_n$ causes the latter to vanish. Because all scales in the constituting integrals of $\overline{\Gamma}_n$ are expanded out, the resulting individual terms produce scaleless integrals which vanish in dimensional regularisation. Therefore, the matching is entirely established by an IR expansion of the full theory and the construction in eq. (2.38) is understood as subtracting out the IR dynamics of the theory. Hence, the matching is only affected by UV scales and thus IR-safe.

To guarantee the equivalence of the Green's functions they are *matched*. In a scale separated TFT such as described in the context of dimensional reduction this is accomplished by equating

$$\overline{\Gamma}_n(q_1, \dots, q_n; \overline{g}, \overline{m})(\phi_1 \dots \phi_n)_{3d} = \frac{1}{T}\Gamma_n(q_1, \dots, q_n; g, m, G, M)(\phi_1 \dots \phi_n)_{4d} \,, \tag{2.39}$$

for a general set of n-external fields, and T-dependent parameters. The inverse factor of $1/T$ accounts for the explicit T-integration in the action of a static Lagrangian. By fixing the low energy parameters $\overline{m}$ to fulfill the above equality up to a given order in perturbation theory the dimensionally reduced theory is fully determined. The normalisation factor for the fields $(\phi_i)_{3d}$ of the effective theory is then related to the matching of their 2-point functions.

A dimensionally reduced thermal field theory restricts to the static regime of utility (see sec. 2.4.1). Since matching computations are conducted therein, it is necessary to decompose tensor structures of correlation functions and isolate static components. Resembling zero-temperature, now this approach involves one additional tensor, namely the proper velocity of the heat bath $u_\mu = (1, \mathbf{u})$ with condition

$$u^2 = u_\mu u^\mu = 1 \,. \tag{2.40}$$

The temperature T is defined in the rest frame of the heat bath where it is timelike with the Euclidean velocity $u_\mu = (1, \mathbf{0})$. Because of this distinguished frame the heat bath breaks $\mathrm{O}(1, d)$ Lorentz symmetry explicitly to the group of spatial rotations $\mathrm{O}(d)$. The metric tensor $\delta_{\mu\nu}$ respects this disjunct structure separately with a spatial $S_{\mu\nu}$ and temporal $T_{\mu\nu}$ spacetime metric (cf. appendix A of [1])

$$\delta_{\mu\nu} \equiv T_{\mu\nu} + S_{\mu\nu} \,, \quad T_{\mu\nu} \equiv \delta_{\mu 0}\delta_{\nu 0} \,, \quad S_{\mu\nu} \equiv \delta_{\mu i}\delta_{\nu i} \,, \quad q_\mu = \delta_{\mu i} q_i \,. \tag{2.41}$$

At some places it is then more illuminating to use a S/T-basis instead of the full δ-function and velocity u_μ. When advancing to higher-point correlators this becomes practical.

A static external Euclidean momentum Q is purely spatial ($q_0 = 0$), of the order of a soft scale $q_i \sim \mathcal{O}(gT)$, and orthogonal to u_μ with $Q_\mu = (0, \mathbf{q})$ and permits the scalar products $u \cdot Q = 0$ and $u \cdot K_i = k_{i_0}$. For a 2-point function of gauge bosons the propagator, its inverse and the self-energy are all symmetric second rank tensors, and a linear combination of

$$\delta_{\mu\nu} \,, \quad Q_\mu Q_\nu \,, \quad u_\mu u_\nu \,, \quad u_\mu Q_\nu + u_\nu Q_\mu \,, \tag{2.42}$$

is the most general tensor thereof.

2.5 QCD in Euclidean spacetime

Describing the strong nuclear force, the four-dimensional action and Lagrangian of Quantum Chromodynamics (QCD) at finite temperature composes of

$$S_{\mathrm{QCD}} = \int_0^\beta \mathrm{d}\tau \int_{\mathbf{x}} \mathcal{L}_{\mathrm{QCD}} \,, \tag{2.43}$$

$$\mathcal{L}_{\mathrm{QCD}} = \mathcal{L}_{\mathrm{gauge}} + \mathcal{L}_{\mathrm{ghost}} + \mathcal{L}_{\mathrm{gf}} + \mathcal{L}_{\mathrm{fermion}} + \delta\mathcal{L}_{\mathrm{QCD}} \,, \tag{2.44}$$

with counterterms necessary for renormalisation at $T = 0$ contained in $\delta\mathcal{L}_{\mathrm{QCD}}$. The different sectors assume

$$\begin{aligned}\mathcal{L}_{\mathrm{gauge}} &= \frac{1}{4}F^a_{\mu\nu}F^a_{\mu\nu} \,, \\ \mathcal{L}_{\mathrm{ghost}} &= \partial_\mu \bar{c}^{\,a} D_\mu c^a \,, \\ \mathcal{L}_{\mathrm{gf}} &= \frac{1}{2\xi}(\partial_\mu A^a_\mu)^2 \,, \\ \mathcal{L}_{\mathrm{fermion}} &= \bar{\psi}(\not{D} + m_i)\psi \,, \end{aligned} \tag{2.45}$$

with a local $\mathrm{SU}(N_\mathrm{c})$ symmetry that leaves the Lagrangian invariant. The corresponding local gauge transformation $U(x) = e^{ig\theta^a(x)T^a} \in \mathrm{SU}(N_\mathrm{c})$ transforms the gauge field $A_\mu \to A'_\mu$

$$A'_\mu = U(x)\left(A_\mu + \frac{i}{g}\partial_\mu\right)U^\dagger(x) \,. \tag{2.46}$$

Here, $A_\mu = A^a_\mu T^a \in \mathbb{R}^{d+1} \otimes \mathfrak{su}(N_\mathrm{c})$ are the gauge fields that take real values in $(d+1)$-dimensions and T^a the generators of the non-Abelian $\mathrm{SU}(N_\mathrm{c})$ with structure constants f^{abc}. Their colour index $a = 1, \ldots, N_\mathrm{c}$ depends on the total number of colours N_c. In the fundamental representation the covariant derivative and field strength tensor take the form

$$D_\mu[A] = \partial_\mu - igA_\mu \,, \tag{2.47}$$

$$F^a_{\mu\nu} = \partial_\mu A^a_\nu - \partial_\nu A^a_\mu + g f^{abc} A^b_\mu A^c_\nu \,. \tag{2.48}$$

Quark fields ψ_i carry Dirac, colour, and the flavour indices $i = 1, \ldots, N_\mathrm{f}$ dependent on the number of fermion flavours N_f. We employ Hermitian Dirac matrices $\gamma_\mu^\dagger = \gamma_\mu$ obeying the Clifford algebra $\mathrm{C}\ell_{d+1}(\mathbb{R})$ with $\{\gamma_\mu, \gamma_\nu\} = 2\delta_{\mu\nu}$. The covariant gauge fixing term $\mathcal{L}_{\mathrm{gf}}$ and ghost sector $\mathcal{L}_{\mathrm{ghost}}$ are in accordance with the Faddeev-Popov construction [52].

All fields and couplings $x \in \{A, B, c, \psi_i, g, m_i, \xi\}$ in QCD are renormalised where B accounts for a background field of A (cf. sec. 4.2.1). By fixing the dimensions for the bare fields and couplings to

$$\dim\{A, B, c, \psi_i, g, m_i, \xi\} = \left\{\frac{d-2}{2}, \frac{d-2}{2}, \frac{d-2}{2}, \frac{d-1}{2}, \frac{4-d}{2}, 1, 0\right\} \,, \tag{2.49}$$

a dimensionless action is realised. Recurring thermal logarithms from bosonic and fermionic integrals respect the notation [49]:

$$L_b \equiv \ln\frac{\bar{\mu}e^{\gamma_\mathrm{E}}}{4\pi T} \,, \quad L_f \equiv L_b + 2\ln 2 \,. \tag{2.50}$$

Concretely, the following conventions relate renormalised and bare fields (or wave functions)

$$\begin{aligned} B^a_{\mu,\mathrm{B}} &\equiv Z_B^{1/2} B^a_\mu = (1 + \delta Z_{_B})^{1/2} B^a_\mu \,, \\ A^a_{\mu,\mathrm{B}} &\equiv Z_A^{1/2} A^a_\mu = (1 + \delta Z_{_A})^{1/2} A^a_\mu \,, \\ c^a_\mathrm{B} &\equiv Z_c^{1/2} c^a = (1 + \delta Z_{_c})^{1/2} c^a \,, \\ \psi_\mathrm{B} &\equiv Z_\psi^{1/2}\psi = (1 + \delta Z_{_\psi})^{1/2}\psi \,, \end{aligned} \tag{2.51}$$

while the renormalised coupling g_R, quark masses m_i, and gauge fixing parameter ξ relate to their bare counterparts by

$$\begin{aligned} g^2_\mathrm{B} &\equiv \mu^{2\epsilon} Z_g g^2_\mathrm{R} = \mu^{2\epsilon}(g^2_\mathrm{R} + \delta g^2) \,, \\ m^2_{i,\mathrm{B}} &\equiv Z_m m_i^2 = (m_i^2 + \delta m_i^2) \,, \\ \xi_\mathrm{B} &\equiv Z_\xi \xi = (1 + \delta Z_\xi)\xi \,, \end{aligned} \tag{2.52}$$

where g_{R} is dimensionless. Then, we list the 3-loop renormalisation group equation (RGE) for QCD by following eq. (2.22)

$$\begin{aligned}\frac{\mathrm{d}}{\mathrm{d}\ln\bar{\mu}^2}\frac{g^2(\bar{\mu})}{(4\pi)^2} &= \beta_0\frac{g^4(\bar{\mu})}{(4\pi)^4}+\beta_1\frac{g^6(\bar{\mu})}{(4\pi)^6}+\beta_2\frac{g^8(\bar{\mu})}{(4\pi)^8}+\mathcal{O}(g^{10})\\ &= \sum_{n=0}^{\infty}\beta_n\, a^{n+2}\,, \quad a=\frac{g^2(\bar{\mu})}{(4\pi)^2}\,,\\ \frac{\mathrm{d}\ln m}{\mathrm{d}\ln\bar{\mu}^2} &= \sum_{n=0}^{\infty}(\gamma_m)_n\, a^{n+1}\,, \end{aligned} \tag{2.53}$$

the bare coupling g_{B} and quark masses are re-expanded in terms of the renormalised gauge coupling from eq. (2.52). The RG constants Z_g and Z_m read to 2-loop order

$$Z_g = 1+\frac{g_{\mathrm{R}}^2}{(4\pi)^2}\frac{\beta_0}{\epsilon}+\frac{g_{\mathrm{R}}^4}{(4\pi)^4}\left[\frac{\beta_1}{2\epsilon}+\frac{\beta_0^2}{\epsilon^2}\right]+\mathcal{O}(g^8)\,, \tag{2.54}$$

$$Z_m = 1+\frac{g_{\mathrm{R}}^2}{(4\pi)^2}\frac{2(\gamma_m)_0}{\epsilon}+\frac{g_{\mathrm{R}}^4}{(4\pi)^4}\left[\frac{(\gamma_m)_1}{\epsilon}-\frac{(\gamma_m)_0\beta_0-2(\gamma_m)_0^2}{\epsilon^2}\right]+\mathcal{O}(g^6)\,. \tag{2.55}$$

As a non-Abelian gauge theory QCD exhibits confinement in the IR and asymptotic freedom in the UV. Succeeding the discussion below eq. (2.21), we inspect the one- to three-loop QCD β-function

$$\beta_0 \equiv \frac{1}{3}(-11N_{\mathrm{c}}+4T_{\mathrm{F}}N_{\mathrm{f}})\,, \tag{2.56}$$

$$\beta_1 \equiv -\frac{34}{3}N_{\mathrm{c}}^2+\frac{20}{3}N_{\mathrm{c}}T_{\mathrm{F}}N_{\mathrm{f}}+4C_{\mathrm{F}}T_{\mathrm{F}}N_{\mathrm{f}}\,, \tag{2.57}$$

$$\begin{aligned}\beta_2 \equiv &-\frac{2857}{54}N_{\mathrm{c}}^3+\frac{1415}{27}N_{\mathrm{c}}^2T_{\mathrm{F}}N_{\mathrm{f}}+\frac{205}{9}N_{\mathrm{c}}C_{\mathrm{F}}T_{\mathrm{F}}N_{\mathrm{f}}\\ &-2C_{\mathrm{F}}^2T_{\mathrm{F}}N_{\mathrm{f}}-\frac{158}{27}N_{\mathrm{c}}T_{\mathrm{F}}^2N_{\mathrm{f}}^2-\frac{44}{9}C_{\mathrm{F}}T_{\mathrm{F}}^2N_{\mathrm{f}}^2\,,\end{aligned} \tag{2.58}$$

with further coefficients known up to 5-loops in vacuum [17, 18, 19]. Since its leading order coefficient is negative $\beta_0 < 0$ for $N_{\mathrm{f}} < \frac{11}{2}N_{\mathrm{c}}$ it is also for the physical case $N_{\mathrm{c}} = 3, N_{\mathrm{f}} = 6$ and the coupling diminishes at short distances. Therein, quarks and gluons behave as free particles at high energy scales and perturbation theory holds. In the low-energy regime the scenario is reversed and QCD becomes strongly coupled, the theory confines, colour-neutral bound states are formed, and the theory requires non-perturbative treatment.

The one- and two-loop QCD quark mass anomalous dimension γ_m is

$$(\gamma_m)_0 \equiv -3C_{\mathrm{F}}\,, \tag{2.59}$$

$$(\gamma_m)_1 \equiv -C_{\mathrm{F}}\left(\frac{97}{6}N_{\mathrm{c}}+\frac{3}{2}C_{\mathrm{F}}-\frac{10}{3}T_{\mathrm{F}}\right)\,, \tag{2.60}$$

with respective results up to 5-loops in [20, 21]. Since the anomalous dimension γ_m bears no dependence on the quark masses inside the $\overline{\mathrm{MS}}$-scheme, we suppress the quark flavour index. The relation between the anomalous dimension and the quark mass renormalisation becomes apparent when taking the derivative of the bare mass which is invariant under renormalisation group transformations

$$0 = \frac{\mathrm{d}m_{\mathrm{B}}}{\mathrm{d}\ln\mu^2} = \frac{\mathrm{d}Z_m}{\mathrm{d}\ln\mu^2}+\underbrace{\frac{\mathrm{d}m}{\mathrm{d}\ln\mu^2}}_{\gamma_m}\,, \tag{2.61}$$

where the second term is per definition eq. (2.21) the anomalous dimension.

2.5.1 Thermodynamics of QCD

Finite-temperature QCD allows to study the transition from an unconfined (quark-gluon) to a confined (hadron) phase [53]. In the unconfined phase the theory describes a Quark-Gluon plasma (QGP). Depending on different values of the light quark masses $m_i = m_{u,d,s}$ in the theory the character of the transition is determined at vanishing chemical potential $\mu \sim 0$.

- $m_i \to \infty$. First-order transition.
  Infinite and large quark masses decouple from the theory and in the resulting pure SU(N) Yang-Mills gauge theory the transition is defined by the $Z(N)$ center symmetry (see below).

- $m_i \to 0$. First-order transition.
  Zero and light quark masses induce the global chiral symmetry in the QCD Lagrangian $\mathcal{L}_{\text{QCD}}$ (2.44). Hence, the phase transition can be defined by chiral symmetry breaking and restoration with the chiral condensate $\langle\bar{\psi}\psi\rangle$ as order parameter.

- Physical quark masses m_i. Crossover transition.
  Since symmetry features remain unaltered across the transition, its nature is one of a smooth crossover. Both chiral and center symmetry are explicitly broken by the quark masses.

Because the latter transition is a smooth crossover for physical quark masses [54, 55] its phase transition critical temperature (T_c) is not uniquely defined. Relating it to observables affected by chiral symmetry such as the chiral condensate and susceptibility, the crossover temperature of $T_\text{c} \simeq 155$ MeV was readily determined by refs. [12, 13] and recently extended to finite chemical potential by refs. [14, 15]. Studying static observables non-perturbatively with both the fundamental theory of QCD and its dimensionally reduced one, agreement was found up to $T \sim 2T_\text{c}$ for e.g. spatial string tension [56, 57, 58] or spatial correlation lengths [59].

As mentioned above, in Yang-Mills theory (YM), the pure-gluonic sector of QCD[1], the breaking of the $Z(N_\text{c})$ center symmetry governs the confinement-deconfinement transition [60, 61]. This is a global symmetry of the theory at finite temperature. While the bosonic fields have to obey periodic boundary conditions in the path integral (2.5) once the time direction is compactified in the ITF, this need not be true for the gauge transformation itself

$$U(\tau + \beta, x) = z\, U(\tau, x) \;, \tag{2.62}$$

where $z \in \text{SU}(N_\text{c})$ is a twist. However, for a transformation (2.46) of gauge fields to be invariant

$$A'_\mu(\tau, \mathbf{x}) = z\left(A_\mu(\tau, \mathbf{x}) + \frac{i}{g}\partial_\mu\right)z^\dagger \;, \tag{2.63}$$

z must be independent of spacetime and commute with all elements of SU(N_c). This condition is only realised if the z-twist is in the center of the gauge group $z \in Z(N_\text{c})$ such that $z = e^{2\pi i n/N_\text{c}}\mathbb{1}$ with integer values $n \in \{0, \ldots, N_\text{c} - 1\}$.

The action of SU(N_c) hot YM without matter in the fundamental representation, is invariant under the $Z(N_\text{c})$ center symmetry. A phase transition always relates to an order parameter which for the center symmetry in QCD is given by the Polyakov loop. The latter is in general not invariant under a $Z(N_\text{c})$ transformation. At low temperatures the Polyakov loop vanishes and center symmetry is restored while at high temperatures it is spontaneously broken to one of the N_c physically equivalent vacuum states. The transition is first order.

The symmetry breaking patterns that drive the phase transition in the full theory need to be either respected or restored by the dimensionally reduced theory. The above Yang-Mills

[1] In comparison to eq. (2.44), the Yang-Mills Lagrangian composes of $\mathcal{L}_{\text{YM}} = \mathcal{L}_{\text{gauge}} + \mathcal{L}_{\text{ghost}} + \mathcal{L}_{\text{gf}}$.

example shows that the spontaneous breaking of center symmetry is essential for the dynamics at the phase transition and its realisation. Chapter 4 discusses how the dimensionally reduced theory of QCD tackles this issue.

Chapter 3

Computer-algebra tools for thermal perturbation theory

Thermal perturbation theory entails great potential of automation in analogy with zero-temperature computations. As indicated in the motivation, the pipeline undergoes a combinatorial, algebraic, and analytic evaluation that stretches from the generation of Feynman diagrams to the treatment of a small set of master integrals. Once the theories of interest contain multiple fields and scales or the computation reaches loop or leg orders that surpass the 1-loop level, their systematic treatment becomes indispensable. Dimensional reduction, as a purely perturbative process, is an ideal candidate to demonstrate the implementation of this kind of systemised algebraic manipulation.

This chapter introduces the cornerstones of automated dimensional reduction, the corresponding computer-algebra tools and in-house algorithmic implementations.

3.1 Automated Dimensional Reduction

How automated is automated? To showcase this question, we monitor various stages of a perturbative computation inside a thermal field theory and show the journey of the 2-loop 2-point QCD diagram including one fermionic line within the most complicated topology

$$(-1)$$  , (3.1)

with the negative sign (-1) for the respective fermion loop.

3.1.1 Computer algebraic implementation

The necessity of precise predictions for hadron collider physics sparked the development of a wealth of zero-temperature algorithms to handle the computation of Feynman diagrams. Their different stages of computation are cast to a succession of pre-existing public packages. The standard procedure consists of a diagram generator like `qgraf` [62] or `FeynArts` [63] based on a model file that codifies particle and vertex properties of the theory. It determines topologies and combinatorial symmetry factors in accordance with the external and internal field content, loop-, and leg number.

What follows is an algebraic stage that simplifies the arising integrals and tackles group-, Lorentz- and Dirac algebra. One all-purpose software implementation is `FeynCalc` [64]. The final reduction and analytic solution of integrals involves methods as Integration-by-parts (IBP) [65, 66], difference equations [67], or Mellin-Barnes transformations [68]. Software that offer these features amongst others are `reduze` [69] or `FIRE` [70] using s-bases, region-bases or explicit integration by sub-diagrams.

The main complication of finite-temperature perturbative calculations presents itself only when analytically evaluating sum-integrals. Thus, this thesis establishes the following algorithm which holds for a generic EFT matching computation. While implemented in `FORM` [71], the loop computer's best pattern matching friend, it handles most levels of Feynman integral calculus. Its central steps are

(i) Feynman rule generation

(ii) Graph generation with `qgraf` [62] and visualisation with `axodraw` [72]

(iii) Momentum shifts to canonical bases

(iv) Feynman rule insertion and algebraic manipulations

(v) Taylor expansion in (soft) external momenta q_i^2 and heavy mass scales

(vi) Scalarisation and decoupling of external momenta via tensor decomposition

(vii) Integral reduction with IBP identities based on a Laporta type [67] algorithm

(viii) Analytical or numerical solution of the remaining master integrals (cf. appendix A.1)

The following summary addresses various waypoints how to exploit the prevailing information of the integrals to algebraically simplify them towards a few calculable integrals. Otherwise the scaling of the problem is far from linear when examining higher-loop orders.

3.1.2 Feynman rules and model generation

Merely starting from the model Lagrangian requires the direct generation of a model file and the corresponding Feynman rules. This allows `qgraf` to assemble all the topologies with the given field and vertex content. Their group-, Lorentz- and Dirac structures are automatically determined by (cycle)symmetrising over individual fields and maximally symmetrising terms in the input Lagrangian. To ensure correct relative signs in the rules, tests against known correlators are run.

The corresponding QCD Feynman rules are generated based on the particle content and the Lagrangian in eq. (2.44) exemplified in listing 3.1 for the QCD gluon 3-point vertex with functions

- `vrtx()` for vertices,
- `prop()` for propagators,
- `ext()` for external lines,

in agreement with [73]. The contributing QCD particles are denoted with

- (`ge3`), `gl3` for (external) SU(3) gauge field $(B_\mu), A_\mu$,
- (`hg3`), `gh3` for (anti-)ghosts $(\bar{c}^a), c^a$,
- (`uq`), `qu` for (anti-)quarks $(\bar{\psi}), \psi$.

Inserted into diagram (3.1) and based on external and internal momenta this creates the corresponding topology in listing 3.2.

Listing 3.1: Feynman rule for the QCD 3-gluon vertex by matching patterns `id lhs = rhs` in `FORM` notation with `d_(m1,m2)`$= \delta_{m_1,m_2}$ and `p1(m1)` momenta p_{1,m_1}. The functions `tr3()` correspond to traces over SU(3) group generators defined in eq. (3.48) while `sg3` is the QCD gauge coupling,

```
id vrtx(gl3(a31?,m1?,p1?),gl3(a32?,m2?,p2?),gl3(a33?,m3?,p3?)) =
  +tr3(a31,a32,a33)*(p1(m2)-p3(m2))*(2*d_(m1,m3)*sg3)
  +tr3(a31,a32,a33)*(p1(m3)-p2(m3))*(-2*d_(m1,m2)*sg3)
  +tr3(a31,a32,a33)*(p2(m1)-p3(m1))*(-2*d_(m2,m3)*sg3)
  +tr3(a31,a33,a32)*(p1(m2)-p3(m2))*(-2*d_(m1,m3)*sg3)
  +tr3(a31,a33,a32)*(p1(m3)-p2(m3))*(2*d_(m1,m2)*sg3)
  +tr3(a31,a33,a32)*(p2(m1)-p3(m1))*(2*d_(m2,m3)*sg3);
```

Listing 3.2: Topology eq. (3.1) generated by `qgraf` in `FORM` notation with functions `vrtx()` for vertices, `prop()` for propagators, and `ext()` for external lines.

```
+(-1)*
ext(ge3(-1,kq1),ge3(-2,-kq1))*
prop(qu(1,-k1),uq(2,k1))*
prop(qu(3,-k1+kq1),uq(4,k1-kq1))*
prop(qu(5,k2),uq(6,-k2))*
prop(qu(7,k2+kq1),uq(8,-k2-kq1))*
prop(gl3(9,-k1-k2),gl3(10,k1+k2))*
vrtx(ge3(-1,kq1),uq(4,k1-kq1),qu(1,-k1))*
vrtx(ge3(-2,-kq1),uq(6,-k2),qu(7,k2+kq1))*
vrtx(gl3(9,-k1-k2),uq(2,k1),qu(5,k2))*
vrtx(gl3(10,k1+k2),uq(8,-k2-kq1),qu(3,-k1+kq1))
```

3.2 Combinatorics

3.2.1 Momentum shifts and expansion

A generic Feynman diagram is classified by N_k internal loops, its number of N_e external lines, $N_q = N_e - 1$ independent external lines, and N_d internal lines or propagators. Its integral is expressed in the form

$$I^{\mu_1\cdots\mu_n}(s_1,\ldots,s_{N_d};m_1,\ldots,m_{N_d}) = \int_{\{k\}} \frac{N^{\mu_1\cdots\mu_n}}{\prod_{i=1}^{N_d}\Delta_i^{s_i}}\,, \quad \underline{s}\in\mathbb{Z}^{N_d}\,, \tag{3.2}$$

with propagators $\Delta_i = p_i^2 + m_i^2$ and explicit numerator Lorentz structure $N^{\mu_1\cdots\mu_n}$. The latter consists of all potential tensor structures of N_e independent external momenta q_i and N_k loop momenta k_i. This especially includes all possible scalar products amongst loop momenta $(k_i\cdot k_j)$ and mixed momenta $(p_i\cdot k_j)$ where p_i are composed of linear combinations

$$p_i = \sum_{j=1}^{N_k}\lambda_{ij}k_j + \sum_{j=1}^{N_e}\sigma_{ij}q_j\,. \tag{3.3}$$

The index i is restricted only by letting the matrices $\lambda_{ij},\sigma_{ij}\in\{-1,0,1\}$. Then the number of unique propagator momenta corresponds to the fixed number N_s of irreducible scalar products within a diagram

$$N_s = \frac{1}{2}N_k(N_k+1) + N_kN_q\,. \tag{3.4}$$

Here the first term amounts to the number of scalar products between loop momenta while the second term counts mixed loop and external momenta. In essence there is a redundancy in eq. (3.2) because the possible number of scalar products is limited by N_s.

Scalarisation casts integrals with explicit tensorial Lorentz signature to purely scalar integrals. Since open Lorentz indices of n-point functions relate to external lines, one either

Listing 3.3: Topology eq. (3.1) generated by `qgraf` in `FORM` notation with functions `vrtx()` for vertices, `prop()` for propagators, and `ext()` for external lines. Momentum shifts from eq. (3.3) onto the corresponding 2-point 2-loop auxiliary topology are applied.

```
+(-1)*
ext(ge3(-1,kq1),ge3(-2,-kq1))*
prop(qu(1,-k1),uq(2,k1))*
prop(qu(3,-k1+kq1),uq(4,k1-kq1))*
prop(qu(5,-k2),uq(6,k2))*
prop(qu(7,-k2+kq1),uq(8,k2-kq1)))*
prop(gl3(9,k2-k1),gl3(10,-k2+k1))*
vrtx(ge3(-1,kq1),uq(4,k1-kq1),qu(1,-k1))*
vrtx(ge3(-2,-kq1),uq(6,k2),qu(7,-k2+kq1))*
vrtx(gl3(9,k2-k1),uq(2,k1),qu(5,-k2))*
vrtx(gl3(10,-k2+k1),uq(8,k2-kq1),qu(3,-k1+kq1))
```

projects out their dependence or shifts these indices onto external momenta and metric tensors. This facilitates the subsequent computations.

An auxiliary topology or integral family A is an ordered, minimal, and complete set of M propagators with $M = N_s$. Concretely, minimality requires the inverse propagators to be linearly independent while completeness ensures that all N_s scalar products can be expressed by inverse propagators. This corresponds to the basis of momenta:

$$A_{N_k,N_e} = \left\{ p_i \,\middle|\, i = 1,\dots,M;\ \{p_i\} \text{ linearly independent} \right\} . \tag{3.5}$$

Momentum shifts onto the auxiliary topology canonise the integral in (3.2)

$$I(s_1,\dots,s_{N_d};m_1,\dots,m_{N_d}) \to I(s_1,\dots,s_M;m_1,\dots,m_M) , \tag{3.6}$$

and reduce the different momenta in the topology of eq. (3.1) to one representation with minimal amount of scalar products; see listing 3.3. Furthermore, this moves the information of contracted Lorentz indices of scalar integrals from the numerator into the denominators and mitigates complicated polynomials of different scalar products in the numerator to the maximal amount of N_s.

This fixes the content of propagators but still allows N_s different scalar products in the numerator. Because they are also contained in the propagators this is another redundancy. We remove it through an expression with inverse propagators and by iteratively applying the identity

$$\frac{(p\cdot k)_i}{\Delta_i} = \frac{1}{C_i}\left(1 - \frac{\Delta_i - C_i(p\cdot k)_i}{\Delta_i}\right) , \quad i \in 1,\dots,M , \tag{3.7}$$

where the propagator $\Delta_i = C_i(p\cdot k)_i + (\dots)$ contains the corresponding scalar product with coefficient C_i. This systematically moves scalar products from the numerator into the denominator on the cost of additional but canonised terms. The resulting integrals

$$I(s_1,\dots,s_M) = I_{s_1\dots s_M} = \int_{\{k\}} \frac{1}{\Delta_1^{s_1}\dots\Delta_M^{s_M}} , \quad \underline{s} \in \mathbb{Z}^M , \tag{3.8}$$

are characterised by points $\underline{s}$ in the M-dimensional parameter space of powers s_i.

The possibility to uniquely identify integrals benefits their further algebraic treatment. One such unique classification separates recurring integrals into sectors and tags them with a sector identification number sID. In this sense a sector is a unique binary base representation indicating which of the M propagators are present in the set A_{N_k,N_e} and sID assigns every possible combination of denominators to a unique sector. Further unique classification of a

whole integral is achieved in accordance with [69] using the scheme:

$$\mathrm{sID}(I_{\underline{s}}) = \sum_i \theta(s_i) 2^{M-i} \;, \qquad \text{sector ID} \;, \tag{3.9}$$

$$t(I_{\underline{s}}) = \sum_i \theta(s_i) \;, \qquad \text{number of denominators} \;, \tag{3.10}$$

$$r(I_{\underline{s}}) = \sum_i \theta(s_i) s_i \;, \qquad \text{denominator powers} \;, \tag{3.11}$$

$$s(I_{\underline{s}}) = \sum_i -\theta(-s_i) s_i \;, \qquad \text{numerator powers (dots)} \;, \tag{3.12}$$

$$q(Z^{\underline{\alpha}}_{\underline{s}}) = \sum_i \theta(\alpha_i) \alpha_i \;, \qquad \text{Matsubara mode powers} \;, \tag{3.13}$$

where $\theta(x)$ is the Heaviside theta function. Starting from the basis eq. (3.5) in a given integral I, then $t(I_{\underline{s}})$ counts the number of different propagators, $r(I_{\underline{s}})$ the total number of positive powers of these propagators, and $s(I_{\underline{s}})$ the total number of negative powers. In case of a sum-integral $Z^{\underline{\alpha}}_{\underline{s}}$ (see below eq. (3.49)), $q(Z^{\underline{\alpha}}_{\underline{s}})$ gives the total power of the zero-momentum components. Conversely, these classifiers were chosen such that for a given sID its binary base representation and complexity are uniquely determined by the set $\{t, r, s, q\}$.

The integral family of a given loop and leg level depends on its maximally difficult integral with $t_{\max}$ propagators. Typically, it suffices to characterise integrals with $M = t_{\max}$ at low loop levels. However, sometimes also more than one maximally difficult topology exists and one needs $M \geq t_{\max}$ propagators to capture all sectors.

The maximal amount of combinations in a binary system with M digits amounts to 2^M but in general not all sectors are relevant or physical. To decide which of them are relevant sectors, we see that there are multiple possible sectors sID for every t-level but only

$$S = \sum_{t=N_k}^{M} \binom{M}{t} < 2^M \;, \tag{3.14}$$

are physical sectors. Additionally, we already disposed of the trivial zero-sectors that have less propagators than loops ($t < N_k$).

In this discrimination certain sectors describe the same topology. Such redundancies are related to symmetries of the integral measure and the propagators. They can be eliminated upon linear transformations of the loop momenta

$$k_i \to \sum_{j=1}^{N_k} M_{ij} k_j + \sum_{j=1}^{N_q} N_{ij} q_j \;, \quad i = 1, \ldots, N_k \;. \tag{3.15}$$

Where we consider M_{ij} as an invertible $[N_k \times N_k]$-matrix and $|\det M| = \pm 1$ to avoid possible d-dimensional dependences in the exponent of the Jacobian matrix. When only vacuum diagrams ($N_e = 0$) are considered eq. (3.15) simplifies to its first term.

By definition, the complete auxiliary topology A_{N_k} in eq. (3.5) expresses every propagator as a linear combination of elements of the basis after acting with M_{ij}

$$\Delta_i \to \Delta'_i = \sum_{n=1}^{M} c_n \Delta_n + c \;, \quad c_n, c = \text{const.} \;, \tag{3.16}$$

such that integrals remain within the same integral family. Figure 3.1 collects all unique sectors and relations amongst them for 2-loop tadpoles with auxiliary topology A_2 and 3-loop with A_3. To summarise, the above classification and momentum shifts allow to group certain sectors:

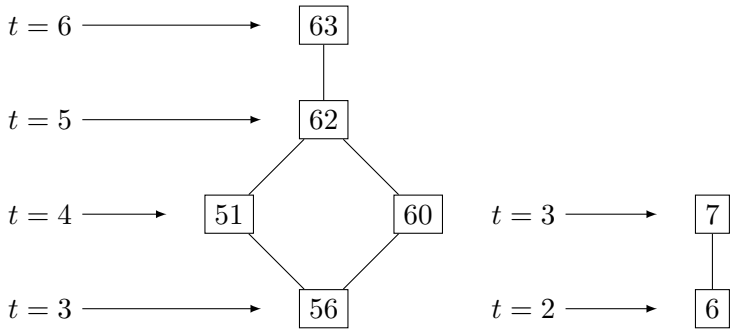

Figure 3.1: The subsector tree of tadpole auxiliary topologies A_2 (right) and A_3 (left) for different sector identities sID and number of denominators t.

(i) *Physical sectors.* A non-vanishing integral possible to map onto a graph with given momenta.

(ii) *Trivial zeros* $t < N_k$. The number of propagators t is less than the number of loops N_k in the diagram but dimensional reduction sets the integral identical to zero.

(iii) *Non-trivial zeros* $\mathrm{rank}(M) < N_k$. The number of propagators t is larger or equal than the number of loops N_k in the diagram but an adequate momentum shift eq. (3.15) sets the integral to zero.

(iv) *Trivial antisectors* $t > t_{\max}$. The number of propagators t is larger than the number of propagators of the maximally difficult topology $t_{\max}$.

(v) *Non-trivial antisectors.* The number of propagators t is less or equal than the number of propagators of the maximally difficult topology $t_{\max}$ but it is impossible to map the integral onto a graph.

The complexity of the integrals decreases further by expanding in external momenta q_i. The resulting terms are Taylor coefficients evaluated at $q_i = 0$ up to the relevant order in q_i. As argued in sec. 2.4.2, external and loop momenta exhibit a scale separation $q_i \ll k_i$ because in the matching the full theory is expanded in IR scales. The exact identity

$$\frac{1}{(k+q)^2+m^2} = \frac{1}{k^2+m^2} - \frac{2k\cdot q+q^2}{k^2+m^2}\frac{1}{(k+q)^2+m^2}\,, \tag{3.17}$$

permits an iterative treatment where m is an arbitrary mass scale on the propagator. While the first term is independent of external momenta it comes with the same UV and IR behaviour as the original integral. However, subsequent terms in eq. (3.17) decrease the superficial degree of UV divergence and increase the degree of IR divergence.

We need to apply eq. (3.17) iteratively to reproduce the correct terms up to fixed order in q. This cancels all poles at $q^2 = 0$ of the correlators that may arise at diagram level. To be specific, the expansion generalises

$$\frac{1}{[(k+q)^2+m^2]^n} = \sum_{i=0}^{\infty}\binom{n+i-1}{i}\frac{(-2k\cdot q-q^2)^i}{[k^2+m^2]^{n+i}}\,, \tag{3.18}$$

with $n > 0$. Inside the resulting integrals the presence of external momenta is removed from the propagators and entirely contained in the numerators. There they still appear in scalar products but the corresponding topologies are all vacuum tadpoles.

Thereafter, external momenta inside scalar products are extracted. This is achieved by Tensor Integral Decomposition (TID) based on the rotational symmetric structure of the

integrals. The decoupling of the remaining tensor indices is performed with totally symmetric tensor structures combining external momenta or metric tensors such as

$$\delta_{\mu\nu} \ , \quad \delta_{\mu\nu\rho\sigma} = \delta_{\mu\nu}\delta_{\rho\sigma} + \delta_{\mu\rho}\delta_{\nu\sigma} + \delta_{\mu\sigma}\delta_{\nu\rho} \ , \tag{3.19}$$

with the generalised Kronecker symbol

$$\delta_{i_1\dots i_{2n}} \equiv \delta_{i_1 i_2}\dots\delta_{i_{2n-1}i_{2n}} + (2n-1)!! \text{ permutations} \ . \tag{3.20}$$

A non-trivial illustration is the decomposition of $\langle k^\mu k^\nu k^\alpha k^\beta \rangle$ which corresponds the rotationally invariant expectation value. We arrive at a composition of metric tensors by anticipating its most general ansatz

$$\langle k^\mu k^\nu k^\rho k^\sigma \rangle = A(k^2)\delta_{\mu\nu}\delta_{\rho\sigma} + B(k^2)\delta_{\mu\rho}\delta_{\nu\sigma} + C(k^2)\delta_{\mu\sigma}\delta_{\nu\rho} \ , \tag{3.21}$$

where the coefficients are functions of k^2. To recover these, both sides of the above are multiplied by either $\delta_{\mu\nu}\delta_{\rho\sigma}$, $\delta_{\mu\rho}\delta_{\nu\sigma}$, or $\delta_{\mu\sigma}\delta_{\nu\rho}$ and the system of equations is solved

$$\langle k^4 \rangle = Ad^2 + Bd + Cd = Ad + Bd^2 + Cd = Ad + Bd + Cd^2 \ , \tag{3.22}$$

which yields $A = B = C$, where

$$A(k^2) = \frac{1}{d(d+2)}\langle k^4 \rangle \ . \tag{3.23}$$

Moreover, all emerging structures are systematically decomposed to decouple external momenta. While the above example shows a specific case, a generalisation of this decomposition of external Lorentz indices is desired. For a generic tensor decomposition and decoupling of the external momentum and loop momenta, one can insert factors $\delta_{i_1\dots i_\alpha}\delta_{i_1\dots i_\alpha}$ yielding

$$I_{i_1\dots i_\alpha} \equiv \int_k k_{i_1}\dots k_{i_\alpha} = \frac{\delta_{i_1\dots i_\alpha}}{\delta_{i_1\dots i_\alpha}\delta_{i_1\dots i_\alpha}} \int_k k_{i_1}\dots k_{i_\alpha}\delta_{i_1\dots i_\alpha} \ . \tag{3.24}$$

The factors in the denominator of eq. (3.24) are evaluated exactly. The special case gives $i_1 \neq \dots \neq i_\alpha$

$$\delta_{i_1\dots i_\alpha}\delta_{i_1\dots i_\alpha} = (\alpha-1)!!\frac{(d+\alpha-2)!!}{(d-2)!!} \ . \tag{3.25}$$

This shifts the open tensorial indices into open Lorentz structures. Their pre-factor is then of combinatorial nature and in general a d-dimensional polynomial. After contraction the external momenta factorise completely from the integral. Odd numbers of loop momenta vanish by integration such that $\alpha \in \{2k : k \in \mathbb{N}\}$ in eq. (3.24).

Thus, the tensor decomposition simplifies the initial auxiliary topology to vacuum tadpole diagrams with a reduced mass scale. This means also N_s only consists of the pure-loop part $N_s = N_k(N_k+1)/2$ in eq. (3.4) and N_k-loop vacuum topologies $T_{t,\text{sID}}$ pictorially identify

$$T_{t,\text{sID}} = \quad \boxed{N_k}_{t,\text{sID}} \ , \tag{3.26}$$

represented by their sector (sID) and number of propagators (t).

3.2.2 Feynman graph polynomials

Internal symmetries reduce the number of Feynman diagrams when applied systematically. Such a method ideally accesses all the symmetry information inside a given diagram in order to find all sector shifts and sector symmetries. One strategy is to construct all possible shifts

by eq. (3.15) and select only those that map onto the targeted sector. This is less obvious because with an increased loop order the number of possible shifts becomes large.

Most internal symmetry information is encoded in graph polynomials which are the first and second Symanzik polynomials. These parametrically represent Feynman integrals and permit a classification

$$I(\underline{s}) = \frac{\Gamma(\nu - \frac{d}{2}N_k)}{\prod_{i=1}^{N_d}\Gamma(s_i)} \int_{x_i \geq 0} \mathrm{d}^{N_d}x \left[\prod_{i=1}^{N_d} \mathrm{d}x_i\, x_i^{s_i-1}\right] \delta\left(1 - \sum_{i=1}^{N_d} x_i\right) \frac{\mathcal{U}^{\nu-\frac{d}{2}(N_k+1)}}{\mathcal{F}^{\nu-\frac{d}{2}N_k}} \,, \tag{3.27}$$

where $\nu = \sum_{N_d} s_i$ sums over exponents of N_d internal lines. Many variants arrive at the Symanzik polynomials with definitions outlined in [74]. $\mathcal{U}$ and $\mathcal{F}$ depend on the Feynman parameters x_i in the sum of denominators

$$\sum_{i=1}^{N_d} x_i(p_i^2 + m_i^2) = \sum_{r,s=1}^{N_k} k_r M_{rs} k_s + 2\sum_{r=1}^{N_k} Q_r \cdot k_r + J \,, \tag{3.28}$$

where M is a $[N_k \times N_k]$-matrix and Q is a N_k-vector of external momenta. Performing a general momentum shift $k_i \to k_j + \sum_k M^{-1}_{jk} Q_k$ fixes the graph polynomials to

$$\mathcal{U} = \det(M) \,, \tag{3.29}$$

$$\mathcal{F} = \det(M)[QM^{-1}Q + J]\mu^{-2} \,, \tag{3.30}$$

where μ is an arbitrary scale to render the integral (3.27) dimensionless. The graph polynomials are homogeneous in x_i with degree N_k for $\mathcal{U}$ and $N_k + 1$ for $\mathcal{F}$, where $\mathcal{U}$ is a positive semi-definite function in the domain where all $x_i \geq 0$; concretely each monomial has coefficient $+1$.

Vacuum integrals simplify the situation because then their graph polynomials agree up to a proportionality constant $\mathcal{U} \propto \mathcal{F}$ once $Q = 0$ and $J = \text{const.}$ in eq. (3.28). This holds for the fully equal massive case $J = \sum_{N_d} x_i m_i = m$ and for the massless case $m_i = 0$. Otherwise the metric is best derived in the space of products $\mathcal{U}\mathcal{F}$. Based on a specific binomial sector representation one can read off the polynomial by computing the determinants $\det(M)$. For example, the binary representation of the integral in sector sID=62 is I_{111110} defined in eq. (3.49). Its massless limit translates to

$$\sum_{i=1}^{5} x_i p_j^2 = x_{145}\, k_1^2 - 2x_4\,(k_1 \cdot k_2) + x_{24}\, k_2^2 - 2x_5\,(k_1 \cdot k_3) + x_{35}\, k_3^2 \,, \tag{3.31}$$

using the notation $x_{ij\ldots k} = x_i + x_j + \cdots + x_k$. Without external sources the matrix

$$M = \begin{bmatrix} x_{145} & -x_4 & -x_5 \\ -x_4 & x_{24} & 0 \\ -x_5 & 0 & x_{35} \end{bmatrix} \tag{3.32}$$

permits a single graph polynomial

$$\mathcal{U} = x_1x_{25}x_{34} + x_2x_5x_{34} + x_3x_4x_{25} \,. \tag{3.33}$$

Note that as expected every monomial in $\mathcal{U}$ has coefficient $(+1)$. When characterising Feynman integrals there are various options for arriving at the first Symanzik polynomial. In fact, in our example even six sectors $\{31, 47, 55, 59, 61, 62\}$ attain eq. (3.33). These are grouped into equivalence classes labelled by their highest valued sector. To compare two polynomials $\mathcal{U}_1$ with $\mathcal{U}_2$ a normal ordering of the terms in the polynomials per sector becomes necessary to determine equal sectors. A metric is defined using a variant of the algorithm described

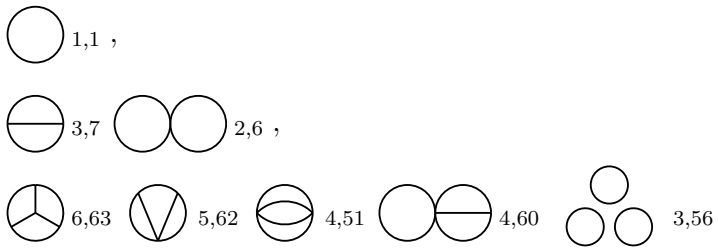

Figure 3.2: Vacuum topologies up to 3-loops consisting of the 1-loop tadpole, 2-loop Sunset, factorised 2-loop tadpole, 3-loop Mercedes-, Spectacles-, Basketball diagrams and two factorised 3-loop topologies. Sector identities sID and number of propagators t are given.

in [75]. This retrieves the graph isomorphism which is known to belong to the NP complexity class.

As an example we can *a priori* determine the number of vacuum topologies at different ℓ-loop levels. They are fixed and at 3-loop order, 5 different vacuum topologies feature (cf. fig. 3.2) which are $T_{6,63}, T_{5,62}, T_{4,51}$ of the form $3 \times (3\ell)$, $T_{4,60}$ of $(2\ell) \times (1\ell)$, and $T_{3,56}$ of factorised $(1\ell)^3$. The sector symmetry of $T_{6,63}$ is equivalent to a regular tetrahedron and thus isomorphic to the symmetric group S_4.

3.3 Algebra

Once integrals are condensed to a scalarised set, the remaining task is to deal with the different algebraic sectors of the theory. This necessitates an automatic implementation of Lorentz algebra, group Algebra, and Dirac algebra using either projectors to avoid open indices or explicit treatment of tensor structures.

3.3.1 Lorentz algebra

In the previous section, we described how Lorentz tensor indices are shifted onto the external momenta in the computation. In case of multiple external momenta it is still non-trivial to deal with the decoupled q_i.

In the following, the case of a rank-2 tensor is illuminated, namely the gluon self-energy $\Pi_{\mu\nu}$. Owing to the presence of the heat bath, eq. (2.42) constrains the possible allowed structures such that for a spatial external momentum $q_\mu = \delta_{\mu i} q_i$ three independent components $\Pi_{\mathrm{E}}, \Pi_{\mathrm{T}}$ and Π_{L} remain

$$\begin{aligned} \Pi_{00}(\mathbf{q}) &\equiv \Pi_{\mathrm{E}}(q^2) \ , \\ \Pi_{ij}(\mathbf{q}) &\equiv \left(\delta_{ij} - \frac{q_i q_j}{q^2}\right) \Pi_{\mathrm{T}}(q^2) + \frac{q_i q_j}{q^2} \Pi_{\mathrm{L}}(q^2) \ , \end{aligned} \tag{3.34}$$

which are scalar functions. The spatial part is d-dimensionally transverse ($q_j \Pi_{ij} = 0$) as required by the Slavnonv-Taylor identity [76, 77] wherefore longitudinal contributions Π_{L} vanish consistently order-by-order and possible time-spatial cross-terms Π_{0i}, Π_{i0} vanish identically.

At 2-point, Lorentz projectors are especially practical because particle conservation at the vertex fixes all external indices. Relevant for the loop calculation are

$$\begin{aligned} \mathbb{P}^{\mathrm{E}}_{\mu\nu} &= \delta_{\mu 0}\delta_{\nu 0} \ , \\ \mathbb{P}^{\mathrm{T}}_{\mu\nu} &= \delta_{\mu\nu} - \frac{q_\mu q_\nu}{q^2} \ , \\ \mathbb{P}^{\mathrm{L}}_{\mu\nu} &= \frac{q_\mu q_\nu}{q^2} \ , \end{aligned} \tag{3.35}$$

which denote the transverse $\mathbb{P}^{\mathrm{T}}_{\mu\nu}$, longitudinal $\mathbb{P}^{\mathrm{L}}_{\mu\nu}$, and temporal $\mathbb{P}^{\mathrm{E}}_{\mu\nu}$ projection operators. Contracting the generic tensor structure of the self-energy amplitude in eq. (3.34) with these projectors fixes the transverse part Π_{T}

$$\Pi = \left(P_{\mathrm{T}}\,\mathbb{P}^{\mathrm{T}}_{\mu\nu} + P_{\mathrm{L}}\,\mathbb{P}^{\mathrm{L}}_{\mu\nu} + P_{\mathrm{E}}\,\mathbb{P}^{\mathrm{E}}_{\mu\nu}\right)\Pi_{\mu\nu} = (P_{\mathrm{T}} + P_{\mathrm{E}})\Pi_{\mathrm{E}} + (d-1)P_{\mathrm{T}}\,\Pi_{\mathrm{T}} + P_{\mathrm{L}}\,\Pi_{\mathrm{L}}\,, \tag{3.36}$$

with coefficients $P_{\mathrm{E,T,L}}$. Substituting in eq. (3.35) and setting the following values for the projector coefficients P gives

$$\begin{aligned}
\Pi_{\mathrm{T}} &= \frac{1}{d-1}\left(\mathbb{P}^{\mathrm{T}}_{\mu\nu} - \mathbb{P}^{\mathrm{E}}_{\mu\nu}\right)\Pi_{\mu\nu} = \Pi\big|_{P_{\mathrm{E}}=-\frac{1}{d-1},P_{\mathrm{T}}=\frac{1}{d-1},P_{\mathrm{L}}=0}\,,\\
\Pi_{\mathrm{L}} &= \Pi\big|_{P_{\mathrm{E}}=0,P_{\mathrm{T}}=0,P_{\mathrm{L}}=1}\,,\\
\Pi_{\mathrm{E}} &= \Pi\big|_{P_{\mathrm{E}}=1,P_{\mathrm{T}}=0,P_{\mathrm{L}}=0}\,.
\end{aligned} \tag{3.37}$$

We note that within the dimensionally reduced theory tensor structures are purely spatial. Hence, the temporal Π_{E} is not present. While the simplicity of the 2-point function is particularly convenient such a treatment is less apparent and unique at higher-point correlators.

3.3.2 Group algebra

The generators T^a_{R} of a compact semi-simple Lie group form a Lie algebra

$$\left[T^a_{\mathrm{R}}, T^b_{\mathrm{R}}\right] = i f^{abc} T^c_{\mathrm{R}}\,, \tag{3.38}$$

with representation R and its totally antisymmetric structure constants f^{abc} that are independent of any representation. After normalising the structure constant also the normalisation of the generators is set for any representation. Taking traces over generators is encountered throughout almost any computation of Feynman diagrams in QCD. The appearing structures are group invariants defined as quadratic, cubic, and n-th order Casimirs $C_n(R)$

$$\delta^{ab} T^a_{\mathrm{R}} T^b_{\mathrm{R}} = C_2(R)\,, \quad d_{abc} T^a_{\mathrm{R}} T^b_{\mathrm{R}} T^c_{\mathrm{R}} = C_3(R)\,, \quad \ldots \tag{3.39}$$

Furthermore, the generators satisfy an inner product relation

$$\mathrm{Tr}\left(T^a_{\mathrm{R}} T^b_{\mathrm{R}}\right) = T(R)\delta^{ab}\,, \tag{3.40}$$

where $T(R)$ is the Dynkin index of the corresponding representation. Multiplying both sides of eq. (3.40) with δ^{ab} relates the quadratic Casimir to the index

$$d(R)C_2(R) = T(R)d(G)\,. \tag{3.41}$$

Two prominent representations of generators for the $\mathfrak{su}(N)$ algebra are the adjoint (T^a_{A}) and fundamental (T^a_{F}) representation with

$$(T^a_{\mathrm{F}})_{ij} = (T^a)_{ij}\,, \quad (T^a_{\mathrm{A}})_{bc} = -i f^{abc}\,, \tag{3.42}$$

where $i,j \in \{1,\ldots,N\}$ and $a,b \in \{1,\ldots,N^2-1\}$. Using that the group dimension $d(\mathrm{SU}(N)) = N^2-1$, distinct values of dimensions and group invariants of these two representations for a general $\mathrm{SU}(N)$ are

$$\begin{aligned}
\text{adj.:}\quad & d_{\mathrm{A}} = (N^2-1)\,, \quad C_{\mathrm{A}} = N\,, \quad T_{\mathrm{A}} = N\,,\\
\text{fund.:}\quad & d_{\mathrm{F}} = N\,, \quad C_{\mathrm{F}} = \frac{(N^2-1)}{2N}\,, \quad T_{\mathrm{F}} = \frac{1}{2}\,,
\end{aligned} \tag{3.43}$$

Listing 3.4: Factorised colour structure of eq. (3.1) with fundamental traces of the form `tr3(a1,...,an)` from eq. (3.48).

```
1 [diag]=
2   +tr3(a3i9,a3i10)*tr3(a3e1,a3e2)*
3   tr3(a3i9,t3(i3i5,i3i2))*
4   tr3(a3i10,t3(i3i3,i3i8))*
5   tr3(a3e1,t3(i3i1,i3i4))*
6   tr3(a3e2,t3(i3i7,i3i6))*
7   d_(i3i1,i3i2)*d_(i3i3,i3i4)*d_(i3i5,i3i6)*d_(i3i7,i3i8)*
8   (499 terms);
```

Listing 3.5: Factorised colour structure of eq. (3.1) after applying the Fierz identity (3.46). `Ca3` is the adjoint and `Cf3` the fundamental quadratic Casimir

```
1 [diag]=
2   +Cf3*( 499 terms)
3   +Ca3*( 499 terms);
```

using $\delta^{ab}\delta^{ab} = d(R)$. This allows to project open group indices of n-point gauge field correlators and is practical to treat the 2-point colour gauge field external structure. For any representation, the relation

$$\mathrm{Tr}\left(\left[T^a_{\mathrm{R}}, T^b_{\mathrm{R}}\right]T^c_{\mathrm{R}}\right) = if^{abd}\mathrm{Tr}\left(T^d_{\mathrm{R}}T^c_{\mathrm{R}}\right) = if^{abc}T(R)\,, \tag{3.44}$$

translates traces over generators to the structure constants of the group up to the index of the representation. Ultimately adjoint generators are traded for traces over fundamental ones

$$if^{abc}T_{\mathrm{F}} = \mathrm{Tr}\left(\left[T^a, T^b\right]T^c\right)\,. \tag{3.45}$$

The latter decomposes further by using the Fierz identity

$$(T^a)_{ij}(T^a)_{kl} = \frac{1}{2}\left(\delta_{il}\delta_{kj} - \frac{1}{N}\delta_{ij}\delta_{kl}\right)\,, \tag{3.46}$$

that splits contracted fundamental $\mathfrak{su}(N)$ generators where a is summed implicitly. The identity states that the generators form a complete set of traceless $N \times N$ matrices, where tracelesness is implemented by the $1/N$-term. A powerful application is that, any trace in any representation can be brought back to traces over fundamental generators and products of traces are translated to single traces.

Typical terms that appear in a computation contract T^a from multiple traces

$$\mathrm{Tr}\left(\ldots T^a \ldots\right)\mathrm{Tr}\left(\ldots T^a \ldots\right)\,. \tag{3.47}$$

In case of external particles in the fundamental representation the overall colour structure consists of T^a-strings $(T^{a_1}\ldots T^{a_n})_{ij}$. In our example (3.1) the following colour structure is factored off the remaining terms and takes the form in listing 3.4 with fundamental traces and strings of generators

$$\begin{aligned}\texttt{tr3(a1,...,an)} &= \mathrm{Tr}\left(T^{a_1}\ldots T^{a_n}\right)\,,\\ \texttt{tr3(a1,...,an,t3(i1,i2))} &= \left(T^{a_1}\ldots T^{a_n}\right)_{i_1 i_2}\,.\end{aligned} \tag{3.48}$$

After applying the Fierz identity eq. (3.46) the colour factor simplifies significantly giving rise to its adjoint (`Ca3`) and fundamental quadratic Casimirs (`Cf3`); see listing 3.5.

In general higher-loop computations introduce higher-order group invariants [78]. The reason for this is that traces can span over many more group generators than the ones outlined above. Therefore, the colour structures of different terms after applying the Fierz identity can always be mapped onto the basis of group invariants.

3.4 Automated sum-integral reduction

In the passing, we establish a compact parameterisation for tadpole sum-integrals with vectors $\underline{s} \in \mathbb{Z}^M$ and $\underline{\alpha} \in \mathbb{N}^{N_k}$

$$\begin{aligned} Z^{\alpha_1}_{s_1;\sigma_1} &\equiv \sum\!\!\!\!\!\!\int_{K\{\sigma_1\}} \frac{k_0^{\alpha_1}}{\Delta_K^{s_1}} \,, \\ Z^{\alpha_1\alpha_2}_{s_1s_2s_3;\sigma_1\sigma_2} &\equiv \sum\!\!\!\!\!\!\int_{K_1\{\sigma_1\}K_2\{\sigma_2\}} \frac{k_{1_0}^{\alpha_1} k_{2_0}^{\alpha_2}}{\Delta_{K_1}^{s_1}\Delta_{K_2}^{s_2}\Delta_{K_1-K_2}^{s_3}} \,, \\ Z^{\alpha_1\alpha_2\alpha_3}_{s_1s_2s_3s_4s_5s_6;\sigma_1\sigma_2\sigma_3} &\equiv \sum\!\!\!\!\!\!\int_{K_1\{\sigma_1\}K_2\{\sigma_2\}K_3\{\sigma_3\}} \frac{k_{1_0}^{\alpha_1} k_{2_0}^{\alpha_2} k_{3_0}^{\alpha_3}}{\Delta_{K_1}^{s_1}\Delta_{K_2}^{s_2}\Delta_{K_3}^{s_3}\Delta_{K_1-K_2}^{s_4}\Delta_{K_1-K_3}^{s_5}\Delta_{K_2-K_3}^{s_6}} \,, \end{aligned} \tag{3.49}$$

employing propagators $\Delta_K = K^2$ with implicit masses on the lines when unambiguous. Otherwise they are made explicit $\Delta_{K,m} = K^2 + m^2$. Also the fermion signature is implied in the Matsubara four-momenta $K^2 = [(2n + \sigma_i)\pi T]^2 + \mathbf{k}^2$ and $\sigma_i = 0(1)$ for bosons(fermions). The inclusion of a chemical potential in the partition function eq. (2.1) induces a shift in the zero-component of the fermionic momenta $K_{\mathrm{F}} \to K_{\mathrm{F}} + (i\mu, \mathbf{0})$ or accordingly in the Matsubara frequencies

$$\omega_n^{\mathrm{F}} \to \tilde{\omega}_n^{\mathrm{F}} = \omega_n^{\mathrm{F}} + i\mu = (2n+1)\pi T + i\mu \,. \tag{3.50}$$

Generally also bosonic and fermionic masses are allowed. Full bosonic integrals with $\{\sigma_i\} = \underline{\sigma} = \mathbf{0}$ or $\{\alpha_i\} = \underline{\alpha} = \mathbf{0}$ are identified as

$$Z^{\mathbf{0}}_{\underline{s};\mathbf{0}} \equiv Z_{\underline{s}} \,. \tag{3.51}$$

For computations with massless bosons different fermionic masses $\{m_i\} = \underline{m} \neq \mathbf{0}$ allow a compressed notation

$$Z^{\underline{\alpha}}_{\underline{s};\underline{m};\underline{\sigma}} \equiv Z^{\underline{\alpha}}_{\underline{s};\{m_i\sigma_i\}} \,. \tag{3.52}$$

Vacuum integrals in d-dimensions will be denoted in equal fashion but as

$$I_{\underline{s};\underline{m}} \,, \tag{3.53}$$

only consisting of subscripts.

The computation becomes more involved when considering fermionic lines since traces over gamma matrices require correct monitoring of fermion chains inside the diagrams. Open fermionic lines can only appear on external legs while internally fermions form only closed loops due to fermion number conservation at each vertex. Therefore, every vertex reduces the number of independent line signatures σ_i by one. For the 2-loop tadpole sum-integral in eq. (3.49) one relation exists:

$$\sigma_1 = (\sigma_2 + \sigma_3) \pmod 2 \,. \tag{3.54}$$

Most efficiently one iteratively contracts vertices and propagators around the loop to obtain an ordered list of Lorentz indices and colour indices. Those can be used for γ_μ-matrix- and colour tensor contraction. As from 3-loop level onwards more than one fermion loop is encountered, these need to be treated separately handling both Dirac and colour algebra along the loop.

After all the above considerations, the final list of vacuum integrals is in general still large. For the example in eq. (3.1) there are $\sim \mathcal{O}(100)$ integrals to be calculated as seen in listing 3.6 using the internal representations

$$Z^{\underline{\alpha}}_{\underline{s};\underline{m};\underline{\sigma}} = \texttt{Z}(\texttt{fb}(\underline{\texttt{s}}), \texttt{fm}(\underline{\texttt{m}}), \texttt{fc}(\underline{\sigma}), \texttt{fq0}(\underline{\alpha})) \,, \tag{3.55}$$

$$I_{\underline{s};\underline{m}} = \texttt{Z}(\texttt{fb}(\underline{\texttt{s}}), \texttt{fm}(\underline{\texttt{m}})) \,. \tag{3.56}$$

Listing 3.6: List of vacuum diagrams for eq. (3.1) after external momentum expansion and tensor integral decomposition. The different integrals correspond to the notation in eq. (3.55).

```
[diag]=
  +Z(fb(1,1,1),fm(1,1,0),fc(1,1),fq0(0,0))*( 6 terms)
  +Z(fb(1,1,2),fm(1,1,0),fc(1,1),fq0(0,0))*( 10 terms)
  +Z(fb(1,1,2),fm(1,1,0),fc(1,1),fq0(1,1))*( 4 terms)
  +Z(fb(2,1,0),fm(1,0,0),fc(1,0),fq0(0,0))*( 4 terms)
  +Z(fb(2,1,0),fm(1,1,0),fc(1,1),fq0(0,0))*( 4 terms)
  +Z(fb(2,1,1),fm(1,1,0),fc(1,1),fq0(0,0))*( 10 terms)
  +( 65 lines)
  +Z(fb(5,1,1),fm(1,1,0),fc(1,1),fq0(4,0))*( 2 terms);
```

3.4.1 Integration-by-parts identities

Integration-by-parts (IBP) identities [65, 66] take a pivotal role in multi-loop calculations. Their ability to reduce the number of Feynman integrals by extracting linear relations amongst them provides a powerful tool using the differential operator

$$O_{ij} = \frac{\partial}{\partial k_i^\mu} k_j^\mu \,, \tag{3.57}$$

and inserting it into the integrand I'. The resulting integral, a surface term,

$$0 = \int_{k_i} \frac{\partial}{\partial k_{i,\mu}} p_\mu \, I'(k_1, \ldots, k_{N_k}, q_1, \ldots, q_{N_q}) \,, \quad i = 1, \ldots, N_k \,, \tag{3.58}$$

vanishes according to the d-dimensional divergence theorem where p_μ is a linear combination of loop- and external momenta in line with eq. (3.3). The index i is not summed over as it holds individually for every loop momentum k_i.

A generalisation to finite temperature is straightforward [22]. In eq. (2.8) we have seen that the $(d+1)$-theory in the ITF is one of a sum over an infinite number of massive fields that live in d-dimensions. The dynamical degrees of freedom are the d-dimensional momenta and the Matsubara frequencies act as masses. The salient point is that by applying the d-dimensional differential operators of eq. (3.58) under a sum-integral every term in the sum equates to zero individually. As an example, we look at the 1-loop tadpole integral $Z^{\alpha_1}_{s_1;\sigma_1}$ with general mass on the propagator $\Delta_{K,m} = K^2 + m^2$ with particle signature $\sigma_1 = 0(1)$ and $D = d + 1$

$$\begin{aligned}
0 &= \sum\!\!\!\!\!\!\int_{K\{\sigma_1\}} \frac{\partial}{\partial k_i} \left\{ k_i \, \frac{k_0^{\alpha_1}}{\Delta_{K,m}^{s_1}} \right\} = \sum\!\!\!\!\!\!\int_{K\{\sigma_1\}} \left\{ d \, \frac{k_0^{\alpha_1}}{\Delta_{K,m}^{s_1}} - 2s_1 \mathbf{k}^2 \frac{k_0^{\alpha_1}}{\Delta_{K,m}^{s_1+1}} \right\} \\
&= \sum\!\!\!\!\!\!\int_{K\{\sigma_1\}} \left\{ (d - 2s_1) \frac{k_0^{\alpha_1}}{\Delta_{K,m}^{s_1}} + 2s_1 \frac{k_0^{\alpha_1+2}}{\Delta_{K,m}^{s_1+1}} + 2s_1 m^2 \frac{k_0^{\alpha_1}}{\Delta_{K,m}^{s_1+1}} \right\} \\
&= (d - 2s_1) \, Z^{\alpha_1}_{s_1;\sigma_1} + 2s_1 \, Z^{\alpha_1+2}_{s_1+1;\sigma_1} + 2s_1 m^2 \, Z^{\alpha_1}_{s_1+1;\sigma_1} \,.
\end{aligned} \tag{3.59}$$

Arising scalar products are converted into propagators by replacing

$$\mathbf{k}^2 = \Delta_{K,m} - k_0^2 - m^2 \,. \tag{3.60}$$

The final recurrence relation yields

$$\begin{aligned}
Z^{\alpha_1+2}_{s_1+1;\sigma_1} &= \frac{2s_1 - d}{2s_1} \, Z^{\alpha_1}_{s_1;\sigma_1} - m^2 \, Z^{\alpha_1}_{s_1+1;\sigma_1} \,, \\
\mathbf{1}_+ \mathbf{1}^+ &= \frac{2s_1 - d}{2s_1} - m^2 \mathbf{1}_+ \,,
\end{aligned} \tag{3.61}$$

where the last line uses the raising and lowering operators for propagators ($\mathbf{n}_\pm$) and Matsubara frequencies ($\mathbf{n}^\pm$)

$$\begin{aligned}\mathbf{n}_\pm\, Z^{\underline{\alpha}}_{\underline{s}} &= Z^{\underline{\alpha}}_{\dots s_n \pm 1 \dots}\,,\\ \mathbf{n}^\pm\, Z^{\underline{\alpha}}_{\underline{s}} &= Z^{\dots \alpha_n \pm 2 \dots}_{\underline{s}}\,.\end{aligned} \tag{3.62}$$

This allows to translate thermal massive IBPs to either vacuum zero-temperature IBPs by setting all $\mathbf{n}^\pm = 0$ or massless IBPs by letting all $m_i = 0$. Analogously the O_{ij} generate a set of $N_{\text{IBP}} = N_k(N_k + N_q)$ relations. The vacuum diagrammatic result at 2-loop order produces $O_{ij} = \{O_{11}, O_{12}, O_{21}, O_{22}\}$ that form a coupled system of partial recurrence relations

$$\begin{aligned}0 &= (d - 2s_1 - s_3) + s_3\,\mathbf{3}_+(\mathbf{2}_- - \mathbf{1}_-) + 2s_1\,\mathbf{1}_+(\mathbf{1}^+ + m_1^2)\\ &\quad + s_3\,\mathbf{3}_+(\mathbf{1}^+ - \mathbf{2}^+ + \mathbf{3}^+ + m_1^2 - m_2^2 + m_3^2)\,,\\ 0 &= (s_3 - s_2) + s_2\,\mathbf{2}_+(\mathbf{3}_- - \mathbf{1}_-) + s_3\,\mathbf{3}_+(\mathbf{1}_- - \mathbf{2}_-)\\ &\quad + s_2\,\mathbf{2}_+(\mathbf{1}^+ + \mathbf{2}^+ - \mathbf{3}^+ + m_1^2 + m_2^2 - m_3^2) - s_3\,\mathbf{3}_+(\mathbf{1}^+ - \mathbf{2}^+ + \mathbf{3}^+ + m_1^2 - m_2^2 + m_3^2)\,,\\ 0 &= (s_3 - s_1) + s_1\,\mathbf{1}_+(\mathbf{3}_- - \mathbf{2}_-) + s_3\,\mathbf{3}_+(\mathbf{2}_- - \mathbf{1}_-)\\ &\quad + s_1\,\mathbf{1}_+(\mathbf{2}^+ + \mathbf{1}^+ - \mathbf{3}^+ + m_2^2 + m_1^2 - m_3^2) - s_3\,\mathbf{3}_+(\mathbf{2}^+ - \mathbf{1}^+ + \mathbf{3}^+ + m_2^2 - m_1^2 + m_3^2)\,,\\ 0 &= (d - 2s_2 - s_3) + s_3\,\mathbf{3}_+(\mathbf{1}_- - \mathbf{2}_-) + 2s_2\,\mathbf{2}_+(\mathbf{2}^+ + m_2^2)\\ &\quad + s_3\,\mathbf{3}_+(\mathbf{2}^+ - \mathbf{1}^+ + \mathbf{3}^+ + m_2^2 - m_1^2 + m_3^2)\,.\end{aligned} \tag{3.63}$$

The linear transformations of the IBP relations are exploited to map amplitudes as a sum over irreducible Master Integrals (MI) I_i [79]

$$I(\underline{s}) = \sum_i r_i(d, \xi) I_i(d)\,, \tag{3.64}$$

where r_i are rational functions of the form $\text{poly}_i(d, \xi)/\text{poly}_i(d)$. This subset is irreducible and integrals cannot be expressed as a linear combination of others. Their number is known to be always finite [23] and possible to be determined *a priori* the reduction process [79].

The generators O_{ij} have properties of elements of a Lie group [80]. That is they fulfill the commutation relations

$$[O_{ij}, O_{i'j'}] = \delta_{ij'} O_{i'j} - \delta_{i'j} O_{ij'}\,, \tag{3.65}$$

which decimates the effective set of IBP relations to a total amount of $N_{\text{IBP}} = N_k + N_e + 1$ for a given point in parameter space $\underline{s}$. Since the system of equations of an IBP reduction is overdetermined knowing *a priori* which information is redundant decreases the computational effort in the solution.

One can also show that Lorentz-invariance (LI) identities are merely a composition of IBP relations. IBP relations are part of the class of generalised recurrence relations [81, 82, 83]. These relate integrals of different spacetime dimensions and reduce them even further.

3.4.2 The Laporta algorithm

With growing system size, number of loop momenta $N_k > 1$ and IBPs in eq. (3.58) one is confronted with a system of multivariate difference equations. In order to tackle this problem with discrete mathematics, extreme efforts have to be taken and in most cases no closed solution can be found with current methods. Practically, certain algorithms allow to solve the system of equations and still find a reduction using direct decomposition-by-intersection methods [84, 85, 86] or systematic Gaussian elimination. The latter is known as the Laporta algorithm [67] and in the following a brief outline is given.

The first step is to establish a unique ordering prescription for integrals using lexicographical ordering. This provides a metric in the parametric search space of integrals and the complexity of an integral is determined unambiguously. From eq. (3.49) the following succession is implemented as the most complex integral using eqs. (3.9)–(3.13):

(1) Largest t,

(2) Largest r,

(3) Largest s,

(4) Largest q,

(5) Greatest power s_i,

(6) Greatest power α_i.

Steps (1)–(4) determine the integral complexity and (5)–(6) its uniqueness. For fixed integral mass dimension with eq. (3.68) steps (1)–(3) already define the integral uniquely.

To cover the search space of all integrals that are needed, IBP generators are applied on a list of initially supplied seed integrals. These consist of all possible integrals up to fixed (t, r, s) at zero-T and (t, r, s, q) for finite-T. Thus, for every combination of (t, r, s, q) one finds

$$\mathcal{N}(I_{trs}) = \binom{r-1}{t-1}\binom{s+M-t-1}{M-t-1}\,, \tag{3.66}$$

$$\mathcal{N}(I_{trsq}) = \mathcal{N}(I_{trs})\binom{N_k+q}{N_k}\,, \tag{3.67}$$

integrals where the first binomial factor counts the number of distributions of positive powers and the second factor counts the remaining combinations for negative powers of denominators. For finite temperature this gets multiplied by the factor of possible powers of Matsubara frequencies producing $\mathcal{N}(I_{trsq})$ thermal seeds.

The resulting system of IBP relations is ordered according to the above prescription. That is first every equation is tagged by its most complicated integral, which we define as its complexity. Then the ordering descends starting from the least complex relation, which is the one with the simplest integral representative. This list is supplied to the Laporta algorithm.

If temperature is the only scale of the integrals, the IBP relations do not mix dimensions amongst the thermal sum-integrals. From eq. (3.57) it is clear that any IBP generator acts dimensionless leaving the mass dimension untouched. This has an immediate implication on massless thermal sum-integrals of eq. (3.49):

$$\dim[Z^{\underline{\alpha}}_{\underline{s}}] = N_k D + \sum_{i=1}^{N_k}\alpha_i - 2\sum_{i=1}^{M} s_i\,, \tag{3.68}$$

for any level in the reduction. This stands in contrast to the scenario where more scales are involved or at $T = 0$. In the latter case mass dimensions allow the whole tower of seeds to take part in the reduction.

The Laporta algorithm (c.f. algorithm 1) starts from the least complex IBP relation

$$0 = \sum_j c_j Z_j\,. \tag{3.69}$$

This contains its most complicated integral Z_j which is brought to the l.h.s. expressing it in terms of simpler ones

$$Z_l = -\sum_{j\neq l} c'_j Z_j\,, \quad c'_j = \frac{c_j}{c_l}\,. \tag{3.70}$$

Listing 3.7: List of master integrals of eq. (3.1) after IBP redcution with relations in eq. (3.63). The integrals correspond to the notation in eq. (3.55).

```
[diag]=
  +Z(fb(1),fm(0),fc(0),fq0(0))*Z(fb(2),fm(1),fc(1),fq0(0))*( 2 terms)
  +Z(fb(1),fm(0),fc(0),fq0(0))*Z(fb(3),fm(1),fc(1),fq0(0))*( 2 terms)
  +Z(fb(1),fm(1),fc(1),fq0(0))*Z(fb(2),fm(0),fc(0),fq0(0))*( 2 terms)
  +Z(fb(1),fm(1),fc(1),fq0(0))*Z(fb(2),fm(1),fc(1),fq0(0))*( 2 terms)
  +Z(fb(1),fm(1),fc(1),fq0(0))*Z(fb(3),fm(1),fc(1),fq0(0))*( 2 terms)
  +Z(fb(2),fm(0),fc(0),fq0(0))*Z(fb(2),fm(1),fc(1),fq0(0))*( 2 terms)
  +Z(fb(2),fm(1),fc(1),fq0(0))^2*( 4 terms)
  +Z(fb(2),fm(1),fc(1),fq0(0))*Z(fb(3),fm(1),fc(1),fq0(0))*( 2 terms)
  +Z(fb(1,1,2),fm(1,1,0),fc(1,1),fq0(0,0))*( 2 terms)
  +Z(fb(2,1,2),fm(1,1,0),fc(1,1),fq0(0,0))*( 2 terms);
```

This has the advantage that resubstitution into previously solved IBPs is unnecessary as it will be the first time Z_j is encountered. The resulting identity is substituted in all other yet to be solved IBP relations. This is the same procedure as Gaussian elimination and the process is repeated until the number of solved equations surpasses the number of degrees of freedom i.e. integrals that need to be solved for.

Algorithm 1 Laporta algorithm [67]

Require: Initialise $i = j = 0$, $k = 0$, $i_{\max} = \mathcal{N}(t, r, s, q)$, $N_{\text{IBP}} = N_k(N_k + N_q)$
  for $i < i_{\max}$ **do**
    for $j < N_{\text{IBP}}$ **do**
      Apply j-th IBP on i-th seed
      Symmetrise integrals of j-th IBP relation
    end for
  end for
  while $N > 0$ **do**
    Solve least complex relation $0 = \sum_j c_j Z_j$ for most complicated integral Z_l therein.
    Resubstitution
  end while

Extra care has to be taken with spurious poles which are singular pre-factors of master diagrams. Sometimes the coefficients in the linear relations of the acquired IBP relations can have poles for certain dimension. To circumvent this issue one needs to find basis transformations by hand or via automation.

Depending on the order in the expansion of external momenta the list of vacuum diagrams reduces significantly. Only a few master integrals of eq. (3.1) remain for leading order in the external momentum q. Some of the 2-loop integrals have factorised to 1-loop tadpoles; see listing 3.7.

3.5 Master sum-integrals

At some point all the information of scale separation and symmetry aspects is depleted and the remaining master sum-integrals are maximally reduced. At zero temperature various algorithms were developed in great extent using difference equations [67], sector decomposition [87], differential equations [88], or Harmonic Polylogarithms [89]. When it comes to sum-integrals this final step is a far less automated process.

Indeed, the sum-integral analytic structure is the root source for a whole set of difficulties. As rotational invariance $\mathrm{O}(d)$ only holds for the spatial components of integration momenta the temporal ones take the role of non-dynamical masses. For every loop order of integration

one additional scale enters the integral such that at N_k-loop integrations one faces a N_k-scale problem. Not only increases this the dimension of the search space during an IBP it also significantly worsens the number of possible master diagrams.

Purely massless integrals permit a semi-automatic treatment employing methods used by Arnold and Zhai [90]. At lower loop levels these approaches work successfully. To reach higher levels the general idea is to exploit analytically known lower-loop sub-topologies of the diagram. Naturally at one-loop most integrals can be solved analytically for the massless case. Once more scales and especially masses are included, only numerical solutions exist even at one-loop order.

3.5.1 Massive sum-integrals

The "Saclay method" [91, 92] allows to handle most of these integrals as shown in [93]. This approach first computes the frequency sums before splitting the integral into vacuum and temperature-dependent pieces. The idea is to convert the N_k-fold summation over Matsubara frequencies into a M-fold one for every propagator by inserting the representation of Kronecker-delta functions

$$\delta(k_0) = T \int_0^\beta \mathrm{d}\tau \, e^{ik_0\tau} \, . \tag{3.71}$$

Thereafter, one iteratively applies the Saclay representations of the propagators $G(\tau)$ and $\tilde{G}(\tau)$ in eqs. (2.12) and (2.13) and integrates over the remaining τ. Exponentials are then removed by converting them into distribution functions

$$e^{\beta\omega} n_{\mathrm{B/F}} = \frac{e^{\beta\omega}}{e^{\beta\omega} \mp 1} = \left(1 \pm \frac{1}{e^{\beta\omega} \mp 1}\right) = (1 \pm n_{\mathrm{B/F}}) \, , \tag{3.72}$$

such that the resulting expression contains monomials of maximal order $(n_{\mathrm{B/F}})^{N_k}$ and fractions of linear combinations of the M energies ω_k.

The simplest example is the 1-loop massive (fermionic) bosonic tadpole $\sigma = 0(1)$ which accords with the $\tau = 0$ special case of their mixed propagators eqs. (2.12) and (2.13). Therein the frequency summation is straightforward and the emergent terms are grouped into a massive vacuum tadpole and a temperature-dependent integral with one power of the distribution function

$$Z_{1;\sigma} = \sum\!\!\!\!\!\!\int_{K\{\sigma\}} \frac{1}{\left[K^2 + m_1^2\right]} = I_1^{\mathrm{vac}}(m_1) + \int_{\mathbf{k}} \frac{1}{2\omega_1} \Big[n_+(\omega_1) + n_-(\omega_1) \Big] \tag{3.73}$$

$$= I_1^{\mathrm{vac}}(m_1) + Z_{1;\sigma}^T \, , \tag{3.74}$$

with $Z_{1;\sigma}^T$ from eq. (A.43). The two distributional cases are defined implicitly

$$n_\pm(\omega) = \begin{cases} n_{\mathrm{B}}(\omega) & \text{(bosons)} \\ -n_{\mathrm{F}}(\omega \pm \mu) & \text{(fermions)} \end{cases} \tag{3.75}$$

In the zero-mass and zero chemical potential limit the momentum integral allows an explicit evaluation eq. (A.39). Special care has to be taken in the summation of the fermionic imaginary-time propagator $\tilde{G}(\tau)$ as it is not symmetric under $\tau \to -\tau$ in the presence of a chemical potential.

However, once $m \neq 0$ no closed form exists[1]. Further denominator powers $s_i > 1$ of $Z_{s_i;1}$ are evaluated in appendix A.3 by taking mass derivatives. A physical interpretation of the second finite-temperature term is that of forward scattering of an external particle off a particle in the plasma. A diagrammatical application of this procedure are the cutting rules of thermal integrals introduced in [94].

[1] Nonetheless, for $\mu \neq 0$ and $m = 0$ closed forms exist with examples in appendix A.3.

Chapter 4

Testing accuracy of Dimensional Reduction: Higher-order operators

This chapter, summarising the work reported in [1], investigates the accuracy of Dimensional Reduction (DR) and motivates the inclusion of higher-order operators when reaching higher accuracy levels in the DR of QCD [95, 96, 97, 98, 99]. As a consequence, their significance for the dynamics at the ultrasoft scale emerges.

Higher levels of accuracy in the matching of the effective field theories necessitate the approach of higher loop levels. Thus, we reproduce the 3-loop gauge coupling from four-dimensional Yang-Mills theory and argue that its $(1/\epsilon)$-logarithmic infrared divergence after renormalisation as found in [100] is a natural consequence of the absence of decoupling in thermal effective theories [50].

As an introduction, we revisit the first appearance of the operator-augmented dimensionally reduced theory of hot QCD in a computation by Chapman [101] in arbitrary dimension and generalise its concepts.

4.1 Dimensionally reduced effective theories of QCD

The dimensional reduction of QCD, by the generic rules in [49], undergoes two stages (cf. table 4.1). First non-zero Matsubara modes are integrated out which encompasses all fermionic ψ_n and non-zero bosonic $A_{n\neq 0}$ degrees of freedom. The resulting dimensionally reduced EFT is purely bosonic, known as Electrostatic QCD (EQCD) and defined by the action

$$S_{\mathrm{EQCD}}[A] \equiv \int_X \mathcal{L}_{\mathrm{EQCD}}[A] \,, \tag{4.1}$$

$$\begin{aligned}\mathcal{L}_{\mathrm{EQCD}}[A] \equiv{}& \frac{1}{4}F_{ij}^a F_{ij}^a + \frac{1}{2}\mathcal{D}_i^{ab}A_0^b\mathcal{D}_i^{ac}A_0^c + \frac{1}{2}m_{\mathrm{E}}^2 A_0^a A_0^a \\ &+ \frac{1}{4!}\lambda_{\mathrm{E}}^{(1)}A_0^a A_0^a A_0^b A_0^b + \frac{1}{4!}\lambda_{\mathrm{E}}^{(2)}X^{abcd}A_0^a A_0^b A_0^c A_0^d \,,\end{aligned} \tag{4.2}$$

where $\int_X \equiv \frac{1}{T}\int_{\mathbf{x}}$ since the fields reside in d-dimensions and the τ-integration yields the prefactor $1/T = \int_0^\beta \mathrm{d}\tau$. The theory was used successfully in the past to study the high temperature behaviour of QCD [95].

Other structures appearing in the Lagrangian are

$$\mathcal{D}_i^{ab} = \delta^{ab}\partial_i - g_{\mathrm{E}}f^{abc}A_i^c \,, \quad (A_0)_{ab} = -if^{abc}A_0^c \,, \quad \mathrm{Tr}\, T^a T^b = -X^{ab} = \delta^{ab}N_{\mathrm{c}} \,. \tag{4.3}$$

Start: **Thermal QCD**

Scale	Validity	Dimension	Lagrangian	Fields	Parameters
Hard	πT	$d+1$	$\mathcal{L}_{\text{QCD}}$ (2.44)	$F_{\mu\nu}, \psi_i, c^a$	g, m_i
		↓ *Integrate out* $n \neq 0$ *modes and fermions*			
Soft	gT	d	$\mathcal{L}_{\text{EQCD}}$ (4.1)	F_{ij}, A_0, c^a	$g_{\text{E}}, m_{\text{E}}, \lambda_{\text{E}}^{(1)}, \lambda_{\text{E}}^{(2)}$
		↓ *Integrate out temporal adjoint scalar* A_0			
Ultrasoft	g^2T/π	d	$\mathcal{L}_{\text{MQCD}}$ (4.14)	F_{ij}, c^a	$g_{\text{M}}, m_{\text{M}}$

End: d**-dimensional Yang-Mills**

Table 4.1: Dimensional reduction of $(d+1)$-dimensional hot QCD into effective d-dimensional theories based on the scale hierarchy at high temperature. The effective couplings are functions of the couplings of their parent theories and temperature and are determined by a matching procedure. The first step integrates out all hard non-zero modes. The second step integrates out the temporal adjoint scalar A_0 with soft Debye mass m_{E}. At the ultrasoft scale, only ultrasoft spatial gauge fields A_i remain.

$(T_{\text{A}}^a)_{bc} = -if^{abc}$ from eq. (3.42) are the Hermitian generators of $\mathfrak{su}(N_{\text{c}})$ in the adjoint representation with the electrostatic coupling g_{E} and the covariant derivative

$$F_{ij} = \frac{i}{g_{\text{E}}}[D_i, D_j] \,, \quad D_i[A] = \partial_i - ig_{\text{E}}A_i \,. \tag{4.4}$$

The general form of colour tensors

$$X^{a_1a_2\ldots a_n} \equiv f^{m_n a_1 m_1} f^{m_1 a_2 m_2} \cdots f^{m_{n-1} a_n m_n} \,, \tag{4.5}$$

compactly denotes traces over n-adjoint generators $\text{Tr}\,(T_{\text{A}}^{a_1} \ldots T_{\text{A}}^{a_n}) = (-i)^n X^{a_1\cdots a_n}$ and captures all arising colour structures of operators in the Lagrangian with symmetry properties filed in appendix A of [1]. These are exploited to generate the arising Feynman rules.

It is to be noted that the operator basis for the adjoint scalars couplings $\lambda_{\text{E}}^{(1)}, \lambda_{\text{E}}^{(2)}$ is redundant because of the linear relation $\text{Tr}\, A_0^4 = \frac{1}{2}(\text{Tr}\, A_0^2)^2$ for $N_{\text{c}} \leq 3$. Focussing on general N_{c}, the distinction between these operators is kept.

Another possibility to represent the scalar operators is the fundamental representation (cf. e.g. [57]). To illustrate their agreement, we rewrite $\lambda_{\text{E}}^{(1,2)} = \lambda_{\text{E,A}}^{(1,2)}$ in the adjoint scalar sector $\mathcal{L}_{\text{A}}$ of the EQCD Lagrangian in eq. (4.2) which provides again a complete basis. The latter is compared with the fundamental scalar sector $\mathcal{L}_{\text{F}}$ of the Lagrangian from [57]

$$\mathcal{L}_{\text{A}} = \frac{1}{4!}\lambda_{\text{E,A}}^{(1)} \left(\text{Tr}_{\text{A}}\big[A_0^2\big]\right)^2 + \frac{1}{4!}\lambda_{\text{E,A}}^{(2)} \,\text{Tr}_{\text{A}}\big[A_0^4\big] \,, \tag{4.6}$$

$$\mathcal{L}_{\text{F}} = \lambda_{\text{E,F}}^{(1)} \left(\text{Tr}_{\text{F}}\big[A_0^2\big]\right)^2 + \lambda_{\text{E,F}}^{(2)} \,\text{Tr}_{\text{F}}\big[A_0^4\big] \,. \tag{4.7}$$

After symmetrisation of both terms, the conversion $\{\lambda_{\text{E,A}}^{(1)}, \lambda_{\text{E,A}}^{(2)}\} \mapsto \{\lambda_{\text{E,F}}^{(1)}, \lambda_{\text{E,F}}^{(2)}\}$ identifies

$$\lambda_{\text{E,F}}^{(1)} = \frac{1}{12}\left(2N_{\text{c}}^2\lambda_{\text{E,A}}^{(1)} + 3\lambda_{\text{E,A}}^{(2)}\right) \,, \quad \lambda_{\text{E,F}}^{(2)} = \frac{N_{\text{c}}}{12}\lambda_{\text{E,A}}^{(2)} \,. \tag{4.8}$$

We drop the subscripts (F, A) retaining $\lambda_{\text{E,A}}^{(1,2)} = \lambda_{\text{E}}^{(1,2)}$ since all coefficients are henceforth in the adjoint representation as instituted in the action (4.1). Upon further notice colour traces are understood in the adjoint representation $\text{Tr}_{\text{A}}\{AB\} = \text{Tr}\,\{AB\} = A_{ab}B_{ba}$ denoting Tr_{R} as the trace in general representation (R). At higher loop orders additional group

invariant structures appear (cf. sec. 3.3.2). Hence, defining the scalar coupling parameters more compactly proves beneficial

$$\begin{aligned}
\lambda &\equiv \frac{(N_\mathrm{c}^2+1)}{12N_\mathrm{c}}\frac{\lambda_\mathrm{E}^{(1)}}{g_\mathrm{E}^2} + \frac{5N_\mathrm{c}}{24}\frac{\lambda_\mathrm{E}^{(2)}}{g_\mathrm{E}^2}\,, \\
\kappa_1 &\equiv \frac{10}{6N_\mathrm{c}}\frac{\lambda_\mathrm{E}^{(1)}}{g_\mathrm{E}^2} + \frac{(N_\mathrm{c}^2+36)}{12N_\mathrm{c}}\frac{\lambda_\mathrm{E}^{(2)}}{g_\mathrm{E}^2}\,, \\
\kappa_2 &\equiv \frac{(N_\mathrm{c}^2+1)}{18N_\mathrm{c}^2}\left(\frac{\lambda_\mathrm{E}^{(1)}}{g_\mathrm{E}^2}\right)^2 + \frac{5}{18}\frac{\lambda_\mathrm{E}^{(1)}\lambda_\mathrm{E}^{(2)}}{g_\mathrm{E}^4} + \frac{(N_\mathrm{c}^2+36)}{144}\left(\frac{\lambda_\mathrm{E}^{(2)}}{g_\mathrm{E}^2}\right)^2 .
\end{aligned} \tag{4.9}$$

The contributing operators in the above action render the dimensionally reduced theory super-renormalisable

$$g_\mathrm{E}^2 = g_\mathrm{ER}^2\mu^{2\epsilon} + \delta g_\mathrm{E}^2\,, \tag{4.10}$$

$$m_\mathrm{E}^2 = m_\mathrm{ER}^2 + \delta m_\mathrm{E}^2\,. \tag{4.11}$$

Only the thermal mass of the colour-electric modes m_E acquires a counterterm [102, 103, 100]

$$\delta g_\mathrm{E}^2 = 0\,, \tag{4.12}$$

$$\delta m_\mathrm{E}^2 = \left(\frac{g_\mathrm{E}^2 N_\mathrm{c} T}{16\pi}\right)^2 \frac{4(\kappa_2 - 4\lambda)}{\epsilon}\,. \tag{4.13}$$

Any left-over IR divergence at 3-loop level on the full theory side fails to cancel against counterterms on the EQCD side. Hence, potential higher operators have been truncated but generally must be accounted for since EQCD is merely an EFT.

The second step of the reduction integrates out the soft dynamics of the adjoint scalar field A_0. The resulting theory is an effective one for static ultrasoft gauge field modes known as Magnetostatic QCD (MQCD) and defined by the action

$$S_\mathrm{MQCD}[A] \equiv \int_X \frac{1}{4}F_{ij}^a F_{ij}^a\,, \tag{4.14}$$

with the magnetostatic coupling g_M inside the covariant derivative

$$F_{ij} = \frac{i}{g_\mathrm{M}}[D_i, D_j]\,, \quad D_i = \partial_i - ig_\mathrm{M}A_i\,, \tag{4.15}$$

which equals purely three-dimensional Yang-Mills theory with truncated higher-dimensional operators. To obtain its effective coupling g_M, the matching of correlation functions with EQCD is conducted. The MQCD gauge coupling then depends on the couplings of the high-scale theory $g_\mathrm{M} = g_\mathrm{M}(g_\mathrm{E}, m_\mathrm{E})$ which in this case are the EQCD gauge coupling g_E and mass scale m_E. Both of are previously determined themselves through matching from full QCD. Through a rescaling of the gauge fields $A_i^a \to A_i^a T^{1/2}$ it is seen that the only scale in the theory is g_M itself.

4.1.1 Deficiencies of dimensionally reduced QCD

One of the main pillars of constructing a successful EFT is to preserve symmetries. In the following, we inspect what influences the pure-gluonic phase transition in dimensionally reduced QCD and which aspects of the fundamental theory are maintained.

Electrostatic QCD, the dimensionally reduced effective theory of hot QCD, reproduces the center symmetry only partially. Instead of spontaneously, EQCD breaks the symmetry explicitly [104], singling out one vacuum state instead of N_c physically equivalent ones. The

culprit is that a transformation under $Z(N_c)$ produces N_c vacua that are of $A_0 \sim 2\pi T/g$ originating from the second "twist" term in eq. (2.63). Now their scale $\mathcal{O}(g^{-1}T)$ is even well above the hard scale and thus the dimensionally reduced theory cannot resolve this UV scale. The only vacuum that is in reach of the validity of the theory is $A_0 \approx 0$ around which the EFT is an expansion of.

Another issue is the lack of light fermionic degrees of freedom. On the one hand, it is convenient that the effective theory is one of purely bosonic modes which obviates all complications related to fermions on the lattice. The only place they appear is through the effective couplings. On the downside, the absence of fermions obstructs the EFT from respecting the full parent symmetries such as flavour structures or chiral symmetry breaking.

Different observables exhibit different sensitivity to the given scales in the theory. In this context non-perturbative EQCD dynamics yields less satisfactory results concerning the pressure of hot QCD [105] which is affected by all three scales: hard, soft, and ultrasoft.

4.2 Dimension-six operators in EQCD

The sole source of a remaining divergence after renormalisation identifies as higher-dimensional operators that were previously neglected when truncating EQCD. A standard procedure to construct the higher-order Lagrangian was already pursued in [101] for coupling coefficients in $d = 3$. Following the strategy there, a covariant derivative expansion of the heat kernel is applied to assemble an operator basis. Later, through a more economical approach, we construct a different basis which generalises the higher-dimensional operator inclusion beyond YM and QCD.

The advantage of a covariant derivative expansion of the effective action of the static modes is that the resulting 3-dimensional effective action will be inherently invariant under spatially-dependent gauge transformations. For pure gauge SU(N) this amounts to expanding the functional determinants in

$$S_{\text{eff}}[A] = \ln \frac{\det(-D^2)}{\det(-\partial^2)} - \frac{1}{2} \ln \frac{\det(-D^2\delta_{\mu\nu} - 2[D_\mu, D_\nu])}{\det(-\partial^2\delta_{\mu\nu})} \,, \tag{4.16}$$

always subtracting the zero-gluon field contributions. Since

$$\ln x = -\lim_{\epsilon\to 0^+} \left(\int_\epsilon^\infty \frac{\mathrm{d}t}{t} e^{-xt} + (\gamma_{\text{E}} + \ln\epsilon) \right) , \tag{4.17}$$

regulates the logarithm, it implies the identity for ratios of various determinants in the Schwinger proper time representation [106]

$$\ln \frac{\det(K)}{\det(K_0)} = -\int_0^\infty \frac{\mathrm{d}t}{t} \mathrm{Tr}\, (e^{-tK} - e^{-tK_0}) \,. \tag{4.18}$$

To evaluate the determinant, the functional trace in eq. (4.18) is taken by employing any kind of complete set of states for the spacetime degrees of freedom

$$\mathrm{Tr}\, e^{-tK} = \int \mathrm{d}^d x\, \mathrm{Tr}\, \langle x|e^{-tK}|x\rangle \,, \tag{4.19}$$

while internal indices are left untouched. Conveniently a plane wave basis $|x\rangle \sim \exp(ip_\mu x_\mu)$ is introduced expanding the covariant derivative and commuting it to the right

$$\lim_{x'\to x} \int \frac{\mathrm{d}^3 p}{(2\pi)^3} e^{-ipx'} D^2 e^{ipx} = \lim_{x'\to x} \int \frac{\mathrm{d}^3 p}{(2\pi)^3} e^{ip(x-x')} (D^2 + 2iD_\mu p_\mu - p^2) \,, \tag{4.20}$$

which has the effect of a shift $\partial_\mu \to \partial_\mu + ip_\mu$ inside the derivatives. The ghost functional determinant expands as

$$\ln \frac{\det(-D^2)}{\det(-\partial^2)} = -\int_0^\infty \frac{\mathrm{d}t}{t} \int_X T\sum_n \int \frac{\mathrm{d}^3p}{(2\pi)^3} e^{-p^2t} \operatorname{Tr} \left\{ \exp\left[(D^2 + 2iD_\mu p_\mu)t \right] \mathbb{1} - 1 \right\} . \quad (4.21)$$

Since the trace over spacetime degrees of freedom was performed, the above left-over trace is understood over internal indices only i.e. colour or Lorentz indices. Due to the compactification of the Euclidean time coordinate at finite temperature neither x_0, running from 0 to $1/T$, nor p_0, in the sum over Matsubara modes, are dynamical.

A t-expansion up to first non-zero terms after spatial momentum integration is given by

$$\begin{aligned} &\operatorname{Tr} \int_X T\sum_n \int \frac{\mathrm{d}^3p}{(2\pi)^3} e^{-p^2t} \left[D^2 t + \frac{(2i)^2}{2!} (p\cdot D)^2 t^2 \right] \mathbb{1} = \\ &\quad \frac{t}{(4\pi t)^{\frac{3}{2}}} \operatorname{Tr} \int_X T\sum_n e^{-p_0^2 t} (1 - 2p_0^2 t) D_0^2 . \end{aligned} \quad (4.22)$$

Rotational invariance allows only even powers in D. Hence, the next valid order are four powers of D assuming

$$\begin{aligned} &\operatorname{Tr} \int_X T\sum_n \int \frac{\mathrm{d}^3p}{(2\pi)^3} e^{-p^2t} \left[\frac{1}{2!} D^4 t^2 + 3\frac{(2i)^2}{3!} (p\cdot D)^2 D^2 t^3 + \frac{(2i)^4}{4!} (p\cdot D)^4 t^4 \right] \mathbb{1} = \\ &\quad \frac{1}{(4\pi t)^{\frac{3}{2}}} \operatorname{Tr} \int_X \frac{1}{180} T\sum_n e^{-p_0^2 t} \\ &\qquad \times \left\{ 15t^2 [D_\mu, D_\nu]^2 + 30t^2(1 - 2p_0^2 t)([D_i, D_0]^2 + \{[D_i, [D_i, D_0]], D_0\}) \right\} . \end{aligned} \quad (4.23)$$

Similarly the operators for D^6 are acquired in [101]. The last line uses the cyclicity of the trace to trade strings of covariant derivatives for commutators. Terms consisting only of D_0 are grouped in the effective potential

$$V_{\text{eff}} = -\int_0^\infty \frac{\mathrm{d}t}{t} \frac{T}{(4\pi t)^{\frac{3}{2}}} \sum_n \operatorname{Tr} \left\{ \exp\left[(D_0 + ip_0)^2 t \right] - e^{-p_0^2 t} \right\} \mathbb{1} , \quad (4.24)$$

which gives rise to mass terms A_0^2, quartic A_0^4, and sextic couplings A_0^6 of the adjoint scalar field. The gauge field determinant

$$\ln \frac{\det(-D^2\delta_{\mu\nu} - 2[D_\mu, D_\nu])}{\det(-\partial^2\delta_{\mu\nu})} , \quad (4.25)$$

expands similarly as the functional ghost determinant. After integration-by-parts and trace-cyclicity eliminate redundancies, the integration over proper time is performed. This yields an effective action for static modes and specifically the augmentation of the action eq. (4.1) by dimension-six operators [1]

$$\begin{aligned} \delta S_{\text{EQCD}}[A] = 2g_{\text{E}}^2 \int_X \operatorname{Tr} \Big\{ &\mathcal{C}_1 \, (D_\mu F_{\mu\nu})^2 + \mathcal{C}_2 \, (D_\mu F_{\mu 0})^2 \\ &+ ig_{\text{E}} \big[\mathcal{C}_3 \, F_{\mu\nu} F_{\nu\rho} F_{\rho\mu} + \mathcal{C}_4 \, F_{0\mu} F_{\mu\nu} F_{\nu 0} + \mathcal{C}_5 \, A_0 (D_\mu F_{\mu\nu}) F_{0\nu} \big] \\ &+ g_{\text{E}}^2 \big[\mathcal{C}_6 \, A_0^2 F_{\mu\nu}^2 + \mathcal{C}_7 \, A_0 F_{\mu\nu} A_0 F_{\mu\nu} + \mathcal{C}_8 \, A_0^2 F_{0\mu}^2 + \mathcal{C}_9 \, A_0 F_{0\mu} A_0 F_{0\mu} \big] \\ &+ g_{\text{E}}^4 \big[\mathcal{C}_{10} \, A_0^6 \big] \Big\} . \end{aligned} \quad (4.26)$$

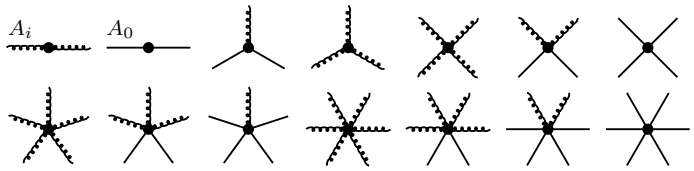

Figure 4.1: Dimension-six operator induced vertices for EQCD in eq. (4.26) containing the "Chapman vertices" as filled blobs. Solid lines represent the adjoint scalar A_0 and curly lines the spatial gauge boson A_i.

The coefficients $\mathcal{C}_i$ are obtained through thermal integration of the c_i of [1],

$$\mathcal{C}_i = \sum\!\!\!\!\!\!\int_K{}' \frac{c_i}{K^6} = Z_{3;0} c_i \,. \tag{4.27}$$

We note that $Z_{3;0} \sim \left(\frac{\zeta_3}{128\pi^4 T^2}\right)$ shows a $1/T^2$ suppression in temperature which justifies the success of the truncated eq. (4.2) at high-temperature studies [95]. The effective action eq. (4.26) introduces the effective vertices depicted in fig. 4.1 which represent 1-loop insertions of the full theory by a filled blob. These vertices are dubbed "Chapman vertices" in accordance with [101]. In contrast to the strategy pursed there, we compute them in general dimensions through matching.

Therefore, the next section introduces a facilitating formalism.

4.2.1 Background Field Formalism

Matching computations usually necessitate the evaluation of many n-point functions. The Background Field Gauge (BFG) [107] formalism facilitates this vastly. While keeping gauge invariance explicit at all levels also the gauge coupling renormalisation in QCD can be performed by only computing self-energies.

We revisit the original partition function in the conventional functional approach [108]

$$\mathcal{Z}[J] = \int \mathcal{D}A \, \det\left[\frac{\delta G^a}{\delta \theta^b}\right] \exp\left\{-\left(S[A] + \frac{1}{2\xi} G^a G^a - J^a_\mu A^a_\mu\right)\right\} \,, \tag{4.28}$$

with source J and implicit integration over X in e.g. $\int_X G^a G^a$. This is the generating functional for the disconnected n-point Green's functions $G^{(n)}$ by taking functional J-derivatives of $\mathcal{Z}[J]$. Connected Green's functions $G_c^{(n)}$ are contained in the generating functional

$$W[J] = \ln \mathcal{Z}[J] \,. \tag{4.29}$$

Its derivative with respect to J yields

$$\bar{A}^a_\mu = \frac{\delta W[J]}{\delta J^a_\mu} \,, \tag{4.30}$$

where $\bar{A}$ assumes the role of a vacuum expectation value of A in the presence of a source J. A Legendre transform of $W[J]$ defines the one-particle irreducible (1PI) effective action

$$\Gamma[\bar{A}] = W[J] - \int_X J\bar{A} \,, \tag{4.31}$$

which gives the one-particle irreducible (1PI) Green's functions $\Gamma^{(n)}$ of the theory. An expansion in powers of external sources J or $\bar{A}$ shows how the different generating functionals

are composed

$$\mathcal{Z}[J] = \sum_{n=0}^{\infty} \frac{1}{n!} \int \mathrm{d}^4x_1 \dots \mathrm{d}^4x_n \, G^{(n)}(x_1, \dots, x_n) \, J(x_1) \dots J(x_n) \; , \tag{4.32}$$

$$W[J] = \sum_{n=0}^{\infty} \frac{1}{n!} \int \mathrm{d}^4x_1 \dots \mathrm{d}^4x_n \, G_c^{(n)}(x_1, \dots, x_n) \, J(x_1) \dots J(x_n) \; , \tag{4.33}$$

$$\Gamma[\bar{A}] = \sum_{n=0}^{\infty} \frac{1}{n!} \int \mathrm{d}^4x_1 \dots \mathrm{d}^4x_n \, \Gamma^{(n)}(x_1, \dots, x_n) \, \bar{A}(x_1) \dots \bar{A}(x_n) \; , \tag{4.34}$$

and which derivatives can be taken.

In contrast to the conventional approach above, the background field approach encounters an analogous set of generating functionals subscripted with b. Their relation to the original quantities

$$\{\mathcal{Z}, W, \Gamma\} \to \{\mathcal{Z}_b, W_b, \Gamma_b\} \; , \tag{4.35}$$

is subject of the following discussion. The background field generating functional is retrieved after expanding the gauge fields A_μ around a non-dynamical, classical background field B_μ^a and introducing quantum fluctuations A_μ

$$A_\mu \to B_\mu + A_\mu \; . \tag{4.36}$$

Only the A_μ are the dynamical variables of integration. The shift is understood only in the classical action

$$\begin{aligned} \mathcal{Z}_b[J, B] &= \int \mathcal{D}A \, \det\left[\frac{\delta \widetilde{G}^a}{\delta \theta^b}\right] \exp\left\{-\left(S[A+B] + \frac{1}{2\xi}\widetilde{G}^a\widetilde{G}^a - J_\mu^a A_\mu^a\right)\right\} \; , \\ &= \int \mathcal{D}(A+B) \, \det\left[\frac{\delta \widetilde{G}^a}{\delta \theta^b}\right] \exp\left\{-\left(S[A+B] + \frac{1}{2\xi}\widetilde{G}^a\widetilde{G}^a - J_\mu^a (A+B)_\mu^a\right)\right\} e^{-J\cdot B} \; , \\ &= \mathcal{Z}[J] e^{-J\cdot B} \; . \end{aligned} \tag{4.37}$$

where the second step recovers the initial effective action up to a multiplicative factor. Taking the logarithm, the generating functional for connected Green's functions $G_c^{(n)}$ becomes

$$W_b[J, B] = \ln \mathcal{Z}_b[J, B] = W[J] - \int_X JB \; . \tag{4.38}$$

Equivalently to the conventional approach eq. (4.30) defining a vacuum expectation value of A in the presence of a source in the BFG formalism gives

$$\tilde{A}_\mu^a = \frac{\delta W_b[J, B]}{\delta J_\mu^a} = \frac{\delta W[J]}{\delta J_\mu^a} - B_\mu^a = \bar{A}_\mu^a - B_\mu^a \; , \tag{4.39}$$

which relates $\tilde{A}$ to its conventional value $\bar{A}$. Both are now related through a shift with the background field B. Finally, the modified effective action is the Legendre transform

$$\begin{aligned} \Gamma_b[\tilde{A}, B] &= W_b[J, B] - \int_X J\tilde{A} \; , \\ &= W[J] - \int_X J(B + \tilde{A}) \; , \\ &= W[J] - \int_X J\bar{A} = \Gamma[\bar{A}] = \Gamma[\tilde{A} + B] \; , \end{aligned} \tag{4.40}$$

where the last line expresses $\bar{A} = \tilde{A} + B$ from the relation (4.39). Consequently, the modified and conventional effective action are equivalent and by setting $\tilde{A} = 0$ it follows that

$$\Gamma_b[0, B] = \Gamma[B] \; . \tag{4.41}$$

Thus, the effective action can be determined through $\Gamma_b[0, B]$. Eventually the background field in $\Gamma[B]$ is replaced by the original field by a field redefinition $A_\mu = B_\mu(1 + \mathcal{O}(g_{\mathrm{B}}^2))$. The striking difference between both sides in eq. (4.41) is the gauge condition in Γ_b

$$\widetilde{G}^a = (\partial_\mu + g f^{abc} B_\mu^c) A_\mu^b = \mathcal{D}_\mu^{ab}[B] A_\mu^b \; . \tag{4.42}$$

This is the background field gauge. It is an unconventional but entirely valid gauge that mixes B and A compared to the usual covariant gauge-fixing in Γ. The latter is equivalent to computing graphs with no B-fields in the loops and no A-fields as external lines. Concretely this involves summing all 1PI vacuum graphs of the theory in the presence of the background B-field. The major advantage of the BFG is that only vacuum graphs have to be considered. The equality eq. (4.41) guarantees gauge independent physical quantities to be identical on both sides. For deriving the Feynman rules, recall that vertices including one regular gauge field have no contribution to 1PI diagrams and are therefore safely discarded. The gauge parameter ξ becomes also explicit in 3-point and 4-point gauge vertices [107].

Renormalisation is another virtue of the background field gauge. Since the gluon and ghost fields appear strictly inside loops, their renormalisation constants cancel mutually. Thus, their renormalisation is unnecessary. The gauge invariant effective YM action should exhibit only a multiplicative divergent factor, renormalising such that

$$F_{\mu\nu}^a = Z_A^{\frac{1}{2}} \Big[\partial_\mu A_\nu^a - \partial_\nu A_\mu^a + g Z_g Z_A^{\frac{1}{2}} f^{abc} A_\mu^b A_\mu^c \Big] \; , \tag{4.43}$$

which is only gauge-covariant by demanding

$$Z_g = Z_A^{-\frac{1}{2}} \; . \tag{4.44}$$

Introducing a background field gauge in the EQCD action shifts the spatial gauge fields and leaves the electrostatic A_0 unaltered

$$A_i \to B_i + A_i \; , \quad A_0 \to A_0 \; . \tag{4.45}$$

After adding a general covariant gauge term the electrostatic Lagrangian (4.2) produces

$$\begin{aligned} S_{\mathrm{EQCD}}[A] \equiv \int_X \Big\{ & \frac{1}{4} F_{ij}^a[B + A]^2 + \frac{1}{2} \big(\mathcal{D}_i^{ab}[B + A] A_0^b \big)^2 \\ & + \frac{1}{2} m_{\mathrm{E}}^2 A_0^a A_0^a + \frac{1}{4!} \lambda_{\mathrm{E}}^{(1)} A_0^a A_0^a A_0^b A_0^b + \frac{1}{4!} \lambda_{\mathrm{E}}^{(2)} X^{abcd} A_0^a A_0^b A_0^c A_0^d \\ & + \frac{1}{2\xi} \big(\mathcal{D}_i^{ab}[B] A_i^b \big)^2 + \delta \mathcal{L}_{\mathrm{E}} \Big\} \; , \end{aligned} \tag{4.46}$$

where A_0^a denotes the adjoint field, A_i^a the colour-magnetic gauge field and $\delta\mathcal{L}_{\mathrm{E}}$ incorporates higher-order operators *viz.* eq. (4.26). The background field gauge-fixing condition shows explicitly $\mathcal{D}_i^{ab}[A] \to \mathcal{D}_i^{ab}[B]$ as from eq. (4.42); see [56] for corresponding Feynman rules.

Since the effective action is now both gauge invariant under the effective B_{eff} and the original background field B, we obtain the effective coupling g_{E} (or g_{M}) through a 2-point computations of the background gauge potentials denoted by B_μ^a [57]. Therefrom, we Taylor-expand the gluon self-energy (3.34) in both the bare gauge coupling g_{B} and the soft (or ultrasoft) external momentum $|\mathbf{q}| = q \sim \mathcal{O}(gT)$

$$\Pi(q^2) = \sum_{n=0}^{\infty} q^{2n} \sum_{\ell=1}^{\infty} g_{\mathrm{B}}^{2\ell} \, \Pi_\ell^{(n)}(0) \; , \tag{4.47}$$

with transversal and temporal components $\Pi = \{\Pi_{\mathrm{E}}, \Pi_{\mathrm{T}}\}$. The gauge coupling then yields (cf. ref. [57])

$$\begin{aligned} g_{\mathrm{E}}^2 = g^2 T \Big\{ & 1 - g^2\, \Pi'_{\mathrm{T}1}(0) \\ & + g^4 \left[(\Pi'_{\mathrm{T}1}(0))^2 - \Pi'_{\mathrm{T}2}(0) \right] \\ & - g^6 \left[(\Pi'_{\mathrm{T}1}(0))^3 - 2\Pi'_{\mathrm{T}1}(0)\Pi'_{\mathrm{T}2}(0) + \Pi'_{\mathrm{T}3}(0) \right] \Big\} \,, \end{aligned} \tag{4.48}$$

to second order in the external momentum q^2. It is to be noted that all Taylor coefficients $\Pi'_{\mathrm{T}1}(0)$ are manifestly gauge-invariant. Because the external momentum is decoupled only massive tadpole integrals arise which facilitates the computation. The method to regularise the theory will be dimensional regularisation as it is convenient when facing scaleless sub-loops which render the whole graph zero in the chosen scheme.

4.2.2 Determination of dimension-six coefficients

As mentioned, the Chapman vertices [101] were previously obtained in three-dimensions. Generally, computations that insert these operators can lead to ultraviolet-divergent integrals. In strict dimensional regularisation the generalisation of the c_i to arbitrary d-dimensions lifts said divergences and is therefore indispensable.

To achieve this, a matching computation is conducted starting from the full theory eq. (2.44). Utilising the background field gauge, this necessitates the computations of the corresponding n-point correlation functions present in the 1PI action eq. (4.34)

$$\Gamma^{(2)}_{\mathrm{EQCD}}[B] = \frac{1}{2!} g_{\mathrm{B}}^2 N_{\mathrm{c}}\, B^a_\mu(q_1) B^b_\nu(q_2)\, \delta^{ab} \delta(q_1+q_2)\, \gamma^{(2)}_{\mu\nu}(q_1) \,, \tag{4.49}$$

$$\Gamma^{(n)}_{\mathrm{EQCD}}[B] = \frac{(i)^n}{n!} g_{\mathrm{B}}^n\, B^{a_1}_{\mu_1}(q_1) \dots B^{a_n}_{\mu_n}(q_n)\, \delta(q_1 + \dots + q_n)\, \gamma^{(n) a_1 \dots a_n}_{\mu_1 \dots \mu_n}(q_1, \dots, q_n) \,, \tag{4.50}$$

focussing on 1-loop contributions. More generally, in any matching procedure the coefficients of higher-dimensional operators will depend on the couplings of the theory and on possible mass scales in the loops. For EQCD this means that the c_i in eq. (4.27) are functions of g^2 and possible fermionic mass contributions. While the former are regarded as higher order effects, fermionic masses generate no IR divergences and are omitted in this section but we return to them in chapter 5.

In the next step the n-point correlation functions are matched onto the effective vertices in the action $\delta S^{(n)}_{\mathrm{EQCD}}$. The latter composes of all the appearing group and Lorentz tensor structures that respect the external field content of the vertex up to a fixed order in mass dimension. One example is the dimension-six electrostatic QCD gluon 3-point vertex which can be chosen to have the minimal basis

$$\begin{aligned} \delta S^{(3)}_{\mathrm{EQCD}} = {} & A^a_\mu(q)\, A^b_\mu(r)\, A^c_\mu(s)\, f^{abc}\, \delta(q+r+s) \left(\sum\!\!\!\!\!\!\int_K{}' \frac{i g_{\mathrm{E}}^3 N_{\mathrm{c}}}{K^6} \right) \\ & \times \Big\{ \xi_1\, q_\mu q_\nu q_\rho + \xi_2\, q_\mu q_\nu r_\rho + \xi_3\, q_\mu r_\nu q_\rho + \xi_4\, r_\mu q_\nu q_\rho \\ & \quad + S_{\mu\nu} \left[\xi_5\, q^2 q_\rho + \xi_6\, q^2 r_\rho + \xi_7\, s^2 q_\rho \right] + T_{\mu\nu} \left[\xi_8\, q^2 q_\rho + \xi_9\, q^2 r_\rho + \xi_{10}\, s^2 q_\rho \right] \Big\} \,. \end{aligned} \tag{4.51}$$

One economical strategy to approach a minimal set of basis operators is to symmetrise in all external (gauge) fields $A^{a_i}_{\mu_i}(q_i)$. This first relabels the entire set of indices (q_i, μ_i, a_i) of every term such that $(q_i \leftrightarrow q_j, \mu_i \leftrightarrow \mu_j, a_i \leftrightarrow a_j)$ and then acts with the full symmetries of the tensor structures to remove redundancies. This leaves only the choice to consistently pick the

"simplest" basis which is straightforwardly implemented using the lexicographical ordering of a computer algebra system.

By applying the same symmetrisation on both $\delta S^{(n)}_{\mathrm{EQCD}}$ and the resulting computation $\Gamma^{(n)}_{\mathrm{EQCD}}$, they exhibit the same set of basis operators and the coefficients in the effective action are readily obtained. Finally, by acting with the same symmetry operation on the effective Lagrangian eq. (4.65) a unique mapping between the bases $\{\xi_i\} \to \{c_i\}$ allows to infer the coefficients c_i. The explicit coefficients defined in eq. (4.27) read

$$
\begin{aligned}
\mathcal{C}_1 &= N_{\mathrm{c}}\left[\frac{41-d}{120}+\frac{(8-\alpha)\alpha}{48}\right]Z_{3;0}-\frac{1}{15}\sum_{i=1}^{N_{\mathrm{f}}}Z_{3;i}\;,\\
\mathcal{C}_2 &= N_{\mathrm{c}}\left[\frac{(d-1)(d-5)}{120}+\frac{(d-5)(4+\alpha)\alpha}{48}\right]Z_{3;0}-\sum_{i=1}^{N_{\mathrm{f}}}\left[\frac{d-5}{60}Z_{3;i}+\frac{1}{10}m_i^2 Z_{4;i}\right]\;,\\
c_3 &= \frac{1-d}{180}\;,\\
c_5-c_4 &= \frac{(d-1)(d-5)}{60}+\frac{(d-5)\alpha}{6}\;,\\
c_4-2c_7 &= \frac{(41-d)(5-d)}{60}\;,\\
c_5-2c_7 &= \frac{(21-d)(5-d)}{30}+\frac{(d-5)\alpha}{6}\;,\\
c_6+c_7 &= \frac{(d-25)(5-d)}{24}\;,\\
c_8 &= \frac{(d-5)(d-3)(d-1)}{20}+\frac{(d-5)(d-3)\alpha}{3}\;,\\
c_9 &= \frac{(d-5)(d-3)(d-1)}{30}+\frac{(d-5)(d-3)\alpha}{6}\;,\\
c_{10} &= \frac{(d-5)(d-3)(d-1)^2}{180}\;,
\end{aligned}
\tag{4.52}
$$

in general spatial dimension and gauge with abbreviated parameter

$$
\alpha = (1-\xi)\;, \tag{4.53}
$$

shifted from the conventional one in the gluon propagator. For generality $\mathcal{C}_1, \mathcal{C}_2$ include fermionic effects while $c_3, \ldots, c_{10}$ are given for $N_{\mathrm{f}} = 0$[1]. Curiously, some coefficients $c_8\, A_0^2 F_{0\mu}^2$, $c_9\, A_0 F_{0\mu} A_0 F_{0\mu}$, and $c_{10}\, A_0^6$ couple to evanescent operators wherefore their effect vanishes in $d \approx 3$. To access the coefficient c_{10} requires the computation of the 6-point gluon effective vertex [1].

4.3 The EQCD effective coupling to 3-loop level

The ensuing sections evaluate the 3-loop magnetostatic coupling in d-dimensions following the algorithm sketched in chapter 3. This is to demonstrate that soft and ultrasoft observables are IR finite and indeed influenced by all scales in the QCD hierarchy. Integrating out the hard and soft scales requires all the contributions above and even including the ultrasoft scale.

The strategy is to first determine the EQCD effective gauge coupling g_{E} accounting for genuine hard scale contributions and overlapping insertions (one hard blob) at the soft and

[1] The determination of fermionic effects for $c_3, \ldots, c_{10}$ is technically more challenging and subject of future investigations.

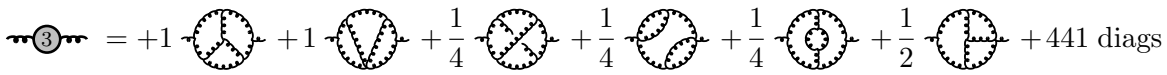

Figure 4.2: 3-loop bosonic contributions to the gluon 2-point function $\mathcal{Z}_B$ in 4-dimensional QCD in the background field B^a_μ (cf. ref. [109]).

ultrasoft scale (cf. sec. 4.3.2). Only then its contribution to $g_{\rm M}$ is given. We restrict to $N_{\rm f} = 0$ contributions at the hard scale such that masses are manifest only in EQCD by the single dynamically generated mass scale $m_i = m_{\rm E}$ from the Lagrangian (4.2). Inverse propagators are labelled to uniquely identify momenta and masses on the diagram lines $\Delta_i = p_i^2 + m_i^2$.

4.3.1 Power counting

At 3-loop order, the full theory generates a precision of $\mathcal{O}(g^6)$. The argument of decoupling in sec. 2.4.1 requires to both take both into account higher-order operators and higher-loop orders to conduct a well defined weak-coupling expansion. Thus, the question remains which operators are to be kept in EQCD and MQCD to cover all terms contributing to g^6.

We have seen that these operators are generated from a "ℓ-loop hard" computation inside the fundamental theory and are of order $g^{2\ell}/T^2$ (cf. sec. 4.2.2). They appear in calculations through their (blob) insertion inside hierarchically lower scales after the DR. At the soft scale they assume at 1-loop order

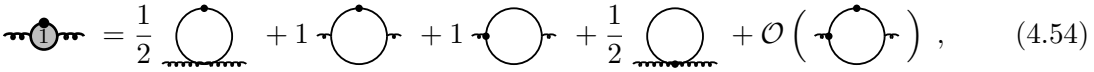

(4.54)

which increases the effective order of the actual computation. A 2-loop soft result eventually competes with 3-loop hard results in the matching. The factor "1-loop soft" is of $\sim g^2 T m_{\rm ER} \sim g^3 T$ and the one from "2-loop soft" of $\sim (g^2 T)^2 \sim g^4 T^2$. For the 1-loop result to be still within the range of accuracy one requires for n-insertions

$$g^3 T^2 \times \left(\frac{g^{2\ell}}{T^2}\right)^n \sim g^{3+2\ell n} \geq g^6 \,, \tag{4.55}$$

which only applies for $\ell = n = 1$. Either one insertion with higher precision of coefficients or multiple insertions of higher-dimensional operators will then exceed the targeted accuracies in the weak-coupling expansion. Therefore the higher-order terms in eq. (4.54) do not contribute in our analysis.

A similar argument follows from the power analysis of even higher-dimensional operators. Their leading order hard coefficient is of $\sim g^2/T^4$. Inside a soft loop they are even further suppressed.

4.3.2 The hard contribution

The 3-loop contribution to the effective gauge coupling $g_{\rm E}^2$ originates from the 2-point background field computation; its diagrams are depicted in fig. 4.2. After renormalisation by using QCD vacuum counterterms for the gauge coupling eq. (2.52) and fields eq. (2.51), the

resulting expression still contains a logarithmic $(1/\epsilon)$-divergence [109],

$$\Gamma^{(2)}_{\mathrm{EQCD}}[B] = \frac{1}{2}\, B^a_i(q)\, B^b_j(r)\, \delta^{ab}\, \delta(q+r)\, (q^2\delta_{ij} - q_i q_j)\, (\mathcal{Z}_{\scriptscriptstyle B} + \delta\mathcal{Z}_{\scriptscriptstyle B})\,, \tag{4.56}$$

$$\begin{aligned}\mathcal{Z}_{\scriptscriptstyle B} = 1 &- \frac{g^2 N_{\mathrm{c}}}{(4\pi)^2}\left[\frac{22}{3}L_b + \frac{1}{3}\right] - \frac{g^4 N_{\mathrm{c}}^2}{(4\pi)^4}\left[\frac{68}{3}L_b + \frac{341}{18} - \frac{10\zeta_3}{9}\right] \\ &- \frac{g^6 N_{\mathrm{c}}^3}{(4\pi)^6}\left[\frac{748}{9}L_b^2 + \left(\frac{6608}{27} - \frac{10982\zeta_3}{135}\right)L_b + (\text{finite})\right] + \mathcal{O}(g^8)\ ,\end{aligned} \tag{4.57}$$

$$\delta\mathcal{Z}_{\scriptscriptstyle B} = \frac{g^6 N_{\mathrm{c}}^3}{(4\pi)^6}\frac{61\zeta_3}{5\epsilon} + \mathcal{O}(g^8)\,, \tag{4.58}$$

with $\zeta_n = \zeta(n)$ the zeta-function from eq. (A.7) and L_b defined in eq. (2.50). We know already that the theory receives no UV counterterms from the full theory side. EQCD is, however, also super-renormalisable such that the left-over divergence $\delta\mathcal{Z}_{\scriptscriptstyle B}$ appears as a puzzle at first sight. The following sections reason why the cancellation of such a divergence in the hard-soft matching fails and still is rather natural in dimensionally reduced thermal field theories.

To distinguish contributions that affect the ultrasoft scale, we define analogously to eq. (4.56), the d-dimensional self-energy in the background field formalism with the quadratic part

$$\Gamma^{(2)}_{\mathrm{MQCD}}[B] = \frac{1}{2} B^a_i(q)\, B^b_j(-q)\, (q^2\delta_{ij} - q_i q_j)\, (Z_{\scriptscriptstyle B} + \delta Z_{\scriptscriptstyle B})\,, \tag{4.59}$$

casting possible divergences into $\delta Z_{\scriptscriptstyle B}$ and denoting finite parts $Z_{\scriptscriptstyle B}$ in contrast to the hard result ($\mathcal{Z}_{\scriptscriptstyle B}$).

4.3.3 Soft/hard overlap contribution

Insertions of dimension-six operators originating from 2- to 6-point Chapman vertices manifest themselves as hard blobs in the diagrams consisting of soft (and later ultrasoft) fields.

According to the power counting scheme in sec. 4.3.1 the first relevant order is 2-loop[2] where contributions to both $Z_{\scriptscriptstyle B}$ and $\delta Z_{\scriptscriptstyle B}$ emerge. Its explicit form is

$$\begin{aligned}\delta_2\Gamma^{(2)}_{\mathrm{MQCD}}[B] = \frac{1}{2}\, B^a_i(q)\, B^b_j(r)\, \delta^{ab}\delta(q+r)&\left(\sum\!\!\!\!\!\!\int_K{}' \frac{g_{\mathrm{E}}^6 N_{\mathrm{c}}^3}{K^6}\right) H_2(m_{\mathrm{E}}) \\ &\times\left\{\frac{m_{\mathrm{E}}^2\delta_{ij}}{4d}C_1 + \frac{(q^2\delta_{ij} - q_i q_j)}{4d}C_2 + \frac{q_i q_j}{4d}C_3 + \mathcal{O}\left(\frac{q^4}{m_{\mathrm{E}}^2}\right)\right\}\,,\end{aligned} \tag{4.60}$$

using the covariant gauge parameter ξ from eq. (4.46) and the 2-loop two-mass sunset integral H_2 from eq. (A.24). The coefficients C_1, C_2, C_3 (cf. ref. [1]) are determined from diagrams with a single insertion of higher-dimensional n-point vertices. Here, all 2- to 6-point Chapman vertices contribute to the effective action; for the corresponding diagrams see fig. 4.3. Substituting the coefficients $\mathcal{C}_i$ from eq. (4.52), we get

[2] The 1-loop contributions inside EQCD from eq. (4.54) are of $\mathcal{O}(g^4 m_{\mathrm{E}}/T) \sim \mathcal{O}(g^5)$ which is of higher order than the hard IR divergence. Nevertheless, it is the largest finite hard part of $Z_{\scriptscriptstyle B}$ stemming from the soft scale theory but without effect on $\delta Z_{\scriptscriptstyle B}$.

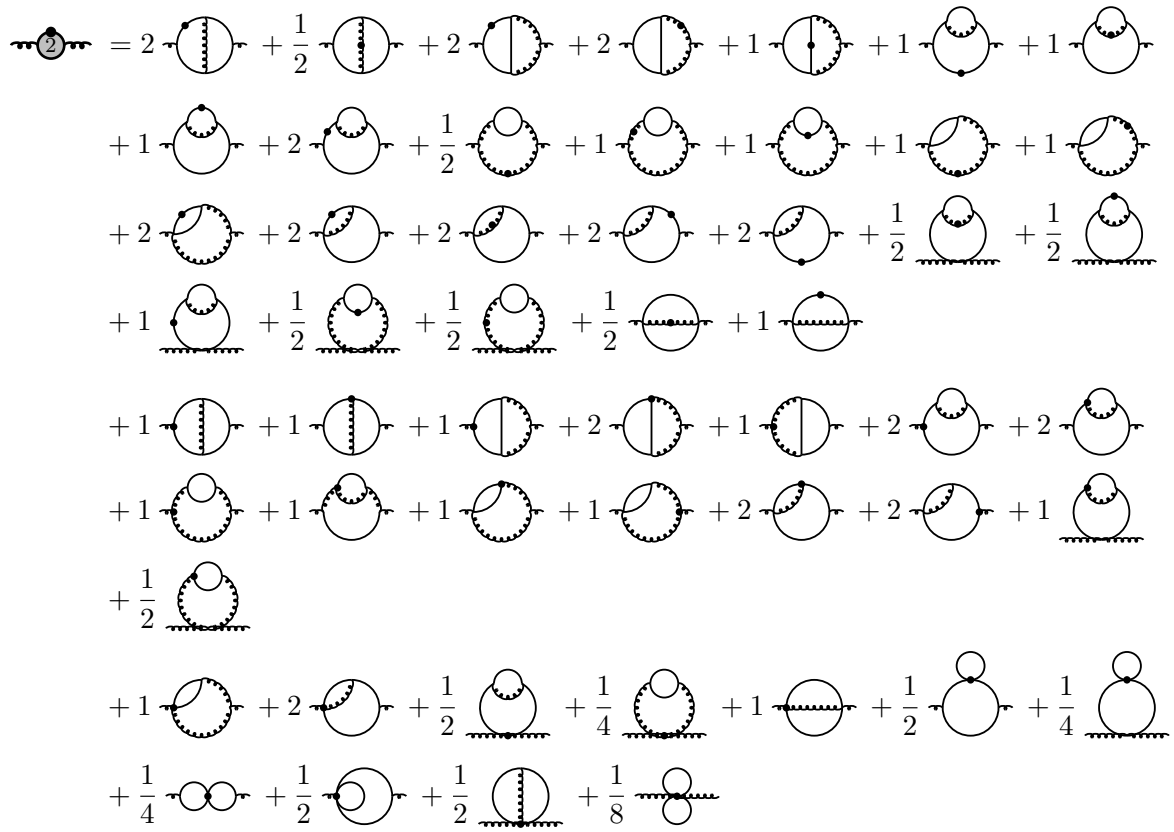

Figure 4.3: 2-loop 2-point EQCD gluon contribution to Z_B in the background field B_i^a with insertion of one dimension-6 vertex denoted by a filled blob (cf. fig. 4.1). This is the soft/hard overlap contribution (cf. ref. [1]).

$$\begin{aligned}\delta_2\Gamma^{(2)}_{\mathrm{MQCD}}[B] = -\frac{1}{2}B_i^a(q)\,B_j^b(r)\,\delta^{ab}\delta(q+r)(q^2\delta_{ij}-q_iq_j)(g_{\mathrm{E}}^6N_{\mathrm{c}}^3)\,H_2(m_{\mathrm{E}})\\ \times\left\{\frac{(d-3)(d-4)^2(d^3-10d^2+23d-44)(\mathcal{C}_1+\mathcal{C}_2)}{3d(d-5)(d-7)}\right.\\ +\frac{(d^4-18d^3+95d^2-210d+192)\,\mathcal{C}_3}{d(d-5)}+\frac{(d^3-13d^2+36d-36)(\mathcal{C}_4-2\mathcal{C}_7)}{3d}\\ \left.+\frac{4(d^3-13d^2+21d-6)(\mathcal{C}_6+\mathcal{C}_7)}{3d}+\frac{(d-3)(d-4)(2\mathcal{C}_8+\mathcal{C}_9)}{3}\right\},\end{aligned}\tag{4.61}$$

with $H_2(m_{\mathrm{E}})\sim 1/(4\epsilon)$. Taking the limit of $d=3-2\epsilon$ yields the 1- and 2-loop overlapping soft/hard contributions to the background field 2-point effective action (4.59). Indeed, these bear a divergent part at $\mathcal{O}(g^6)$

$$\begin{aligned}Z_{_B} = 1+\left(\frac{g_{\mathrm{ER}}^2N_{\mathrm{c}}}{(4\pi)^2}\right)^2\frac{m_{\mathrm{ER}}}{2\pi T}\left(\frac{875\zeta_3}{72}\right)\\ -\left(\frac{g_{\mathrm{ER}}^2N_{\mathrm{c}}}{(4\pi)^2}\right)^3\left(\frac{1097}{549}\right)\frac{61\zeta_3}{5}\left\{L_b+2\ln\left(\frac{\bar{\mu}}{2m_{\mathrm{ER}}}\right)+\frac{\zeta_3'}{\zeta_3}-\gamma_{\mathrm{E}}+\frac{103771}{52656}\right\},\end{aligned}\tag{4.62}$$

$$\delta Z_{_B} = -\left(\frac{g_{\mathrm{ER}}^2N_{\mathrm{c}}}{(4\pi)^2}\right)^3\left(\frac{1097}{1098}\right)\frac{61\zeta_3}{5\epsilon}\,,\tag{4.63}$$

employing $g_{\mathrm{ER}}^2=g^2(1+\mathcal{O}(g))$ to leading order. Summing up the two left-over logarithmic IR divergences $\delta\mathcal{Z}_{_B}$ in eq. (4.58) and $\delta Z_{_B}$ in (4.63), we witness a cancellation of 1097/1098

of the $1/\epsilon$-poles resulting from EQCD

$$\delta\mathcal{Z}_{B} + \delta Z_{B} = \frac{g^6 N_{\mathrm{c}}^3 T^2}{(8\pi)^2}\left(\frac{\zeta_3}{128\pi^4 T^2}\right)\frac{1}{45\epsilon} + \mathcal{O}(g^8)\,, \tag{4.64}$$

where the bracket $(\dots) \propto Z_{3;0}$ factors the contribution from the six-dimensional bosonic sum-integral.

4.3.4 Ultrasoft/hard overlap contribution

The hard modes also induce dimension-six operators at the ultrasoft scale. In resemblance with the spatial part of δS_{EQCD} (4.26), the higher-dimensional part of the MQCD action is

$$\delta S_{\mathrm{MQCD}}[A] = 2g_{\mathrm{M}}^2 \int_X \mathrm{Tr}\left\{\mathcal{C}_1\,(D_i F_{ij})^2 + i g_{\mathrm{M}} \mathcal{C}_3\, F_{ij}F_{jk}F_{ki}\right\}. \tag{4.65}$$

These operators contribute to infrared dynamics and physical quantities which are accessible non-perturbatively. We want to determine if those dimension-six operators generate an ultraviolet divergence cancelling the one in eq. (4.64). However, inside loops, MQCD is a scaleless theory and all integrals computed perturbatively vanish in dimensional regularisation.

To retrieve only the ultraviolet divergent part stemming from the MQCD dynamics, we introduce an infrared regulator. Resorting to [110], this is implemented by dealing an equal fictitious ultrasoft mass parameter $m_{\mathrm{G}} \sim \mathcal{O}(g_{\mathrm{M}}^2 T/\pi)$ to the gauge fields A_i^a and the (anti-) ghost fields $c^a, \bar{c}^{\,b}$ which renders their propagators massive

$$\begin{aligned}\Big\langle A_k^a(p) A_l^b(q)\Big\rangle &\equiv \frac{\delta^{ab}\delta(p+q)}{p^2+m_{\mathrm{G}}^2}\left(\delta_{kl} - (1-\xi)\frac{p_k p_l}{p^2+m_{\mathrm{G}}^2}\right)\,,\\ \Big\langle c^a(p)\bar{c}^{\,b}(q)\Big\rangle &\equiv \frac{\delta^{ab}\delta(p-q)}{p^2+m_{\mathrm{G}}^2}\,.\end{aligned} \tag{4.66}$$

The resulting theory is IR-safe and its IR dynamics is shielded by the cut-off which, in the limit $m_{\mathrm{G}} \to 0$, retains only the UV dimensionally regularised contribution.

In analogy with soft/hard eq. (4.60), we inspect the 2-loop[3] IR cut-off result. The coefficients D_1, D_2, D_3 define as

$$\begin{aligned}\delta_2\Gamma_{\mathrm{IR}}^{(2)}[B] = \frac{1}{2}\,B_i^a(q)\,B_j^b(r)\,\delta^{ab}\delta(q+r)(g_{\mathrm{M}}^6 N_{\mathrm{c}}^3)\\ \times\left\{\frac{m_{\mathrm{G}}^2\delta_{ij}}{4d}D_1 + \frac{(q^2\delta_{ij}-q_iq_j)}{4d}D_2 + \frac{q_iq_j}{4d}D_3 + \mathcal{O}\left(\frac{q^4}{m_{\mathrm{G}}^2}\right)\right\}.\end{aligned} \tag{4.67}$$

Two master integrals remain within the explicit expression of the D_i, namely the two-mass $H_2(m_{\mathrm{G}})$ and three-mass $H_3(m_{\mathrm{G}})$ sunset diagram in eq. (A.24)

$$\begin{aligned}D_1 &= \frac{d-3}{d-2}D_{12}\,H_2(m_{\mathrm{G}}) + D_{13}\,H_3(m_{\mathrm{G}})\,,\\ D_2 &= (d-3)D_{22}\,H_2(m_{\mathrm{G}}) + D_{23}\,H_3(m_{\mathrm{G}})\,,\\ D_3 &= \widetilde{D}_3\left(-2(d-3)(d-2)^2 H_2(m_{\mathrm{G}}) + \frac{9d^2-28d+24}{3}H_3(m_{\mathrm{G}})\right)\,,\end{aligned} \tag{4.68}$$

with coefficients D_{ij} summarised in eqs. (C.1)–(C.3). Inserting values for the coefficients $\eta_1, \dots, \chi_{17}$ from ref. [1] both D_1 and D_3 vanish exactly. The finite part of the remaining D_2

[3]The 1-loop IR cut-off result, proportional to $I(m_{\mathrm{G}}) \sim m_{\mathrm{G}}$, vanishes duly in the limit $m_{\mathrm{G}} \to 0$.

is ξ-dependent while the relevant $1/\epsilon$-pole is not. Proceeding in Feynman gauge, the result resembles the form of eq. (4.60):

$$\begin{aligned}\delta_2\Gamma^{(2)}_{\mathrm{IR}}[B] \,=\, & \frac{1}{2}B^a_i(q)\,B^b_j(r)\,\delta^{ab}\delta(q+r)\,(q^2\delta_{ij}-q_iq_j)\frac{g_{\mathrm{M}}^6N_{\mathrm{c}}^3}{4d}\\ & \times\Bigg\{H_2(m_{\mathrm{G}})\bigg(\frac{4}{9}(d-3)(3d^5-105d^4+1058d^3-4536d^2+8602d-5808)\,\mathcal{C}_1\\ & \qquad -4(d-3)(d-2)(19d^2-135d+332)\,\mathcal{C}_3\bigg)\\ & -H_3(m_{\mathrm{G}})\bigg(\frac{4}{27}(d-3)(15d^4-440d^3+3231d^2-8332d+5808)\,\mathcal{C}_1\\ & \qquad +\frac{2}{3}(d-2)(5d^3-291d^2+1480d-1992)\,\mathcal{C}_3\bigg)\Bigg\}\,, \end{aligned}\tag{4.69}$$

wherein, by construction of the higher-dimensional MQCD action (4.65), only the coefficients $\mathcal{C}_1$ and $\mathcal{C}_3$ appear. The two remaining master integrals contain the same UV divergence $H_{2,3}(m) = T^2\mu^{-4\epsilon}/[(4\pi)^2 4\epsilon] + \mathcal{O}(1)$. Therefore, terms $\mathcal{C}_1H_2$, $\mathcal{C}_3H_2$, and $\mathcal{C}_1H_3$ with overall factor $(d-3)$ are of $\mathcal{O}(\epsilon^0)$. Only the term proportional to the three-mass sunset $\mathcal{C}_3H_3$ contributes $1/\epsilon$-divergently.

Together with the coefficient $\mathcal{C}_3$ (4.52), the UV contribution originating from MQCD becomes

$$\begin{aligned}\delta_2\Gamma^{(2)}_{\mathrm{IR}}[B] = & \frac{1}{2}B^a_i(q)\,B^b_j(r)\,\delta^{ab}\delta(q+r)\,(q^2\delta_{ij}-q_iq_j)\\ & \times\frac{g^6N_{\mathrm{c}}^3T^2}{(8\pi)^2}\left(\frac{\zeta_3}{128\pi^4T^2}\right)\left(-\frac{1}{45}\right)\left\{\frac{1}{\epsilon}+2L_b+4\ln\left(\frac{\bar{\mu}}{3m_{\mathrm{G}}}\right)+\mathcal{O}(1)\right\}\,. \end{aligned}\tag{4.70}$$

Really, by comparing with the joint left-over divergence related to the genuine hard $\delta\mathcal{Z}_{_B}$ and soft/hard $\delta Z_{_B}$ computation in eq. (4.64), the result is rendered finite

$$\delta\mathcal{Z}_{_B}+\delta Z_{_B}+\delta Z_{_{B,\mathrm{IR}}}=0\,. \tag{4.71}$$

This demonstrates the principles of a strict expansion in the weak-coupling for dimensionally reduced thermal effective theories. Only when including higher-dimensional operators that contribute at equal coupling order, the g-expansion is well defined and thus physical results are finite such as g^2_{M} from EQCD.

4.4 Can we proceed to MQCD?

Since also the soft scale $\mathcal{O}(gT)$ contributes to the construction of the ultrasoft effective action, we may pose the question if it can be integrated out as well. As parent theory to MQCD, following the usual EFT recipe, the effective coupling at the infrared theory g_{M} is determined by the parameters of the soft scale theory which are g_{E} and m_{E}[4]. Since this is essentially a computation where we already know the EQCD gauge coupling, now genuine soft scale contributions and overlapping insertions (one soft blob) at the ultrasoft scale are required.

While reproducing known results for the background field 2-point function in super-renormalisable truncated EQCD at 1- and 2-loop [56, 57], in the following stages, we review its 3-loop extension attained in ref. [1]. Henceforth, $\widetilde{Z}_{_B}$ denotes these purely soft contributions to $Z_{_B}$ in eq. (4.59).

[4] $g_{\mathrm{E}} = g_{\mathrm{E}}(g, m_i)$ and $m_{\mathrm{E}} = m_{\mathrm{E}}(g, m_i)$ are themselves effective couplings of the hard scale theory and therefore functions of the QCD gauge coupling g and possibly also quark masses m_i although in this computation we set $N_{\mathrm{f}} = 0$.

Already the 1-loop contribution exemplifies all important algorithmic steps. Its single loop momentum $\{k\} = \{k_1\}$ and external momentum q form the canonical basis of the form eq. (3.5)

$$A_{1,1}[q] = \{k_1, k_1 - q\} \ . \tag{4.72}$$

As a non-trivial example, we evaluate the transversal self-energy $\Pi_{\mathrm{T}}(q^2)$ explicitly from the two non-vanishing 1-loop diagrams in dimensional regularisation with symmetry factors

$$\frac{1}{2}$$  $$= -g_{\mathrm{E}}^2 N_{\mathrm{c}} T \frac{dP_{\mathrm{G}} - P_{\mathrm{L}}}{q^2[k_1^2 + m_{\mathrm{E}}^2]} \ ,$$

$$\frac{1}{2}$$  $$= \frac{g_{\mathrm{E}}^2 N_{\mathrm{c}} T}{2} \frac{P_{\mathrm{G}}[-4\,(k_1 \cdot q) + 4k_1^2 + q^2] - P_{\mathrm{L}}[2\,(k_1 \cdot q) + q^2]^2 \frac{1}{q^2}}{q^2[k_1^2 + m_{\mathrm{E}}^2][(k_1 - q)^2 + m_{\mathrm{E}}^2]} \ , \tag{4.73}$$

after contraction with projectors $P_{\mathrm{G}}\,(\mathbb{P}^{\mathrm{T}}_{\mu\nu} + \mathbb{P}^{\mathrm{L}}_{\mu\nu})$ and $P_{\mathrm{L}}\,\mathbb{P}^{\mathrm{L}}_{\mu\nu}$ from eq. (3.35). Concentrating on the strictly transverse terms proportional to P_{G}, we perform the scalarisation utilising $(k_1 \cdot q) = (k_1^2 + q^2 - (k_1 - q)^2)/2$ before expanding q-dependent denominators up to $\mathcal{O}(q^0)$ in accordance with eq. (3.17) . Summing both diagrams and abbreviating the notation via the momentum basis eq. (4.72) and explicit propagator masses with notation in eq. (3.6), the remaining terms take the form

$$\Pi_{\mathrm{T}}(q^2) = \frac{g_{\mathrm{E}}^2 N_{\mathrm{c}} T}{q^2} \left((1-d) I_{10;10} + I_{01;01} - \left(2m^2 + \frac{q^2}{2} \right) I_{11;11} \right) \ . \tag{4.74}$$

Next, we carry out the Taylor expansion in the external momentum described in eq. (3.17) which affects the last two integrals $I_{01;10}$ and $I_{11;11}$. This splits-off the external momentum q and the remaining integrals are purely massive tadpoles with the basis

$$A_1 = \{k_1\} \ , \tag{4.75}$$

and a total sector number of $2^1 = 2$. These discriminate between the zero sector and the sector with powers of $\Delta_1 = k_1^2 + m_{\mathrm{E}}^2$. Given the overall factor q^{-2}, we need to expand up to $\mathcal{O}(q^2)$ to account for all contributions

$$\begin{aligned} I_{01;01} &= I_{1;1} - q^2 I_{2;1} + 4(k_1 \cdot q)^2 I_{3;1} = I_{1;1} \ , \\ I_{11;11} &= I_{2;1} - q^2 I_{3;1} + 4(k_1 \cdot q)^2 I_{4;1} = I_{1;1} \left(-\frac{d-2}{2m_{\mathrm{E}}^2} - q^2 \frac{(d-4)(d-2)}{24 m_{\mathrm{E}}^2} \right) \ , \end{aligned} \tag{4.76}$$

where odd powers in the loop-momentum k_1 vanish due to symmetries $k_1 \to -k_1$ of $I_{s_1;1}$ and the tensor decomposition eq. (3.24) splits-off q in scalar products of even power. Recall that the aim of the decomposition was to remain with a small number of tadpole integrals which becomes explicit in the above steps. For the vacuum 1-loop tadpole a single IBP relation exists when evaluating the total derivative inside $I_{s_1;1}$ producing the recursion

$$I_{s_1+1;1} = \frac{2s_1 - d}{2s_1} \frac{1}{m_{\mathrm{E}}^2} I_{s_1;1} \tag{4.77}$$

for positive integers $s_1 \in \mathbb{Z}^+$. In fact, this is a special case of eq. (3.61) for $\mathbf{1}^+ = 0$. Inserting eq. (4.76) into (4.74) and keeping terms up to $\mathcal{O}(q^0)$ retrieves

$$\widetilde{Z}_B^{(1)} = -\frac{g_{\mathrm{E}}^2 N_{\mathrm{c}}}{m_{\mathrm{E}}^2} \frac{d-2}{12} I(m_{\mathrm{E}}) \ , \tag{4.78}$$

where individual longitudinal parts cancel mutually permitting the transverse contribution. After dimensional regularisation, the insertion of the 1-loop tadpole master integral $I(m_{\mathrm{E}})$ in eq. (A.16) yields

$$\widetilde{Z}_B^{(1)} = \left(\frac{g_{\mathrm{E}}^2 N_{\mathrm{c}} T \mu^{-2\epsilon}}{16\pi m_{\mathrm{E}}} \right) \left(\frac{\bar{\mu}}{2m_{\mathrm{E}}} \right)^{2\epsilon} \left[\frac{1}{3} + \mathcal{O}(\epsilon^2) \right] \ . \tag{4.79}$$

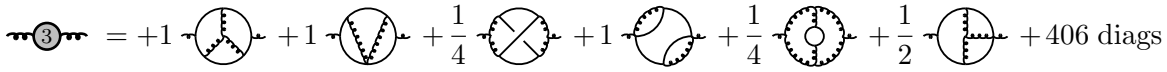

Figure 4.4: 3-loop gluon 2-point function $\widetilde{Z}_B$ in EQCD in the background field B_i^a (cf. sec. C.1) with leading diagrammatic symmetry factors. Curly lines denote spatial gauge fields A_i and solid lines the adjoint scalar field A_0.

The resulting expression exhibits no ξ-dependence. These properties are only valid for the combined result of all sub-graphs while on diagram level a gauge parameter dependence could be explicit. Additionally, we witness UV convergence as all $1/\epsilon$-poles vanish.

At 2-loop level, the momenta in the reduction procedure adapt analogously $\{k\} = \{k_1, k_2\}$ which constitute the vacuum-integral basis

$$A_2 = \{k_1, k_2, k_1 - k_2\} \ , \tag{4.80}$$

after the integrals are expanded and the external momentum is stripped off. The present symmetry of the integrand

$$k_1 \to -k_2 \ , \quad k_2 \to -k_1 \ , \tag{4.81}$$

nullifies terms with odd combined powers of k_1 and k_2 in the numerator as they vanish under the symmetric integration boundaries. Similarly, within the $2^3 = 8$ sectors, the algorithmic computation gives a ξ-independent result in the numerator of eq. (3.64) and contributing diagrams in [56]

$$\widetilde{Z}_B^{(2)} = \left(\frac{g_{\mathrm{E}}^2 N_{\mathrm{c}}}{m_{\mathrm{E}}^2}\right)^2 \frac{(d-4)(d-2)}{12} \left[\frac{d^3 - 10d^2 + 23d - 44}{2(d-7)(d-5)d} - \lambda\right] I(m_{\mathrm{E}})^2 \ , \tag{4.82}$$

showing transverse structure and utilising λ from eq. (4.9). Insertion of the massive 1-loop tadpole master $I(m_{\mathrm{E}})$ yields

$$\widetilde{Z}_B^{(2)} = \left(\frac{g_{\mathrm{E}}^2 N_{\mathrm{c}} T \mu^{-2\epsilon}}{16\pi m_{\mathrm{E}}}\right)^2 \left(\frac{\bar{\mu}}{2m_{\mathrm{E}}}\right)^{4\epsilon} \left[\frac{19}{18} + \frac{4}{3}\lambda + \mathcal{O}(\epsilon)\right] \ . \tag{4.83}$$

The arising ϵ and d dependences originate from products of both the scalarisation and the expansion in the master integrals. All divergent parts vanish in the expansion leaving only a finite contribution and terms of $\mathcal{O}(\epsilon)$ which vanish when $\epsilon \to 0$. Notably, the scalar λ_{E}-dependent part accords with ref. [57] which, however, is stated for the fundamental representation. The conversion (4.8) transforms $\widetilde{Z}_B^{(2)}$ in eq. (4.83) to coincide with [57].

When facing computations at 3-loop level, efficiency becomes indispensable. The genuine EQCD 3-loop background field self-energy demands all tools outlined in chapter 3. The loop-momenta $\{k\} = \{k_1, k_2, k_3\}$ employ the auxiliary vacuum topology

$$A_3 = \Big\{k_1, k_2, k_3, k_1 - k_2, k_1 - k_3, k_2 - k_3\Big\} \ . \tag{4.84}$$

The number of possible massive lines is $M = 6$ with $2^M = 2^6 = 64$ discriminable sectors. *A priori* the computation features 5 different vacuum topologies (*viz.* fig. 3.2) which are $3 \times 3\ell$, $2\ell \times 1\ell$ and $1\ell^3$, with totally $\mathcal{O}(450)$ diagrams. Some representatives are listed in fig. 4.4.

Luckily only three topologies namely, the basketball and the two factorised 1- and 2-loop diagrams enter the 2-point EQCD gluon self-energy when expanding in the external momentum. The remaining integrals project onto a few mass footprints[5] by exploiting momentum shifts. Consecutively, left-over integrals reduce with integration-by-parts identities.

[5]The signature of masses $\underline{m} = (m_1, \ldots, m_M)$ on the lines of an integral in a parameterisation as in eq. (3.49).

Compactly, the 3-loop contribution to Z_B with generic gauge parameter ξ writes as

$$\widetilde{Z}_B^{(3)} = \left(\frac{g_{\mathrm{E}}^2 N_{\mathrm{c}}}{m_{\mathrm{E}}^2}\right)^3 \Big[(r_1+\tilde{r}_1)(d)\, I(m_{\mathrm{E}})^3 + r_2(d)\, m_{\mathrm{E}}^2\, B_2(m_{\mathrm{E}}) + (r_3+\tilde{r}_3)(d)\, m_{\mathrm{E}}^2\, B_4(m_{\mathrm{E}})\Big]\,, \quad (4.85)$$

with the four-mass B_4 and two-mass B_2 basketball diagrams from eq. (A.30). The d-dimensional polynomials $r_i(d)$ employ a condensed notation for the gauge part summarised in eq. (C.5) and $\tilde{r}_i(d)$ for the scalar part in (C.7).

All ξ-proportional terms cancel duly and the result is completely gauge-independent. The remaining three master integrals, namely the factorised tadpole I^3 and the two massive basketball integrals B_4 and B_2 are worked out in appendix A.1. By counting ϵ-powers at $d = 3-2\epsilon$ in eq. (4.85), we need to expand to $\mathcal{O}(\epsilon^2)$ for I, $\mathcal{O}(\epsilon^1)$ for B_2, and $\mathcal{O}(\epsilon^0)$ for B_4 to reproduce all divergent and finite ϵ-parts. Their explicit forms are put into eq. (4.85) from which the dimensionally regularised result is attained

$$\begin{aligned}\widetilde{Z}_B^{(3)} = \left(\frac{g_{\mathrm{E}}^2 N_{\mathrm{c}} T \mu^{-2\epsilon}}{16\pi m_{\mathrm{E}}}\right)^3 \left(\frac{\bar{\mu}}{2m_{\mathrm{E}}}\right)^{6\epsilon} \Bigg[&\frac{1}{6\epsilon} + \frac{4(\kappa_2-4\lambda)}{6\epsilon} \\ &+ \frac{2(23510+12600\zeta_2-1101\ln 2)}{945} \\ &+ \frac{4\lambda+24\lambda^2-\kappa_1(5-8\ln 2)+\kappa_2(31-24\ln 2)}{9} + \mathcal{O}(\epsilon)\Bigg]\,, \end{aligned} \quad (4.86)$$

including scalar contributions of $\lambda_{\mathrm{E}}^{(1)}$ and $\lambda_{\mathrm{E}}^{(2)}$ in terms of λ, κ_1 and κ_2 given in eq. (4.9).

We encounter $1/\epsilon$-divergences from both the vector and scalar field sector. However, the question remains if they originate from the infrared or ultraviolet. To clarify this, an IR regulator separates the UV analogously as displayed for MQCD in eq. (4.66) and we reiterate the 3-loop EQCD computation although now giving an equal fictitious mass $m_{\mathrm{E}} \sim \mathcal{O}(gT)$ (instead of m_{G}) to all three fields, the adjoint scalars A_0, gluons B_i^a, A_i^a, and ghosts $c^a, \bar{c}^b$; the associated diagrams are those depicted in appendix C.1 extended by the ghost field sector. The resulting divergence is the scalar one for the $(\kappa_2 - 4\lambda)$-term in eq. (4.86). Two intermediate consequences can be stated at this point: (i) the scalar-sector divergence is purely UV and (ii) the vector-sector divergence is purely IR.

The single parameter that receives renormalisation in EQCD is the electrostatic adjoint scalar mass parameter m_{E}. Because the operator-truncated theory is super-renormalisable only the proper mass counterterm (4.13) is scale-dependent $\delta m_{\mathrm{E}}^2 \neq 0$. It is retrieved from the 2-loop[6] adjoint scalar self-energy $\Pi_{A_0A_0}(q^2)$ at zero-external momentum; for corresponding diagrams see fig. 4.5. It is noteworthy that the result is not manifestly gauge invariant and can bear an explicit gauge parameter ξ. To check against the IR sensitivity, the computation is conducted with and without the above IR regulator (cf. eq. (4.66)) yielding the $1/\epsilon$-parts

$$\Pi_{A_0A_0}(0) = \left(\frac{g_{\mathrm{E}}^2 N_{\mathrm{c}}}{16\pi}\right)^2 \left[-\frac{4(\kappa_2-4\lambda)}{\epsilon} + \frac{2(8-\xi)}{\epsilon} + \mathcal{O}(1)\right]\,, \quad (4.87)$$

$$\Pi_{A_0A_0,\mathrm{IR}}(0) = \left(\frac{g_{\mathrm{E}}^2 N_{\mathrm{c}}}{16\pi}\right)^2 \left[-\frac{4(\kappa_2-4\lambda)}{\epsilon} + \mathcal{O}(1)\right]\,, \quad (4.88)$$

which resembles the 3-loop divergent part of $\widetilde{Z}_B$. The IR-shielded $\Pi_{A_0A_0,\mathrm{IR}}$ shows a gauge-independent UV divergence, identified as the mass counterterm δm_{E}^2 in eq. (4.13) in adjoint representation.

[6]The 1-loop A_0 self-energy is proportional to $I(m_{\mathrm{G}})$ which carries no UV divergence in $d = 3-2\epsilon$ *viz.* eq. (A.16).

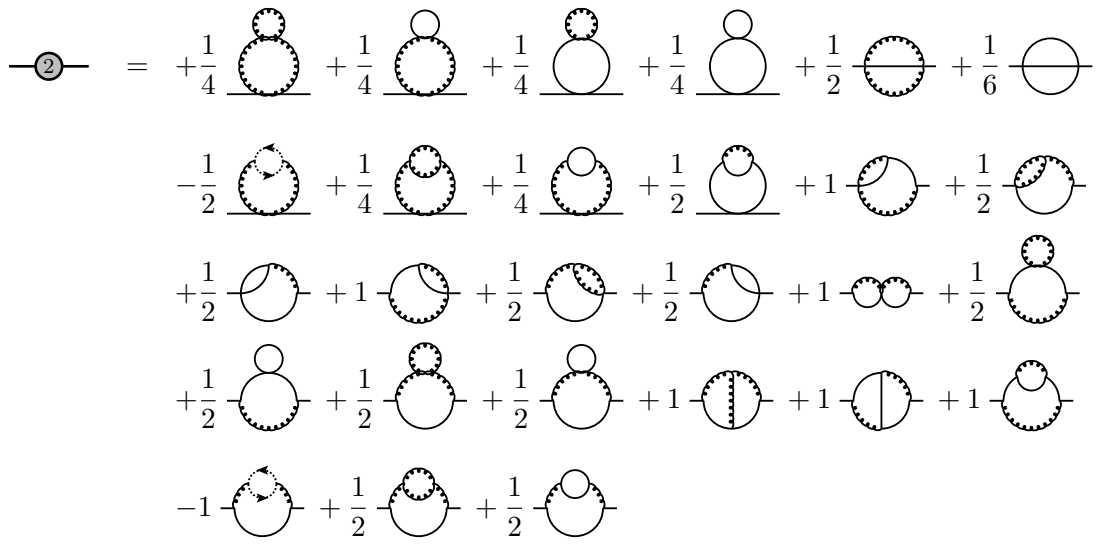

Figure 4.5: Diagrams contributing to the 2-loop EQCD adjoint scalar-field (A_0) self-energy $\Pi_{A_0A_0}$. Curly lines denote spatial gauge fields A_i, dotted lines ghost fields c^a, and solid lines the adjoint scalar field A_0.

The EQCD mass counterterm renormalises the scalar sector of eq. (4.86). This is achieved by re-expressing the 1-loop result $\widetilde{Z}_B^{(1)}$ in eq. (4.79) by the renormalised mass $m_{\rm E}^2 = m_{\rm ER}^2 + \delta m_{\rm E}^2$, assuming a counterterm of the form

$$\delta m_{\rm E}^2 = \frac{\beta}{\epsilon}\left(\frac{g_{\rm E}^2 N_{\rm c} T}{16\pi}\right)^2 , \tag{4.89}$$

with a general parameter β, and re-expanded up to first order in $\delta m_{\rm ER}^2$

$$\begin{aligned}\widetilde{Z}_B^{(1)}[m_{\rm ER}^2 + \delta m_{\rm E}^2] - \widetilde{Z}_B^{(1)}[m_{\rm ER}^2] &= -\left(\frac{1}{2}+\epsilon\right)\frac{\delta m_{\rm E}^2}{m_{\rm E}^2}\widetilde{Z}_B^{(1)}[m_{\rm ER}^2] \,, \\ &= -\frac{\beta}{6\epsilon}\left(\frac{g_{\rm E}^2 N_{\rm c} T}{16\pi m_{\rm ER}}\right)^3 + \mathcal{O}(1) \,. \end{aligned} \tag{4.90}$$

From now on subscripts "R" are dropped and renormalised quantities are assumed. Finally, inserting the adjoint counterterm eq. (4.13) with $\beta = 4(\kappa_2 - 4\lambda)$ gives

$$\delta\widetilde{Z}_B^{(3)} = -\left(\frac{g_{\rm E}^2 N_{\rm c} T \mu^{-2\epsilon}}{16\pi m_{\rm E}}\right)^3 \left(\frac{\bar{\mu}}{2m_{\rm E}}\right)^{6\epsilon}\left[\frac{4(\kappa_2-4\lambda)}{6\epsilon} + \mathcal{O}(\epsilon)\right] . \tag{4.91}$$

According to our source analysis above, the scalar $1/\epsilon$-divergences of λ- and κ_2-dependent contributions at 3-loop level renormalise and render the result finite in the UV

$$\begin{aligned}\widetilde{Z}_B = 1 &+ \left(\frac{g_{\rm E}^2 N_{\rm c} T}{16\pi m_{\rm E}}\right)\frac{1}{3} + \left(\frac{g_{\rm E}^2 N_{\rm c} T}{16\pi m_{\rm E}}\right)^2\left[\frac{19}{18}+\frac{4}{3}\lambda\right] \\ &+ \left(\frac{g_{\rm E}^2 N_{\rm c} T}{16\pi m_{\rm E}}\right)^3\left[\left(1+\frac{8(\kappa_2-4\lambda)}{3}\right)\ln\left(\frac{\bar{\mu}}{2m_{\rm E}}\right)\right. \\ &\qquad + \frac{2(23510+12600\zeta_2-1101\ln 2)}{945} \\ &\qquad \left. + \frac{52\lambda+24\lambda^2-\kappa_1(5-8\ln 2)+\kappa_2(19-24\ln 2)}{9}\right] + \mathcal{O}(g^8) \,, \end{aligned} \tag{4.92}$$

$$\delta\widetilde{Z}_B = \left(\frac{g_{\rm E}^2 N_{\rm c} T}{16\pi m_{\rm E}}\right)^3 \frac{1}{6\epsilon} + \mathcal{O}(g^8) \,. \tag{4.93}$$

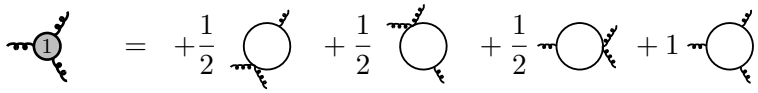

Figure 4.6: Contributing 4 diagrams to 3-point 1-loop EQCD gluon correlation function in the background field B_i^a.

We showed that both the residual vector divergence $\delta\widetilde{Z}_B \sim (g_{\mathrm{E}}^2/m_{\mathrm{E}})^3$ and the additional gauge-dependent divergence in eq. (4.87) originate from the infrared. It therefore appears that further IR contributions are required for δm_{E}^2 with $\beta \neq 0$ in the counterterm (4.89) to match this divergence. In the next section another source of IR divergences is envisaged.

4.4.1 Ultrasoft/soft overlap contribution

Also the soft scale induces higher-dimensional operators at the ultrasoft scale. In a similar manner, the MQCD coefficients in eq. (4.65) are extended by a soft dimension-six term

$$\mathcal{C}_i = \sum\!\!\!\!\!\!\int_K{}' \frac{c_i}{K^6} + T\int_k \frac{\tilde{c}_i}{[k^2+m_{\mathrm{E}}^2]^3}\,, \quad i=1,3\,, \tag{4.94}$$

allowing to identify the coefficients built up from EQCD as to first order $g_{\mathrm{M}}^2 = g_{\mathrm{ER}}^2\mu^{2\epsilon}(1+\mathcal{O}(g))$. The difference to EQCD (4.27) is that now the suppression follows $I_{3;m_{\mathrm{E}}} \sim 1/m_{\mathrm{E}}^3$.

The soft dimension-six coefficients $\tilde{c}_i$ are determined by matching of effective n-point vertex functions at 1-loop level in EQCD. Because the space of parameters only consists of $\tilde{c}_1, \tilde{c}_3$ they are uniquely fixed by computing the 3-point vertex; for diagrams see fig. 4.6. The effective action $\delta S_{\mathrm{MQCD}}^{(3)}$ assumes the spatial part of eq. (4.51) with relabelled $\xi_i \to \tilde{\xi}_i$. By projecting the MQCD Lagrangian eq. (4.65) onto the same operator-set, a unique mapping between the bases $\{\tilde{\xi}_i\} \to \{\tilde{c}_i\}$ infers the coefficients in eq. (4.94)

$$\begin{aligned}
&\tilde{\xi}_1 = 0\,, \quad \tilde{\xi}_2 = 2\tilde{c}_3\,, \quad \tilde{\xi}_3 = -4\tilde{c}_1\,, \quad \tilde{\xi}_4 = -2\tilde{c}_3\,,\\
&\tilde{\xi}_5 = -3\tilde{c}_3\,, \quad \tilde{\xi}_6 = 8\tilde{c}_1 - 3\tilde{c}_3\,, \quad \tilde{\xi}_7 = 3\tilde{c}_3 - 4\tilde{c}_1\,.
\end{aligned} \tag{4.95}$$

Thereafter, also the six-dimensional contributions to the EQCD 3-point correlation function $\Gamma_{\mathrm{MQCD}}^{(3)}$ is projected onto the $\tilde{\xi}$-basis reading

$$\begin{aligned}
&\tilde{\xi}_1 = 0\,, \quad \tilde{\xi}_2 = -\frac{1}{90}\,, \quad \tilde{\xi}_3 = -\frac{1}{30}\,, \quad \tilde{\xi}_4 = \frac{1}{90}\,,\\
&\tilde{\xi}_5 = \frac{1}{60}\,, \quad \tilde{\xi}_6 = -\frac{1}{20}\,, \quad \tilde{\xi}_7 = \frac{1}{60}\,,
\end{aligned} \tag{4.96}$$

which solves for $\tilde{c}_i$ with eq. (4.95)

$$\tilde{c}_1 = -\frac{1}{120}\,, \quad \tilde{c}_3 = -\frac{1}{180}\,. \tag{4.97}$$

Alternatively a covariant derivative expansion of the EQCD effective action gives rise to the same coefficients [111]. More non-trivial cross-checks are possible by inspecting higher n-point vertices with $n > 3$.

Together with the second terms of the coefficients in eq. (4.94) and the recycled soft/hard result $c_i \to \tilde{c}_i$ (4.69), the UV contribution originating from MQCD becomes

$$\begin{aligned}
\delta_2\widetilde{\Gamma}_{\mathrm{IR}}^{(2)}[B] = {}& \frac{1}{2}B_i^a(q)\,B_j^b(r)\,\delta^{ab}\delta(q+r)\,(q^2\delta_{ij}-q_iq_j)\\
&\times\left(\frac{g_{\mathrm{M}}^2 N_{\mathrm{c}} T\mu^{-2\epsilon}}{16\pi m_{\mathrm{E}}}\right)^3\left(-\frac{1}{45}\right)\left\{\frac{1}{\epsilon}+2\ln\left(\frac{\bar{\mu}}{2m_{\mathrm{E}}}\right)+4\ln\left(\frac{\bar{\mu}}{3m_{\mathrm{G}}}\right)+\mathcal{O}(1)\right\}\,.
\end{aligned} \tag{4.98}$$

By comparing with the left-over divergence related to the genuine soft computation eq. (4.93), the magnetostatic gauge coupling is *not* rendered finite

$$\delta\widetilde{Z}_B + \delta\widetilde{Z}_{B,\mathrm{IR}} = \left(\frac{g_{\mathrm{M}}^2 N_{\mathrm{c}} T}{16\pi m_{\mathrm{E}}}\right)^3 \left(\frac{13}{90}\right) \frac{1}{\epsilon}\,, \tag{4.99}$$

and bears a residual soft gauge-independent IR divergence. Only if the mass parameter receives a contribution of the form of eq. (4.89) with $\beta = -\frac{13}{15}$ the result becomes finite.

In conclusion, by including higher dimensional operators in EQCD and MQCD, we inspected the computation of soft IR observables in sec. 4.3 and ultrasoft ones in sec. 4.4. The main implications are as follows:

(i) Soft observables $\langle \mathcal{O}_{\mathrm{E}} \rangle \sim g_{\mathrm{E}}^2 [1 + \ldots]$ are finite and all contributing divergences cancel duly in eq. (4.71).

(ii) Ultrasoft observables $\langle \mathcal{O}_{\mathrm{M}} \rangle \sim g_{\mathrm{M}}^2 [1 + \ldots]$ experience a partial cancellation of IR divergent terms in eq. (4.99).

Chapter 5

Improving accuracy of Dimensional Reduction: A two-loop QCD Debye mass

Along the lines of [2], we review the determination of the Debye mass $m_{\rm D}$ as a matching coefficient of a dimensionally reduced thermal theory. Concretely, we focus on 4-dimensional thermal QCD and increase its precision at two-loop order by incorporating massive quarks. As a consequence, the ensuing chapter analyses the crossing of quark mass thresholds of the Debye mass at high temperatures $T \gtrsim 1$ GeV relevant for cosmological applications.

5.1 Debye screening

Screening is a collective effect that emerges when particles that propagate through a plasma interact with light constituents of that plasma. In an Abelian gauge theory such as QED propagating charges attract a net amount of opposite charged particles that engulf them – screen them – by a finite radius. Beyond that radius the electric field decreases exponentially with the distance r from the charge. The potential then takes a Yukawa form $\propto e^{-m_{\rm E} r}/r$, where the parameter $m_{\rm E}$ is dubbed an electric or Debye mass which characterises the strength of the exponential fall-off with the distance from the particle.

In non-Abelian gauge theories different modes are screened at different length scales. Based on the scale hierarchy in sec. 2.4.1, we discriminate the degrees of freedom and inspect which screening length applies. Recall that thermal masses (2.29) arises as particles that propagate in a heat bath are affected by their constant interaction with the medium. For a non-Abelian plasma, of a SU($N_{\rm c}$) gauge theory with $N_{\rm f}$ fermions in the fundamental representation, colour-electric fields get screened at the order of $m_{\rm E} \sim gT$

$$m_{\rm E}^2 = g^2 T^2 \left(\frac{N_{\rm c}}{3} + \frac{N_{\rm f}}{6} \right) + \mathcal{O}(g^3 T^2) \,, \tag{5.1}$$

which was first evaluated in [112]. Colour-magnetic fields, however, are not screened at this order $m_{\rm M} \sim 0 \times gT$. Only at the next natural order we find a non-zero contribution for their screening mass $m_{\rm M} \sim g^2 T$. Its computation is unattainable with a finite set of diagrams [113], particularly, since at this order QCD modes are non-perturbative [16].

Various definitions of a gauge-invariant and infrared-safe Debye mass are known. A non-perturbative definition in [114] relates it to the inverse correlation length of time-reflection odd operators. The first few terms including non-perturbative contributions [115, 116] yield

$$m_{\rm D} = m_{\rm D}^{\rm LO} + (g^2 T) \frac{N}{4\pi} \ln \frac{m_{\rm D}^{\rm LO}}{g^2 T} + c_N g^2 T + d_{N,N_{\rm f}} g^3 T + \mathcal{O}(g^4 T) \,, \tag{5.2}$$

where the leading order term $m_{\mathrm{D}}^{\mathrm{LO}}$ equals the one in eq. (5.1). The higher-order corrections c_N and $d_{N,N_{\mathrm{f}}}$ are already non-perturbative and computed numerically [115] and analytically [117]. The issue with the above definition is that the constructed correlator depends on the choice of the operators and their quantum numbers.

Another account [118] of an infrared-safe and gauge-independent Debye mass in full thermal QCD defines it in terms of the pole of the static gluon propagator. Besides the above ones, for the remainder of this thesis we focus on a different definition.

5.2 A Debye mass at high temperatures

The Debye mass is defined uniquely and gauge-independently as a matching coefficient of a dimensionally reduced effective theory. Thereby it is purely perturbative, part of a broader concept inside an EFT, and furthermore infrared safe because dimensional reduction is an ultraviolet process. Henceforth, the Debye mass refers to the purely perturbative contribution of eq. (5.2).

Analytic computations of the Debye mass reach up to levels of 3-loop in pure Yang-Mills [119, 100] and 2-loop including massless fermions [120]. Strikingly, little improvement was achieved on the inclusion of fermionic mass effects. Most of all, the inclusion of quark masses is technically challenging already for the 1-loop massive case [93]. Additionally it introduces many yet unknown master diagrams that show a delicate IR behaviour. In [2], we extend the current limit to 2-loop order.

The EQCD mass parameter is determined through the matching of the poles of the static gluon propagator. Therefore, the zeros of the inverse propagators for the QCD and EQCD side amount to

$$\mathbf{q}^2 + \Pi_{\mathrm{E}}(\mathbf{q}^2)\big|_{\mathbf{q}^2=-m_{\mathrm{D}}^2} = 0 \,, \quad \text{QCD} \,, \tag{5.3}$$

$$\mathbf{q}^2 + m_{\mathrm{E}}^2 + \Pi_{A_0A_0}(\mathbf{q}^2)\big|_{\mathbf{q}^2=-m_{\mathrm{D}}^2} = 0 \,, \quad \text{EQCD} \,, \tag{5.4}$$

where $\Pi_{00}(\mathbf{q}) \equiv \Pi_{\mathrm{E}}(q^2)$. Note that this follows the prescription for general correlators in eq. (2.39).

Taylor-expanding the 2-point correlation functions $\Pi(\mathbf{q}^2)$ both in the bare gauge coupling g_{B} and the soft external momentum $|\mathbf{q}| = q \sim \mathcal{O}(gT)$ for QCD reads

$$\Pi_{\mathrm{E}}(q^2) = \sum_{n=0}^{\infty} q^{2n} \sum_{\ell=1}^{\infty} g_{\mathrm{B}}^{2\ell}\, \Pi_{\mathrm{E}\ell}^{(n)}(0) \,, \tag{5.5}$$

with the Taylor coefficients $\Pi_{\mathrm{E}\ell}^{(n)}$ up to ℓ-loops containing vacuum sum-integrals. An analogous treatment for EQCD has now perturbatively small $m_{\mathrm{E}} \sim \mathcal{O}(gT)$ and $q \sim \mathcal{O}(gT)$ which are, compared to T, allowed scales to expand in. Since these are the only two scales in EQCD, all surviving integrals are vacuum ones with scaleless propagators. In turn, these are rendered zero in dimensional regularisation and especially all self-energy coefficients $\Pi_{\mathrm{E}\ell}$ give a vanishing result $\Pi_{A_0A_0}^{(n)}(0) = 0$. As a consequence eq. (5.4) identifies

$$m_{\mathrm{E}}^2 = m_{\mathrm{D}}^2 \,. \tag{5.6}$$

Indeed, m_{E}^2 is merely a matching coefficient in the EQCD Lagrangian (4.2) and, through its fully perturbative determination, captures the perturbative contribution to the Debye mass and is only sensitive to the hard scale. The expansion (5.5) iteratively solves the first matching condition eq. (5.3) order by order. The leading order is 1-loop which composes of

$$m_{\mathrm{E},1\ell}^2 = \Pi_{\mathrm{E}1\ell}(0) = g^2\, \Pi_{\mathrm{E}1}(0) \,, \tag{5.7}$$

with extension to 2-loop next-to-leading order (NLO)

$$\begin{aligned} m^2_{\mathrm{E},2\ell} &= \Pi_{\mathrm{E}2\ell}(0) - m^2_{\mathrm{E},1\ell}\Pi'_{\mathrm{E}1\ell}(0) \\ &= g^2\,\Pi_{\mathrm{E}1}(0) + g^4\left[\Pi_{\mathrm{E}2}(0) - \Pi_{\mathrm{E}1}(0)\Pi'_{\mathrm{E}1}(0)\right], \end{aligned} \tag{5.8}$$

and 3-loop next-to-next-leading order (NNLO)

$$\begin{aligned} m^2_{\mathrm{E},3\ell} &= \Pi_{\mathrm{E}3\ell}(0) - m^2_{\mathrm{E},2\ell}\Pi'_{\mathrm{E}1\ell}(0) + (-m^2_{\mathrm{E},1\ell})^2\Pi''_{\mathrm{E}1\ell}(0) \\ &= g^2\,\Pi_{\mathrm{E}1}(0) + g^4\left[\Pi_{\mathrm{E}2}(0) - \Pi_{\mathrm{E}1}(0)\Pi'_{\mathrm{E}1}(0)\right] \\ &+ g^6\Big[\Pi_{\mathrm{E}3}(0) - \Pi_{\mathrm{E}1}(0)\Pi'_{\mathrm{E}2}(0) - \Pi'_{\mathrm{E}1}(0)\Pi_{\mathrm{E}2}(0) + \Pi_{\mathrm{E}1}(0)(\Pi'_{\mathrm{E}1}(0))^2 + (\Pi_{\mathrm{E}1}(0))^2\Pi'_{\mathrm{E}1}(0)\Big]. \end{aligned} \tag{5.9}$$

With regard to the 2-loop QCD Debye mass $m^2_{\mathrm{E},2\ell}$ in eq. (5.8), the diagrams that contribute to the different self-energy orders $\Pi^{(n)}_{\mathrm{E}\ell} = \{\Pi_{\mathrm{E}1}, \Pi'_{\mathrm{E}1}, \Pi_{\mathrm{E}2}\}$ are both fermionic, displayed in ref. [2], and bosonic in [120]. The 2-loop QCD Debye mass requires renormalisation

$$\begin{aligned} m^2_{\mathrm{E},2\ell} &= g^2_{\mathrm{R}}\,\Pi_{\mathrm{E}1}(0) \\ &+ g^4_{\mathrm{R}}\left[\Pi_{\mathrm{E}2}(0) - \Pi_{\mathrm{E}1}(0)\Pi'_{\mathrm{E}1}(0) + (\delta_1 g + \delta_2 g)\Pi_{\mathrm{E}1}(0) + \sum_{i=1}^{N_{\mathrm{f}}} m_i^2\delta_1 m_i^2 \frac{\mathrm{d}\Pi_{\mathrm{E}1}(0)}{\mathrm{d}m_i^2}\right], \end{aligned} \tag{5.10}$$

where we inserted the counterterms for the gauge coupling $\delta_1 g, \delta_2 g$ and quark masses δm_i^2 from eqs. (2.54) and (2.55)

$$\delta_1 g = -\frac{1}{(4\pi)^2}\frac{11N_{\mathrm{c}}}{3\epsilon}, \quad \delta_2 g = \frac{1}{(4\pi)^2}\frac{4T_{\mathrm{F}}\sum_{i=1}^{N_{\mathrm{f}}}}{3\epsilon}, \quad \delta_1 m_i^2 = -\frac{1}{(4\pi)^2}\frac{6C_{\mathrm{F}}}{\epsilon}. \tag{5.11}$$

Whereas massless terms receive contributions only from the gauge coupling renormalisation Z_g, masses are renormalised by the RG constant Z_m.

5.2.1 The reduction

Since the integrals that compose the contributing diagrams are vacuum sum-integrals and aware of the temperature scale T, all the thermal integral reduction machinery introduced in chapter 3 applies. The starting point for the following discussion are the integration-by-parts relations eq. (3.63) for 2-loop massive vacuum sum-integrals $Z^{\alpha_1\alpha_2}_{s_1s_2s_3;ii}$ parameterised (without masses) in eq. (3.49).

The list of integration-by-parts relations with a single scale inside the integral is exhaustive. The system eq. (3.49) simplifies parametrically and the mass scale can be factored out of the integrals which is the case in massive vacuum integrals. Since the Matsubara frequencies act as masses every loop order introduces one extra scale in the computation and an ℓ-loop computation becomes an ℓ-scale problem.

The generated massless ($m_i = 0$) system of 2-loop equations eq. (3.63), after systematically combined, drastically decimates the number of master integrals and gives rise to many

identities that factorise into 1-loop sum-integrals

$$\begin{aligned}
Z_{111;11} &= 0 \,, \\
Z_{211;11} &= -\frac{1}{(d-2)(d-5)} Z_{2;1} Z_{2;1} \,, \\
Z_{112;11} &= \frac{1}{(d-2)(d-5)} (Z_{2;1} Z_{2;1} - 2 Z_{2;1} Z_{2;0}) \,, \\
Z_{212;11} &= \frac{2}{(d-2)(d-7)} (Z_{3;1} Z_{2;1} - Z_{3;1} Z_{2;0}) \,, \\
Z_{311;11} &= -\frac{2}{(d-2)(d-7)} (Z_{3;1} Z_{2;1} + Z_{3;1} Z_{2;0}) \,,
\end{aligned} \tag{5.12}$$

among integrals without irreducible scalar products; which is indicated by the lack of superscripts. A similar reduction for general masses is not guaranteed.

Once quark masses are included, the number of integration-by-parts relations diminishes and becomes highly constraint. However, for some special mass configurations non-trivial relations exist – even among massive 2-loop thermal integrals. The two identities pertinent to our analysis, originate from vanishing surface terms of the symmetric integrals

$$\begin{aligned}
0 = {} & \sum\!\!\!\!\!\!\int_{\{K_1 K_2\}} \frac{\partial}{\partial k_{1_i}} \left\{ \frac{(d-2s) k_{1_i}}{\Delta_{K_1} \Delta_{K_2} \delta^s_{K_1-K_2}} + \frac{2 k_{1_0} (k_{1_0} k_{2_i} - k_{2_0} k_{1_i})}{\Delta_{K_1} \Delta^2_{K_2} \delta^s_{K_1-K_2}} - \frac{k_{1_i}}{\Delta_{K_1} \Delta^2_{K_2} \delta^{s-1}_{K_1-K_2}} + \frac{k_{1_i} - k_{2_i}}{\Delta^2_{K_2} \delta^s_{K_1-K_2}} \right\} \\
& + \sum\!\!\!\!\!\!\int_{\{K_1 K_2\}} \frac{\partial}{\partial k_{2_i}} \left\{ \frac{(d-2s) k_{1_i}}{\Delta_{K_1} \Delta_{K_2} \delta^s_{K_1-K_2}} - \frac{2 k_{1_0} (k_{1_0} k_{2_i} - k_{2_0} k_{1_i})}{\Delta^2_{K_1} \Delta_{K_2} \delta^s_{K_1-K_2}} - \frac{(s-1) k_{1_i}}{\Delta^2_{K_1} \Delta_{K_2} \delta^{s-1}_{K_1-K_2}} \right\} ,
\end{aligned} \tag{5.13}$$

with massive propagators $\Delta_K = K^2 + m^2$ and massless ones $\delta_K = K^2$. For $s \in \mathbb{Z}$ the above yield the IBP relations eqs. (B.3) for $Z_{211;110;11}$ at $s = 1$ and (B.4) for $Z_{221;110;11}$ at $s = 2$. Higher s-values still yield IBP relations but not necessarily without superscripts. Applying these reductions to the Taylor coefficients of Π_{E} and Π_{T} with the sum over $N_{\mathrm{f}} = 3, \ldots, 6$ massive fermion flavours, produces a small set of master integrals. At 1-loop level these acquire eqs. (B.6)–(B.12), whereas at 2-loop the results amount to eqs. (B.13)–(B.11).

The fermionic contribution to the 1-loop Debye mass is manifestly of thermal nature. This is reassuring since the Debye mass, as a purely thermal effect, should vanish in vacuum. At 1-loop this is particularly obvious due to the separation of zero-temperature parts in the sum-integrals in accord with eq. (3.73) such that $Z_{s_1;i} = I^{\mathrm{vac}}_{s_1;i} + Z^T_{s_1;i}$. We proceed on a purely algebraic level using IBP relations eq. (3.61), $I^{\mathrm{vac}}_{2;i} = -(d-1)/(2m_i^2) I^{\mathrm{vac}}_{1;i}$. Since vacuum integrals come in $(d+1)$-dimensions, the remaining terms take the following form

$$\Pi_{\mathrm{E1}}(0) = N_{\mathrm{c}} (d-1)^2 Z_{1;0} - 2 \sum_{i=1}^{N_{\mathrm{f}}} \left[(d-1) Z^T_{1;i} + 2 m_i^2 Z^T_{2;i} \right] , \tag{5.14}$$

$$\begin{aligned}
\Pi'_{\mathrm{E1}}(0) = {} & - \left[\frac{d^2 + d + 10}{6} - (d-3)\xi \right] N_{\mathrm{c}} Z_{2;0} \\
& + \frac{1}{3} \sum_{i=1}^{N_{\mathrm{f}}} \left[(d-1) \left(Z^T_{2;i} - \frac{1}{m_i^2} I^{\mathrm{vac}}_{1;i} \right) + 4 m_i^2 Z^T_{3;i} \right] ,
\end{aligned} \tag{5.15}$$

and consequently all mass derivatives of m_{E}^2 are also finite. The last line evaluates the first-order Taylor coefficient of Π_{E1} which shows the divergent vacuum contribution $I^{\mathrm{vac}}_{1;i}$.

A similar dissection applies for the integrals appearing at 2-loop. Vacuum parts cancel upon each other and the remaining contributions are all either purely thermal or factored (thermal)×(vacuum) such as in $\Pi_{\mathrm{E1}} \times \Pi'_{\mathrm{E1}}$, and therefore vanish at zero temperature.

5.2.2 Master sum-integrals

We parameterise both the effective coupling and the Debye mass as in [121] with $\overline{\text{MS}}$-renormalised masses and couplings

$$m_{\text{E}}^2 \equiv T^2\biggl\{g^2(\bar{\mu})\,\alpha_{\text{E4}} + \frac{g^4(\bar{\mu})}{(4\pi)^2}\,\alpha_{\text{E6}} + \mathcal{O}(g^6)\biggr\}\,, \tag{5.16}$$

$$g_{\text{E}}^2 \equiv T\biggl\{g^2(\bar{\mu}) + \frac{g^4(\bar{\mu})}{(4\pi)^2}\,\alpha_{\text{E7}} + \frac{g^6(\bar{\mu})}{(4\pi)^4}\,\gamma_{\text{E1}} + \mathcal{O}(g^8)\biggr\}\,. \tag{5.17}$$

For the renormalised 2-loop contribution to the QCD Debye mass, we obtain

$$\begin{aligned}
\alpha_{\text{E6}} &= N_{\text{c}}^2(d-1)^2 Z_{1;0}\biggl[\frac{d^2-11d+46}{6}Z_{2;0} + \frac{\delta_1 g}{N_{\text{c}}}\biggr] \\
&\quad + N_{\text{c}}\sum_{i=1}^{N_{\text{f}}}\biggl\{-\biggl[(d-1)Z_{1;i} + 2m_i^2 Z_{2;i}\biggr]\biggl[\frac{d^2-5d+28}{3}Z_{2;0} + \frac{2\delta_1 g}{N_{\text{c}}}\biggr] \\
&\qquad\quad + (d-1)^2 Z_{1;0}\biggl[\frac{\delta_2 g}{N_{\text{f}}} - \frac{(d-1)Z_{2;i} + 4m_i^2 Z_{3;i}}{3}\biggr] \\
&\qquad\quad + 2(d-1)(d-3)Z_{1;i}Z_{2;0} + 2m_i^2 Z_{2;i}\bigl[2Z_{2;0} - Z_{2;i}\bigr] \\
&\qquad\quad - 2m_i^2(d-4)\bigl[(d-5)Z_{112;ii} + 4m_i^2 Z_{212;ii}\bigr]\biggr\} \\
&\quad + C_{\text{F}}\sum_{i=1}^{N_{\text{f}}}\biggl[(d-3)Z_{2;i} + 4m_i^2 Z_{3;i}\biggr]\biggl[\biggl(\frac{8}{d-2}Z_{2;i} + \frac{2\delta m_i^2}{C_{\text{F}}}\biggr)m_i^2 + 2(d-1)\bigl[Z_{1;0} - Z_{1;i}\bigr]\biggr] \\
&\quad + \frac{2}{3}\sum_{i,j=1}^{N_{\text{f}}}\biggl[(d-1)Z_{1;i} + 2m_i^2 Z_{2;i}\biggr]\biggl[(d-1)Z_{2;j} + 4m_j^2 Z_{3;j} - \frac{3\delta_2 g}{N_{\text{f}}}\biggr]\,,
\end{aligned} \tag{5.18}$$

using the counterterms from above eq. (5.11) which, after cancelling divergences stemming from fermionic and bosonic $Z_{2;\sigma} = 1/[(4\pi)^2\epsilon] + \mathcal{O}(1)$, yield a finite overall result. Quark mass renormalisation eq. (2.55) evidently affects only $C_{\text{F}}N_{\text{f}}$-proportional terms whereas gauge coupling renormalisation contributes to all N_{c}^2, $N_{\text{c}}N_{\text{f}}$, and N_{f}^2-terms.

A factorisation into 1-loop diagrams parallel to eq. (5.12) fails and more master diagrams require analytic evaluation. Besides 1-loop tadpoles for massless bosons $Z_{s_1;0}$ in eq. (A.39) and massive fermions $Z_{s_1;i}$ in eqs. (A.43)–(A.46), the results for the effective gauge coupling g_{E} and the Debye mass also comprise unfactorised 2-loop master diagrams yielding the following set:

$$m_{\text{E}}^2: \quad Z_{111;ii}\,, \quad Z_{112;ii}\,, \quad Z_{212;ii}\,, \tag{5.19}$$

$$g_{\text{E}}^2: \quad Z_{111;ii}\,, \quad Z_{112;ii}\,, \quad Z_{212;ii}\,, \quad Z_{113;ii}\,, \quad Z^{11}_{111;ii}\,, \quad Z^{11}_{112;ii}\,, \quad Z^{11}_{113;ii}\,. \tag{5.20}$$

The masters $Z_{111;ii}$, $Z_{112;ii}$, and $Z_{212;ii}$ constitute an integral basis[1] for the genuine 2-loop sector of m_{E}^2. Coincidentally, the coefficient of $Z_{111;ii}$ vanishes on an algebraic level. The latter is given in [122] and eq. (A.64) where it was evaluated applying the Saclay method (cf. sec. 3.5.1). Only two masters remain to be evaluated and in principle $Z_{112;ii}$ is attainable from $Z_{111;ii}$ by a mass derivative on the third propagator line. However, since that line is bosonic and eventually massless, the integral is plagued with IR divergences at intermediate stages of its calculation. A thorough discussion that demonstrates that the integral is indeed

[1] Using the IBP relation eq. (B.5) also a different basis is conceivable which replaces $Z_{212;ii} \to Z_{311;ii}$.

finite after taking thorough precautions in dimensional regularisation is summarised in [2] and appendix A.3.1.

Including also massive fermions in $\Pi'_{\mathrm{T}2}$ yields a more precise contribution to the 2-loop effective gauge coupling g_{E}^2 via eq. (4.48). Its set of master diagrams is enhanced by additional ones with non-vanishing Matsubara frequencies in the integral numerators. The computation of $Z_{113;ii}$ demands similar treatment as $Z_{112;ii}$ but its thermal contributions are highly IR-sensitive. We give an IBP reduced expression for the fully massive $\Pi'_{\mathrm{T}2}$ in eq. (B.15) in the basis of eq. (5.20) which agrees with [57] in the limit $m_i \ll T$.

The Debye mass is re-expressed in terms of its explicit masters for the massless fermion limit $m_i \ll T$ reproducing [123]

$$\alpha_{\mathrm{E}4} \overset{d=3-2\epsilon}{=} \frac{N_{\mathrm{c}}}{3} + \frac{N_{\mathrm{f}}}{6} \,, \tag{5.21}$$

$$\begin{aligned}\alpha_{\mathrm{E}6} &\overset{d=3-2\epsilon}{=} \left(\frac{N_{\mathrm{c}}}{3}\right)^2 (22L_b + 5) \\ &+ \frac{N_{\mathrm{c}}N_{\mathrm{f}}}{9}\left(11L_b - 4L_f + \frac{9}{2}\right) - \frac{N_{\mathrm{f}}^2}{9}(2L_f - 1) - C_{\mathrm{F}}N_{\mathrm{f}} \,,\end{aligned} \tag{5.22}$$

$$\alpha_{\mathrm{E}7} \overset{d=3-2\epsilon}{=} \frac{N_{\mathrm{c}}}{3}(22L_b + 1) - \frac{8N_{\mathrm{f}}T_{\mathrm{F}}}{3}L_f \,, \tag{5.23}$$

where L_b and L_f are defined in eq. (2.50) and the first line equals the classic result eq. (5.1).

Once quark masses are included, the α_{E}-coefficients comprise explicit flavour summations. An expansion up to $\mathcal{O}(\epsilon^0)$ yields

$$\alpha_{\mathrm{E}4} \overset{d=3-2\epsilon}{=} \frac{N_{\mathrm{c}}}{3} - 4\sum_{i=1}^{N_{\mathrm{f}}}\left[Z^T_{1;i} + m_i^2 Z^T_{2;i}\right] \,, \tag{5.24}$$

$$\begin{aligned}\alpha_{\mathrm{E}6} &\overset{d=3-2\epsilon}{=} \left(\frac{N_{\mathrm{c}}}{3}\right)^2 (22L_b + 5) \\ &+ N_{\mathrm{c}}(4\pi)^2 \sum_{i=1}^{N_{\mathrm{f}}}\Bigg\{-\frac{2}{9}\left[Z^T_{2;i} + \frac{1}{(4\pi)^2}\ln\frac{\bar{\mu}^2}{m_i^2}\right] - \frac{44}{3(4\pi)^2}\left[Z^T_{1;i} + m_i^2 Z^T_{2;i}\right](2L_b + 1) \\ &\qquad + \frac{8}{(4\pi)^2}Z^T_{1;i} - 2m_i^2\big(Z^T_{2;i}\big)^2 - \frac{4m_i^2}{9}Z^T_{3;i} - 4m_i^2\left[Z^{(\mathrm{FF})}_{112;ii} - 2m_i^2 Z^{(\mathrm{FF})}_{212;ii}\right]\Bigg\} \\ &+ 4C_{\mathrm{F}}(4\pi)^2 \sum_{i=1}^{N_{\mathrm{f}}} m_i^2\left\{\frac{1}{3} + \frac{12m_i^2}{(4\pi)^2}\left[\ln\frac{\bar{\mu}^2}{m_i^2} + \frac{4}{3}\right] - 4\left[Z^T_{1;i} - 2m_i^2 Z^T_{2;i}\right]\right\} Z^T_{3;i} \\ &+ \frac{8}{3}(4\pi)^2 \sum_{i,j=1}^{N_{\mathrm{f}}}\left[Z^T_{1;i} + m_i^2 Z^T_{2;i}\right]\left[Z^T_{2;j} + 2m_j^2 Z^T_{3;j} + \frac{1}{(4\pi)^2}\ln\frac{\bar{\mu}^2}{m_j^2}\right] \,,\end{aligned} \tag{5.25}$$

$$\alpha_{\mathrm{E}7} \overset{d=3-2\epsilon}{=} \frac{N_{\mathrm{c}}}{3}(22L_b + 1) - \frac{2}{3}\sum_{i=1}^{N_{\mathrm{f}}}\left[\ln\frac{\bar{\mu}^2}{m_i^2} + (4\pi)^2 Z^T_{2;i}\right] \,, \tag{5.26}$$

employing massive thermal integrals $Z^T_{s_1;1}$ which we handle in integral representation[2] in appendix A.3 and integrate numerically since they lack a closed form. The genuine 2-loop thermal integral $Z^{(\mathrm{FF})}_{112;ii}$ is evaluated in eq. (A.86) and its mass derivative $Z^{(\mathrm{FF})}_{212;ii}$ in eq. (A.104). The limit $m_i \ll T$ reproduces the zero-mass result eq. (5.22). In all thermal integral expressions the negative-sign convention for fermion distributions is implied (cf. eq. (3.75)).

[2] Alternatively a representation utilising convergent sums over modified Bessel functions is conceivable $Z^T_{1;m;\sigma} = \frac{mT}{2\pi^2}\sum_{n=1}^{\infty}\frac{(2\sigma+1)^n}{n}K_1\big(\frac{nm}{T}\big)$, while K_n are modified Bessel function of the second kind [34].

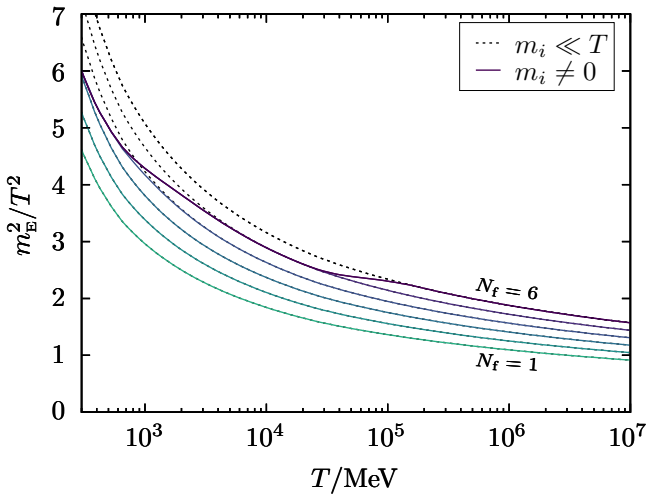

Figure 5.1: The 1-loop QCD Debye mass m_{E}^2/T^2 as a function of the temperature T in units of MeV in the range (300 MeV – 10 TeV). The different solid lines originate from varying the number of quarks in the range $N_{\mathrm{f}} = 1, \ldots, 6$ with chosen renormalisation scale $\bar{\mu} = \bar{\mu}_{\mathrm{opt}} = 2\pi T$. Dashed lines indicate the limit $m_i \ll T$ using eq. (5.21).

5.2.3 Numerical evaluation

The visualisation of the quark mass dependence of the Debye mass (cf. fig. 5.3), follows the strategy in [2]. Therefore, the RGE for $g^2(\bar{\mu})$ in eq. (2.53) is solved numerically in both $\bar{\mu}$-directions with the initial value $\alpha_{\mathrm{s}}(m_Z) = 0.1181 \pm 0.0011$ [3], imposing continuity whenever a quark mass threshold is crossed at $\bar{\mu} \simeq m_i$ and the value of N_{f} is changed. Therefore, 5-loop runnings for the gauge coupling g^2 [17, 18, 19] and quark masses m_i [20, 21] are adopted and their PDG values for m_i [3] are used. As a consequence the running of the quark masses dynamically affects the position of their thresholds $\bar{\mu} = m_i(\bar{\mu})$.

Intuitively the $\overline{\mathrm{MS}}$-renormalisation scale $\bar{\mu}$ is of the order T in the context of the running of the Debye mass. This is justified since m_{E}, in its perturbative generation, is sensitive to only the hard scale. However, to achieve maximal decoupling [50] and convergence in the dimensional reduction, one needs also to account for the non-static modes that make themselves felt in the subtraction scale of the effective theory $\bar{\mu} \propto 2\pi T$ and induce its exact proportionality. This becomes apparent in a renormalisation scheme that demands the slope of the 1-loop effective coupling to vanish and g_{E}^2 is therefore minimally sensitive to changes in $\bar{\mu}$. The latter is known as the procedure of minimal sensitivity [57, 100]. For a specific number of colours and massless fermion flavours one optimises $\bar{\mu}_{\mathrm{opt}} = 4\pi T e^{-(\gamma_{\mathrm{E}}+c)}$ with $c = (N_{\mathrm{c}} - 16 T_{\mathrm{F}} N_{\mathrm{f}} \ln 2)/(22 N_{\mathrm{c}} - 8 T_{\mathrm{F}} N_{\mathrm{f}})$ which is independent of the gauge parameter as it should be in the chosen scheme [124]. For finite quark masses the minimisation condition has to be solved numerically for every value of T.

The influence of non-static modes on the renormalisation scale for the Debye mass as a function of temperature is one of higher-order [2]. Hence, we want to indicate how sensitive the result is on the choice of $\bar{\mu}$ and which magnitude these corrections assume. In our numerical analysis, we retain $\bar{\mu}_{\mathrm{opt}} \sim 2\pi T$ and vary the proportionality in the renormalisation scale $\bar{\mu} = (0.5 \ldots 2.0) \times 2\pi T$.

The thermal 2-loop functions Z_{112} and Z_{212} and also 1-loop $Z_{1;\sigma}$ and various mass-derivatives thereof, are integrated numerically. For efficiency reason starting at 2-loop, the implementation is adapted within `QUADPACK` routines of the `GSL` library in `C++` .

The 1-loop QCD Debye mass for different fermion flavours in the range $N_{\mathrm{f}} = 1, \ldots, 6$ is shown in fig. 5.1 with their limiting case $m_i \ll T$ as a reference according with [100]. Every quark mass threshold is crossed over a broad enough range of temperatures to not be

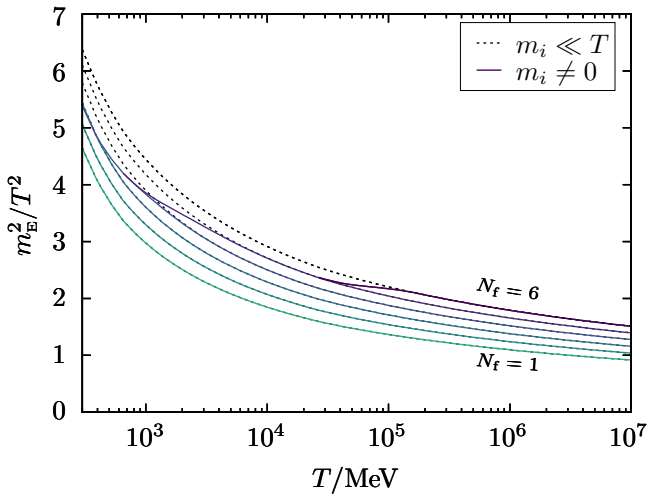

Figure 5.2: The 2-loop QCD Debye mass m_E^2/T^2 as a function of the temperature T in units of MeV in the range (300 MeV – 10 TeV). The different solid lines originate from varying the number of quarks in the range $N_f = 1, \ldots, 6$ with chosen renormalisation scale $\bar{\mu} = \bar{\mu}_{opt} = 2\pi T$. Their lower limit is chosen as $T \gtrsim m_{N_f} \times 0.15$ with m_{N_f} the highest quark mass of the N_f-theory. Dashed lines indicate the limit $m_i \ll T$ using eqs. (5.21) and (5.22).

resolvable on their own. By comparing between N_f-values, various plateau regions become discernible. The most prominent one occurs around $T \sim 70$ GeV when the top quark mass threshold is crossed.

The 2-loop level (cf. fig. 5.2) pronounces the deviation from their $m_i \ll T$ limit at low temperatures even further. Since the effective theory is an EFT founded on the high-temperature scale separation of QCD, results are expected to become increasingly unreliable at low temperature. With a renormalisation scale of the order of the high-scale $\bar{\mu} \sim T$, large logarithms appear in eq. (5.25) once certain masses set the largest scale themselves $m_i \gg T$. In other words the DR fails to resolve these scales at low-T. Therefore, the curves in fig. 5.2 are shown up to values of T where the effective theory is still valid choosing this limit at 15% of the value of the highest quark mass m_{N_f} in the N_f-theory. For $N_f = 6$ this relates to the top mass with a regime of utility $T \gtrsim m_t \times 0.15$.

The crossing of quark thresholds occurs within equivalent temperature intervals as at 1-loop and approaches the high-T limit qualitatively similarly. The dependence on higher-order effects is diminished while precision is increased at 2-loop level. Inspecting the specific case of $N_f = 6$ in fig. 5.3, this is to validate the argument above that higher-order effects are indeed subleading.

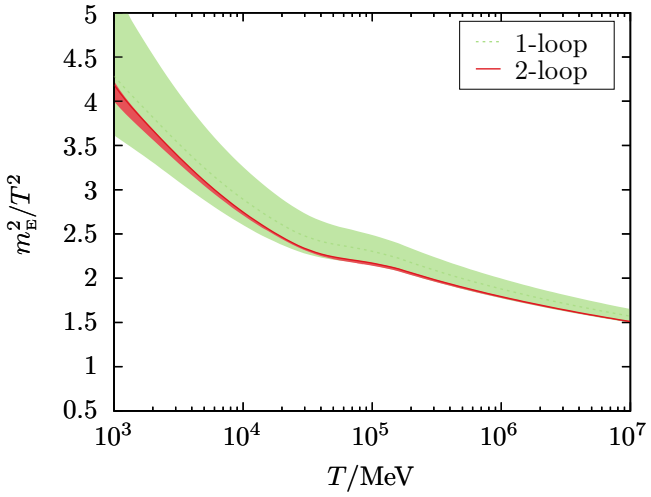

Figure 5.3: 1-loop (green) and 2-loop (red) QCD Debye mass m_E^2/T^2 as function of temperature T, in units of MeV. The variation of $\bar{\mu} = (0.5 \ldots 2.0) \times \bar{\mu}_{\text{opt}}$ with $\bar{\mu}_{\text{opt}} = 2\pi T$ is indicated by the light correspondingly coloured bands. Visible plateau when crossing the top mass threshold around $T \sim 70$ GeV.

Chapter 6

Conclusions and outlook

To fully study the infrared behaviour of dimensionally reduced thermal field theories, contributions from higher-dimensional operators must be included. The intuitive picture is that the non-static modes decouple at high temperatures because their masses become infinitely heavy like in every other effective theory. This is not entirely true. Due to the dynamical generation of the light masses the Appelquist-Carazzone [33] decoupling theorem breaks down at finite temperature. Consequently, corrections from higher-order operators enter at the same level as higher orders in perturbation theory.

The foundation of this thesis is a computer algebraic algorithm that fully automatically streamlines the matching of dimensional reduction as outlined in chapter 3. Its goal is to compute n-point correlation functions of the fundamental theory with different configurations of external legs. These are matched onto the effective vertices in the EFT. The procedure allows for a much more general treatment of DR while bearing enough potential to be scaled up for higher accuracy computations with more loops and legs.

Indeed, we showed [1] how higher-dimensional operators are necessary for understanding the logarithmic divergences of the effective magnetostatic gauge coupling g_{M} in the dimensionally reduced theory of hot Yang-Mills. A remnant IR divergence found at 3-loop level [100] was revealed to reside in the set of dimension-six operators in EQCD and MQCD that is indispensable for a well-defined expansion in the weak-coupling.

Their influence on the IR dynamics could be even more prominent. We found that even though the soft scale $\mathcal{O}(gT)$ is parametrically well above the ultrasoft scale $\mathcal{O}(g^2T)$, it still contributes in the cancellation of the aforementioned IR divergences 1097 times more than the cancelling contribution from higher-dimensional MQCD operators. Including such operators in simulations might allow for an improved accuracy in the description of the IR dynamics in EQCD.

When matching the electrostatic onto the magnetostatic theory, the dimensional reduction integrates out the soft scale or concretely the dynamical mass m_{E}. Therein, the dimension-six operators are generated in the ultrasoft theory, namely MQCD. Contrarily, a full cancellation of mass-suppressed $1/m_{\mathrm{E}}^3$-terms fails. Together with an ambiguity of the Debye mass they render the effective coupling of the ultrasoft theory g_{M} non-perturbative at $\mathcal{O}(\alpha_{\mathrm{s}}^{3/2})$. One explanation is that EQCD is indeed confining rather than barely perturbative as discussed in sec. 2.4. In this case the ambiguities inside m_{E} would then be a natural consequence. To better understand the behaviour of the theory, a computation to access the first non-perturbative orders would be illuminating but also involve investigations of $1/m_{\mathrm{E}}^3$-suppressed operators in MQCD.

Returning to 2-loop level where no such problems are present, the matching computation of the Debye mass m_{E} in QCD with massive fermions is conducted [2]. Aiming for astronomically large scales $T \gtrsim 1$ GeV, we witnessed smooth crossing of the quark mass thresholds (cf. fig. 5.3). The cornerstones of this computation are the non-trivial IBP reductions for

massive 2-loop sum-integrals in eq. (5.13) as well as the evaluation of the remaining master sum-integral Z_{112} filed in appendix A.3.1.

6.1 Outlook and future work

Future work focuses on the automated application of dimensional reduction to various thermal field theories which has one striking advantage: A systematic implementation of all order resummation. An immediate continuation in dimensionally reduced QCD is to put forward extensions of different matching parameters such as the

(i) 3-loop QCD Debye mass including massless fermionic matter in the fundamental representation. This increases its accuracy from current hot Yang-Mills computations at this order [119, 100]. Once fermions are allowed inside diagrams, the set of symmetries that comes to aid for purely bosonic integrals is drastically diminished. The reason is fermion number conservation which constraints the diagram isomorphism founded on momentum shifts that lead back to the same diagram. Consequently more topologies and integrals occur.

(ii) 2-loop EQCD effective gauge coupling g_{E}^2 including quark mass effects. Based on already IBP-reduced expressions eq. (B.15), the set of master integrals is enlarged and receives additional IR-divergent integrals.

(iii) 4-loop Yang-Mills pressure going beyond the currently known contributions up to $g^6 \ln g$. Tackling the next purely perturbative contribution at g^6 fosters new higher-loop sum-integral evaluation techniques especially since present attempts are barely automated for bosonic 3-loop integrals. There genuine vacuum integrals without lower-loop subtopologies are either unknown or demand a case-by-case study. A typical example is the Mercedes type integral (cf. fig. 3.2).

With all this improved understanding from the side of QCD, the same tools can now be applied to other gauge theories, particularly Beyond the Standard Model theories with extended Higgs sectors, which may possess first order phase transitions leading to important cosmological consequences. Studying these effects with dimensional reduction was reinvigorated after staying dormant for some time.

Then dimensional reduction can be used in the electroweak theory to compute the effective potential for the Higgs field. There DR is superior since direct resummations at higher orders are inconsistent. One major culprit is its generalisation to higher-dimensional operators included in the parent theory. In dimensional reduction this necessitates the matching of the corresponding effective n-point functions on both theory sides. Equally, those higher-point functions need to be accounted for in the conventional approach with the Daisy resummed thermal effective potential [125] where they are incorporated in thermal masses. Whereas this procedure is the only way for the effective potential to mitigate the IR problem, it is nevertheless oblivious to some infrared sensitive pieces originating from those higher-order diagrams.

The constructed in-house algorithm provides a framework that generalises dimensional reduction for a whole class of different theories beyond the Standard Model where scalar extensions can assume representations of complex n-tuplets. The salient point is that only the stage of group-algebraic manipulation is the one that needs extra generalisation. Previous attempts address the special cases of complex multiplets for the singlet ($n = 1$) [48], the doublet ($n = 2$) [126, 127], and the real triplet ($n = 3$) [128]. Higher-dimensional representations such as the quintuplet ($n = 5$) and septuplet ($n = 7$) are considered in [129]. However, their application in the context of electroweak phase transitions (EWPT) is less exploited and open for further investigations.

Furthermore, integration-by-parts identities not only offer a strong tool to facilitate the formidable task to compute thousands of Feynman diagrams by finding equalities in their parameter space. They also spark interest in their own understanding. Many IBP relations show a strong sign of systematics during the reduction and the Laporta algorithm offers a brute force method to still apply them. However, there is very little understanding how to uncover the general solutions of the system of relations. One example is the conjectured factorisation of massless thermal integrals at 2-loop order.

Attempts for direct decomposition-by-intersection methods [84, 85, 86] of certain diagrams in the vector space of master integrals demonstrate how this process can be facilitated. The advantage is that the computation of a large number of relations can be omitted and the initial to-be-reduced integral is directly projected onto a minimal basis. Therefore employing these methods at finite temperature is envisaged.

Appendix A

Master integrals

This appendix collects vacuum and thermal master integrals appearing in chapters 4 and 5. Along their evaluation one encounters the dimensionally regularised integration measure

$$\begin{aligned} \mathrm{d}^d p &= p^{d-1}\mathrm{d}p \prod_{i=1}^{d-1} \sin^{i-1}\theta_i \,\mathrm{d}\theta_i \\ &= p^{d-1}\mathrm{d}p\,\mathrm{d}\Omega_{d-1} = p^{d-1}\mathrm{d}p\,\mathrm{d}\Omega_{d-2}\,\sin^{d-2}\theta_{d-1}\,\mathrm{d}\theta_{d-1}\,, \end{aligned} \tag{A.1}$$

where θ_i is the angle to the i-th axis, with $0 \leq \theta_1 < 2\pi$ and $0 \leq \theta_i < \pi$ for $i > 1$ for the $(d-1)$-dimensional surface area. The angle parameterisation $z = \mathbf{p}\cdot\mathbf{k}/|\mathbf{p}||\mathbf{k}|$ with respect to one external vector $\mathbf{k}$ reads [130]

$$\int_{\mathbf{p}} = \int_p = \int \frac{\mathrm{d}\Omega_{d-2}}{(2\pi)^d} \int_0^\infty \mathrm{d}p\, p^{d-1} \int_{-1}^{+1} \mathrm{d}z\, (1-z^2)^{\frac{d-3}{2}} \tag{A.2}$$

$$= \int \frac{\mathrm{d}\Omega_{d-1}}{(2\pi)^d} \int_0^\infty \mathrm{d}p\, p^{d-1} = c_d \int_0^\infty \mathrm{d}p\, p^{d-1}\,, \tag{A.3}$$

where the second line shows the special case of a z-independent integrand. The d-dimensional angular integral evaluates directly with abbreviations

$$\Omega_d = \frac{2\pi^{\frac{d+1}{2}}}{\Gamma\left(\frac{d+1}{2}\right)}\,, \quad c_d = \frac{\Omega_{d-1}}{(2\pi)^d} = \frac{2}{(4\pi)^{\frac{d}{2}}\Gamma\left(\frac{d}{2}\right)}\,, \quad \frac{\Omega_{d-2}}{(2\pi)^d} = \frac{4}{(4\pi)^{\frac{d+1}{2}}\Gamma\left(\frac{d-1}{2}\right)}\,. \tag{A.4}$$

A.1 Vacuum integrals

In order to display the results for physical quantities, we define the standard Passarino-Veltman type functions [131], in Euclidean spacetime:

$$I(m) \equiv \int_K \frac{1}{[K^2+m^2]}\,, \tag{A.5}$$

$$B(Q;m_1,m_2) \equiv \int_K \frac{1}{\left[(K+Q)^2+m_1^2\right]\left[K^2+m_2^2\right]}\,. \tag{A.6}$$

When dealing with discrete sums we encounter polylogarithms, generalised (Hurwitz) and Riemann Zeta functions in their sum-representation

$$\mathrm{Li}_s(z) \equiv \sum_{k=1}^\infty \frac{z^k}{k^s}\,, \quad \zeta(s,q) \equiv \sum_{k=0}^\infty (q+k)^{-s}\,, \quad \zeta_s \equiv \sum_{k=1}^\infty k^{-s}\,, \tag{A.7}$$

and integral representations

$$\mathrm{Li}_s(\pm z) = \pm\frac{1}{\Gamma(s)}\int_0^\infty \mathrm{d}x\,\frac{x^{s-1}}{e^x z^{-1}\mp 1}\,, \tag{A.8}$$

$$\zeta(s,q) = \frac{1}{\Gamma(s)}\int_0^\infty \mathrm{d}x\,\frac{x^{s-1}}{e^{qx}\,(1-e^{-x})}\,, \tag{A.9}$$

$$\begin{aligned}\zeta_s &= \frac{1}{\Gamma(s)}\int_0^\infty \mathrm{d}x\,\frac{x^{s-1}}{e^x-1}\\ &= \frac{1}{(1-2^{1-s})}\frac{1}{\Gamma(s)}\int_0^\infty \mathrm{d}x\,\frac{x^{s-1}}{e^x+1}\,,\end{aligned} \tag{A.10}$$

for $\mathrm{Re}(s)>1$. Sum-representations of Hypergeometric functions and Hypergeometric Appell functions are defined as

$${}_pF_q[\alpha_1,\ldots,\alpha_p;\beta_1,\ldots,\beta_q;z] = \sum_{n=0}^\infty \frac{(\alpha_1)_n\ldots(\alpha_p)_n}{(\beta_1)_n\ldots(\beta_q)_n}\frac{z^n}{n!}\,, \tag{A.11}$$

$$F_1\left[\alpha_1;\beta_1,\beta_2;\gamma_1;z_1,z_2\right] = \sum_{m,n=0}^\infty \frac{(\alpha_1)_{m+n}(\beta_1)_m(\beta_2)_n}{(\gamma_1)_{m+n}}\frac{z_1^m}{m!}\frac{z_2^n}{n!}\,, \tag{A.12}$$

with $(a)_n = \Gamma(a+n)/\Gamma(a)$ the Pochhammer symbol. The integral representations of two special cases of Hypergeometric functions are given as

$$\begin{aligned}{}_2F_1[\alpha_1,\alpha_2;\beta_1;z] &= \frac{\Gamma(\beta_1)}{\Gamma(\alpha_2)\Gamma(\beta_1-\alpha_2)}\\ &\quad\times\int_0^1 \mathrm{d}x\,x^{\alpha_2-1}(1-x)^{\beta_1-\alpha_2-1}(1-zx)^{-\alpha_1}\,,\end{aligned} \tag{A.13}$$

$$\begin{aligned}F_1\left[\alpha_1;\beta_1,\beta_2;\gamma_1;z_1,z_2\right] &= \frac{\Gamma(\gamma_1)}{\Gamma(\alpha_1)\Gamma(\gamma_1-\alpha_1)}\\ &\quad\times\int_0^1 \mathrm{d}x\,x^{\alpha_1-1}(1-x)^{\gamma_1-\alpha_1-1}(1-z_1x)^{-\beta_1}(1-z_2x)^{-\beta_2}\,.\end{aligned} \tag{A.14}$$

Below we derive and list the set of master integrals encountered in this thesis in dimensional regularisation. We utilise the case of denominators $\Delta_{k_1}\equiv k_1^2+m^2$ that depend on a single mass scale m.

The one-loop tadpole integral has an analytic solution in terms of Gamma functions

$$\begin{aligned}I_{s_1;m} &= \quad\bigcirc\\ &\equiv \int_{k_1}\frac{T}{\Delta_{k_1,m}^{s_1}} = \left(\frac{\bar\mu^2 e^{\gamma_\mathrm{E}}}{4\pi}\right)^\epsilon \frac{[m^2]^{\frac{d}{2}-s_1}}{(4\pi)^{\frac{d}{2}}}\frac{\Gamma\left(s_1-\frac{d}{2}\right)}{\Gamma\left(s_1\right)}\,,\end{aligned} \tag{A.15}$$

$$\begin{aligned}I_{1;m} &\overset{d=3-2\epsilon}{=} -\frac{m\mu^{-2\epsilon}T}{4\pi}\left(\frac{\bar\mu}{2m}\right)^{2\epsilon}\left\{1+2\epsilon+\epsilon^2\left[4+\frac{3\zeta_2}{2}\right]\right.\\ &\qquad\left.+\epsilon^3\left[8+3\zeta_2-\frac{7\zeta_3}{3}\right]+\mathcal{O}(\epsilon^4)\right\}\,,\end{aligned} \tag{A.16}$$

$$\begin{aligned}I_{1;m} &\overset{d=4-2\epsilon}{=} -\frac{m^2\mu^{-2\epsilon}T}{(4\pi)^2}\left(\frac{\bar\mu}{m}\right)^{2\epsilon}\left\{\frac{1}{\epsilon}+1+\epsilon\left[1+\frac{\zeta_2}{2}\right]\right.\\ &\qquad\left.+\epsilon^2\left[1+\frac{\zeta_2}{2}-\frac{\zeta_3}{3}\right]+\mathcal{O}(\epsilon^3)\right\}\,,\end{aligned} \tag{A.17}$$

where $I(m) = I_{1;m}$.

For the generalised 2-point function first Feynman parameterisation is applied before the integral is symmetrised in m_1, m_2

$$B(Q;m_1,m_2) = \quad \text{(bubble)}$$
$$\equiv \int_0^1 \mathrm{d}x \int_K \frac{1}{\left[K^2 + x(1-x)Q^2 + (1-x)m_1^2 + xm_2^2\right]^2}$$
$$= \frac{\mu^{-2\epsilon}}{(4\pi)^2}\left[\frac{1}{\epsilon} + 2 + \ln\frac{\bar{\mu}^2}{m_1 m_2} + \frac{m_1^2 - m_2^2}{Q^2}\ln\frac{m_1}{m_2}\right.$$
$$\left. - \frac{2\sqrt{(m_1-m_2)^2+Q^2}\sqrt{(m_1+m_2)^2+Q^2}}{Q^2}\operatorname{artanh}\left(\frac{\sqrt{(m_1-m_2)^2+Q^2}}{\sqrt{(m_1+m_2)^2+Q^2}}\right)\right]. \qquad \text{(A.18)}$$

Moreover, the two-loop sunset integral [51, 132] with masses m_i and $m_{123} = \sum_i^3 m_i$ and mass fractions

$$x = \left(\frac{m_2}{m_1}\right)^2, \quad y = \left(\frac{m_3}{m_1}\right)^2, \qquad \text{(A.19)}$$

yields in d-dimensions

$$I_{s_1 s_2 s_3, \underline{m}} = \quad \text{(sunset: 1, 2, 3)}$$
$$\equiv \int_{k_1,k_2} \frac{T^2}{\Delta_{k_1,m_1}^{s_1}\Delta_{k_2,m_2}^{s_2}\Delta_{k_1-k_2,m_3}^{s_3}}$$
$$= \left(\frac{\bar{\mu}^2 e^{\gamma_\mathrm{E}}}{4\pi}\right)^{2\epsilon}\frac{[m_1^2]^{d-s_{123}}}{(4\pi)^d}\frac{1}{\Gamma(s_1)\Gamma(s_2)\Gamma(s_3)\Gamma\left(\frac{d}{2}\right)}$$
$$\times \sum_{nm}\frac{y^n}{n!}\frac{x^m}{m!}\frac{\Gamma\left(\frac{d}{2}-s_3\right)}{\left(s_3-\frac{d}{2}+1\right)_n}\frac{\Gamma\left(\frac{d}{2}-s_2\right)}{\left(s_2-\frac{d}{2}+1\right)_m}$$
$$\times\left[\Gamma\Big(s_{23}+n+m-\frac{d}{2}\Big)\Gamma\Big(s_{123}+n+m-d\Big)\right.$$
$$+ y^{s_3-\frac{d}{2}}\Gamma\Big(s_2+n+m\Big)\Gamma\Big(s_{12}+n+m-\frac{d}{2}\Big)$$
$$+ x^{s_2-\frac{d}{2}}\left[\Gamma\Big(s_3+n+m\Big)\Gamma\Big(s_{12}+n+m-\frac{d}{2}\Big)\right.$$
$$\left.\left. + y^{s_3-\frac{d}{2}}\Gamma\Big(s_1+n+m\Big)\Gamma\Big(n+m+\frac{d}{2}\Big)\right]\right], \qquad \text{(A.20)}$$

$$I_{111;\underline{m}} \overset{d=3-2\epsilon}{=} \frac{\mu^{-4\epsilon}T^2}{(4\pi)^2}\left(\frac{\bar{\mu}}{m_{123}}\right)^{4\epsilon}\left\{\frac{1}{4\epsilon}+\frac{1}{2}\right.$$
$$\left. + \epsilon\left[1 - \frac{\zeta_2}{4} + \sum_{i=1}^{3}\mathrm{Li}_2\left(1-\frac{2m_i}{m_{123}}\right)\right] + \mathcal{O}(\epsilon^2)\right\}, \qquad \text{(A.21)}$$

where the last line evaluated the sunset in $d = 3 - 2\epsilon$ and with general masses while abbreviating sums over denominator powers s_i and masses m_i

$$s_{\{i\}} = \sum_{j\in\{i\}} s_j\,, \quad m_{\{i\}} = \sum_{j\in\{i\}} m_j\,. \qquad \text{(A.22)}$$

The sunset $I_{111;\underline{m}}$ with equal masses $m_i = m$ occurs in two variations which decompose in

terms of hypergeometric functions ${}_2F_1$ and factor 1-loop tadpole diagrams [133, 134]

$$
\begin{aligned}
I_{111;mm0} &= -\frac{d-2}{d-3}\frac{1}{2m^2}(I_{1;m})^2 \,, \\
I_{111;mmm} &= -\frac{d-2}{d-3}\frac{3}{4m^2}\left({}_2F_1\left[\frac{4-d}{2},1;\frac{5-d}{2};\frac{3}{4}\right] - 3^{\frac{d-5}{2}}\frac{2\pi\Gamma(5-d)}{\Gamma\left(\frac{4-d}{2}\right)\Gamma\left(\frac{6-d}{2}\right)}\right)(I_{1;m})^2 \,,
\end{aligned}
\tag{A.23}
$$

where the first line is generated by the two-loop IBP relations eq. (3.63). The triply massive $H_3(m)$ or doubly massive $H_2(m)$ abbreviate

$$
H_3(m) = I_{111;mmm} \,, \quad H_2(m) = I_{111;mm0} \,. \tag{A.24}
$$

Special mass configurations with higher denominator powers for the sunset (A.20) have the closed forms

$$
\begin{aligned}
I_{s_1s_2s_3;m_1m_2 0} &= \quad \text{(sunset: 1, 2, 3)} \\
&= \left(\frac{\bar\mu^2 e^{\gamma_\mathrm{E}}}{4\pi}\right)^{2\epsilon}\frac{[m_1^2]^{d-s_{123}}}{(4\pi)^d} \\
&\qquad \times \frac{\Gamma\left(\frac{d}{2}-s_3\right)\Gamma\left(s_{23}-\frac{d}{2}\right)\Gamma\left(s_{13}-\frac{d}{2}\right)\Gamma\left(s_{123}-d\right)}{\Gamma\left(\frac{d}{2}\right)\Gamma\left(s_1\right)\Gamma\left(s_2\right)\Gamma\left(s_{123}+s_3-d\right)} \\
&\qquad \times {}_2F_1\left[s_{23}-\frac{d}{2}, s_{123}-d; s_{123}+s_3-d; 1-\rho\right] \,,
\end{aligned}
\tag{A.25}
$$

$$
\begin{aligned}
I_{s_1s_2s_3;mm0} &= \left(\frac{\bar\mu^2 e^{\gamma_\mathrm{E}}}{4\pi}\right)^{2\epsilon}\frac{[m^2]^{d-s_{123}}}{(4\pi)^d} \\
&\qquad \times \frac{\Gamma\left(\frac{d}{2}-s_3\right)\Gamma\left(s_{23}-\frac{d}{2}\right)\Gamma\left(s_{13}-\frac{d}{2}\right)\Gamma\left(s_{123}-d\right)}{\Gamma\left(\frac{d}{2}\right)\Gamma\left(s_1\right)\Gamma\left(s_2\right)\Gamma\left(s_{123}+s_3-d\right)} \,,
\end{aligned}
\tag{A.26}
$$

$$
\begin{aligned}
I_{s_1s_2s_3;m00} &= \left(\frac{\bar\mu^2 e^{\gamma_\mathrm{E}}}{4\pi}\right)^{2\epsilon}\frac{[m^2]^{d-s_{123}}}{(4\pi)^d} \\
&\qquad \times \frac{\Gamma\left(\frac{d}{2}-s_2\right)\Gamma\left(\frac{d}{2}-s_3\right)\Gamma\left(s_{23}-\frac{d}{2}\right)\Gamma\left(s_{123}-d\right)}{\Gamma\left(\frac{d}{2}\right)\Gamma\left(s_1\right)\Gamma\left(s_2\right)\Gamma\left(s_3\right)} \,,
\end{aligned}
\tag{A.27}
$$

where $\rho = \left(\frac{m_2}{m_1}\right)^2$ for $m_2 \leq m_1$ with an apparent symmetry $s_1 \leftrightarrow s_2$. The result in eq. (A.26) is recovered from eq. (A.25) in the limit $m_1 \to m_2$ or conversely $\rho \to 1$. The limit $m_2 \to 0$ in eq. (A.27) is achieved by $\rho \to 0$ and the identity

$$
\begin{aligned}
{}_2F_1[a,b;c;z] &= \frac{\Gamma(c)\Gamma(a+b-c)}{\Gamma(a)\Gamma(b)}{}_2F_1[c-a,c-b;c-a-b+1;1-z](1-z)^{c-a-b} \\
&\quad + \frac{\Gamma(c)\Gamma(c-a-b)}{\Gamma(c-a)\Gamma(c-b)}{}_2F_1[a,b;a+b-c+1;1-z] \,,
\end{aligned}
\tag{A.28}
$$

inducing symmetry in $s_2 \leftrightarrow s_3$.

The 3-loop level encounters integrals such as cubic powers of one-loop tadpoles but also

basketball integrals (cf. [110, 135]) which have the structure

$$
\begin{aligned}
I_{110011,\underline{m}} \quad &= \quad \text{  } \\
&\equiv \quad \int_{k_1,k_2,k_3} \frac{T^3}{\Delta^{s_1}_{k_1,m_1}\Delta^{s_2}_{k_2,m_2}\Delta^{s_3}_{k_1-k_3,m_3}\Delta^{s_4}_{k_2-k_3,m_4}} \\
&\overset{d=3-2\epsilon}{=} \quad -\frac{m_{1234}\mu^{-6\epsilon}T^3}{(4\pi)^3}\left(\frac{\bar{\mu}}{m_{1234}}\right)^{6\epsilon}\left\{\frac{1}{4\epsilon}+2+\frac{1}{2}\sum_{i=1}^{4}\frac{m_i}{m_{1234}}\ln\frac{m_{1234}}{2m_i}\right. \\
&\qquad +\epsilon\left[13+\frac{9\zeta_2}{8}+\sum_{i=1}^{4}\left(\left(1-\frac{2m_i}{m_{1234}}\right)\mathrm{Li}_2\left(1-\frac{2m_i}{m_{1234}}\right)\right.\right. \\
&\qquad\qquad \left.\left.\left.+\frac{1}{2}\frac{m_i}{m_{1234}}\left(\ln^2\frac{m_{1234}}{2m_i}+8\ln\frac{m_{1234}}{2m_i}\right)\right)\right]+\mathcal{O}(\epsilon^2)\right\}, \qquad \text{(A.29)}
\end{aligned}
$$

where $m_{1234}=\sum_{i=1}^{4}m_i$ is the sum over all massive lines and Li_2 is the dilogarithm. The two cases featuring in the three-loop EQCD gluon self-energy in eq. (4.85), namely the two-mass B_2 and four-mass B_4 basketball diagram abbreviate special mass configurations of $I_{110011,\underline{m}}$

$$
B_4(m)=I_{110011;mm00mm}\,, \quad B_2(m)=I_{110011;mm0000}\,, \qquad \text{(A.30)}
$$

which equate to

$$
\begin{aligned}
B_4(m)=\ &\text{  } \\
&=-\frac{m\mu^{-6\epsilon}T^3}{(4\pi)^3}\left(\frac{\bar{\mu}}{2m}\right)^{6\epsilon} \\
&\quad\times\left\{\frac{1}{\epsilon}+8-4\ln 2+\epsilon\left[52+\frac{17\zeta_2}{2}-32\ln 2+4\ln^2 2\right]+\mathcal{O}(\epsilon^2)\right\}, \qquad \text{(A.31)}
\end{aligned}
$$

$$
B_2(m)=\ \text{  } =-\frac{m\mu^{-6\epsilon}T^3}{(4\pi)^3}\left(\frac{\bar{\mu}}{2m}\right)^{6\epsilon}\left\{\frac{1}{2\epsilon}+4+\epsilon\left[26+\frac{25\zeta_2}{4}\right]+\mathcal{O}(\epsilon^2)\right\}, \qquad \text{(A.32)}
$$

using $\mathrm{Li}_2(1)=\zeta_2=\pi^2/6$.

A.2 Massless sum-integrals

The tensor decomposition outlined in sec. 3.2.1 consists of the extraction of the sum-integral tensor structure onto the tensors defined in eqs. (2.41) and (3.20) and the decoupling of the external momentum (cf. eq. (3.25)). In one-loop tadpole sum-integrals with bosonic or fermionic four-momentum dependence denoted by $K=(k_n,\mathbf{k})$, non-vanishing tensor sum-integrals carry an even number of Lorentz indices. Its simplest example with two open indices μ,ν establishes the relation

$$
\begin{aligned}
\sum\!\!\!\!\!\!\int_K \frac{K_\mu K_\nu}{[K^2]^{s_1}} &= \delta_{\mu 0}\delta_{\nu 0}\sum\!\!\!\!\!\!\int_K \frac{k_0k_0}{[K^2]^{s_1}}+\delta_{\mu i}\delta_{\nu j}\sum\!\!\!\!\!\!\int_K \frac{k_ik_j}{[K^2]^{s_1}} \\
&= \delta_{\mu 0}\delta_{\nu 0}\sum\!\!\!\!\!\!\int_K \frac{k_n^2}{[K^2]^{s_1}}+\delta_{\mu i}\delta_{\nu j}\delta_{ij}\frac{1}{d}\sum\!\!\!\!\!\!\int_K \frac{k^2}{[K^2]^{s_1}} \\
&= \delta_{\mu 0}\delta_{\nu 0}\sum\!\!\!\!\!\!\int_K \frac{k_n^2}{[K^2]^{s_1}}+\delta_{\mu i}\delta_{\nu i}\frac{1}{d}\sum\!\!\!\!\!\!\int_K \frac{K^2-k_n^2}{[K^2]^{s_1}} \\
&= \delta_{\mu 0}\delta_{\nu 0}Z^2_{s_1;\sigma}+\frac{\delta_{\mu i}\delta_{\nu i}}{d}\left[Z^0_{s_1;\sigma}-Z^2_{s_1;\sigma}\right] \\
&= \left[\delta_{\mu 0}\delta_{\nu 0}\frac{2s_1-2-d}{2(s_1-1)}+\frac{\delta_{\mu i}\delta_{\nu i}}{d}\left(1-\frac{2s_1-2-d}{2(s_1-1)}\right)\right]Z^0_{s_1-1;\sigma} \\
&= \frac{T_{\mu\nu}(2s_1-3-d)+\delta_{\mu\nu}}{2(s_1-1)}\,Z^0_{s_1-1;\sigma}\,, \qquad \text{(A.33)}
\end{aligned}
$$

which extends the list of basic sum-integrals in appendix B in [1]. Once more indices appear in the tensor structure all possible combinations of $T_{\mu\nu}$ and $\delta_{\mu\nu}$ appear and their combinatorial factors are determined through tensor decomposition. By changing basis onto the S/T-basis eq. (2.41) we show how some of the relevant sum-integral relations are altered *viz.*

$$\sum\!\!\!\!\!\!\int_K \frac{K_\mu K_\nu}{K^8} = \sum\!\!\!\!\!\!\int_K \frac{(6-d)\,T_{\mu\nu}+S_{\mu\nu}}{6K^6}\,, \tag{A.34}$$

$$\begin{aligned}\sum\!\!\!\!\!\!\int_K \frac{K_\mu K_\nu K_\rho K_\sigma}{K^{10}} &= \sum\!\!\!\!\!\!\int_K \left\{\frac{(8-d)(6-d)T_{\mu\nu\rho\sigma}}{48K^6}\right.\\ &\left.+\frac{(6-d)(T_{\mu\nu}S_{\rho\sigma}+5\text{ permutations})+S_{\mu\nu\rho\sigma}}{48K^6}\right\},\end{aligned} \tag{A.35}$$

$$\begin{aligned}\sum\!\!\!\!\!\!\int_K \frac{K_\mu K_\nu K_\rho K_\sigma K_\alpha K_\beta}{K^{12}} &= \sum\!\!\!\!\!\!\int_K \left\{\frac{(10-d)(8-d)(6-d)T_{\mu\nu\rho\sigma\alpha\beta}}{480K^6}\right.\\ &+\frac{(8-d)(6-d)(T_{\mu\nu\rho\sigma}S_{\alpha\beta}+14\text{ permutations})}{480K^6}\\ &\left.+\frac{(6-d)\,(T_{\mu\nu}S_{\rho\sigma\alpha\beta}+14\text{ permutations})+S_{\mu\nu\rho\sigma\alpha\beta}}{480K^6}\right\}.\end{aligned} \tag{A.36}$$

When considering a rescaling of the spatial momenta $k_i \to 2k_i$ and a partition of the Matsubara sums as

$$\sum_{n\in\mathbb{Z}} = \sum_{\text{even}} + \sum_{\text{odd}}\,, \tag{A.37}$$

one can relate fermionic sum-integrals to bosonic ones:

$$Z^{\alpha_1}_{s_1;f} = \left(2^{2s_1-\alpha_1-d+1}-1\right) Z^{\alpha_1}_{s_1;b}\,. \tag{A.38}$$

The explicit solutions for the bosonic and massless fermionic one-loop sum-integrals evaluate to

$Z^{\alpha_1}_{s_1;b} =$ 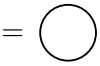

$$\equiv \sum\!\!\!\!\!\!\int_K \frac{k_0^{\alpha_1}}{\Delta_K^{s_1}} = \left(\frac{\bar\mu^2 e^{\gamma_\text{E}}}{4\pi}\right)^\epsilon 2T\,\frac{[2\pi T]^{d-2s_1+\alpha_1}}{(4\pi)^{\frac{d}{2}}}\,\frac{\Gamma\left(s_1-\frac{d}{2}\right)}{\Gamma\left(s_1\right)}\zeta_{2s_1-\alpha_1-d}\,, \tag{A.39}$$

$Z^{\alpha_1}_{s_1;f} =$ 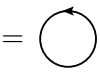

$$\begin{aligned}\equiv \sum\!\!\!\!\!\!\int_{\{K\}} \frac{k_0^{\alpha_1}}{\Delta_K^{s_1}} &= \left(\frac{\bar\mu^2 e^{\gamma_\text{E}}}{4\pi}\right)^\epsilon T\,\frac{[2\pi T]^{d-2s_1+\alpha_1}}{(4\pi)^{\frac{d}{2}}}\,\frac{\Gamma\left(s_1-\frac{d}{2}\right)}{\Gamma\left(s_1\right)}\\ &\times\left[\zeta\left(2s_1-\alpha_1-d,\frac{1}{2}-i\frac{\mu}{2\pi}\right)+(-1)^{\alpha_1}\zeta\left(2s_1-\alpha_1-d,\frac{1}{2}+i\frac{\mu}{2\pi}\right)\right]\,,\end{aligned} \tag{A.40}$$

where in the latter a non-zero chemical potential μ is included after first integrating over d spatial dimensions and then summing over Matsubara modes. In the limit $\mu \to 0$ the scaling behaviour eq. (A.38) is recovered.

A.3 Massive sum-integrals

The massive 1-loop tadpoles need a different treatment when evaluated in one of the two regions of high- ($T \gg m$) and low-temperature ($T \ll m$). Only the former guarantees a formal evaluation in closed form because the sum over Matsubara frequencies is absolutely convergent.

However, in accordance with the Saclay method (cf. sec. 3.5.1), we carry out the summation explicitly and higher powers of denominators of eq. (3.73) are obtained by taking mass derivatives. The different spatial integration parts are parameterised using units of temperature. In $d = 3 - 2\epsilon$ the ϵ-expansion for the thermal part of eq. (3.73) gives

$$\begin{aligned} Z^T_{1;1} &= T^{d-1} c_d \int_0^\infty \mathrm{d}p\, \frac{p^{d-1}}{2\omega_p} \Big[n_+(\omega_p) + n_-(\omega_p) \Big] \,, \\ &= \left(\frac{\bar{\mu}^2 e^{\gamma_\mathrm{E}}}{4\pi} \right)^\epsilon T^{2-2\epsilon} \frac{c_{3-2\epsilon}}{2} \int_0^\infty \mathrm{d}p\, p^{-2\epsilon}\, \frac{p^2}{\omega_p} \Big[n_+(\omega_p) + n_-(\omega_p) \Big] \,. \end{aligned} \tag{A.41}$$

By taking momentum derivatives of $n_\pm(\omega_p)$ relates

$$\int_p p^n \frac{\mathrm{d}}{\mathrm{d}p} n_\mathrm{F}(\omega_p) = \Big[p^{d-1+n} n_\mathrm{F}(\omega_p) \Big]_0^\infty - (d-1+n) \int_p p^{n-1} n_\mathrm{F}(\omega_p) \,, \tag{A.42}$$

for $(d-1+n) \in \mathbb{Z}^+$. The thermal part of the 1-loop sum-integral tadpoles becomes

$$Z^T_{1;1} = \frac{T^{d-1}}{2} \int_p \frac{1}{\omega_p} \Big[n_+(\omega_p) + n_-(\omega_p) \Big] \,, \tag{A.43}$$

$$Z^T_{2;1} = \frac{T^{d-3}}{4} (d-2) \int_p \frac{1}{p^2 \omega_p} \Big[n_+(\omega_p) + n_-(\omega_p) \Big] \,, \tag{A.44}$$

$$Z^T_{3;1} = \frac{T^{d-5}}{16} (d-2) \int_p \frac{n_+(\omega_p)}{p^2 \omega_p^2} \left[\frac{1}{\omega_p} + \frac{1 - n_+(\omega_p)}{1} \right] \quad + \quad (+ \leftrightarrow -) \,, \tag{A.45}$$

$$\begin{aligned} Z^T_{4;1} = \frac{T^{d-7}}{32} (d-2) \int_p \frac{n_+(\omega_p)}{p^2 \omega_p^3} \left[\frac{1}{\omega_p^2} + \frac{1 - n_+(\omega_p)}{\omega_p} + \frac{(1 - n_+(\omega_p))(1 - 2n_+(\omega_p))}{3} \right] \\ + \quad (+ \leftrightarrow -) \,. \end{aligned} \tag{A.46}$$

Their $m_i \to 0$ for fermions

$$Z_{1;1} = -\frac{1}{2} \left[\zeta\left(-1, \frac{1}{2} - i\frac{\mu}{2\pi} \right) + \zeta\left(-1, \frac{1}{2} + i\frac{\mu}{2\pi} \right) \right] = \frac{1}{24} + \frac{\mu^2}{8\pi^2} \,, \tag{A.47}$$

$$Z_{2;1} = -\left[\Psi\left(\frac{1}{2} - i\frac{\mu}{2\pi} \right) + \Psi\left(\frac{1}{2} + i\frac{\mu}{2\pi} \right) \right] \,, \tag{A.48}$$

$$Z_{3;1} = \frac{1}{(4\pi)^4} \left[\zeta\left(3, \frac{1}{2} - i\frac{\mu}{2\pi} \right) + \zeta\left(3, \frac{1}{2} + i\frac{\mu}{2\pi} \right) \right] \,, \tag{A.49}$$

agrees with eq. (A.40) relating the n-th derivative of the Digamma function

$$\Psi_n(z) = (-1)^{n+1}\, n!\, \zeta(n+1, z) \,. \tag{A.50}$$

A.3.1 Two-loop massive sum-integrals

The calculation of the general sunset sum-integral with arbitrary masses m_i with $i = 1, 2, 3$ on the basis of [47] is of the form

$$\begin{aligned} Z^{\alpha_1\alpha_2}_{111;\underline{m}} = \sum\!\!\!\!\!\!\int_{K_1,K_2} \frac{k_{1_0}^{\alpha_1} k_{2_0}^{\alpha_2}}{\Delta_{K_1,m_1} \Delta_{K_2,m_2} \Delta_{K_1-K_2,m_3}} = \int_{k_1,k_2,k_3} (2\pi)^d \delta(k_1 - k_2 + k_3) \sum_{k_{1_0} k_{2_0} k_{3_0}} \delta(k_{1_0} - k_{2_0} + k_{3_0}) \\ \times \frac{k_{1_0}^{\alpha_1} k_{2_0}^{\alpha_2}}{\big[k_{1_0}^2 + (\omega_1^{k_1})^2 \big] \big[k_{2_0}^2 + (\omega_2^{k_2})^2 \big] \big[k_{3_0}^2 + (\omega_3^{k_3})^2 \big]} \,. \end{aligned} \tag{A.51}$$

Thus, the twofold sum over Matsubara frequencies is rewritten as a threefold sum with the Kronecker δ-function eq. (3.72) and the fermionic and bosonic imaginary-time propagators

eqs. (2.12) and (2.13) employed. Additional variants of the sunset sum-integral eq. (A.51) are required, where lines are weighted with powers of Matsubara frequencies or irreducible scalar products. Hence, both sides of the propagators in $G(\tau)$ and $\tilde{G}(\tau)$ are differentiated

$$(\partial_\tau)^{\alpha_1} G(\tau) = T \sum_{\omega_n} \frac{(i\omega_n)^{\alpha_1} e^{i\omega_n \tau}}{[\omega_n^2 + \omega^2]} \,. \tag{A.52}$$

However, the propagators $G(\tau)$ exhibit a kink at $\tau = 0$. Already a second order derivation needs to identify recurring instances of the original propagator and arising δ-functions

$$\begin{aligned}(\partial_\tau)^2 G(\tau) &= T \sum_{\omega_n} \frac{(-\omega_n^2) e^{i\omega_n \tau}}{[\omega_n^2 + \omega^2]} = T \sum_{\omega_n} \left(-1 + \frac{\omega^2}{[\omega_n^2 + \omega^2]} \right) e^{i\omega_n \tau} \\ &= -\delta(\tau) + \omega^2 G(\tau) \,, \end{aligned} \tag{A.53}$$

$$(\partial_\tau)^{2n} G(\tau) = -\sum_{i=1}^{n} \omega^{2i-2} \delta^{(2n-2i)}(\tau) + \omega^{2n} G(\tau) \,, \tag{A.54}$$

which permits an extension to higher-order derivatives. Here the standard summation formula for bosons and fermions is used

$$\begin{aligned} T \sum_{\omega_n^{\mathrm{B}}} e^{i\omega_n^{\mathrm{B}} \tau} &= \delta(\tau \mod \beta) \,, \\ T \sum_{\omega_n^{\mathrm{F}}} e^{i\omega_n^{\mathrm{F}} \tau} &= 2\delta(\tau \mod 2\beta) - \delta(\tau \mod \beta) \,. \end{aligned} \tag{A.55}$$

On the integration domain $\tau \in [0, \beta]$ both sums act in the same way. Focussing primarily on the basic sunset ($\alpha_i = 0$), the sum over Matsubara modes is executed using the Saclay-Method, outlined in sec. 3.5.1, to arrive at

$$Z_{111;\underline{m}} = \int_{k_1,k_2,k_3} (2\pi)^d \delta(k_1 - k_2 + k_3)\, D(\omega_1, \omega_2, \omega_3) \,. \tag{A.56}$$

For the case $Z_{111} = Z^{00}_{111;\underline{m}}$ and including a chemical potential eq. (3.50), we get the integrand

$$\begin{aligned} D(\omega_1, \omega_2, \omega_2) &= \frac{1}{4\omega_1\omega_2\omega_3(\omega_1 + \omega_2 + \omega_3)} \\ &\quad + \frac{1}{8\omega_1\omega_2\omega_3} \sum_{i\neq j\neq k} \sum_{\sigma=\pm 1} n_\sigma(\omega_i) D_1(\omega_i, \omega_j, \omega_k) \\ &\quad + \frac{1}{8\omega_1\omega_2\omega_3} \sum_{i\neq j\neq k} \sum_{\sigma,\tau=\pm 1} n_\sigma(\omega_j) n_\tau(\omega_k) D_2(\omega_i, \sigma\omega_j, \tau\omega_k) \,, \end{aligned} \tag{A.57}$$

where the sum $\sum_{i\neq j\neq k} = \sum_{(i,j,k)=(1,2,3),(2,3,1),(3,1,2)}$ accounts for all cyclic permutations of mass signatures

$$\begin{aligned} D_1(\omega_i, \omega_j, \omega_k) &= \frac{1}{\omega_i + \omega_j + \omega_k} - \frac{1}{\omega_i - \omega_j - \omega_k} \,, \\ D_2(\omega_i, \omega_j, \omega_k) &= \frac{1}{\omega_i - \omega_j + \omega_k} + \frac{1}{\omega_i + \omega_j - \omega_k} \,. \end{aligned} \tag{A.58}$$

The compactly denoted distribution functions $n_\pm(\omega_i)$ in eq. (3.75) are fermionic for $i = 1, 2$ and bosonic for $i = 3$. The energy fractions are reorganised by identifying zero-temperature objects. To verify their correspondence one explicitly integrates over zero-momenta k_{1_0}, k_{2_0}

in the vacuum part. By inspecting its poles the integration is determined using the method of residues. Thereafter, the sunset reads

$$\begin{aligned} Z_{111} &= Z_{111}^{\text{vac}} \\ &+ \sum_{i\neq j\neq k} \sum_{\sigma=\pm 1} \int_{\mathbf{k}_i} \frac{n_\sigma(\omega_i)}{2\omega_i} B(-im_i; m_j, m_k) \\ &+ \sum_{i\neq j\neq k} \sum_{\sigma,\tau=\pm 1} \int_{\mathbf{k}_i}\int_{\mathbf{k}_j} \frac{n_\sigma(\omega_i)}{2\omega_i}\frac{n_\tau(\omega_j)}{2\omega_j}\left[\frac{1}{-(\sigma\mathcal{K}_i-\tau\mathcal{K}_j)^2+m_k^2}\right], \end{aligned} \tag{A.59}$$

inserting $B(Q; m_1, m_2)$ from eq. (A.6). For compactness the notation with on-shell Minkowskian four-vectors is introduced:

$$\mathcal{K}_i \cdot \mathcal{K}_j = \omega_i\omega_j - \mathbf{k}_i\cdot\mathbf{k}_j\ , \quad \mathcal{K}_i \equiv (\omega_i, \mathbf{k}_i)\ . \tag{A.60}$$

The result in eq. (A.59) corresponds to the application of cutting rules [94] splitting the sum-integral into a vacuum part, one-cut parts and two-cut parts. Where the cut line is put on-shell and weighted by the corresponding thermal distribution. The double integration over $[\ldots]$ in the third line is split into a 2-dimensional radial integral over $k_i \equiv |\mathbf{k}_i|$ and two angular integrals parametrising the angle between the integration momenta $z = \mathbf{k}_i\cdot\mathbf{k}_j/|\mathbf{k}_i||\mathbf{k}_j|$. Using symmetries $\mathbf{k}_i \to -\mathbf{k}_i$ rewrites this integral

$$\begin{aligned} &\int_{\mathbf{k}_i}\int_0^\infty \frac{\mathrm{d}k_j\, k_j^{d-1}}{(2\pi)^d}\frac{n_\sigma(\omega_i)}{2\omega_i}\frac{n_\tau(\omega_j)}{2\omega_j}\int \mathrm{d}\Omega_{d-2}\int_{-1}^{+1}\mathrm{d}z\,\frac{(1-z^2)^{\frac{d-3}{2}}}{2\sigma\tau\omega_i\omega_j+m_k^2-m_j^2-m_i^2+2k_ik_jz} \overset{d=3}{=} \\ &\qquad \int_{\mathbf{k}_i}\int_0^\infty \frac{\mathrm{d}k_j\, k_j^2}{(2\pi)^2}\frac{n_\sigma(\omega_i)}{2\omega_i}\frac{n_\tau(\omega_j)}{2\omega_j}\frac{1}{2k_ik_j}\int_{-1}^{+1}\mathrm{d}z\,\frac{\mathrm{d}}{\mathrm{d}z}\,\ln\left[2\sigma\tau\omega_i\omega_j+m_k^2-m_j^2-m_i^2+2k_ik_jz\right]\ . \end{aligned} \tag{A.61}$$

Here the angular integral in d-dimensions identifies as the hypergeometric function ${}_2F_1$ in eq. (A.11):

$$\begin{aligned} \int_{-1}^{+1}\mathrm{d}z\,\frac{(1-z^2)^{\frac{d-3}{2}}}{2\sigma\tau\omega_i\omega_j+m_k^2-m_j^2-m_i^2+2k_ik_jz} &= \frac{\Gamma\left(\frac{d-1}{2}\right)^2}{\Gamma(d-1)}\frac{4^{\frac{d-2}{2}}}{2\sigma\tau\omega_i\omega_j+m_k^2-m_j^2-m_i^2-2k_ik_j} \\ \times {}_2F_1\left[1, \frac{d-1}{2}; d-1; \frac{-4k_ik_j}{2\sigma\tau\omega_i\omega_j+m_k^2-m_j^2-m_i^2-2k_ik_j}\right]&. \end{aligned} \tag{A.62}$$

Since momenta get integrated out, the integral only depends on the ordering of the masses. Internal propagators of the two-cut thermal contributions go on-shell when the momenta of the cut lines become collinear in some Lorentz frame. In dimensional regularisation collinear divergences are regulated via the $\sin^{d-2}\theta$ term in the Jacobian eq. (A.1).

Inserting the thermal part $Z^T_{s_1;i}$ of the 1-loop master from eq. (3.73) into eq. (A.59), yields

$$\begin{aligned} Z_{111} &= Z_{111}^{\text{vac}} \\ &+ \sum_{i\neq j\neq k} Z^T_{1,i}\, B(-im_i; m_j, m_k) \\ &+ \sum_{i\neq j\neq k} \sum_{\sigma,\tau=\pm 1} \int_0^\infty \frac{\mathrm{d}p\, p}{(2\pi)^2}\frac{\mathrm{d}q\, q}{(2\pi)^2}\frac{n_\sigma(\omega_i^p)}{2\omega_i^p}\frac{n_\tau(\omega_j^q)}{2\omega_j^q} \\ &\qquad\qquad \times \ln\left[\frac{2\sigma\tau\omega_i^p\omega_j^q+m_k^2-m_j^2-m_i^2+2pq}{2\sigma\tau\omega_i^p\omega_j^q+m_k^2-m_j^2-m_i^2-2pq}\right]. \end{aligned} \tag{A.63}$$

Two further configurations of eq. (A.51) involve $(\alpha_1 = 1, \alpha_2 = 1)$ and $(\alpha_1 = 2, \alpha_2 = 0)$. Focussing on the latter its integrand is

$$\begin{aligned} D(\omega_1,\omega_2,\omega_2) = {} & \frac{\omega_1}{4\omega_2\omega_3(\omega_1+\omega_2+\omega_3)} - \frac{1}{4\omega_2\omega_3} \\ & + \frac{\omega_1}{8\omega_2\omega_3} \sum_{i\neq j\neq k} \sum_{\sigma=\pm 1} n_\sigma(\omega_i) D_1(\omega_i,\omega_j,\omega_k) - \frac{1}{4\omega_2\omega_3} \sum_{i>1} \sum_{\sigma=\pm 1} n_\sigma(\omega_i) \\ & + \frac{\omega_1}{8\omega_2\omega_3} \sum_{i\neq j\neq k} \sum_{\sigma,\tau=\pm 1} n_\sigma(\omega_j) n_\tau(\omega_k) D_2(\omega_i,\sigma\omega_j,\tau\omega_k) \\ & - \frac{1}{4\omega_2\omega_3} \sum_{i,j>1} \sum_{\sigma,\tau=\pm 1} n_\sigma(\omega_i) n_\tau(\omega_j) \,. \end{aligned} \tag{A.64}$$

Again it is possible to identify a pure vacuum piece that corresponds to the first line. It is obtained by carrying out the integrals over k_{1_0}, k_{2_0} in

$$Z^{20,\mathrm{vac}}_{111;\underline{m}} = \int_{K_1,K_2} \frac{k_{1_0}^2}{\Delta_{K_1,m_1}\Delta_{K_2,m_2}\Delta_{K_1-K_2,m_3}} = \frac{1}{d+1}\left[-m_1^2 Z^{\mathrm{vac}}_{111} + Z^{\mathrm{vac}}_{1;2}\, Z^{\mathrm{vac}}_{1;3}\right] \,, \tag{A.65}$$

where Lorentz symmetry permits to decompose the vacuum part even further. Similarly, the one-cut terms get modified

$$B^{(2,0)}(Q;m_1,m_2) = \int_{K_1} \frac{k_{1_0}^2}{\Delta_{K_1,m_1}\Delta_{K_1-Q,m_2}} = \frac{1}{d+1}\left[-m_1^2 B(Q;m_1,m_2) + Z^{\mathrm{vac}}_{1;2}\right] \,. \tag{A.66}$$

In order to write the result in closed form, we employ

$$\begin{aligned} Z^{20}_{111} = {} & Z^{20,\mathrm{vac}}_{111} \\ & + \sum_{i\neq j\neq k} \sum_{\sigma=\pm 1} \int_{\mathbf{k}_i} \frac{n_\sigma(\omega_i)}{2\omega_i} B^{(2,0)}(-im_i;m_j,m_k) \\ & + \sum_{i\neq j\neq k} \sum_{\sigma,\tau=\pm 1} \int_{\mathbf{k}_i}\int_{\mathbf{k}_j} \omega_1 \frac{n_\sigma(\omega_i)}{2\omega_i}\frac{n_\tau(\omega_j)}{2\omega_j}\left[\frac{1}{-(\sigma\mathcal{K}_i - \tau\mathcal{K}_j)^2 + m_k^2}\right] \\ & - \sum_{i,j>1} \sum_{\sigma,\tau=\pm 1} \left(\int_{\mathbf{k}_i} \frac{n_\sigma(\omega_i)}{2\omega_i}\right)\left(\int_{\mathbf{k}_j} \frac{n_\tau(\omega_j)}{2\omega_j}\right) \,. \end{aligned} \tag{A.67}$$

Inserting thermal 1-loop parts from eq. (3.73)

$$\begin{aligned} Z^{20}_{111} = {} & Z^{20,\mathrm{vac}}_{111} \\ & + \sum_{i\neq j\neq k} Z^T_{1;i}\, B^{(2,0)}(-im_i;m_j,m_k) \\ & + \sum_{j,k>1} \sum_{\sigma,\tau=\pm 1} \int_0^\infty \frac{\mathrm{d}k_i\, k_i^2}{(2\pi)^2}\frac{\mathrm{d}k_j\, k_j^2}{(2\pi)^2}\frac{n_\sigma(\omega_1)}{2\omega_1}\frac{n_\tau(\omega_j)}{2\omega_j}\omega_1^2 \\ & \qquad \times 2\int_{-1}^{+1} \mathrm{d}z \frac{1}{2\sigma\tau\omega_1\omega_j + m_k^2 - m_j^2 - m_1^2 + 2k_1k_jz} \\ & + \sum_{\sigma,\tau=\pm 1} \int_0^\infty \frac{\mathrm{d}p\, p^2}{(2\pi)^2}\frac{\mathrm{d}q\, q^2}{(2\pi)^2}\frac{n_\sigma(\omega_2^p)}{2\omega_2^p}\frac{n_\tau(\omega_3^q)}{2\omega_3^q} \\ & \qquad \times 2\int_{-1}^{+1} \mathrm{d}z\, \frac{p^2+q^2+m_1^2+2pqz}{2\sigma\tau\omega_2^p\omega_3^q + m_1^2 - m_2^2 - m_3^2 + 2pqz} \\ & - Z^T_{1;2}Z^T_{1;3} \,, \end{aligned} \tag{A.68}$$

and evaluating the radial integrals on the right

$$
\begin{aligned}
Z^{20}_{111} &= Z^{20,\mathrm{vac}}_{111} \\
&\quad + \sum_{i\neq j\neq k} Z^{T}_{1;i}\, B^{(2,0)}(-im_i; m_j, m_k) \\
&\quad + \sum_{j,k>1} \sum_{\sigma,\tau=\pm 1} \int_0^\infty \frac{\mathrm{d}p\, p}{(2\pi)^2} \frac{\mathrm{d}q\, q}{(2\pi)^2} \frac{n_\sigma(\omega_1^p)}{2\omega_1^p} \frac{n_\tau(\omega_j^q)}{2\omega_j^q} (\omega_1^p)^2 \\
&\qquad\qquad \times \ln\left[\frac{2\sigma\tau\omega_1^p\omega_j^q + m_k^2 - m_j^2 - m_1^2 + 2pq}{2\sigma\tau\omega_i^p\omega_j^q + m_k^2 - m_j^2 - m_1^2 - 2pq}\right] \\
&\quad + \sum_{\sigma,\tau=\pm 1} \int_0^\infty \frac{\mathrm{d}p\, p}{(2\pi)^2} \frac{\mathrm{d}q\, q}{(2\pi)^2} \frac{n_\sigma(\omega_2^p)}{2\omega_2^p} \frac{n_\tau(\omega_3^q)}{2\omega_3^q} \frac{(\sigma\omega_2^p - \tau\omega_3^q)^2}{pq} \\
&\qquad\qquad \times \ln\left[\frac{2\sigma\tau\omega_2^p\omega_3^q + m_1^2 - m_2^2 - m_3^2 + 2pq}{2\sigma\tau\omega_2^p\omega_3^q + m_1^2 - m_2^2 - m_3^2 - 2pq}\right] ,
\end{aligned}
\tag{A.69}
$$

the quadratic 1-loop thermal contribution in the last line combines duly with the integrand in the second radial integral. The encountered integrals are

$$
\begin{aligned}
\int_{-1}^{+1} \mathrm{d}z \frac{(a+bz)^\alpha}{(c+dz)^\beta} &= 2\frac{(a-b)^\alpha}{(c-d)^\beta} F_1\left[1; -\alpha, \beta; 2; \frac{2b}{b-a}, \frac{2d}{d-c}\right] , \\
\int_{-1}^{+1} \mathrm{d}z \frac{(a+bz)^\alpha}{c+dz} &= \frac{1}{\alpha}\frac{(a+bz)^{1+\alpha}}{(c+dz)b}\, {}_2F_1\left[1, 1; 1-\alpha; \frac{bc-ad}{(c+dz)b}\right]\Bigg|_{-1}^{+1} , \\
\int_{-1}^{+1} \mathrm{d}z \frac{a+bz}{c+dz} &= \frac{b}{d}z + \frac{ad-bc}{d^2} \ln\left[c+dz\right]\Big|_{-1}^{+1} , \\
\int_{-1}^{+1} \mathrm{d}z \frac{1}{c+dz} &= \frac{1}{d} \ln\left[c+dz\right]\Big|_{-1}^{+1} ,
\end{aligned}
\tag{A.70}
$$

in the limits $\alpha \to \{0, 1\}$.

A.3.2 Two equal heavy masses

The cases of physical interest

$$
m_1 = m_2 = m\ , \quad m_3 = 0\ , \tag{A.71}
$$

are encountered in the Taylor parameters of the Debye mass eq. (5.18). To achieve higher powers in the denominators, mass derivatives of the form

$$
Z^{\alpha_1\alpha_2}_{\ldots,s_i,\ldots}(\ldots, m_i, \ldots) = \frac{(-1)^{s_i-1}}{(s_i-1)!} \left(\frac{\mathrm{d}}{\mathrm{d}m_i^2}\right)^{s_i-1} Z^{\alpha_1\alpha_2}_{\ldots,1,\ldots}(\ldots, m_i, \ldots)\ , \tag{A.72}
$$

are taken before enforcing zero-mass limits. The vacuum contributions can be taken from eq. (A.20) in $d = 4 - 2\epsilon$. In dimensional regularisation, we expand eq. (A.51)

$$
Z_{111;\underline{m}} = \frac{1}{\epsilon^2} Z^{(-2)}_{111;\underline{m}} + \frac{1}{\epsilon} Z^{(-1)}_{111;\underline{m}} + Z^{(0)}_{111;\underline{m}} + \mathcal{O}(\epsilon)\ , \tag{A.73}
$$

with the corresponding expansion parameters

$$
\begin{aligned}
Z^{(-2)}_{111;\underline{m}} &= -\frac{m_1^2+m_2^2+m_3^2}{2(4\pi)^4}\,, \\
Z^{(-1)}_{111;\underline{m}} &= -\frac{1}{(4\pi)^4}\sum_{i=1}^{3} m_i^2\left(\ln\frac{\bar{\mu}^2}{m_i^2}+\frac{3}{2}\right)+\sum_{i=1}^{3}\frac{Z^{T(0)}_{1;i}}{(4\pi)^2}\,, \\
Z^{(0)}_{111;\underline{m}} &= -\frac{1}{(4\pi)^4}\Bigg\{\sum_{i=1}^{3} m_i^2\left[\frac{1}{2}\ln^2\frac{\bar{\mu}^2}{m_i^2}+3\ln\frac{\bar{\mu}^2}{m_i^2}+\frac{7}{2}+\frac{\zeta_2}{2}\right] \\
&\qquad +\frac{1}{2}\sum_{i\neq j\neq k}(m_i^2+m_j^2-m_k^2)\ln\frac{\bar{\mu}^2}{m_i^2}\ln\frac{\bar{\mu}^2}{m_j^2}-R(m_1^2,m_2^2,m_3^2)L(m_1^2,m_2^2,m_3^2)\Bigg\} \\
&\quad +\sum_{i\neq j\neq k} Z^{T(0)}_{1;i}\,\mathrm{Re}\,B^{(0)}(-im_i;m_j,m_k)+\sum_{i=1}^{3}\frac{Z^{T(1)}_{1;i}}{(4\pi)^2} \\
&\quad +\sum_{i\neq j\neq k}\sum_{\sigma,\tau=\pm1}\int_0^\infty \frac{\mathrm{d}p\,p}{(2\pi)^2}\frac{\mathrm{d}q\,q}{(2\pi)^2}\frac{n_\sigma(\omega_i^p)}{2\omega_i^p}\frac{n_\tau(\omega_j^q)}{2\omega_j^q} \\
&\qquad\qquad \times\ln\left[\frac{2\sigma\tau\omega_i^p\omega_j^q+m_k^2-m_j^2-m_i^2+2pq}{2\sigma\tau\omega_i^p\omega_j^q+m_k^2-m_j^2-m_i^2-2pq}\right]\,,
\end{aligned}
\tag{A.74}
$$

and vacuum parts taken from [132]:

$$
\begin{aligned}
R\left(m_1^2,m_2^2,m_3^2\right) &= \sqrt{m_1^2-2m_2m_1-2m_3m_1+m_2^2+m_3^2-2m_2m_3}\,, \\
L\left(m_1^2,m_2^2,m_3^2\right) &= \mathrm{Li}_2\left(-\frac{t_3m_2}{m_1}\right)+\mathrm{Li}_2\left(-\frac{t_3m_1}{m_2}\right)+\zeta_2+\frac{\ln^2 t_3}{2} \\
&\quad +\frac{1}{2}\left[\ln\left(t_3+\frac{m_2}{m_1}\right)-\ln\left(t_3+\frac{m_1}{m_2}\right)+\frac{3}{4}\ln\frac{m_1^2}{m_2^2}\right]\ln\frac{m_1^2}{m_2^2}\,, \\
t_3 &= \frac{m_3^2-m_1^2-m_2^2+R\left(m_1^2,m_2^2,m_3^2\right)}{2m_1m_2}\,.
\end{aligned}
\tag{A.75}
$$

When approaching the physical scenario with the denominator power configurations as in eq. (5.20), individual terms per diagram exhibit both UV and various IR divergences. The most transparent way to control them is to establish a regulator for the UV via dimensional regularisation and for the IR using a mass regulator for massless lines. Thus, the two fermionic masses are identified and a fictitious mass regulator M is kept finite on the bosonic line

$$
m_1=m_2=m\,,\quad m_3=M\,. \tag{A.76}
$$

Acting with mass derivatives

$$
Z_{s_1s_2s_3}(m,m,M)=\frac{(-1)^{s_3-1}}{(s_3-1)!}\left(\frac{\mathrm{d}}{\mathrm{d}M^2}\right)^{s_3-1}Z_{s_1s_21}(m,m,M)\,, \tag{A.77}
$$

$$
Z_{21s_3}(m,m,M)=-\frac{1}{2}\frac{\mathrm{d}}{\mathrm{d}m^2}Z_{11s_3}(m,m,M)\,, \tag{A.78}
$$

first on the bosonic line, the zero-mass limit $M\to 0$ is taken. Thereafter, mass derivatives with respect to finite physical masses are performed. The sum-integral splits into a vacuum part, two one-cut parts, and two two-cut parts, with "cut" meaning that the corresponding

line is put on-shell and weighted by its thermal distribution:

$$Z_{112} = Z_{112}^{\rm vac} + Z_{112}^{\rm (B)} + Z_{112}^{\rm (F)} + Z_{112}^{\rm (BF)} + Z_{112}^{\rm (FF)} \,, \tag{A.79}$$

$$Z_{112}^{\rm (B)} = -\lim_{M\to 0}\frac{\mathrm{d}}{\mathrm{d}M^2}\int_p \frac{n_{\rm F}(\Omega_p)}{\Omega_p}\left[\int_Q \frac{1}{[Q^2+m^2]\,[(P-Q)^2+m^2]}\right]_{P^2=-M^2} , \tag{A.80}$$

$$Z_{112}^{\rm (F)} = -2\lim_{M\to 0}\int_p \frac{n_{\rm F}(\omega_p)}{\omega_p}\left[\int_Q \frac{1}{[Q^2+M^2]^2\,[(P-Q)^2+m^2]}\right]_{P^2=-m^2} , \tag{A.81}$$

$$Z_{112}^{\rm (BF)} = 2\lim_{M\to 0}\frac{\mathrm{d}}{\mathrm{d}M^2}\int_{p,q} \frac{n_{\rm B}(\Omega_p)}{\Omega_p}\frac{n_{\rm F}(\omega_q)}{\omega_q}\left[\frac{1}{(P-Q)^2+m^2}\right]_{P^2=-M^2,Q^2=-m^2} , \tag{A.82}$$

$$Z_{112}^{\rm (FF)} = \lim_{M\to 0}\frac{\mathrm{d}}{\mathrm{d}M^2}\int_{p,q} \frac{n_{\rm F}(\omega_p)}{\omega_p}\frac{n_{\rm F}(\omega_q)}{\omega_q}\left[\frac{1}{(P-Q)^2+M^2}\right]_{P^2=-m^2,Q^2=-m^2} . \tag{A.83}$$

The cuts are

$$\begin{aligned}[\ldots]_{P^2=-m^2} &\equiv \frac{1}{2}\sum_{p_n=\pm i\omega_p}[\ldots] \,, \\ [\ldots]_{P^2=-M^2,Q^2=-m^2} &\equiv \frac{1}{4}\sum_{p_n=\pm i\Omega_p}\sum_{q_n=\pm i\omega_q}[\ldots] \,. \end{aligned} \tag{A.84}$$

To finite order in ϵ, we obtain for the $n_{\rm F}$ one-cut fermion line contribution

$$Z_{112}^{\rm (F)} = \frac{2}{(4\pi)^2 m^2}\int_p \frac{n_{\rm F}(\omega_p)}{\omega_p}\left[-\frac{\pi}{2}\frac{m}{M} + \ln\frac{m}{M} + \frac{1}{2}\right] , \tag{A.85}$$

using the expanded B-function (A.6). Considering the $n_{\rm F}n_{\rm F}$ two-cut term and by keeping the mass regulator M finite reads

$$\begin{aligned} Z_{112}^{\rm (FF)} &= \frac{1}{2}\int_{p,q}\frac{n_{\rm F}(\omega_p)}{\omega_p}\frac{n_{\rm F}(\omega_q)}{\omega_q}\left\{\frac{1}{M^4-4M^2(m^2+\omega_p\omega_q)+4m^2(\omega_p+\omega_q)^2}\right. \\ &\qquad \left. + (\omega_q\to-\omega_q)\right\} , \\ &= \frac{1}{16m^4}\int_{p,q}\frac{1}{\omega_p\omega_q}\left\{\frac{[n_{\rm F}(\omega_p)+n_{\rm F}(\omega_q)]^2}{(\omega_p+\omega_q)^2} - \frac{[n_{\rm F}(\omega_p)-n_{\rm F}(\omega_q)]^2}{(\omega_p-\omega_q)^2}\right\} + \delta Z_{112}^{\rm (FF)} \,, \end{aligned} \tag{A.86}$$

$$\begin{aligned} \delta Z_{112}^{\rm (FF)} &= \frac{1}{2}\int_p \frac{n_{\rm F}^2(\omega_p)}{\omega_p}\int_q \frac{1}{\omega_q}\left\{\frac{1}{M^4-4M^2(m^2-\omega_p\omega_q)+4m^2(\omega_p-\omega_q)^2} - (\omega_q\to-\omega_q)\right\} \\ &= \frac{1}{(4\pi)^2m^2}\int_p \frac{n_{\rm F}^2(\omega_p)}{\omega_p}\int_0^\infty \mathrm{d}q\,\frac{q^{d-1}}{\omega_q} \\ &\qquad \times\left\{\frac{1}{\left[\omega_q-\omega_p\left(1-\frac{1}{2}\frac{M^2}{m^2}\right)\right]^2+p^2\frac{M^2}{m^2}\left(1-\frac{1}{4}\frac{M^2}{m^2}\right)} - (\omega_q\to-\omega_q)\right\} \\ &\overset{M\to 0}{=} \frac{1}{(4\pi)^2m^2}\int_p \frac{n_{\rm F}^2(\omega_p)}{\omega_p}\int_0^\infty \mathrm{d}q\,\frac{q^{d-1}}{\omega_q} \\ &\qquad \times\left\{\frac{1}{(\omega_q-\omega_p)^2+p^2\frac{M^2}{m^2}} - (\omega_q\to-\omega_q)\right\} . \end{aligned} \tag{A.87}$$

Here only the first term in the brackets diverges at the pole when $M\to 0$ and $p=q$. The identity

$$\lim_{\epsilon\to 0}\frac{1}{\Delta\pm i\epsilon} = \mathbb{P}\left(\frac{1}{\Delta}\right) \mp i\pi\delta(\Delta) \,, \tag{A.88}$$

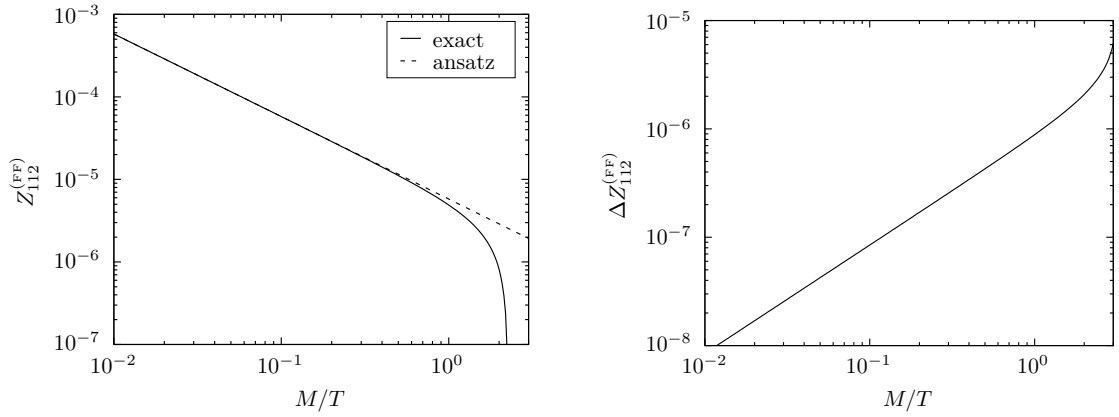

Figure A.1: $m/T = 1.6,\ q/T = 1$. Left: $\delta Z_{112}^{(\mathrm{FF})}$ as a function of M for both the exact numerical result from eq. (A.87) and the ansatz in eq. (A.89). Right: Remainder $\Delta Z_{112}^{(\mathrm{FF})}$.

is employed where $\mathbb{P}$ stands for the Cauchy principal value. For this reason the q-integral is extended over the whole real axis which allows to combine both terms. We find the resulting ansatz for this contribution

$$\delta Z_{112}^{(\mathrm{FF})} = \frac{2}{(4\pi)^2 m^2} \int_p \frac{n_{\mathrm{F}}^2(\omega_p)}{\omega_p} \frac{\pi}{2} \frac{m}{M} \,, \tag{A.89}$$

which is depicted in contrast to the exact expression eq. (A.87) in fig. A.1. The remainder scales as $\mathcal{O}(M)$ for $M \to 0$ and is then exact for $M = 0$. However, the finite contribution of $\mathcal{O}(M^0)$ in eq. (A.87) has the form

$$\delta Z_{112}^{(\mathrm{FF})} = \int_p \frac{n_{\mathrm{F}}^2(\omega_p)}{2m^2} \int_q \frac{1}{(q^2 - p^2)^2} \,. \tag{A.90}$$

The remaining vacuum integral is evaluated as a function of $-p^2$

$$\int_q \frac{1}{(q^2 - p^2)^2} = -\frac{i}{8\pi} \frac{1}{\sqrt{p^2}} \,. \tag{A.91}$$

Alternatively the q-integration in eq. (A.87) can be performed exactly yielding the same $1/M$ pole. The ansatz in eq. (A.89) can also be derived by splitting the q-integral into the three domains $[0, p-\Lambda], [p-\Lambda, p+\Lambda], [p+\Lambda, \infty]$ using a cut-off regulator Λ. Thus showing that in the neighborhood of $p = q$ one can expand ω_q in the denominator of the integrand while outside of this neighborhood one can safely set $M \to 0$.

For the mixed $n_{\mathrm{F}} n_{\mathrm{B}}$ two-cut contribution mass derivatives are converted into derivatives with respect to momentum and the angular integration is carried out

$$\begin{aligned}
Z_{112}^{(\mathrm{BF})} &= -\int_{p,q} \frac{n_{\mathrm{B}}(\Omega_p)}{\Omega_p} \frac{n_{\mathrm{F}}(\omega_q)}{\omega_q} 2q \left[\frac{(2pq - M^2)(p+q)}{(2pq - M^2)^2 - 4\Omega_p^2 \omega_q^2} + (p \to -p) \right] \\
&= \frac{2}{(2\pi)^2 m^2} \int_q \frac{n_{\mathrm{F}}(\omega_q)}{\omega_q} \int_{-\infty}^{\infty} \mathrm{d}p \, \frac{n_{\mathrm{B}}(\Omega_p)}{\Omega_p} \frac{\left(p - \frac{M^2}{2q}\right)(p+q)}{\left(p + \frac{M^2}{m^2}\frac{q}{2}\right)^2 + \omega_q^2 \frac{M^2}{m^2}\left(1 - \frac{M^2}{4m^2}\right)} \\
&\overset{M\to 0}{=} \frac{2}{(2\pi)^2 m^2} \int_q \frac{n_{\mathrm{F}}(\omega_q)}{\omega_q} \int_0^{\infty} \mathrm{d}p \, \frac{n_{\mathrm{B}}(\Omega_p)}{\Omega_p} \left[\frac{p(p+q) - \frac{M^2}{2}}{p^2 + \frac{M^2}{m^2}\left(\omega_q^2 + pq + \frac{M^2}{m^2}\frac{q^2}{4}\right)} + (p \to -p) \right] \\
&\overset{M\to 0}{=} \frac{2}{(2\pi)^2 m^2} \int_q \frac{n_{\mathrm{F}}(\omega_q)}{\omega_q} \int_0^{\infty} \mathrm{d}p \, \frac{n_{\mathrm{B}}(\Omega_p)}{\Omega_p} 2 \left[\frac{\left(p^2 + \frac{M^2}{m^2}\omega_q^2\right)\left(p^2 - \frac{M^2}{2}\right) - \frac{M^2}{m^2} p^2 q^2}{\left(p^2 + \frac{M^2}{m^2}\omega_q^2\right)^2 - \left(\frac{M^2}{m^2} pq\right)^2} \right] \\
&\overset{M\to 0}{=} \frac{2}{(2\pi)^2 m^2} \int_q \frac{n_{\mathrm{F}}(\omega_q)}{\omega_q} \int_0^{\infty} \mathrm{d}p \, p^{d-3} \frac{n_{\mathrm{B}}(\Omega_p)}{\Omega_p} \frac{2p^4 + M^2 p^2 - \frac{M^4}{m^2}\omega_q^2}{\left(p^2 + \frac{M^2}{m^2}\omega_q^2\right)^2} \,.
\end{aligned} \tag{A.92}$$

In the first line integration-by-parts allows to trade mass derivatives of thermal distribution functions for momentum derivatives $M^2\frac{\mathrm{d}}{\mathrm{d}M^2} \to p^2\frac{\mathrm{d}}{\mathrm{d}p^2}$ of the logarithmic factor in $Z_{111}^{(\mathrm{BF})}$. In the second line $-\frac{2q}{4m^2}$ is factored out and the integration range is extended over the whole real axis. In lines 3–5 vanishing terms in the limit $M \to 0$ are omitted and remaining terms combined.

Given the complexity of the integrals the strategy is to first re-expand the distribution functions, perform the d-dimensional integral and then take care of the Matsubara summation. Starting from the identity for the distribution functions

$$n_{\mathrm{B}}(\omega_p) = +\frac{1}{2}\left(\coth\frac{\omega_p}{2} - 1\right) , \tag{A.93}$$

$$n_{\mathrm{F}}(\omega_p) = -\frac{1}{2}\left(\tanh\frac{\omega_p}{2} - 1\right) , \tag{A.94}$$

with the application of the series expansion

$$\sum_{n=-\infty}^{\infty} \frac{y}{y^2 + n^2\pi^2} = \coth(y) , \tag{A.95}$$

$$\sum_{n=-\infty}^{\infty} \frac{y}{y^2 + \left(n+\frac{1}{2}\right)^2\pi^2} = \tanh(y) , \tag{A.96}$$

this is equivalent to reverting the integral to its full sum-integral where the vacuum part has been subtracted. Thus, the integral eq. (A.92) is split into two parts and evaluated in strict dimensional regularisation

$$\int_0^\infty \mathrm{d}p\, p^{d-3}\Bigg(\underbrace{\sum_{n=-\infty}^{\infty} \frac{1}{\Omega_p^2 + (2\pi n)^2}}_{\text{(A.97.1)}} \underbrace{- \frac{1}{2\Omega_p}}_{\text{(A.97.2)}}\Bigg) \frac{2p^4 + M^2p^2 - \frac{M^4}{m^2}\omega_q^2}{\left(p^2 + \frac{M^2}{m^2}\omega_q^2\right)^2} . \tag{A.97}$$

In the sum-integral

$$\begin{aligned}
\text{(A.97.1)} \quad &= \quad \frac{\pi}{2}\left(\frac{m}{M}\right)^{4-d} \frac{m^{d-2} - \omega_q^{d-4}((d-2)\omega_q^2 - (d-3)m^2)}{(\omega_q + m)(\omega_q - m)} \frac{1}{\sin\left(\frac{d\pi}{2}\right)} \\
&- \quad \pi\Bigg\{(2\pi)^{d-4}\zeta_{4-d} + \sum_{n=1}^{\infty}(2\pi n)^{d-4}\left[\left(1 + \frac{M^2}{4\pi^2n^2}\right)^{\frac{d}{2}} - 1\right]\Bigg\}\frac{1}{\sin\left(\frac{d\pi}{2}\right)} + \mathcal{O}(M^2) \\
&\overset{d=3-2\epsilon}{=} \quad \frac{1}{2\epsilon} + \frac{\pi}{2}\frac{T}{M}\frac{m}{\omega_q + m} + \ln\frac{e^{\gamma_{\mathrm{E}}}}{2\pi} ,
\end{aligned} \tag{A.98}$$

the zero-mode contribution ($n = 0$) is isolated in the first line and yields the expected $\propto 1/M$ infrared divergence. In the second line finite contributions of $\mathcal{O}(M^0)$ are summed while remaining terms are of $\mathcal{O}(M)$. This means that only the p^4-term in eq. (A.97) contributes for $n > 0$ in the zero-mass limit. The vacuum contribution is modified by respective variable transformations such that a representation with ${}_2F_1$ from eq. (A.13) is possible

$$\begin{aligned}
\text{(A.97.2)} \quad &= \quad \frac{1}{4}M^{d-3}\int_0^1 \mathrm{d}z\, z^{\frac{1-d}{2}}(1-z)^{\frac{d-4}{2}}(1 + \frac{q^2}{m^2}z)^{-2}\left(2 - 3z - \frac{q^2}{m^2}z^2\right) \\
&= \quad \frac{1}{4}M^{d-3}\frac{\Gamma\left(\frac{3-d}{2}\right)\Gamma\left(\frac{d-2}{2}\right)}{2\Gamma\left(\frac{3}{2}\right)}\Bigg((d-2)\,{}_2F_1\left[2, \frac{3-d}{2}; \frac{3}{2}; -\frac{q^2}{m^2}\right] \\
&\qquad\qquad - (d-3)\,{}_2F_1\left[1, \frac{5-d}{2}; \frac{3}{2}; -\frac{q^2}{m^2}\right]\Bigg) \\
&\overset{d=3-2\epsilon}{=} \quad -\frac{1}{2\epsilon} + \ln\frac{M}{2T} + \frac{1}{2} + \frac{\omega_q}{2q}\ln\left(\frac{\omega_q + q}{\omega_q - q}\right) .
\end{aligned} \tag{A.99}$$

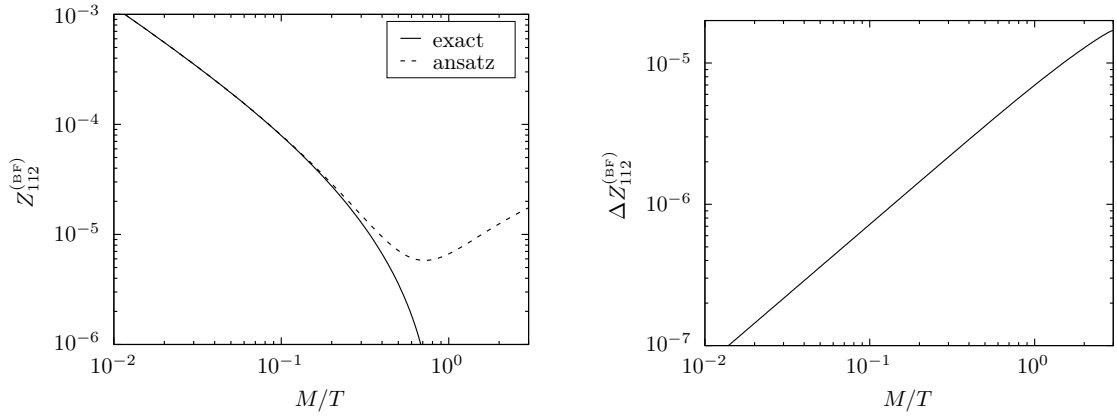

Figure A.2: $m/T = 1.6,\ q/T = 1$. Left: $Z_{112}^{(\mathrm{BF})}$ as a function of M for both the exact numerical result from eq. (A.82) and the ansatz in eq. (A.100). Right: Remainder $\Delta Z_{112}^{(\mathrm{BF})}$.

Combining results from eq. (A.98) and eq. (A.99), the final form of the ansatz approaches

$$Z_{112}^{(\mathrm{BF})} = \frac{2}{(4\pi)^2 m^2} \int_p \frac{n_{\mathrm{F}}(\omega_p)}{\omega_p} \left[\frac{\pi}{2} \frac{T}{M} \frac{m}{\omega_p + m} + \ln\left(\frac{M e^{\gamma_{\mathrm{E}}}}{4\pi T}\right) + \frac{1}{2} + \frac{\omega_p}{2p} \ln\left(\frac{\omega_p + p}{\omega_p - p}\right) \right] , \quad \text{(A.100)}$$

which is plotted in fig. A.2 in comparison with the exact numerical result in eq. (A.82). The remainder behaves as $\mathcal{O}(M)$ and thus vanishes in the limit $M \to 0$ numerically validating the representation of the IR divergence. In the sum $Z_{112}^{(\mathrm{F})} + Z_{112}^{(\mathrm{BF})} + Z_{112}^{(\mathrm{FF})}$ all $(1/M)$-divergences combine to the Matsubara zero-mode contribution

$$T \int_k \frac{1}{[k^2 + M^2]^2} Z_{2;i} \, . \quad \text{(A.101)}$$

To verify that the behaviour in the limit $m_i \to 0$ is consistent with the result obtained from IBP eq. (5.12) individual terms are expanded up to $\mathcal{O}(m_i^2)$

$$\begin{aligned} Z_{112}^{(\mathrm{F})} + Z_{112}^{(\mathrm{BF})} &\propto \int_p \frac{n_{\mathrm{F}}(\omega_p)}{\omega_p} \left[\ln\left(\frac{m e^{\gamma_{\mathrm{E}}}}{4\pi T}\right) + 1 + \frac{\omega_p}{2p} \ln\left(\frac{\omega_p + p}{\omega_p - p}\right) \right] \\ &= \frac{T^2}{24} [2 + (\ln \zeta_2)' - \ln \pi] \\ &\quad + \frac{2m^2}{(4\pi)^2} \left[\ln^2\left(\frac{m e^{\gamma_{\mathrm{E}}}}{4\pi T}\right) + (1 + 2\ln 2) \ln\left(\frac{m e^{\gamma_{\mathrm{E}}}}{4\pi T}\right) + 3\ln 2 - \frac{1}{2} \right] + \mathcal{O}(m^4) \, , \end{aligned} \quad \text{(A.102)}$$

$$\begin{aligned} Z_{112}^{(\mathrm{FF})} &\propto \int_{p,q} \frac{1}{\omega_p \omega_q} \left\{ \frac{[n_{\mathrm{F}}(\omega_p) + n_{\mathrm{F}}(\omega_q)]^2}{(\omega_p + \omega_q)^2} - \frac{[n_{\mathrm{F}}(\omega_p) - n_{\mathrm{F}}(\omega_q)]^2}{(\omega_p - \omega_q)^2} \right\} \\ &= -\frac{4T^2}{3(4\pi)^2} \left[\frac{11}{6} + (\ln \zeta_2)' - \ln \pi \right] \\ &\quad - \frac{32 m^2}{(4\pi)^4} \left[\ln^2\left(\frac{m e^{\gamma_{\mathrm{E}}}}{4\pi T}\right) + \ln\left(\frac{m e^{\gamma_{\mathrm{E}}}}{4\pi T}\right) + 4\ln 2 - \frac{5}{2} \right] + \mathcal{O}(m^4) \, . \end{aligned} \quad \text{(A.103)}$$

Strategically the expansion in eq. (A.102) first performs the integration before executing the summation. Furthermore the expansion in eq. (A.103) is verified numerically.

Taking another mass derivative as in eq. (A.78) the contributions to Z_{212} starting from

eq. (A.79) are worked out independently

$$\begin{aligned}
Z_{212}^{(\mathrm{FF})} &= -\frac{1}{2}\frac{\mathrm{d}}{\mathrm{d}m^2} Z_{112}^{(\mathrm{FF})} \\
&= \frac{1}{32m^4}\int_{p,q}\frac{1}{2}\left(\frac{p^2}{p^2}+\frac{q^2}{q^2}\right)\frac{1}{\omega_p\omega_q}\left\{\frac{[n_{\mathrm{F}}(\omega_p)+n_{\mathrm{F}}(\omega_q)]^2}{(\omega_p+\omega_q)^2}-\frac{[n_{\mathrm{F}}(\omega_p)-n_{\mathrm{F}}(\omega_q)]^2}{(\omega_p-\omega_q)^2}\right\} \\
&- \frac{1}{32m^2}\int_{p,q}\frac{1}{2}\left(\frac{1}{p}\partial_p+\frac{1}{q}\partial_q\right)\frac{1}{\omega_p\omega_q}\left\{\frac{[n_{\mathrm{F}}(\omega_p)+n_{\mathrm{F}}(\omega_q)]^2}{(\omega_p+\omega_q)^2}-\frac{[n_{\mathrm{F}}(\omega_p)-n_{\mathrm{F}}(\omega_q)]^2}{(\omega_p-\omega_q)^2}\right\} \\
&= \frac{1}{64m^4}\int_{p,q}\left(\frac{\omega_p^2}{p^2}+\frac{\omega_q^2}{q^2}\right)\frac{1}{\omega_p\omega_q}\left\{\frac{[n_{\mathrm{F}}(\omega_p)+n_{\mathrm{F}}(\omega_q)]^2}{(\omega_p+\omega_q)^2}-\frac{[n_{\mathrm{F}}(\omega_p)-n_{\mathrm{F}}(\omega_q)]^2}{(\omega_p-\omega_q)^2}\right\}. \qquad \text{(A.104)}
\end{aligned}$$

In the second line the mass derivative was exchanged for a linear combination of momentum derivatives which could be computed using partial integration. We further verify that

$$\begin{aligned}
Z_{212}^{(\mathrm{F})}+Z_{212}^{(\mathrm{BF})} &= -\frac{1}{2}\frac{\mathrm{d}}{\mathrm{d}m^2}\left(Z_{112}^{(\mathrm{F})}+Z_{112}^{(\mathrm{BF})}\right) \\
&= \frac{1}{(4\pi)^2m^4}\int_p\frac{n_{\mathrm{F}}(\omega_p)}{\omega_p}\left[\ln\left(\frac{me^{\gamma_{\mathrm{E}}}}{4\pi T}\right)+1+\frac{\omega_p}{2p}\ln\left(\frac{\omega_p+p}{\omega_p-p}\right)\right] \\
&- \frac{1}{(4\pi)^2m^4}\int_p\frac{n_{\mathrm{F}}(\omega_p)}{\omega_p}\left[1+\frac{1}{2}\frac{1}{\omega_p}\frac{m^2}{2p}\ln\left(\frac{\omega_p+p}{\omega_p-p}\right)\right] \\
&+ \frac{1}{2}\frac{(d-2)}{(4\pi)^2m^4}\int_p\frac{n_{\mathrm{F}}(\omega_p)}{\omega_p}\frac{m^2}{p^2}\left[\ln\left(\frac{me^{\gamma_{\mathrm{E}}}}{4\pi T}\right)+1+\frac{\omega_p}{2p}\ln\left(\frac{\omega_p+p}{\omega_p-p}\right)\right] \\
&+ \frac{1}{2}\frac{1}{(4\pi)^2m^4}\int_p\frac{n_{\mathrm{F}}(\omega_p)}{\omega_p}\left[\frac{1}{\omega_p}\frac{m^2}{2p}\ln\left(\frac{\omega_p+p}{\omega_p-p}\right)-\frac{m^2}{p^2}\frac{\omega_p}{2p}\ln\left(\frac{\omega_p+p}{\omega_p-p}\right)+1+\frac{\omega_p^2}{p^2}\right] \\
&= \frac{1}{(4\pi)^2m^4}\int_p\frac{n_{\mathrm{F}}(\omega_p)}{\omega_p}\left[\left(1+\frac{m^2}{2p^2}\right)\ln\left(\frac{me^{\gamma_{\mathrm{E}}}}{4\pi T}\right)+\frac{\omega_p^2}{p^2}+\frac{\omega_p}{2p}\ln\left(\frac{\omega_p+p}{\omega_p-p}\right)\right], \qquad \text{(A.105)}
\end{aligned}$$

using partial integration in lines 4 and 5. Checking the corresponding massless IBP relation eq. (5.12), individual terms are expanded up to $\mathcal{O}(m_i^4)$

$$\begin{aligned}
Z_{212}^{(\mathrm{F})}+Z_{212}^{(\mathrm{BF})} &\propto \int_p\frac{n_{\mathrm{F}}(\omega_p)}{\omega_p}\left[\left(1+\frac{m^2}{2p^2}\right)\ln\left(\frac{me^{\gamma_{\mathrm{E}}}}{4\pi T}\right)+\frac{\omega_p^2}{p^2}+\frac{\omega_p}{2p}\ln\left(\frac{\omega_p+p}{\omega_p-p}\right)\right] \\
&= \frac{T^2}{24}[2+(\ln\zeta_2)'-\ln\pi] \\
&- \frac{2m^2}{(4\pi)^2}\left[\ln\left(\frac{me^{\gamma_{\mathrm{E}}}}{4\pi T}\right)+\ln 2+\frac{1}{2}\right]+\frac{14\zeta_3 m^4}{(4\pi)^4T^2}\left[\ln\left(\frac{me^{\gamma_{\mathrm{E}}}}{4\pi T}\right)+\frac{9}{4}\right]+\mathcal{O}(m^6), \qquad \text{(A.106)}
\end{aligned}$$

$$\begin{aligned}
Z_{212}^{(\mathrm{FF})} &\propto \frac{1}{64}\int_{p,q}\frac{1}{\omega_p\omega_q}\left(\frac{\omega_p^2}{p^2}+\frac{\omega_q^2}{q^2}\right)\left\{\frac{[n_{\mathrm{F}}(\omega_p)+n_{\mathrm{F}}(\omega_q)]^2}{(\omega_p+\omega_q)^2}-\frac{[n_{\mathrm{F}}(\omega_p)-n_{\mathrm{F}}(\omega_q)]^2}{(\omega_p-\omega_q)^2}\right\} \\
&= -\frac{T^2}{24(4\pi)^2}\left[\frac{11}{6}+(\ln\zeta_2)'-\ln\pi\right] \\
&+ \frac{m^2}{(4\pi)^4}\left[\ln\left(\frac{me^{\gamma_{\mathrm{E}}}}{4\pi T}\right)+\frac{1}{2}\right]-\frac{14\zeta_3 m^4}{(4\pi)^6T^2}\left[\ln\left(\frac{me^{\gamma_{\mathrm{E}}}}{4\pi T}\right)+\frac{9}{4}\right]+\mathcal{O}(m^6), \qquad \text{(A.107)}
\end{aligned}$$

confirming eq. (A.107) numerically and eq. (A.106) both analytically and numerically.

Appendix B

Integration-by-parts relations

The 2-loop QCD Debye mass eq. (5.18) requires the evaluation of the 2-loop Taylor coefficients eq. (B.13). These are obtained by a succession of massive 2-loop integration-by-parts relations which are derived in eq. (3.63) and constructively combined in this section. The integrals that require reduction are the massive fermionic sum-integrals with convention

$$Z^{\alpha_1\alpha_2\alpha_3}_{s_1s_2s_3;110;\sigma_1\sigma_2} \equiv \sum\!\!\!\!\!\!\int_{K_1K_2} \frac{k_{1_0}^{\alpha_1} k_{2_0}^{\alpha_2} (k_{1_0}-k_{2_0})^{\alpha_3}}{\left[K_1^2+m^2\right]^{s_1}\left[K_2^2+m^2\right]^{s_2}\left[(K_1-K_2)^2\right]^{s_3}} \;, \tag{B.1}$$

such that

$$\begin{aligned}
Z^{200}_{122;110;11} &= \frac{(d-2)(d-5)}{32m^4}\left(2Z^0_{1;1}Z^0_{1;0}-Z^0_{1;1}Z^0_{1;1}\right) - \frac{(d-3)^2(d-6)}{16m^2(d-4)}Z^{000}_{111;110;11} \\
&\quad - \frac{(d-3)(d-5)}{16m^4}Z^{110}_{111;110;11} - \frac{1}{2(d-4)}Z^{000}_{112;110;11} - \frac{3(d-5)}{4m^2}Z^{200}_{112;110;11} \\
&\quad + \frac{3(d-3)}{4m^2}Z^0_{1;1}Z^0_{2;0} + \frac{1}{4m^2}\left(Z^0_{2;1}Z^0_{1;0}-Z^0_{2;1}Z^0_{1;1}\right) \\
&\quad + \frac{2d-7}{4(d-4)}\left(2Z^0_{2;1}Z^0_{2;0}-\frac{1}{(d-2)}Z^0_{2;1}Z^0_{2;1}\right) + \frac{2m^2}{(d-4)}Z^{000}_{311;110;11} \\
&\quad - \frac{2m^2}{(d-2)(d-4)}Z^0_{3;1}Z^0_{2;1} \;, \\
Z^{020}_{122;110;11} &= -\frac{(d-2)(d-5)}{32m^4}\left(2Z^0_{1;1}Z^0_{1;0}-Z^0_{1;1}Z^0_{1;1}\right) + \frac{(d-3)(d^2-9d+22)}{16m^2(d-4)}Z^{000}_{111;110;11} \\
&\quad + \frac{(d-3)(d-5)}{16m^4}Z^{110}_{111;110;11} - \frac{1}{2(d-4)}Z^{000}_{112;110;11} + \frac{(d-5)}{4m^2}Z^{200}_{112;110;11} \\
&\quad - \frac{(d-3)}{4m^2}Z^0_{1;1}Z^0_{2;0} + \frac{1}{4(d-4)}\left(2Z^0_{2;1}Z^0_{2;0}-\frac{1}{(d-2)}Z^0_{2;1}Z^0_{2;1}\right) \\
&\quad + \frac{2m^2}{(d-4)}Z^{000}_{311;110;11} - \frac{2m^2}{(d-2)(d-4)}Z^0_{3;1}Z^0_{2;1} \;, \\
Z^{002}_{122;110;11} &= -\frac{(d-2)(d-5)}{16m^4}\left(2Z^0_{1;1}Z^0_{1;0}-Z^0_{1;1}Z^0_{1;1}\right) + \frac{(d-3)^2}{8m^2}Z^{000}_{111;110;11} \\
&\quad + \frac{(d-3)(d-5)}{8m^4}Z^{110}_{111;110;11} + \frac{1}{4m^2}\left(Z^0_{2;1}Z^0_{1;0}-Z^0_{2;1}Z^0_{1;1}\right) \;, \\
Z^{200}_{221;110;11} &= \frac{(d-3)}{8m^2}Z^{000}_{111;110;11} - \frac{1}{2}Z^{000}_{112;110;11} + \frac{(d-5)}{2m^2}Z^{200}_{112;110;11} - \frac{(d-3)}{2m^2}Z^0_{1;1}Z^0_{2;0} \\
&\quad - \frac{1}{4m^2}\left(Z^0_{2;1}Z^0_{1;0}-Z_{2;1}Z^0_{1;1}\right) + \frac{1}{4(d-2)}Z^0_{2;1}Z^0_{2;1} \\
&\quad + 2m^2Z^{000}_{311;110;11} - \frac{2m^2}{(d-2)}Z^0_{3;1}Z^0_{2;1} \;,
\end{aligned}$$

$$
\begin{aligned}
Z^{002}_{221;110;11} &= \frac{(d-2)(d-5)}{8m^4}\left(2Z^0_{1;1}Z^0_{1;0} - Z^0_{1;1}Z^0_{1;1}\right) + \frac{(d-3)}{4m^2}Z^{000}_{111;110;11} \\
&\quad - \frac{(d-3)(d-5)}{4m^4}Z^{110}_{111;110;11} - \frac{1}{2m^2}\left(Z^0_{2;1}Z^0_{1;0} - Z^0_{2;1}Z^0_{1;1}\right) + Z^0_{2;1}Z^0_{2;1}\,, \\
Z^{002}_{113;110;11} &= \frac{(d-2)(d-5)}{32m^4}\left(2Z^0_{1;1}Z^0_{1;0} - Z^0_{1;1}Z^0_{1;1}\right) - \frac{(d-3)^2}{16m^2}Z^{000}_{111;110;11} \\
&\quad - \frac{(d-3)(d-5)}{16m^4}Z^{110}_{111;110;11} - \frac{(d-5)}{4}Z^{000}_{112;110;11} - \frac{(d-5)}{4m^2}Z^{200}_{112;110;11} \\
&\quad + \frac{(d-3)}{4m^2}Z^0_{1;1}Z^0_{2;0}\,, \\
Z^{200}_{311;110;11} &= \frac{(d-2)(d-5)}{32m^4}\left(2Z^0_{1;1}Z^0_{1;0} - Z^0_{1;1}Z^0_{1;1}\right) - \frac{(d-3)}{16m^2}Z^{000}_{111;110;11} \\
&\quad - \frac{(d-3)(d-5)}{16m^4}Z^{110}_{111;110;11} + \frac{1}{4}Z^{000}_{112;110;11} - \frac{(d-5)}{4m^2}Z^{200}_{112;110;11} \\
&\quad + \frac{(d-3)}{4m^2}Z^0_{1;1}Z^0_{2;0} - \frac{1}{8}\frac{(d-4)}{(d-2)}Z^0_{2;1}Z^0_{2;1} - m^2 Z^{000}_{311;110;11}\,.
\end{aligned}
\tag{B.2}
$$

Special cases are found for

$$
Z_{211;110;11} = -\frac{(d-3)}{4m^2}Z_{111;110;11} + \frac{1}{2(d-2)}Z_{2;1}Z_{2;1}\,, \tag{B.3}
$$

$$
Z_{221;110;11} = \frac{(d-2)(d-5)}{4m^2}Z_{112;110;11} + (d-4)Z_{212;110;11} + \frac{1}{4m^2}(2Z_{2;1}Z_{2;0} - Z_{2;1}Z_{2;1})\,, \tag{B.4}
$$

$$
\begin{aligned}
Z_{311;110;11} &= \frac{(d-3)(d-5)}{16m^4}Z_{111;110;11} - \frac{(d-2)(d-5)}{8m^2}Z_{112;110;11} - \frac{(d-4)}{2}Z_{212;110;11} \\
&\quad - \frac{1}{8m^2}\left(2Z_{2;1}Z_{2;0} - \frac{1}{(d-2)}Z_{2;1}Z_{2;1}\right) + \frac{1}{(d-2)}Z_{3;1}Z_{2;1}\,.
\end{aligned}
\tag{B.5}
$$

B.1 Taylor coefficients

The next-to-leading order contributions to the Taylor coefficients of the QCD gluon self-energy also contribute directly to the matching of the EQCD effective gauge coupling g_{E}^2 via eq. (4.48).

At 1-loop level the Taylor coefficients of Π_{E} and Π_{T} with the sum over $N_{\mathrm{f}} = 3, \ldots, 6$ massive fermion flavours acquire

$$
\Pi_{\mathrm{E}1}(0) = N_{\mathrm{c}}(d-1)^2 Z_{1;0} - 2\sum_{i=1}^{N_{\mathrm{f}}}\left[(d-1)Z_{1;i} + 2m_i^2 Z_{2;i}\right]\,, \tag{B.6}
$$

$$
\frac{\mathrm{d}\Pi_{\mathrm{E}1}(0)}{\mathrm{d}m_i^2} = 2\left[(d-3)Z_{2;i} + 4m_i^2 Z_{3;i}\right]\,, \tag{B.7}
$$

$$
\Pi'_{\mathrm{E}1}(0) = -\left[\frac{d^2+d+10}{6} - (d-3)\xi\right]N_{\mathrm{c}}Z_{2;0} + \frac{1}{3}\sum_{i=1}^{N_{\mathrm{f}}}\left[(d-1)Z_{2;i} + 4m_i^2 Z_{3;i}\right]\,, \tag{B.8}
$$

$$
\begin{aligned}
\Pi''_{\mathrm{E}1}(0) &= \left[\frac{2d^2+11d+2}{60} + \xi\frac{(d-6)\xi - 6(d-4)}{12}\right]N_{\mathrm{c}}Z_{3;0} \\
&\quad - \frac{1}{5}\sum_{i=1}^{N_{\mathrm{f}}}\left[\frac{d-1}{3}Z_{3;i} + 2m_i^2 Z_{4;i}\right]\,,
\end{aligned}
\tag{B.9}
$$

$$
\Pi_{\mathrm{T}1}(0) = 0\,, \tag{B.10}
$$

$$\Pi'_{\mathrm{T1}}(0) = \frac{d-25}{6}N_{\mathrm{c}}Z_{2;0} + \frac{2}{3}\sum_{i=1}^{N_{\mathrm{f}}} Z_{2;i} \,, \tag{B.11}$$

$$\Pi''_{\mathrm{T1}}(0) = \left[\frac{117-2d}{60} - \frac{(6+\xi)\xi}{12}\right] N_{\mathrm{c}}Z_{3;0} - \frac{4}{15}\sum_{i=1}^{N_{\mathrm{f}}} Z_{3;i} \,. \tag{B.12}$$

We report also an IBP reduced expression for the fully massive 2-loop Π_{E2} and Π'_{T2} in the basis of eq. (5.20)

$$\begin{aligned}
\Pi_{\mathrm{E2}}(0) = {} & -(d-1)^2(d-3)(2-\xi)N_{\mathrm{c}}^2 Z_{1;0}Z_{2;0} \\
& + \sum_{i=1}^{N_{\mathrm{f}}}\Bigg\{(d-1)(d-3)\left(2(2-\xi)N_{\mathrm{c}}Z_{1;i}Z_{2;0} + 2C_{\mathrm{F}}\left[Z_{1;0}-Z_{1;i}\right]Z_{2;i}\right) \\
& \quad + 2m_i^2\Bigg(2N_{\mathrm{c}}\left[(d-2)-(d-3)\xi\right]Z_{2;i}Z_{2;0} + \left[4C_{\mathrm{F}}\frac{d-3}{d-2} - N_{\mathrm{c}}\right](Z_{2;i})^2 \\
& \quad\quad + 4(d-1)C_{\mathrm{F}}\left[Z_{1;0}-Z_{1;i}\right]Z_{3;i} - N_{\mathrm{c}}(d-5)(d-4)Z^{00}_{112;ii}\Bigg) \\
& \quad + 8m_i^4\left(C_{\mathrm{F}}\frac{4}{d-2}Z_{2;i}Z_{3;i} - N_{\mathrm{c}}(d-4)Z^{00}_{212;ii}\right)\Bigg\} \,,
\end{aligned} \tag{B.13}$$

$$\Pi_{\mathrm{T2}}(0) = 0 \,, \tag{B.14}$$

$$\begin{aligned}
\Pi'_{\mathrm{T2}}(0) = {} & \frac{N_{\mathrm{c}}^2}{(d-7)d}\Bigg\{2\frac{(d-3)(d-4)}{(d-5)(d-2)}(4d^2-21d-7)(Z_{2;0})^2 \\
& \quad - \frac{(d-1)^2}{3}(d^2-31d+144)Z_{1;0}Z_{3;0}\Bigg\} \\
& + \sum_{i=1}^{N_{\mathrm{f}}}\Bigg\{\frac{C_{\mathrm{F}}}{m_i^4}\frac{(d-1)(d-2)(d-5)}{d}\left(Z_{1;i}Z_{1;0} - \frac{1}{2}Z_{1;i}Z_{1;i} - Z^{11}_{111;ii}\right) \\
& \quad - \frac{1}{m_i^2}\frac{(d-3)(d-4)}{d}\left[\frac{(d-1)}{4}N_{\mathrm{c}} + \frac{d+1}{3}C_{\mathrm{F}}\right]Z^{00}_{111;ii} \\
& \quad + \frac{2}{m_i^2}\left[(d-1)N_{\mathrm{c}} + \frac{(d+5)}{3}C_{\mathrm{F}}\right]\left(\frac{(d-5)}{d}Z^{11}_{112;ii} - \frac{(d-3)}{d}Z_{1;i}Z_{2;0}\right) \\
& \quad + \frac{C_{\mathrm{F}}}{m_i^2}\frac{2(d-1)}{d}\left(Z_{1;i}-Z_{1;0}\right)Z_{2;i} \\
& \quad + \left[\frac{3d^3-21d^2+58d-52}{6d}N_{\mathrm{c}} - \frac{d^3-9d^2+26d-6}{3d}C_{\mathrm{F}}\right]Z^{00}_{112;ii} \\
& \quad + \frac{2(d^2-21d+32)}{3d}N_{\mathrm{c}}Z_{1;i}Z_{3;0} - \frac{8(d+5)}{3d}N_{\mathrm{c}}Z^{11}_{113;ii} \\
& \quad - \left[3N_{\mathrm{c}} + \frac{2(d-4)}{3d}C_{\mathrm{F}}\right]Z_{2;i}Z_{2;0} \\
& \quad + \left[\frac{(d-4)(3d^2-12d+4)}{3d(d-2)}C_{\mathrm{F}} - \frac{d^2-7d+9}{2(d-2)}N_{\mathrm{c}}\right]Z_{2;i}Z_{2;i} \\
& \quad + \frac{4(d-1)}{3}C_{\mathrm{F}}\left(Z_{1;i}-Z_{1;0}\right)Z_{3;i} \\
& \quad + m_i^2(d-4)\left[2N_{\mathrm{c}} - \frac{4(d-2)}{3d}C_{\mathrm{F}}\right]Z^{00}_{212;ii} \\
& \quad + m_i^2\left(\frac{4(d-22)}{3d}N_{\mathrm{c}}Z^{00}_{113;ii} - \frac{16}{3(d-2)}C_{\mathrm{F}}Z_{3;i}Z_{2;i}\right)\Bigg\} \,.
\end{aligned} \tag{B.15}$$

All the above concur with [57] in the limit $m_i \ll T$.

The situation is more delicate for $\Pi'_{\mathrm{T}2}$. Strikingly, terms inversely proportional to the mass arise in $\Pi'_{\mathrm{T}2}$ when using this integral basis. To safely take the zero-mass limit requires high orders in the mass expansion. Also the integrals need then to be evaluated numerically to high precision at high temperatures. A different basis is in principle conceivable but in general generates even higher powers $s_3 \sim 7$ of the third denominator in eq. (B.1) which is highly IR-sensitive already. However, in that basis the mass dependence becomes explicit and the limit $m_i = 0$ is taken immediately to recover [57].

Appendix C

Matching of the ultrasoft gauge coupling

Towards the account of chapter 4, this appendix collects additional details on the 3-loop computation of the matching of the ultrasoft coupling $g_{\rm M}$. We utilise the parameterisation of n-point vertices established in [1], which for the 2-point vertex reads η_1, η_2, for the 3-point vertex $\xi_1, \ldots, \xi_{10}$, for the 4-point vertex $\psi_1, \ldots, \psi_{44}$ and $\omega_1, \ldots, \omega_{35}$, for the 5-point vertex $\kappa_1, \ldots, \kappa_{10}$ and $\lambda_1, \ldots, \lambda_{10}$, and for the 6-point vertex $\chi_1, \ldots, \chi_{16}$. The redundancy of this operator basis is visible through the recurring appearance of certain combinations of coefficients and provides a strong cross check for the consistency of the computation.

We report the coefficients $D_{1i}, D_{2i}, \widetilde{D}_3$ from eq. (4.68) in Feynman gauge ($\xi = 1$):

$$
\begin{aligned}
D_{12} = {} & 8(d-1)(2d+3)(d^2-3d-2)\eta_1 - 2(d-3)(d-1)\omega_{24} \\
& + (d-1)(2d+3)\left[(d+3)(\lambda_1-3\kappa_1) + 5\lambda_2 + (2d+1)(2\lambda_3-\kappa_2)\right] \\
& + 4(d-1)\big[3(\xi_2+\xi_3-2\xi_4) + 2(d^3-2d^2-8d-8)\xi_5 \\
& \qquad - 2(d^3-d^2-11d-7)\xi_6 - 2(d^2-2)\xi_7\big] \\
& + 12d\big[(4d^2+18d+13)\chi_1 + (2d^2+14d+19)\chi_2 + (4d^2+13d+18)\chi_3 \\
& \qquad + 5(3d+4)\chi_4 + (d^2+12d+22)\chi_5\big] \\
& + 2(3d^4-11d^3-39d^2+16d+11)\psi_1 - 2(3d^3-25d^2+7d+5)\psi_3 \\
& + 4(d+1)(2d^3-11d^2-5d+9)\psi_{10} - 4(2d^4-12d^3+d^2+d+3)\psi_{12} \\
& + (6d^3-33d^2-22d+9)\psi_{22} - (d-21)d\psi_{23} + 2d(d+9)\psi_{24} - (12d^2+31d-3)\psi_{25} \\
& + 2(4d^3-27d^2-8d+11)\psi_{30} - 2(4d^3-27d^2+2d+11)\psi_{31} - 2(8d^2+9d+3)\psi_{38} \\
& + 4d(4d+1)\psi_{39} + 4(4d^2-2d+3)\psi_{40} \\
& - 2(d-1)(d^3-6d^2+d-7)\omega_1 - 2(d-1)(d^2-3)\omega_3 - (d-1)(2d^2-19d-13)\omega_{22} \\
& + (d-6)(d-1)\omega_{23} + (d-1)(4d-9)\omega_{25} - 6(d-1)^2\omega_{31}\,,
\end{aligned}
$$

$$
\begin{aligned}
D_{13} = {} & -\frac{4}{3}(18d^2+41d+18)\eta_1(d-1) \\
& + \frac{3(d-1)}{2}\left[(d+3)(\lambda_1-3\kappa_1) + 5\lambda_2 + (2d+1)(2\lambda_3-\kappa_2)\right] \\
& + (d-1)\bigg[\frac{1}{3}(9d^2-d+21)\omega_1 + 3(\omega_3+\omega_{24}) + \frac{1}{2}(15d+13)\omega_{22} \\
& \qquad + \frac{3}{2}(d-2)\omega_{23} + \frac{1}{6}(4d-27)\omega_{25} - 3(d-1)\omega_{31}\bigg] \\
& + \frac{2}{3}(4d^2+17d-9)(\xi_2+\xi_3) + \frac{4}{3}(2d^2-5d+9)\xi_4 - \frac{4}{3}(9d^2+26d+24)(d-1)\xi_5
\end{aligned}
$$

$$
\begin{aligned}
&+\frac{4}{3}(9d^3+26d^2-8d-21)\xi_6+8(2d-1)\xi_7\\
&-\frac{1}{3}(27d^3+60d^2-34d-33)\psi_1+\frac{1}{3}(36d^2-13d-15)\psi_3\\
&-\frac{2}{3}(18d^3+25d^2-6d-27)\psi_{10}+\frac{2}{3}(18d^3-2d^2-3d-9)\psi_{12}\\
&-\frac{1}{6}(45d^2+22d-27)\psi_{22}-\frac{1}{6}d(9d-25)\psi_{23}+\frac{8d\psi_{24}}{3}-\frac{1}{6}(12d^2+37d-9)\psi_{25}\\
&-\frac{1}{3}(45d^2+8d-33)\psi_{30}+\frac{1}{3}(45d^2-4d-33)\psi_{31}-\frac{1}{3}(8d^2+3d+9)\psi_{38}\\
&+\frac{8d^2\psi_{39}}{3}+\frac{2}{3}(4d^2-9d+9)\psi_{40}\,, \qquad \text{(C.1)}
\end{aligned}
$$

$$
\begin{aligned}
D_{22} = &\frac{2}{9}(3d^5-81d^4+302d^3+1916d^2-8026d+6032)\eta_1\\
&+\frac{(d-19)d}{6}\left[(d+3)(\lambda_1-3\kappa_1)+5\lambda_2+(2d+1)(2\lambda_3-\kappa_2)\right]\\
&-\frac{2}{27}(2d^2+456d-1217)(\xi_2+\xi_3)-\frac{2}{27}(353d^2-2460d+2158)\xi_4\\
&+\frac{2}{9}(3d^4-69d^3+1085d^2-2669d+1514)\xi_5\\
&-\frac{2}{27}(9d^4-207d^3+2951d^2-7542d+4162)\xi_6\\
&-\frac{2}{27}(342d^3-3346d^2+7035d-4790)\xi_7-\frac{1}{3}(3d^4-53d^3-63d^2+276d+139)\psi_1\\
&+\frac{1}{9}(15d^3-226d^2+180d+187)\psi_3-\frac{2}{3}(2d^4-37d^3-17d^2+84d+101)\psi_{10}\\
&+\frac{2}{9}(6d^4-120d^3+154d^2+144d-187)\psi_{12}-\frac{1}{18}(18d^3-321d^2-566d+2491)\psi_{22}\\
&+\frac{1}{18}(45d^2-481d+1166)\psi_{23}+\frac{1}{9}(6d^2-284d+547)\psi_{24}\\
&-\frac{1}{18}(18d^3-426d^2-163d+2045)\psi_{25}-\frac{1}{9}(12d^3-219d^2-274d+1109)\psi_{30}\\
&+\frac{1}{3}(4d^3-79d^2+86d+125)\psi_{31}-\frac{1}{9}(12d^3-294d^2+43d+835)\psi_{38}\\
&+\frac{2}{9}(6d^3-156d^2+262d+7)\psi_{39}+\frac{2}{9}(6d^3-156d^2+313d+94)\psi_{40}\\
&+\frac{1}{3}(d^4-21d^3+29d^2-108d+63)\omega_1-\frac{1}{3}(d^3-12d^2-108d+149)\omega_3\\
&+\frac{1}{6}(2d^3-39d^2+6d-91)\omega_{22}-\frac{1}{6}(d-7)(7d+20)\omega_{23}\\
&+\frac{1}{3}(2d^2-5d+24)\omega_{24}+\frac{1}{6}(2d^3-54d^2+83d-125)\omega_{25}+\frac{1}{3}(11d^2+12d-5)\omega_{31}\,,
\end{aligned}
$$

$$
\begin{aligned}
D_{23} = &-\frac{2}{27}(15d^5-335d^4+568d^3+4276d^2-16592+12912)\eta_1\\
&+\frac{1}{81}(65d^3-1320d^2+4945d-7302)(\xi_2+\xi_3)-\frac{2}{81}(35d^3-2661d^2+9853d-6474)\xi_4\\
&-\frac{2}{27}(30d^4-581d^3+2318d^2-4085d+1950)\xi_5\\
&+\frac{2}{81}(90d^4-1859d^3+7995d^2-15115d+7302)\xi_6\\
&-\frac{2}{81}(45d^4-2467d^3+10578d^2-16427d+11778)\xi_7
\end{aligned}
$$

$$
\begin{aligned}
&+\frac{1}{18}(161d^3-162d^2-569d+834)\psi_1+\frac{1}{54}(d^3-864d^2+2741d-1122)\psi_3\\
&+\frac{1}{9}(109d^3-138d^2-391d+606)\psi_{10}-\frac{1}{27}(325d^3-1008d^2+1157d-1122)\psi_{12}\\
&+\frac{1}{108}(15d^3+952d^2-3185d+2850)\psi_{22}-\frac{1}{108}(15d^3-379d^2+848d+84)\psi_{23}\\
&-\frac{1}{54}(10d^2+91d-174)\psi_{24}+\frac{1}{108}(53d^2-109d+174)(\psi_{25}-2\psi_{38}+3\omega_{25})\\
&-\frac{1}{54}(15d^3-668d^2+1855d-1470)\psi_{30}+\frac{1}{18}(5d^3-258d^2+775d-750)\psi_{31}\\
&-\frac{1}{27}(d^2-35d+42)\psi_{39}-\frac{2}{27}(26d^2-163d+282)\psi_{40}\\
&-\frac{1}{6}(19d^3-38d^2-71d+126)\omega_1+\frac{1}{18}(d^3+144d^2-787d+894)\omega_3\\
&+\frac{1}{36}(5d-1)(3d^2-25d+30)\omega_{22}+\frac{1}{36}(5d^3-231d^2+790d-840)\omega_{23}\\
&-\frac{1}{6}(5d^2-30d+48)\omega_{24}-\frac{1}{18}(5d^3-150d^2+319d-30)\omega_{31}\ ,
\end{aligned}
\tag{C.2}
$$

$$
\begin{aligned}
\widetilde{D}_3 &= (d-1)\left[4\eta_1+4\xi_5-\omega_1-\omega_{25}\right]-4d\left[\psi_{12}+\psi_{39}+\psi_{40}\right]+(d+1)\xi_7\\
&+2(2d+3)\left[\psi_{10}+\psi_{38}\right]+(3d+7)\left[\psi_1+\psi_{25}\right]+8\left[\xi_2+\xi_3+\xi_4+\xi_6\right]\\
&-4\left[\psi_3+\psi_{23}+\psi_{24}+\psi_{31}\right]+10\left[\psi_{22}+\psi_{30}\right]\ .
\end{aligned}
\tag{C.3}
$$

As most coefficients are not fully independent, one can observe that all Θ_i , $i=1,\ldots,12$ relations listed in [1] are satisfied including

$$
\begin{aligned}
\Theta_{13}:&\quad \delta\lambda_1=3\delta\kappa_1\ ,\\
\Theta_{14}:&\quad \delta\kappa_2=2\delta\lambda_3\ .
\end{aligned}
\tag{C.4}
$$

C.1 3-loop diagrams

The genuine soft EQCD contribution to the ultrasoft gauge coupling in hot Yang-Mills in sec. 4.4 requires a 3-loop computation of the self-energy of the spatial gluons A_i^a. We depict all the occurring diagrams in the background field gauge with their respective symmetry factors. The background field B_i^a is implied at the endpoint of a line.

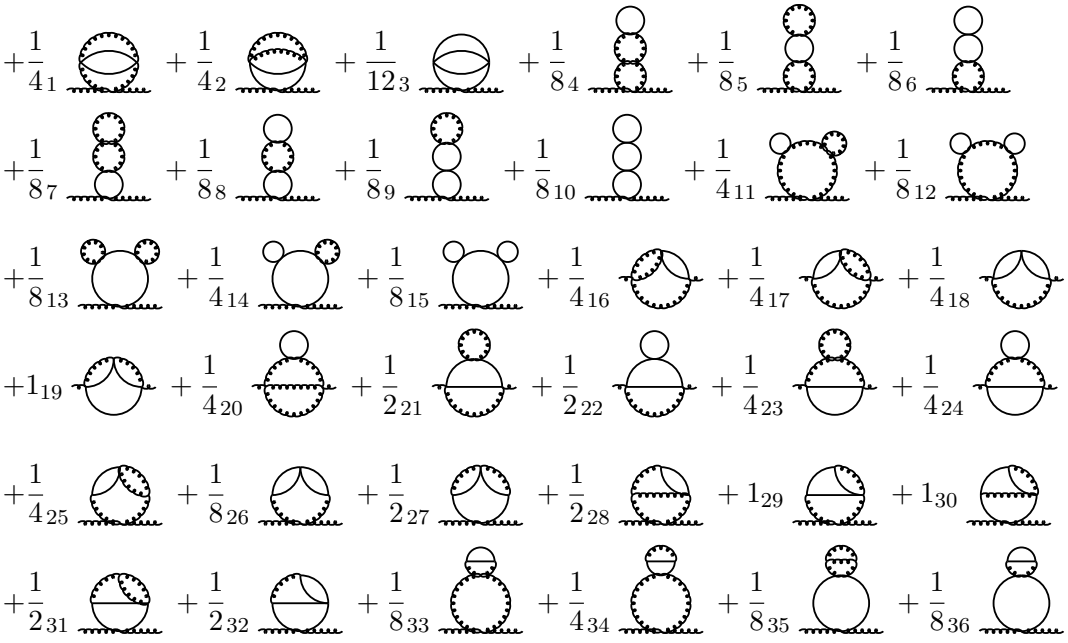

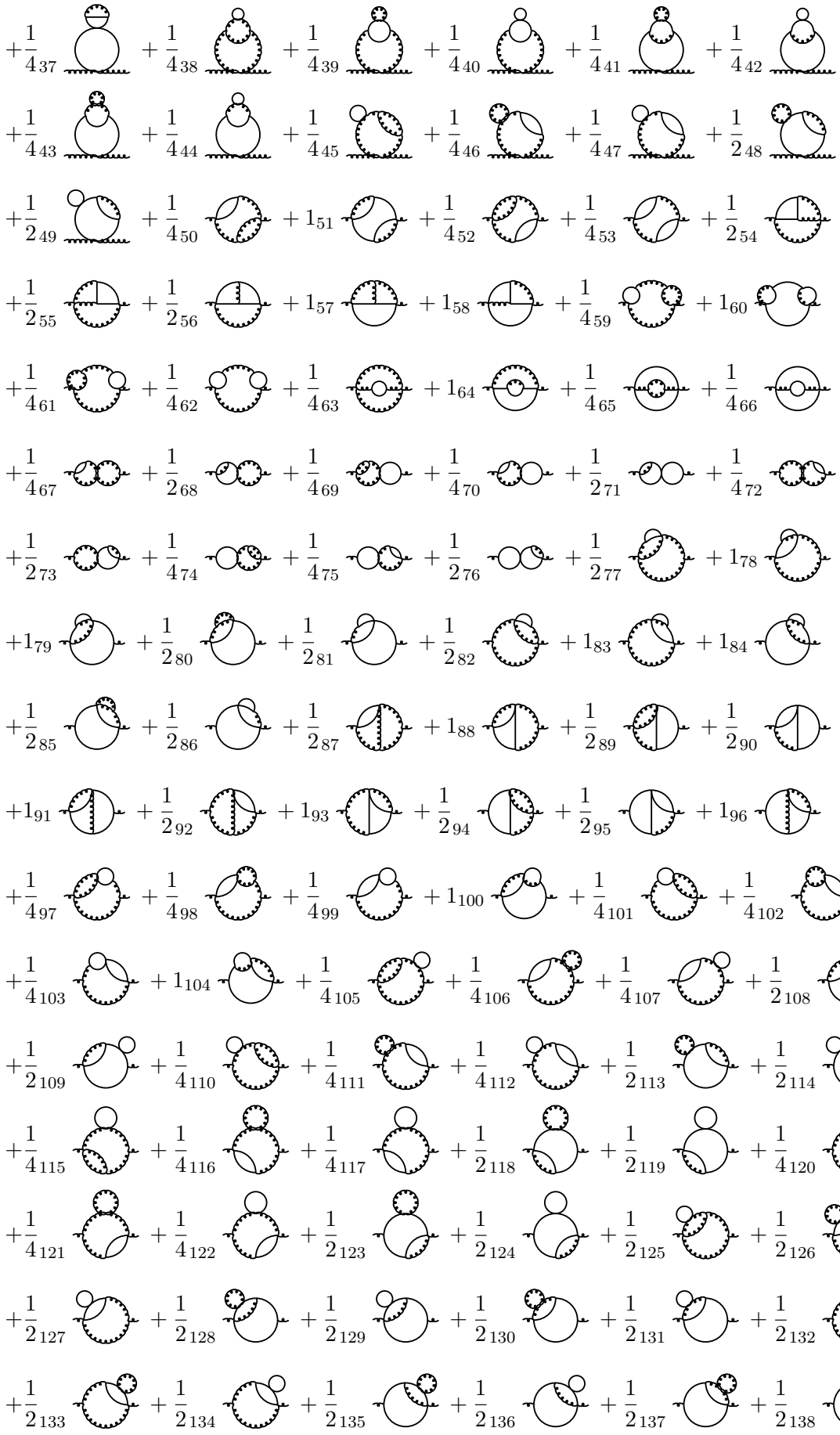

$+\frac{1}{4}_{139}$  $+\frac{1}{2}_{140}$  $+\frac{1}{2}_{141}$  $+\frac{1}{4}_{142}$  $+\frac{1}{4}_{143}$  $+\frac{1}{8}_{144}$ 

$+\frac{1}{8}_{145}$  $+\frac{1}{8}_{146}$  $+\frac{1}{8}_{147}$  $+\frac{1}{8}_{148}$  $+\frac{1}{8}_{149}$  $+\frac{1}{8}_{150}$ 

$+\frac{1}{2}_{151}$  $+\frac{1}{2}_{152}$  $+\frac{1}{6}_{153}$  $+\frac{1}{4}_{154}$  $+\frac{1}{4}_{155}$  $+\frac{1}{4}_{156}$ 

$+\frac{1}{4}_{157}$  $+\frac{1}{4}_{158}$  $+\frac{1}{4}_{159}$  $+\frac{1}{4}_{160}$  $+\frac{1}{4}_{161}$  $+\frac{1}{4}_{162}$ 

$+\frac{1}{4}_{163}$  $+\frac{1}{4}_{164}$  $+\frac{1}{4}_{165}$  $+\frac{1}{4}_{166}$  $+\frac{1}{4}_{167}$  $+\frac{1}{4}_{168}$ 

$+\frac{1}{4}_{169}$  $+\frac{1}{4}_{170}$  $+\frac{1}{4}_{171}$ 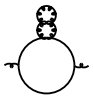 $+\frac{1}{4}_{172}$ 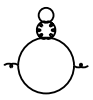 $+\frac{1}{4}_{173}$ 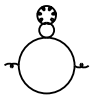 $+\frac{1}{4}_{174}$ 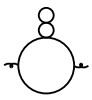

$+\frac{1}{4}_{175}$ 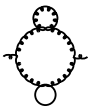 $+\frac{1}{8}_{176}$ 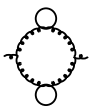 $+\frac{1}{8}_{177}$ 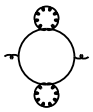 $+\frac{1}{4}_{178}$ 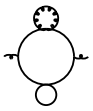 $+\frac{1}{8}_{179}$ $+\frac{1}{4}_{180}$

$+\frac{1}{4}_{181}$ $+\frac{1}{4}_{182}$ $+\frac{1}{4}_{183}$ $+\frac{1}{4}_{184}$ $+\frac{1}{4}_{185}$ $+\frac{1}{4}_{186}$

$+\frac{1}{4}_{187}$ $+\frac{1}{2}_{188}$ $+\frac{1}{2}_{189}$ $+\frac{1}{2}_{190}$ $+\frac{1}{4}_{191}$ $+\frac{1}{8}_{192}$

$+\frac{1}{2}_{193}$ $+\frac{1}{4}_{194}$ $+\frac{1}{2}_{195}$ $+\frac{1}{2}_{196}$ $+\frac{1}{4}_{197}$ $+\frac{1}{4}_{198}$

$+\frac{1}{2}_{199}$ $+1_{200}$ $+1_{201}$ $+\frac{1}{2}_{202}$ $+\frac{1}{2}_{203}$ $+\frac{1}{2}_{204}$

$+1_{205}$ $+1_{206}$ $+\frac{1}{2}_{207}$ $+\frac{1}{2}_{208}$ $+\frac{1}{2}_{209}$ $+\frac{1}{2}_{210}$

$+\frac{1}{2}_{211}$ $+1_{212}$ $+1_{213}$ $+\frac{1}{2}_{214}$ $+\frac{1}{2}_{215}$ $+\frac{1}{2}_{216}$

$+1_{217}$ $+1_{218}$ $+\frac{1}{4}_{219}$ $+\frac{1}{4}_{220}$ $+\frac{1}{4}_{221}$ $+1_{222}$

$+\frac{1}{4}_{223}$ $+\frac{1}{4}_{224}$ $+\frac{1}{4}_{225}$ $+1_{226}$ $+1_{227}$ $+\frac{1}{2}_{228}$

$+\frac{1}{2}_{229}$ $+1_{230}$ $+\frac{1}{2}_{231}$ $+1_{232}$ $+\frac{1}{2}_{233}$ $+\frac{1}{2}_{234}$

$+1_{235}$ $+\frac{1}{2}_{236}$ $+\frac{1}{4}_{237}$ $+\frac{1}{4}_{238}$ $+\frac{1}{4}_{239}$ $+1_{240}$

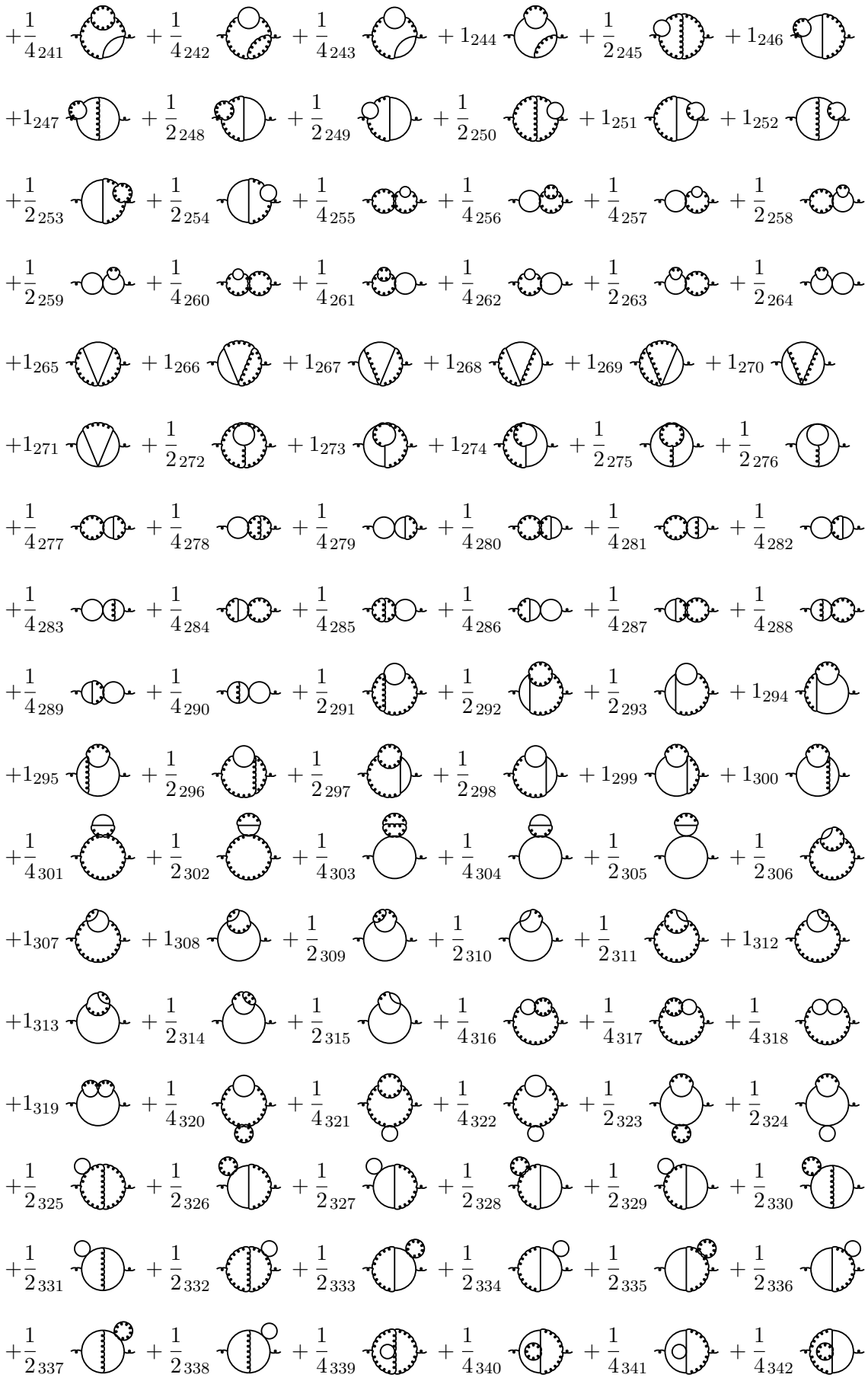

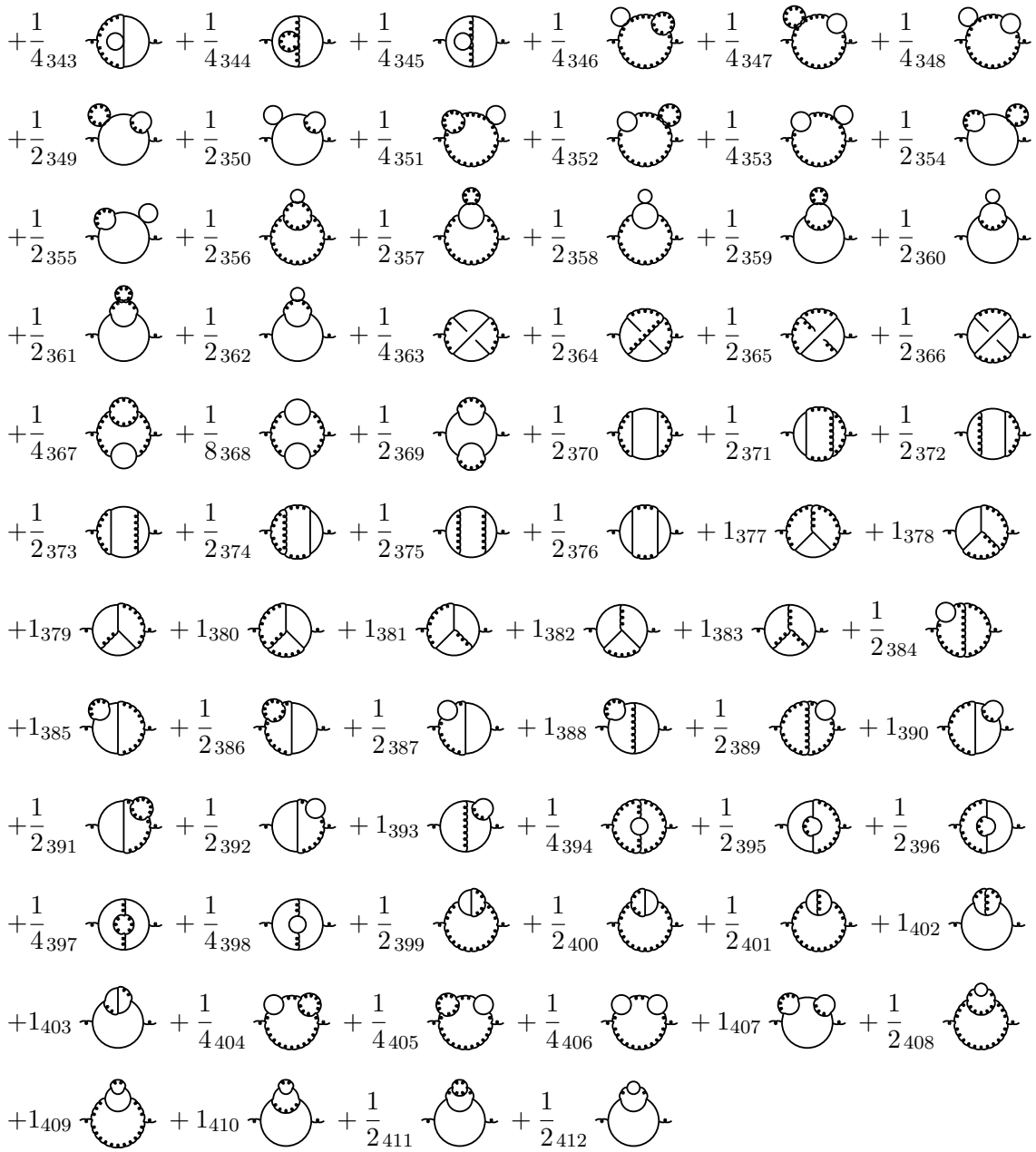

The contributing d-dimensional polynomials of the 3-loop soft contribution to the MQCD gauge coupling in eq. (4.85) are parameterised by

$$
\begin{aligned}
r_1(d) &= -\frac{(d-2)p_1(d)}{384(d-10)(d-8)(d-7)(d-6)(d-5)(d-4)(d-3)^2(d-1)d}\,, \\
r_2(d) &= \frac{(3d-10)(3d-8)p_2(d)}{128(d-3)(d-1)d(2d-11)(2d-9)(2d-7)}\,, \\
r_3(d) &= \frac{(3d-10)(3d-8)p_3(d)}{256(d-10)(d-8)(d-6)(d-4)(d-1)d}\,,
\end{aligned}
\tag{C.5}
$$

with residual non-factorisable polynomials $p_i(d)$

$$
\begin{aligned}
p_1(d) = {} & 12d^{12} - 628d^{11} + 14447d^{10} - 193505d^9 + 1689420d^8 - 10234582d^7 \\
& + 44883931d^6 - 147059385d^5 + 366585830d^4 - 689809244d^3 \\
& + 929595256d^2 - 791686464d + 314842752\,,
\end{aligned}
$$

$$p_2(d) = 12d^7 - 308d^6 + 3175d^5 - 17441d^4 + 57347d^3 - 117419d^2 + 138786d - 70872 \,,$$
$$p_3(d) = 3d^5 - 60d^4 + 359d^3 - 670d^2 + 400d + 736 \,. \tag{C.6}$$

Finally scalar coupling effects are inspected where the respective abbreviated polynomials of the factorised result read

$$\begin{aligned}\tilde{r}_1(d) = \frac{d-2}{8}\Bigg(&\frac{(d-4)(3d^5-49d^4+283d^3-779d^2+1238d-1056)}{3(d-7)(d-5)(d-3)d}\lambda \\ &- \frac{(d-4)(3d-10)}{3}\lambda^2 \\ &+ \frac{(d-2)^2(9d^2-77d+158)}{16(d-6)(d-4)(d-3)d}\kappa_1 + \frac{(d-10)(d-2)^2}{16(d-4)d}\kappa_2\Bigg) \,, \\ \tilde{r}_3(d) = \frac{(3d-10)(3d-8)(d^2-5d-2)}{256(d-6)(d-4)d}&(\kappa_1 + (d-6)\kappa_2) \,. \end{aligned} \tag{C.7}$$

Bibliography

[1] M. Laine, P. Schicho, and Y. Schröder, *Soft thermal contributions to 3-loop gauge coupling,* JHEP **2018** (2018) 37 [1803.08689].

[2] M. Laine, P. Schicho, and Y. Schröder, *A QCD Debye mass in a broad temperature range,* Phys. Rev. D **101** (2020) 023532 [1911.09123].

[3] M. Tanabashi, K. Hagiwara, K. Hikasa, *et al.*, *Review of Particle Physics,* Phys. Rev. D **98** (2018) 030001.

[4] M. Laine and K. Rummukainen, *What's new with the electroweak phase transition?,* Nucl. Phys. B - Proc. Suppl. **73** (1999) 180 [hep-lat/9809045].

[5] K. Kajantie, M. Laine, K. Rummukainen, and M. Shaposhnikov, *The electroweak phase transition: a non-perturbative analysis,* Nucl. Phys. B **466** (1996) 189 [hep-lat/9510020].

[6] K. Kajantie, M. Laine, K. Rummukainen, and M. Shaposhnikov, *Is There a Hot Electroweak Phase Transition at $m_H \gtrsim m_W$?,* Phys. Rev. Lett. **77** (1996) 2887 [hep-ph/9605288].

[7] K. Kajantie, M. Laine, K. Rummukainen, and M. Shaposhnikov, *A non-perturbative analysis of the finite-T phase transition in SU(2)×U(1) electroweak theory,* Nucl. Phys. B **493** (1997) 413 [hep-lat/9612006].

[8] K. G. Wilson, *Confinement of quarks,* Phys. Rev. D **10** (1974) 2445.

[9] D. J. Gross and F. Wilczek, *Asymptotically Free Gauge Theories. I,* Phys. Rev. D **8** (1973) 3633.

[10] H. D. Politzer, *Reliable Perturbative Results for Strong Interactions?,* Phys. Rev. Lett. **30** (1973) 1346.

[11] S. Chin, *Transition to hot quark matter in relativistic heavy-ion collision,* Phys. Lett. B **78** (1978) 552.

[12] S. Borsanyi, Z. Fodor, C. Hoelbling, *et al.*, *Is there still any Tc mystery in lattice QCD? Results with physical masses in the continuum limit III,* JHEP **2010** (2010) 73 [1005.3508].

[13] A. Bazavov, T. Bhattacharya, M. Cheng, *et al.*, *Chiral and deconfinement aspects of the QCD transition,* Phys. Rev. D **85** (2012) 054503 [1111.1710].

[14] A. Bazavov, H.-T. Ding, P. Hegde, *et al.*, *Chiral crossover in QCD at zero and non-zero chemical potentials,* Phys. Lett. B **795** (2019) 15 [1812.08235].

[15] S. Borsanyi, Z. Fodor, J. N. Guenther, *et al.*, *The QCD crossover at finite chemical potential from lattice simulations,* arXiv (2020) [2002.02821].

[16] A. Linde, *Infrared problem in the thermodynamics of the Yang-Mills gas,* Phys. Lett. B **96** (1980) 289.

[17] P. A. Baikov, K. G. Chetyrkin, and J. H. Kühn, *Five-Loop Running of the QCD Coupling Constant,* Phys. Rev. Lett. **118** (2017) 082002 [1606.08659].

[18] F. Herzog, B. Ruijl, T. Ueda, J. A. M. Vermaseren, and A. Vogt, *The five-loop beta function of Yang-Mills theory with fermions,* JHEP **2017** (2017) 90 [1701.01404].

[19] T. Luthe, A. Maier, P. Marquard, and Y. Schröder, *The five-loop Beta function for a general gauge group and anomalous dimensions beyond Feynman gauge,* JHEP **2017** (2017) 166 [1709.07718].

[20] T. Luthe, A. Maier, P. Marquard, and Y. Schröder, *Five-loop quark mass and field anomalous dimensions for a general gauge group,* JHEP **2017** (2017) 81 [1612.05512].

[21] P. Baikov, K. Chetyrkin, and J. Kühn, *Five-loop fermion anomalous dimension for a general gauge group from four-loop massless propagators,* JHEP **2017** (2017) 119 [1702.01458].

[22] M. Nishimura and Y. Schröder, *IBP methods at finite temperature,* JHEP **2012** (2012) 51 [1207.4042].

[23] A. V. Smirnov and A. V. Petukhov, *The Number of Master Integrals is Finite,* Lett. Math. Phys. **97** (2011) 37 [1004.4199].

[24] J. Schwinger, *Brownian Motion of a Quantum Oscillator,* J. Math. Phys. **2** (1961) 407.

[25] L. V. Keldysh, *Diagram technique for nonequilibrium processes,* JETP **20** (1965) 1018.

[26] T. Matsubara, *A New Approach to Quantum-Statistical Mechanics,* Prog. Theor. Phys. **14** (1955) 351.

[27] M. L. Bellac, *Thermal Field Theory.* Cambridge Monographs on Mathematical Physics. Cambridge University Press, Aug, 2011.

[28] J. I. Kapusta and C. Gale, *Finite-Temperature Field Theory.* Cambridge University Press, Cambridge, Jan, 2006.

[29] A. Das, *Finite Temperature Field Theory.* WORLD SCIENTIFIC, May, 1997.

[30] R. Kubo, *Statistical-Mechanical Theory of Irreversible Processes. I. General Theory and Simple Applications to Magnetic and Conduction Problems,* J. Phys. Soc. Japan **12** (1957) 570.

[31] P. C. Martin and J. Schwinger, *Theory of Many-Particle Systems. I,* Phys. Rev. **115** (1959) 1342.

[32] C. Bloch, *Sur la détermination de l'état fondamental d'un système de particules,* Nucl. Phys. **7** (1958) 451.

[33] T. Appelquist and J. Carazzone, *Infrared singularities and massive fields,* Phys. Rev. D **11** (1975) 2856.

[34] M. Laine and A. Vuorinen, *Basics of Thermal Field Theory*, vol. 925 of *Lecture Notes in Physics.* Springer International Publishing, Cham, Jan, 2016, [1701.01554].

[35] J. C. Collins, *Renormalization.* Cambridge University Press, Nov, 1984.

[36] B. Delamotte, *A hint of renormalization,* Am. J. Phys. **72** (2004) 170 [hep-th/0212049].

[37] W. Pauli and F. Villars, *On the Invariant Regularization in Relativistic Quantum Theory,* Rev. Mod. Phys. **21** (1949) 434.

[38] G. 't Hooft and M. Veltman, *Regularization and renormalization of gauge fields,* Nucl. Phys. B **44** (1972) 189.

[39] J. F. Ashmore, *A method of gauge-invariant regularization,* Lett. al Nuovo Cim. **4** (1972) 289.

[40] H. Kleinert and V. Schulte-Frohlinde, *Critical Properties Of Phi4-Theories.* World Scientific Publishing Co. Pte. Ltd., 2001.

[41] J. Collins, *Structure of counterterms in dimensional regularization,* Nucl. Phys. B **80** (1974) 341.

[42] W. A. Bardeen, A. J. Buras, D. W. Duke, and T. Muta, *Deep-inelastic scattering beyond the leading order in asymptotically free gauge theories,* Phys. Rev. D **18** (1978) 3998.

[43] E. Braaten and R. D. Pisarski, *Soft amplitudes in hot gauge theories: A general analysis,* Nucl. Phys. B **337** (1990) 569.

[44] J. O. Andersen and M. Strickland, *Resummation in Hot Field Theories,* Ann. Phys. (N. Y). **317** (2004) 281 [hep-ph/0404164].

[45] F. Karsch, A. Patkós, and P. Petreczky, *Screened perturbation theory,* Phys. Lett. B **401** (1997) 69 [hep-ph/9702376].

[46] J. O. Andersen and L. Kyllingstad, *Four-loop screened perturbation theory,* Phys. Rev. D **78** (2008) 076008 [0805.4478].

[47] M. Laine and M. Losada, *Two-loop dimensional reduction and effective potential without temperature expansions,* Nucl. Phys. B **582** (2000) 277 [hep-ph/0003111].

[48] T. Brauner, T. V. I. Tenkanen, A. Tranberg, A. Vuorinen, and D. J. Weir, *Dimensional reduction of the Standard Model coupled to a new singlet scalar field,* JHEP **2017** (2016) 7 [1609.06230].

[49] K. Kajantie, M. Laine, K. Rummukainen, and M. Shaposhnikov, *Generic Rules for High Temperature Dimensional Reduction and Their Application to the Standard Model,* Nucl. Phys. B **458** (1995) 90 [hep-ph/9508379].

[50] N. Landsman, *Limitations to dimensional reduction at high temperature,* Nucl. Phys. B **322** (1989) 498.

[51] K. Farakos, K. Kajantie, K. Rummukainen, and M. Shaposhnikov, *3D Physics and the Electroweak Phase Transition: Perturbation Theory,* Nucl. Phys. B **425** (1994) 67 [hep-ph/9404201].

[52] L. Faddeev and V. Popov, *Feynman diagrams for the Yang-Mills field,* Phys. Lett. B **25** (1967) 29.

[53] P. Arnold, *Quark-Gluon Plasmas and Thermalization,* Int. J. Mod. Phys. E **16** (2007) 2555 [0708.0812].

[54] Y. Aoki, G. Endrődi, Z. Fodor, S. D. Katz, and K. K. Szabó, *The order of the quantum chromodynamics transition predicted by the standard model of particle physics,* Nature **443** (2006) 675 [hep-lat/0611014].

[55] T. Bhattacharya, M. I. Buchoff, N. H. Christ, *et al.*, *QCD Phase Transition with Chiral Quarks and Physical Quark Masses,* Phys. Rev. Lett. **113** (2014) 082001 [1402.5175].

[56] P. Giovannangeli, *Two loop renormalization of the magnetic coupling and non-perturbative sector in hot QCD,* Nucl. Phys. B **738** (2005) 23 [hep-ph/0506318].

[57] M. Laine and Y. Schröder, *Two-loop QCD gauge coupling at high temperatures,* JHEP **2005** (2005) 067 [hep-ph/0503061].

[58] M. Cheng, S. Datta, J. van der Heide, *et al.*, *The spatial string tension and dimensional reduction in QCD,* Phys. Rev. D **78** (2008) 034506 [0806.3264].

[59] A. Hart, M. Laine, and O. Philipsen, *Static correlation lengths in QCD at high temperatures and finite densities,* Nucl. Phys. B **586** (2000) 443 [hep-ph/0004060].

[60] L. D. McLerran and B. Svetitsky, *Quark liberation at high temperature: A Monte Carlo study of SU(2) gauge theory,* Phys. Rev. D **24** (1981) 450.

[61] B. Svetitsky and L. G. Yaffe, *Critical behavior at finite-temperature confinement transitions,* Nucl. Phys. B **210** (1982) 423.

[62] P. Nogueira, *Automatic Feynman Graph Generation,* J. Comput. Phys. **105** (1993) 279.

[63] T. Hahn, *Generating Feynman Diagrams and Amplitudes with FeynArts 3,* Comput. Phys. Commun. **140** (2000) 418 [hep-ph/0012260].

[64] V. Shtabovenko, R. Mertig, and F. Orellana, *New developments in FeynCalc 9.0* Comput. Phys. Commun. **207** (2016) 432 [1601.01167].

[65] K. Chetyrkin and F. Tkachov, *Integration by parts: The algorithm to calculate β-functions in 4 loops,* Nucl. Phys. B **192** (1981) 159.

[66] F. Tkachov, *A theorem on analytical calculability of 4-loop renormalization group functions,* Phys. Lett. B **100** (1981) 65.

[67] S. Laporta, *High-precision calculation of multi-loop Feynman integrals by difference equations,* Int. J. Mod. Phys. A **15** (2001) 5087 [hep-ph/0102033].

[68] É. É. Boos and A. I. Davydychev, *A method of calculating massive Feynman integrals,* Theor. Math. Phys. **89** (1991) 1052.

[69] A. von Manteuffel and C. Studerus, *Reduze 2 - Distributed Feynman Integral Reduction,* arXiv (2012) [1201.4330].

[70] A. Smirnov, *FIRE5: A C++ implementation of Feynman Integral REduction,* Comput. Phys. Commun. **189** (2015) 182 [1408.2372].

[71] B. Ruijl, T. Ueda, and J. Vermaseren, *FORM version 4.2* arXiv (2017) [1707.06453].

[72] J. C. Collins and J. A. M. Vermaseren, *Axodraw Version 2,* arXiv (2016) [1606.01177].

[73] J. Möller, *Algorithmic approach to finite-temperature QCD,* 2009.

[74] C. Bogner and S. Weinzierl, *Feynman graph polynomials,* Int. J. Mod. Phys. A **25** (2010) 2585 [1002.3458].

[75] A. Pak, *The toolbox of modern multi-loop calculations: novel analytic and semi-analytic techniques,* J. Phys. Conf. Ser. **368** (2011) 012049 [1111.0868].

[76] A. A. Slavnov, *Ward identities in gauge theories,* Theor. Math. Phys. **10** (1972) 99.

[77] J. Taylor, *Ward identities and charge renormalization of the Yang-Mills field,* Nucl. Phys. B **33** (1971) 436.

[78] T. van Ritbergen, A. N. Schellekens, and J. A. M. Vermaseren, *Group theory factors for Feynman diagrams,* Int. J. Mod. Phys. A **14** (1998) 41 [hep-ph/9802376].

[79] R. N. Lee and A. A. Pomeransky, *Critical points and number of master integrals,* JHEP **2013** (2013) 165 [1308.6676].

[80] R. Lee, *Group structure of the integration-by-part identities and its application to the reduction of multiloop integrals,* JHEP **2008** (2008) 031 [0804.3008].

[81] O. V. Tarasov, *Connection between Feynman integrals having different values of the space-time dimension,* Phys. Rev. D **54** (1996) 6479 [hep-th/9606018].

[82] O. V. Tarasov, *A new approach to the momentum expansion of multiloop Feynman diagrams,* Nucl. Phys. B **480** (1996) 397 [hep-ph/9606238].

[83] O. Tarasov, *Generalized recurrence relations for two-loop propagator integrals with arbitrary masses,* Nucl. Phys. B **502** (1997) 455 [hep-ph/9703319].

[84] P. Mastrolia and S. Mizera, *Feynman integrals and intersection theory,* JHEP **2019** (2019) 139 [1810.03818].

[85] H. Frellesvig, F. Gasparotto, S. Laporta, *et al.*, *Decomposition of Feynman Integrals on the Maximal Cut by Intersection Numbers,* JHEP **2019** (2019) 153 [1901.11510].

[86] H. Frellesvig, F. Gasparotto, M. K. Mandal, P. Mastrolia, L. Mattiazzi, and S. Mizera, *Vector Space of Feynman Integrals and Multivariate Intersection Numbers,* Phys. Rev. Lett. **123** (2019) 201602 [1907.02000].

[87] G. Heinrich, *Sector Decomposition,* Int. J. Mod. Phys. A **23** (2008) 1457 [0803.4177].

[88] M. Argeri and P. Mastrolia, *Feynman Diagrams and Differential Equations,* Int. J. Mod. Phys. A **22** (2007) 4375 [0707.4037].

[89] J. A. M. Vermaseren, *Harmonic sums, Mellin transforms and Integrals,* Int. J. Mod. Phys. A **14** (1998) 2037 [hep-ph/9806280].

[90] P. Arnold and C. Zhai, *Three-loop free energy for pure gauge QCD,* Phys. Rev. D **50** (1994) 7603 [hep-ph/9408276].

[91] R. D. Pisarski, *Computing finite-temperature loops with ease,* Nucl. Phys. B **309** (1988) 476.

[92] R. R. Parwani, *Resummation in a hot scalar field theory,* Phys. Rev. D **45** (1992) 4695 [hep-ph/9204216].

[93] J. I. Kapusta, *Quantum chromodynamics at high temperature,* Nucl. Phys. B **148** (1979) 461.

[94] I. Ghişoiu, T. Gorda, A. Kurkela, P. Romatschke, M. Säppi, and A. Vuorinen, *On high-order perturbative calculations at finite density,* Nucl. Phys. B **915** (2017) 102 [1609.04339].

[95] T. Appelquist and R. D. Pisarski, *High-temperature Yang-Mills theories and three-dimensional quantum chromodynamics,* Phys. Rev. D **23** (1981) 2305.

[96] S. Nadkarni, *Dimensional reduction in finite-temperature quantum chromodynamics,* Phys. Rev. D **27** (1983) 917.

[97] S. Nadkarni, *Dimensional reduction in finite-temperature quantum chromodynamics. II,* Phys. Rev. D **38** (1988) 3287.

[98] L. Kärkkäinen, P. Lacock, D. Miller, B. Petersson, and T. Reisz, *Dimensional reduction in SU (3) gauge theory,* Phys. Lett. B **282** (1992) 121.

[99] L. Kärkkäinen, P. Lacock, B. Petersson, and T. Reisz, *Dimensional reduction and colour screening in QCD,* Nucl. Phys. B **395** (1993) 733.

[100] I. Ghisoiu, J. Möller, and Y. Schröder, *Debye screening mass of hot Yang-Mills theory to three-loop order,* JHEP **2015** (2015) 121 [1509.08727].

[101] S. Chapman, *New dimensionally reduced effective action for QCD at high temperature,* Phys. Rev. D **50** (1994) 5308 [hep-ph/9407313].

[102] A. Rajantie, *SU (5) + adjoint Higgs model at finite temperature,* Nucl. Phys. B **501** (1997) 521 [hep-ph/9702255].

[103] M. Laine and A. Rajantie, *Lattice-continuum relations for 3d SU (N) +Higgs theories,* Nucl. Phys. B **513** (1998) 471 [hep-lat/9705003].

[104] K. Kajantie, M. Laine, A. Rajantie, K. Rummukainen, and M. Tsypin, *The phase diagram of three-dimensional SU(3) + adjoint Higgs theory,* JHEP **1998** (1998) 011 [hep-lat/9811004].

[105] A. Hietanen, K. Kajantie, M. Laine, K. Rummukainen, and Y. Schröder, *Three-dimensional physics and the pressure of hot QCD,* Phys. Rev. D **79** (2009) 045018 [0811.4664].

[106] J. Schwinger, *On Gauge Invariance and Vacuum Polarization,* Phys. Rev. **82** (1951) 664.

[107] L. Abbott, *The background field method beyond one loop,* Nucl. Phys. B **185** (1981) 189.

[108] R. Jackiw, *Functional evaluation of the effective potential,* Phys. Rev. D **9** (1974) 1686.

[109] I. Ghisoiu, *Three-loop Debye mass and effective coupling in thermal QCD*, PhD thesis, Universität Bielefeld, Jan, 2013.

[110] K. Kajantie, M. Laine, K. Rummukainen, and Y. Schröder, *Four-loop vacuum energy density of the SU(N_c) + adjoint Higgs theory,* JHEP **2003** (2003) 036 [hep-ph/0304048].

[111] C. P. K. Altes, *The unbearable smallness of magnetostatic QCD corrections,* arXiv (2017) [1801.00019].

[112] E. V. Shuryak, *Theory of Hadronic Plasma,* Sov. Phys. JETP **47** (1978) 212.

[113] A. K. Rebhan, *Non-Abelian Debye mass at next-to-leading order,* Phys. Rev. D **48** (1993) R3967 [hep-ph/9308232].

[114] P. Arnold and L. G. Yaffe, *The non-Abelian Debye screening length beyond leading order,* Phys. Rev. D **52** (1995) 7208 [hep-ph/9508280].

[115] K. Kajantie, M. Laine, J. Peisa, A. Rajantie, K. Rummukainen, and M. Shaposhnikov, *Nonperturbative Debye Mass in Finite Temperature QCD,* Phys. Rev. Lett. **79** (1997) 3130 [hep-ph/9708207].

[116] M. Laine and O. Philipsen, *The non-perturbative QCD Debye mass from a Wilson line operator,* Phys. Lett. B **459** (1999) 259 [hep-lat/9905004].

[117] D. Bieletzki, K. Lessmeier, O. Philipsen, and Y. Schröder, *Resummation scheme for 3d Yang-Mills and the two-loop magnetic mass for hot gauge theories,* JHEP **2012** (2012) 58 [1203.6538].

[118] R. Kobes, G. Kunstatter, and A. Rebhan, *QCD plasma parameters and the gauge-dependent gluon propagator,* Phys. Rev. Lett. **64** (1990) 2992.

[119] J. Möller and Y. Schröder, *Three-loop matching coefficients for hot QCD: reduction and gauge independence,* JHEP **2012** (2012) 25 [1207.1309].

[120] E. Braaten and A. Nieto, *Free energy of QCD at high temperature,* Phys. Rev. D **53** (1996) 3421 [hep-ph/9510408].

[121] M. Laine and Y. Schröder, *Quark mass thresholds in QCD thermodynamics,* Phys. Rev. D **73** (2006) 085009 [hep-ph/0603048].

[122] M. Laine, M. Meyer, and G. Nardini, *Thermal phase transition with full 2-loop effective potential,* Nucl. Phys. B **920** (2017) 565 [1702.07479].

[123] K. Kajantie, M. Laine, K. Rummukainen, and Y. Schröder, *The pressure of hot QCD up to $g^6 ln(1/g)$,* Phys. Rev. D **67** (2002) 105008 [hep-ph/0211321].

[124] S. Huang and M. Lissia, *The relevant scale parameter in the high temperature phase of QCD,* Nucl. Phys. B **438** (1995) 54 [hep-ph/9411293].

[125] P. Arnold and O. Espinosa, *Effective potential and first-order phase transitions: Beyond leading order,* Phys. Rev. D **47** (1993) 3546 [hep-ph/9212235].

[126] A. Helset, *Dimensional reduction of the Two-Higgs Doublet Model with a softly broken Z2 symmetry at one-loop*, PhD thesis, Norwegian U. Sci. Tech., 2017.

[127] T. Gorda, A. Helset, L. Niemi, T. V. I. Tenkanen, and D. J. Weir, *Three-dimensional effective theories for the two Higgs doublet model at high temperature,* JHEP **2019** (2018) 81 [1802.05056].

[128] L. Niemi, H. H. Patel, M. J. Ramsey-Musolf, T. V. I. Tenkanen, and D. J. Weir, *Electroweak phase transition in the real triplet extension of the SM: Dimensional reduction,* Phys. Rev. D **100** (2019) 035002 [1802.10500].

[129] W. Chao, G.-J. Ding, X.-G. He, and M. Ramsey-Musolf, *Scalar electroweak multiplet dark matter,* JHEP **2019** (2019) 58 [1812.07829].

[130] G. Somogyi, *Angular integrals in d dimensions,* J. Math. Phys. **52** (2011) 083501 [1101.3557].

[131] G. Passarino and M. Veltman, *One-loop corrections for e+e- annihilation into mu+mu- in the Weinberg model,* Nucl. Phys. B **160** (1979) 151.

[132] A. Davydychev and J. Tausk, *Two-loop self-energy diagrams with different masses and the momentum expansion,* Nucl. Phys. B **397** (1993) 123.

[133] A. I. Davydychev, *Explicit results for all orders of the epsilon-expansion of certain massive and massless diagrams,* Phys. Rev. D **61** (1999) 087701 [hep-ph/9910224].

[134] Y. Schröder and A. Vuorinen, *High-precision epsilon expansions of single-mass-scale four-loop vacuum bubbles,* JHEP **2005** (2005) 051 [hep-ph/0503209].

[135] A. K. Rajantie, *Feynman diagrams to three loops in three-dimensional field theory,* Nucl. Phys. B **480** (1996) 729 [hep-ph/9606216].

List of Figures

List of Tables

Erklärung
gemäss Art. 18 PromR Phil.-nat. 2019

Name/Vorname:	Philipp Maximilian Schicho
Matrikelnummer:	14-927-669
Studiengang:	Theoretische Physik
	Bachelor ☐ Master ☐ Dissertation ☒
Titel der Arbeit:	Multi-loop investigations of strong interactions at high temperatures
Leiter der Arbeit:	Prof. Dr. Mikko Laine

Ich erkläre hiermit, dass ich diese Arbeit selbständig verfasst und keine anderen als die angegebenen Quellen benutzt habe. Alle Stellen, die wörtlich oder sinngemäss aus Quellen entnommen wurden, habe ich als solche gekennzeichnet. Mir ist bekannt, dass andernfalls der Senat gemäss Artikel 36 Absatz 1 Buchstabe r des Gesetzes über die Universität vom 5. September 1996 und Artikel 69 des Universitätsstatuts vom 7. Juni 2011 zum Entzug des Doktortitels berechtigt ist. Für die Zwecke der Begutachtung und der Überprüfung der Einhaltung der Selbständigkeitserklärung bzw. der Reglemente betreffend Plagiate erteile ich der Universität Bern das Recht, die dazu erforderlichen Personendaten zu bearbeiten und Nutzungshandlungen vorzunehmen, insbesondere die Doktorarbeit zu vervielfältigen und dauerhaft in einer Datenbank zu speichern sowie diese zur Überprüfung von Arbeiten Dritter zu verwenden oder hierzu zur Verfügung zu stellen.

Bern, 23/04/2020

Philipp Maximilian Schicho